

**EVALUATION OF THE THERAPEUTIC EFFICACY OF
NANOPARTICULATED BIO-FLAVONOIDS IN
COMBATING OXIDATIVE HEPATOCELLULAR
DEGENERATION BY NUCLEAR IMAGING
TECHNOLOGY USING Tc-99m
RADIOPHARMACEUTICALS**

Thesis submitted

by

SOUMYA GANGULY

Doctor of Philosophy (Pharmacy)

**Department of Pharmaceutical Technology
Faculty Council of Engineering & Technology
Jadavpur University
Kolkata, India
2023**

JADAVPUR UNIVERSITY
KOLKATA 700032
WEST BENGAL, INDIA

INDEX NO: 261/17/Ph
REGISTRATION NO: 1021713009

1. Title of the thesis:

Evaluation of the therapeutic efficacy of nanoparticulated bio-flavonoids in combating oxidative hepatocellular degeneration by nuclear imaging technology using Tc-99m radiopharmaceuticals.

2. Name, Designation & Institution of the supervisors:

i. Dr. (Mrs.) Mita Chatterjee Debnath

Principal Technical Officer (Retd.),

Infectious Diseases and Immunology Division

CSIR-Indian Institute of Chemical Biology

4, Raja, S. C. Mullick Road, Kolkata 700032

West Bengal, India.

Tel.: +91-9432319250, E mail: mitacd2016@gmail.com

ii. Dr. Saikat Dewanjee

Professor

Department of Pharmaceutical Technology

Jadavpur University

188, Raja S C Mallick Road, Kolkata 700032

West Bengal, India.

Tel.: +91-33-42452-32043, E mail: saikat.dewanjee@jadavpuruniversity.in

3. List of Publications:

A. Related to the thesis works (2)

i. Ganguly S, Dewanjee S, Sen R, Chattopadhyay D, Ganguly S, Gaonkar R, Debnath MC. Apigenin-loaded galactose tailored PLGA nanoparticles: A possible strategy for liver targeting to treat hepatocellular carcinoma. *Colloids Surf B Biointerfaces*. 2021;204:111778. doi: 10.1016/j.colsurfb.2021.111778. (**Impact factor: 5.999**).

ii. Ganguly S, Gaonkar RH, Sinha S, Gupta A, Chattopadhyay D, Chattopadhyay S, Sachdeva SS, Ganguly S, Debnath MC. Fabrication of surfactant-free quercetin-loaded PLGA

nanoparticles: evaluation of hepatoprotective efficacy by nuclear scintigraphy. *J Nanopart Res.* 2016;18(7):196. doi: 10.1007/s11051-016-3504-0. (**Impact factor: 2.533**).

B. Other publications obtained during the period of doctoral research (5)

i. Sen R, **Ganguly S**, Ganguly S, Debnath MC, Chakraborty S, Mukherjee B, Chattopadhyay D. Apigenin-Loaded PLGA-DMSA Nanoparticles: A Novel Strategy to Treat Melanoma Lung Metastasis. *Mol Pharm.* 2021;18(5):1920-1938. doi: 10.1021/acs.molpharmaceut.0c00977. (**Impact factor: 5.364**).

ii. Kazi J, Sen R, Ganguly S, Jha T, **Ganguly S**, Chatterjee Debnath M. Folate decorated epigallocatechin-3-gallate (EGCG) loaded PLGA nanoparticles; in-vitro and in-vivo targeting efficacy against MDA-MB-231 tumor xenograft. *Int J Pharm.* 2020;585:119449. doi: 10.1016/j.ijpharm.2020.119449. (**Impact factor: 6.510**).

iii. Gaonkar RH, Baishya R, Paul B, Dewanjee S, Ganguly S, Debnath MC, **Ganguly S**. Development of a peptide-based bifunctional chelator conjugated to a cytotoxic drug for the treatment of melanotic melanoma. *Med Chem Comm.* 2018;9(5):812-826. doi: 10.1039/c7md00638a. (**Impact factor: 2.495**).

iv. Gaonkar RH, **Ganguly S**, Dewanjee S, Sinha S, Gupta A, Ganguly S, Chattopadhyay D, Chatterjee Debnath M. Garcinol loaded vitamin E TPGS emulsified PLGA nanoparticles: preparation, physicochemical characterization, in vitro and in vivo studies. *Sci Rep.* 2017;7(1):530. doi: 10.1038/s41598-017-00696-6. (**Impact factor: 4.996**).

v. Gaonkar RH, **Ganguly S**, Baishya R, Dewanjee S, Sinha S, Gupta A, Ganguly S, Debnath MC. Exploring the Potential of (99m)Tc(CO)₃-Labeled Triazolyl Peptides for Tumor Diagnosis. *Cancer Biother Radiopharm.* 2016;31(3):110-117. doi: 10.1089/cbr.2015.1915. (**Impact factor: 3.632**).

4. List of patents: Nil

5. List of presentations in national/international seminar/conferences: (5)

i. **Ganguly S**, Debnath MC. Evaluation of Radio-protective Efficacy of Nanoparticulated Myricetin in combating Whole Body Irradiation Induced Liver Tissue Damage in rat model. 70th Indian Pharmaceutical Congress, Amity University, Noida, December 2018.

ii. **Ganguly S**, Debnath MC. Dialysis Method: A Novel Technique for Preparing Surfactant Free Nanoparticles. National Seminar on Pharmacy and Healthcare: Traditional Knowledge to Modern Techniques, Jadavpur University, Kolkata, September 2018.

iii. **Ganguly S**, Debnath MC. Evaluation of The Therapeutic Efficacy of Nanoparticulated Myricetin In Combating Oxidative Hepatocellular Degeneration by Non-Invasive Nuclear

Imaging Technology Using ^{99m}Tc Radiopharmaceuticals. 69th Indian Pharmaceutical Congress, Chandigarh, Punjab, December 2017.

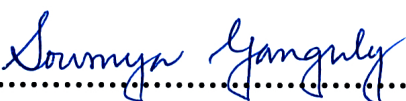
iv. Ganguly S, Gaonkar RH, Debnath MC. Evaluation of the therapeutic efficacy of nanoparticulated apigenin in combating oxidative hepatocellular degeneration by non-invasive nuclear imaging technology using ^{99m}Tc radiopharmaceuticals. ISCBDD 2016 (International Symposium on Chemical Biology and Drug Discovery), Kolkata, March 2016.

v. Ganguly S, Debnath MC. Evaluation of the therapeutic efficacy of Nanoparticulated Quercetin in combating oxidative hepatocellular degeneration by nuclear imaging technology using ^{99m}Tc radiopharmaceuticals. SNMICON 2014 (46th National Annual Conference of Society of Nuclear Medicine India), Kolkata, December 2014.

STATEMENT OF ORIGINALITY

I, **Soumya Ganguly** registered on **18 April 2017** do hereby declare that this thesis entitled "**Evaluation of the therapeutic efficacy of nanoparticulated bio-flavonoids in combating oxidative hepatocellular degeneration by nuclear imaging technology using Tc-99m radiopharmaceuticals**" contains literature survey and original research work done by the undersigned candidate as part of Doctoral studies.

All information in this thesis have been obtained and presented in accordance with existing academic rules and ethical conduct. I declare that, as required by these rules and conduct, I have fully cited and referred all materials and results that are not original to this work. I also declare that I have checked this thesis as per the "Policy on Anti Plagiarism, Jadavpur University, 2019", and the level of similarity as checked by iThenticate software is **10%** (checked on February 26, 2023).


.....

(Soumya Ganguly)

Certified by Supervisors


.....

(Dr. (Mrs.) Mita Chatterjee Debnath)

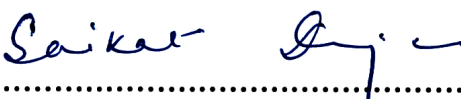
Principal Technical Officer (Retd.)

Infectious Diseases and Immunology Division

CSIR-Indian Institute of Chemical Biology

Kolkata, India.

Dr. (Mrs.) Mita Chatterjee Debnath
M. Pharm. Ph.D.
Retd. Radiological Safety Officer
Nuclear Medicine Division
Indian Institute of Chemical Biology
(A Unit of C.S.I.R. Govt. of India)
Jadavpur, Kolkata - 700 032


.....

(Dr. Saikat Dewanjee)

Professor

Department of Pharmaceutical Technology

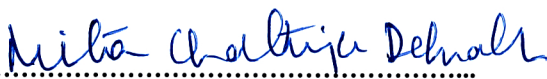
Jadavpur University

Kolkata, India

Prof. Saikat Dewanjee
Dept. of Pharmaceutical Technology
Jadavpur University
Kolkata - 700 032

CERTIFICATE FROM THE SUPERVISORS

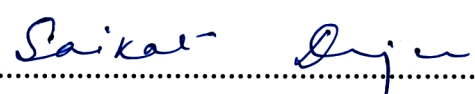
This is to certify that the thesis entitled "Evaluation of the therapeutic efficacy of nanoparticulated bio-flavonoids in combating oxidative hepatocellular degeneration by nuclear imaging technology using Tc-99m radiopharmaceuticals" submitted by Shri. Soumya Ganguly who got his name registered on 18 April 2017 for the award of Ph.D. (Pharmacy) degree of Jadavpur University is absolutely based upon his own work under the supervision of Dr. (Mrs.) Mita Chatterjee Debnath and Prof. Saikat Dewanjee and that neither his thesis nor any part of the thesis has been submitted for any degree/diploma or any other academic award anywhere before.



(Dr. (Mrs.) Mita Chatterjee Debnath)

Principal Technical Officer (Retd.)
Infectious Diseases and Immunology Division
CSIR-Indian Institute of Chemical Biology
Kolkata, India.

Dr. (Mrs.) Mita Chatterjee Debnath
M. Pharm. Ph.D.
~~Retd.~~ Radiological Safety Officer
Nuclear Medicine Division
Indian Institute of Chemical Biology
(A Unit of C.S.I.R. Govt of India)
Jadavpur, Kolkata - 700032



(Dr. Saikat Dewanjee)

Professor
Department of Pharmaceutical Technology
Jadavpur University
Kolkata, India

Prof. Saikat Dewanjee
Dept. of Pharmaceutical Technology
Jadavpur University
Kolkata - 700 032

ACKNOWLEDGEMENTS

The work presented in this thesis would not have been possible without my close association with many people. I take this opportunity to extend my sincere gratitude and appreciation to all those who made this PhD thesis possible.

First and foremost, I would like to extend my deepest gratitude to my research supervisors, **Dr. (Mrs.) Mita Chatterjee Debnath** and **Prof. Saikat Dewanjee**, for introducing me to this exciting domain of scientific research. Their sincere help, advice, inspiration, encouragement, and continuous support throughout my PhD tenure have been invaluable. Madam has been supportive and has given me the freedom to pursue various projects without objection. I am very grateful to her for her scientific advice and knowledge and many insightful discussions and suggestions. I am also very much indebted to Sir for allowing me to register for PhD under his guidance. He has been always supportive and provided necessary advice during my research activities and thesis writing. He has always stood by my side and acted as a pillar throughout this journey.

I am immensely thankful to **Prof. Siddhartha Roy**, ex-Director, Indian Institute of Chemical Biology and **Prof. Samit Chattopadhyay**, Director, Indian Institute of Chemical Biology for providing necessary financial support to carry out my research activities in this prestigious institute, to the **Board of Research in Nuclear Studies (BRNS)** for sanctioning the research project (BRNS project No. 2013/35/25/BRNS/0656 dt. 31 MAY 2013).

I also express my profound gratitude towards my principal collaborators, **Dr. Sankha Chattopadhyay**, VECC, Kolkata and **Dr. Satbir Singh Sachdev**, BRIT, Mumbai for their kind support in the smooth running of the BRNS sponsored research project, **Dr. Santanu Ganguly** (Head of the Department of Nuclear Medicine), **Mr. Samarendu Sinha** and **Mr. Amit Gupta**, Regional Radiation Medicine Centre, Thakurpukur Cancer Research Centre, Kolkata for their active assistance and cooperation during gamma Scintigraphic imaging study, which was an essential part for the completion of this project.

I would like to extend my sincere thanks to **Dr. Dipankar Chattopadhyay**, Professor, Department of Polymer Science and Technology, University of Calcutta for his support and guidance in nanoparticle characterization without which I could not have made any progress.

I would also like to thank **Late Prof. (Dr.) R. Debnath**, Academic Chairman, Calcutta Institute of Pharmaceutical Technology & Allied Health Sciences for having confidence in me and allowing me to teach at CIPT & AHS and **Dr. Susanta Mondal**, Associate Director-DMPK, TCG Lifesciences Pvt. Ltd. for making me a part of his team.

I take this opportunity to convey my thanks to my seniors **Dr. Dipak Kumar Nayak** and **Dr. Rinky Baishya** for their guidance and suggestions and my fellow lab mates **Dr. Raghuvir Gaonkar**, **Dr. Ramkrishna Sen**, **Dr. Julekha Kazi**, **Dr. Kakali De** for their support.

I must thank the office staff of different departments (Central Instrumentation, Animal House, Accounts, Purchase, PME, Library, Canteen) of CSIR-IICB, for their constant support

and guidance, from the procurement of consumables till analysis of samples for my research work, I also thank the security staff and house-keeping personnel of CSIR-IICB for their extensive support during my work,

*I also thank my friends **Mr. Avik Ranjan Chatterjee, Mr. Dibyendu Bhowmick and Miss. Basita Das** for providing support and friendship that I needed. I thank them for being supportive throughout this phase and helping me to regroup whenever I felt tensed and dejected.*

*I especially thank my **Mom, Dad, and Brother** for providing unconditional love and care. My Mom, especially, was a great role model of resilience, strength and character. Their patience and sacrifice will remain my inspiration throughout my life. I love them very much, and I would not have made it this far without them. I knew that I always have my family to count on when times are rough and tough.*

*I owe my deepest gratitude towards my Better half, **Shayari** for her support and understanding of my goals and aspirations. Without her help, I would not have been able to complete much of what I have done and become who I am.*

Soumya Ganguly

(Soumya Ganguly)

Place: Kolkata

Date: 01/06/23

I dedicate this thesis to
The Almighty,
My parents & My wife
for their constant support
and inspiration

PREFACE

Hepatic disorders account for approximately 2 million fatalities per year worldwide. Major liver diseases include non-cancerous liver diseases like alcoholic cirrhosis, viral hepatitis, drug-induced hepatotoxicity, etc. and hepatocellular carcinoma (HCC). Synthetic drug therapy is being used to treat the aforementioned illness, however, the therapeutic regimen is frequently accompanied by serious adverse effects. In contrast, natural products have been quite promising in treating various hepatic disorders including HCC by the virtue of their anti-oxidant, anti-inflammatory, and chemopreventive properties. Consumption of polyphenol-enriched foods can be a suitable alternative in combating these chronic liver disorders. Chemo-preventive effects of plant phenolics, such as flavonoids are progressively rising to confer protection against carcinogenesis in the liver. However, the poor pharmacokinetic attributes of these phytoconstituents limit their therapeutic efficacy and require high and multiple doses for achieving a desired therapeutic effects. In this issue, nanoscale formulations of these flavonoids have come up with the prospect to overcome these limitations and improve their therapeutic efficacy. Biomaterials-based nanoparticles (NPs) have received particular attention because they hold the promise to revolutionize medical treatment with more potent, less toxic, and smart therapeutics. For the purpose of drug delivery, NPs can encapsulate or covalently conjugate hydrophobic drugs to greatly enhance their aqueous solubility and in turn bioavailability. Normally most of the drugs achieve high hepatic concentration, still, their targeting is necessary because the liver is the major organ in the body equipped for uptake, detoxification, metabolic transformation, and excretion of xenobiotics into bile by means of carrier-mediated mechanism. As a consequence, most of the drugs are rapidly cleared from the blood and display high first-pass clearances by the liver which decreases the bioavailability. However, it should be realized that the total hepatic uptake predominantly depends on hepatocytes, whereas Kupffer cells largely contribute to the hepatic uptake of particulate material. Specific targeting of hepatocyte receptors can also be achieved. The most commonly exploited target is the asialoglycoprotein receptor that recognizes carbohydrates (mainly galactose and N-acetylgalactosamine) with variable affinity. This galactose ligand is very important in achieving liver targeting as there is a specific interaction between galactose moiety and the asialoglycoprotein receptors which are found on the surface of hepatocytes. Galactose has been also widely used as targeting moiety to the liver and many research groups have reported this specialized liver targeting.

The thesis comprises the following chapters:

CHAPTER 1 is the introductory section which deals with the current status of chronic liver diseases including HCC and their management using naturally occurring plant metabolites followed by the role of novel drug delivery systems in the delivery of phytoconstituents to improve their therapeutic efficacy.

CHAPTER 2 deals with the thorough literature review of the bioflavonoids (quercetin and apigenin) and the polymer (PLGA) used in the current research.

CHAPTER 3 deals with the development of surfactant-free quercetin-loaded PLGA NPs to investigate the hepatoprotective efficacy of the product non-invasively by nuclear scintigraphy.

CHAPTER 4 deals with the development of galactose-tailored PLGA NPs loaded with apigenin for active liver targeting to treat HCC in an animal model which might serve as a potential therapeutic agent against HCC in the future by achieving improved liver targeting.

Index

Chapters	Contents	Page Nos.
Chapter 1	Introduction	1-18
	1.1. Introduction	1
	1.2. High-risk CLDs	
	1.2.1. Non-cancerous CLDs	2
	1.2.2. HCC	4
	1.3. Challenges associated with the treatment of liver diseases	5
	1.4. Treatments of CLDs and HCC using naturally occurring plant metabolites	5
	1.5. Role of flavonoids in liver ailments	
	1.5.1. Flavonoids in CLDs	7
	1.5.2. Flavonoids against HCC	7
	1.6. Drawback of using flavonoids as a therapeutic option	9
	1.7. Requirements for novel formulations	
	1.7.1. Requirements for novel drug delivery systems for phytoconstituents	10
	1.7.2. NPs: novel formulations with significant promise	12
	1.7.2.1. Polymeric NPs	14
	1.7.2.2. Successes of flavonoid-loaded polymeric NPs in combating against CLDs and HCC	15
	1.8. Nuclear scintigraphy: A non-invasive imaging modality	
	1.8.1. Roles of nuclear scintigraphy	15
	1.8.2. Liver scintigraphic imaging	17
	1.9. Aim & Objectives	18
Chapter 2	Literature Review	19-36
	2.1. Quercetin (Qr)	19
	2.1.1. Physicochemical characteristics	19
	2.1.2. Biological activities of Qr	
	2.1.2.1. Antioxidant activities	20
	2.1.2.2. Anti-inflammatory activity	21
	2.1.2.3. Antidiabetic activity	21
	2.1.2.4. Neuroprotective Activity	22
	2.1.2.5. Hepatoprotective activity	22
	2.1.2.6. Cardioprotective activities	22
	2.1.2.7. Nephroprotective activity	23
	2.1.2.8. Anticancer activity	23
	2.1.2.9. Antimicrobial activity	24
	2.1.2.10. Antiviral activities	24
	2.1.3. Bioavailability of Qr	25
	2.1.4. Nanoformulations of Qr: A potential solution to its poor bioavailability	25
	2.2. Apigenin (API)	26
	2.2.1. Physicochemical characteristics	26
	2.2.2. Biological activities of API	
	2.2.2.1. Antioxidant activity	26
	2.2.2.2. Anti-inflammatory activity	27
	2.2.2.3. Antidiabetic activity	28
	2.2.2.4. Neuroprotective effects	28
	2.2.2.5. Hepatoprotective activity	28

	2.2.2.6. Cardioprotective effect	29
	2.2.2.7. Nephroprotective activity	29
	2.2.2.8. Anticancer effects	30
	2.2.2.9. Antimicrobial properties	30
	2.2.2.10. Antiviral activity	30
	2.2.3. Bioavailability of API	31
	2.2.4. API nanoformulations: A way to overcome its bioavailability issues	31
	2.3. PLGA	32
	2.3.1. Solubility	32
	2.3.2. Molecular weight	33
	2.3.3. Crystallinity	33
	2.3.4. Thermal stability and storage	33
	2.3.5. Degradation	33
	2.3.6. Elimination	33
	2.3.7. Biomedical applications of PLGA	33
Chapter 3	Fabrication of surfactant free quercetin loaded PLGA nanoparticles: Evaluation of hepatoprotective efficacy by nuclear scintigraphy	37-54
	3.1. Introduction	37
	3.2. Materials and methods	
	3.2.1. Materials	39
	3.2.2. Preparation of NPs	39
	3.2.3. Characterization of NPs	
	3.2.3.1. Determination of NP yield, encapsulation efficiency and loading capacity	40
	3.2.3.2. Morphology of NPs	40
	3.2.3.3. Drug physical state characterization	40
	3.2.3.4. Particle size and zeta potential analysis	41
	3.2.3.5. In vitro release studies	41
	3.2.4. In vitro cytotoxicity studies	41
	3.2.5. Confocal laser scanning microscopy	42
	3.2.6. In vivo experiment	42
	3.2.6.1. Serum biochemical analysis	42
	3.2.6.2. Measurement of GSH, catalase, lipid peroxide and SOD in liver homogenate	43
	3.2.6.3. Histopathological analysis	44
	3.2.6.4. Scintigraphic imaging Studies	44
	3.2.7. Statistical analysis	44
	3.3. Results and discussion	45
	3.3.1. Surface morphology, particle size and zeta potential	45
	3.3.2. Drug physical status characterization	46
	3.3.3. In vitro release profile	48
	3.3.4. Cytotoxicity assessment	49
	3.3.5. Cellular uptake	49
	3.3.6. In vivo effects	50
	3.4. Conclusion	54
Chapter 4	Apigenin-loaded galactose tailored PLGA nanoparticles: A possible strategy for liver targeting to treat hepatocellular carcinoma	55-77
	4.1. Introduction	55
	4.2. Materials and Methods	
	4.2.1. Materials	56

4.2.2.	Synthesis of GAL-PLGA	56
4.2.3.	Formulation of NPs	57
4.2.4.	Characterization of NPs	
4.2.4.1.	Particle size distribution and zeta potential analysis	57
4.2.4.2.	Surface morphology of NPs	57
4.2.4.3.	Physicochemical characterization of NPs	57
4.2.5.	In vitro release studies	57
4.2.6.	Stability study	58
4.2.7.	In vitro studies	
4.2.7.1.	Cell culture	58
4.2.7.2.	Cellular uptake studies	58
4.2.7.3.	Cytotoxicity studies	58
4.2.7.4.	Apoptosis assay	58
4.2.8.	In vivo studies	
4.2.8.1.	Pharmacokinetic studies	58
4.2.8.2.	In vivo antitumor efficacy study	59
4.2.8.3.	Serum enzyme parameters	59
4.2.8.4.	Western blot analysis	59
4.2.8.5.	Gelatin zymography analysis	60
4.2.9.	Statistical analysis	60
4.3.	Results	
4.3.1.	Structural confirmation of galactosylation of PLGA	60
4.3.2.	Characterization of NPs	61
4.3.3.	Drug loading and encapsulation efficiency	62
4.3.4.	Surface characteristics of NPs	62
4.3.5.	Physicochemical characteristics of NPs	
4.3.5.1.	DSC and XRD study	63
4.3.5.2.	FTIR spectroscopic analysis	63
4.3.6.	In vitro drug release and kinetic study	64
4.3.7.	In vitro studies	
4.3.7.1.	Cellular uptake and internalization	65
4.3.7.2.	MTT assay	66
4.3.7.3.	Apoptosis study	67
4.3.8.	Pharmacokinetic analysis	68
4.3.9.	Antitumor efficacy of NPs in vivo	
4.3.9.1.	Efficacy of NPs against DEN-induced HCC	69
4.3.9.2.	Histopathological analysis	70
4.3.9.3.	Western blot analysis of apoptosis markers	72
4.3.9.4.	Gelatin zymography analysis	73
4.3.9.5.	Evaluation of hepatoprotective efficacy by scintigraphic imaging analysis	73
4.4.	Discussion	74
Reference		78-123

Figure Captions

Figures	Captions	Page Nos.
Figure 1.1.	The basic mechanism of developing CLDs	4
Figure 1.2.	Anticancer mechanism of flavonoids against HCC	9
Figure 1.3.	Advantages of NPs formulation	14
Figure 2.1.	Structure of Qr	19
Figure 2.2.	The therapeutic mechanism of Qr	20
Figure 2.3.	Structure of API	26
Figure 2.4.	The therapeutic mechanism of API	27
Figure 3.1.	FE-SEM images (A and B), particle size distribution profile (C) and zeta potential distribution profile (D) of Qr-NPs (Batch S1)	46
Figure 3.2.	DSC thermograms (A), XRD spectra (B) of Qr (free), PLGA and Qr-NPs	47
Figure 3.3.	FTIR spectra Qr (free), PLGA and Qr-NPs	48
Figure 3.4.	In vitro drug release profile of Qr-NPs (A), MTT cytotoxicity studies of Qr free and Qr-NPs against HepG2 cells (B) and Fluorescent microscopy images of HepG2 cells treated with FITC loaded PLGA NPs	49
Figure 3.5.	Microscopy images of H & E stained liver of rats treated with olive oil (Normal), CCl ₄ (damaged) and CCl ₄ + Qr-NPs treated	52
Figure 3.6.	(A) Scintigraphic images of ^{99m} Tc-sulphur colloid acquired at 30 min post injection time period of Normal, CCl ₄ - intoxicated and Qr-NPs treated rats. (B) Hepatobiliary clearance curve and (C) scintigraphic images at different post injection time period of ^{99m} Tc-mebrofenin in Normal, CCl ₄ - intoxicated and Qr-NPs treated rats	53
Figure 4.1.	¹ H-NMR spectra of PLGA and GAL-PLGA	61
Figure 4.2.	Size distribution, zeta potential, and morphology of API-NPs and API-GAL-NPs. (A) Particle size distribution profile, (B) zeta potential distribution pattern, (C) FESEM images, and (D) TEM images	62
Figure 4.3.	(A) DSC thermograms, (B) XRD diffractograms, and (C) FTIR spectra of API, PLGA, GAL-PLGA, POLOXAMER, API-NPs, and API-GAL-NPs. (D) in vitro drug release showing cumulative % of drug release of API-NPs and API-GAL-NPs	64

- Figure 4.4.** In vitro cellular uptake of galactosylated and non-galactosylated NPs in HepG2 cells at different time points. (A) Cellular uptake of FITC-NPs. (B) Cellular uptake of FITC-GAL-NPs. (C) Cellular uptake of FITC-GAL-NPs in the presence of galactose (blocking condition). (D) Histogram representing the cellular uptake of FITC-NPs, FITC-GAL-NPs, and FITC-GAL-NPs (blocking condition) at different time points. (E) Confocal microscopic images representing cellular uptake of FITC-NPs and FITC-GAL-NPs in HepG2 cells at a time interval of 2 h. FITC exhibits green fluorescence and DAPI (nuclear stain) exhibits blue fluorescence. 66
- Figure 4.5.** (A) Cytotoxic effect of API, API-NPs, and API-GAL-NPs on HepG2 cells at 24 and 48 h measured by MTT assay. (B) Apoptosis induction by API, API-NPs, and API-GAL-NPs to HepG2 cells measured by flow cytometry. (C) Plasma concentration-time profile of API at different time points following API, API-NPs, and API-GAL-NPs treatments 68
- Figure 4.6.** Images of the livers in experimental animals. Black arrows represent hepatic nodules developed due to DEN treatment in rat 69
- Figure 4.7.** (A) Representative photomicrographs of haematoxylin-eosin-stained liver section. (B) Representative photomicrographs of PAS-stained liver section. (C) Western blot analysis expression of different apoptotic proteins and histogram showing their relative expressions in liver. β -Actin served as a loading control protein. The intensity of normal control band was assigned 1 (D) Zymogram and histogram showing the effect on MMP-9 and MMP-2 in liver. 71
- Figure 4.8.** Nuclear scintigraphic image analyses of normal (Gr-I), HCC control (Gr-II), and API-GAL-NPs-treated rats (Gr-V). (A) Representative scintigraphic images of ^{99m}Tc -sulphur colloid acquired at 1 h post-injection. (B) Representative hepatobiliary clearance curves of ^{99m}Tc -mebrofenin. (C) Representative scintigraphic images at different post-injection time periods of ^{99m}Tc -mebrofenin. White arrows represented area of low uptake of sulphur colloids 73

Table Captions

Tables	Captions	Page Nos.
Table 2.1.	List of PLGA polymeric ratios versus molecular weights	32
Table 2.2.	PLGA nanoparticles developed against different types of diseases	34
Table 3.1.	Particle characterization	45
Table 3.2.	Effect of oral treatment with Qr-NPs on blood serum biochemical parameters in CCl ₄ -induced acute hepatocellular injury. Results are expressed as mean \pm SD of six animals. CCl ₄ treated group was compared with the normal group and Qr-NPs treated group was compared with CCl ₄ treated group	50
Table 3.3.	Effect of oral treatment with Qr-NPs on GSH, catalase, lipid peroxide and SOD activities of liver in CCl ₄ -induced acute hepatocellular injury. Results are expressed as mean \pm SD of six animals. CCl ₄ treated group was compared with the normal group and Qr-NPs treated group was compared with CCl ₄ treated group	51
Table 4.1.	NPs characterization and stability studies	61
Table 4.2.	Data for various kinetic models for NPs obtained from in vitro drug release studies	65
Table 4.3.	IC ₅₀ values of free drug and NPs on HepG2 cells at different time intervals	67
Table 4.4.	Pharmacokinetic data	69
Table 4.5.	Effect of API in free and NP forms on relative liver weight and hepatic nodules in DEN induced hepatocarcinogenic rats	70
Table 4.6.	Effect of API and nanoparticulated API on serum enzyme parameters	70

Abbreviations

2D	2-Dimensional
3CLpro	3-chymotrypsin-like protease
AFP	Alpha-fetoprotein
AFP-L3	Lens culinaris agglutinin-reactive fraction of alpha-fetoprotein
Akt	Protein kinase B
ALP	Alkaline phosphatase
ALT	Alanine transaminase
AMPK	5' adenosine monophosphate-activated protein kinase
AP	Alkaline phosphatase
AP-1	Activator protein-1
API	Apigenin
API-GAL-NPs	Apigenin galactose nanoparticles
API-NPs	Apigenin nanoparticles
ARE	Antioxidant responsive element
ASD	Autism spectrum disorder
ASGP-R	Asialoglycoprotein receptors
AST	Aspartate transaminase
ATP	Adenosine triphosphate
ATP5B	ATP synthase F1 subunit beta
AUC	Area under the curve
A β	Amyloid-beta
b.w.	Body weight
Bax	B-cell lymphoma 2-associated X
BRIT	Board of Radiation and Isotope Technology
CAT	Catalase
CCl ₄	Carbon tetrachloride
CdCl ₂	Cadmium chloride
c-IAP1	Cellular inhibitor of apoptosis protein 1
CLDs	Chronic liver diseases
CNS	Central nervous system
CO ₂	Carbon dioxide
COX-2	Cyclooxygenase-2
CPCSEA	Committee for the Purpose of Control and Supervision of Experiments on Animals
c-Src	Cellular sarcoma kinase
CT	Computerized tomography
CYP2E1	Cytochrome P450 Family 2 Subfamily E Member 1
DAPI	4',6-diamidino-2-phenylindole
DCP	Des- γ -carboxy prothrombin

DEN	Diethylnitrosamine
D-GalN	d-Galactosamine
DISIDA	Diisopropyl iminodiacetic acid
DLS	Dynamic light scattering
DMEM	Dulbecco's Modified Eagle Medium
DMF	Dimethylformamide
DMSO	Dimethyl sulfoxide
DNA	Deoxyribonucleic acid
DSC	Differential scanning calorimetric
DTNB	5,5'-Dithiobis-(2-Nitrobenzoic Acid)
DTPA	Diethylenetriaminepentaacetic acid
ECIL	Electronics Corporation of India Limited
EDTA	Ethylenediaminetetraacetic acid
EMEM	Eagle's minimum essential medium
EPR	Enhanced permeability and retention
ERK	Extracellular signal-regulated kinase
FBS	Fetal bovine serum
FE-SEM	Field emission scanning electron microscope
FITC	Fluorescein isothiocyanate
FTIR	Fourier transform infrared spectroscopy
FXR	Farnesoid X receptor
GAL-PLGA	Galactosylated PLGA
GES-1	Human gastric mucosa epithelial cell
GIT	Gastro intestinal tract
GPx	Glutathione peroxidase
GSH	Reduced glutathione
GSK-3 β	Glycogen synthase kinase-3 beta
GST	Glutathione S-transferase
H ₂ O ₂	Hydrogen peroxide
HBS	Hepatobiliary scintigraphy
HCC	Hepatocellular carcinoma
HepG2	Human liver hepatocellular carcinoma cell
HIF-1 α	Hypoxia-inducible factor 1-alpha
HMGB1	High mobility group box 1
hnRNP	Heterogeneous nuclear ribonucleoprotein
HO-1	Heme oxygenase-1
HPLC	High pressure liquid chromatography
i.p.	Intraperitoneal
i.v.	Intravenous
ICAM-1	Intercellular adhesion molecule 1
IDA	Iminodiacetic acid

IE	Immediate-early
IFN	Interferons
IL	Interleukin
IL-4R	Interleukin 4 receptor
IL-6	Interleukin 6
iNOS	Inducible nitric oxide synthase
IUPAC	International Union of Pure and Applied Chemistry
KCl	Potassium Chloride
kDa	Kilodalton
KMnO ₄	Potassium permanganate
L/G	Poly lactic acid / Poly glycolic acid
LDL	Low density lipoprotein
LPS	Lipopolysaccharide
MAPK	Mitogen-activated protein kinase
MARCH1	Membrane associated ring-CH-type finger 1
MBq	Megabecquerels
miR	MicroRNA
MMP	Matrix metalloproteinases
Mol	Molecular
MRI	Magnetic resonance imaging
mTOR	Mammalian target of rapamycin
MTT	3-(4,5-dimethylthiazol-2-yl)-2,5-diphenyltetrazolium bromide
MWCO	Molecular weight cut-off
NAD	Nicotinamide adenine dinucleotide
NAFLD	Non-alcoholic fatty liver disease
NDDS	Novel drug delivery systems
NDEA	N-nitrosodiethylamine
NEAT1	Nuclear paraspeckle assembly transcript 1
NF-κB	Nuclear factor kappa-light-chain-enhancer of activated B cells
NLRP3	Nucleotide-binding oligomerization domain-like receptor 3
NMR	Nuclear magnetic resonance
NO	Nitric oxide
NPs	Nanoparticles
Nrf-2	Nuclear factor erythroid 2-related factor 2
OLT	Orthotopic liver transplantation
PAC	Poly-alkyl-cyano-acrylates
PBS	Phosphate buffered saline
PCL	Poly-ε-caprolactone
PDI	Polydispersity index
PEG	Polyethylene glycol
PGA	Poly (glycolic acid)

PGC1	Peroxisome proliferator-activated receptor- γ coactivator 1
PI3K	Phosphoinositide 3-kinase
PKC	Protein kinase C
PL pro	Papain-like protease
PLA	Polylactic acid
PLGA	Poly (Lactic-co-glycolic acid)
PON2	Paraoxonase 2
PPAR	Peroxisome proliferator-activated receptor
Qr	Quercetin
RIG-I	Retinoic acid-inducible gene-I
RNS	Reactive nitrogen species
ROS	Reactive oxygen species
s.c.	Subcutaneous
S1P	Sphingosine-1-phosphate
SDS-PAGE	Sodium dodecyl-sulphate polyacrylamide gel electrophoresis
SGPT	Serum glutamate-pyruvate transaminase
SMAD	Suppressor of mothers against decapentaplegic
SOD	Superoxide dismutase
SPECT	Single-photon emission computerized tomography
SphK1	Sphingosine kinase 1
STAT3	Signal transducer and activator of transcription 3
T2D	Type 2 diabetes
TCA	Trichloroacetic acid
TEM	Transmission electron microscope
TGF- β	Transforming growth factor beta
TGPCR	Takeda G-protein-coupled receptor
THP-1	Human monocytic leukaemia cell line
TLR	Toll-like receptor
TNFR	Tumor necrosis factor-alpha receptor
TNF- α	Tumor necrosis factor alpha
TRAF	Tumor necrosis factor receptor-associated factor
TRBP	Transactivation response element RNA-binding protein
UDP	Uridine-5-diphosphate
US	Ultrasonography
USFDA	United States Food and Drug Administration
USP-18	Ubiquitin-specific peptidase 18
UV-Vis	Ultraviolet Visible
VEGF	Vascular endothelial growth factor
WHO	World Health Organization
Wnt	Wingless/Integrated
XRPD	X-Ray powder diffraction

Chapter 1

Introduction

Contents

- 1.1. Introduction
- 1.2. High-risk CLDs
 - 1.2.1. Non-cancerous CLDs
 - 1.2.2. HCC
- 1.3. Challenges associated with the treatment of liver diseases
- 1.4. Treatments of CLDs and HCC using naturally occurring plant metabolites
- 1.5. Role of flavonoids in liver ailments
 - 1.5.1. Flavonoids in CLDs
 - 1.5.2. Flavonoids against HCC
- 1.6. Drawback of using flavonoids as a therapeutic option
- 1.7. Requirements for novel formulations
 - 1.7.1. Requirements for novel drug delivery systems for phytoconstituents
 - 1.7.2. NPs: novel formulations with significant promise
- 1.8. Nuclear scintigraphy: A non-invasive imaging modality
 - 1.8.1. Roles of nuclear scintigraphy
 - 1.8.2. Liver scintigraphic imaging
- 1.9. Aim & Objectives

1.1. Introduction

Hepatic disorders which account for approximately 2 million fatalities per year worldwide are primarily brought on by infections and exposure to xenobiotics (Li et al., 2016). The umbrella phrase "liver disease" refers to a wide range of conditions, some of which are relatively minor histological abnormalities while others have the potential to be fatal. This condition is a major source of worry for public health on a global scale (Zhang et al., 2013). Hepatocellular carcinoma, also known as HCC, is becoming more prevalent as a result of recent food trends and less-than-ideal eating habits, in addition to leading an unhealthy lifestyle. Hepatocellular carcinoma continues to be a major cause of morbidity and mortality, with significant economic and social ramifications (Suresh et al., 2020). According to predictions provided by the WHO, liver disease will be responsible for the deaths of 820,000 individuals in 2021. Cirrhosis and HCC will be the primary causes of mortality associated with this condition. As of 2018, it was projected that a total of 295.8 million people had chronic hepatitis B infection, and it is anticipated that an additional 1.5 million people will get chronic hepatitis B infection this year. There are around 290,000 deaths attributed to hepatitis C each year, despite the fact that there are approximately 58 million people in the globe who are now living with a chronic hepatitis C infection (World health statistics, 2021). Due to the enormous influence that it has had on a global scale, liver illness has become a key issue for the doctors of today (He et al., 2021). Cirrhosis and liver cancer are responsible for 3.5% of all fatalities worldwide when taken together. The condition known as cirrhosis ranks as the eleventh biggest cause of death, and liver cancer places sixteenth (GBD 2017 Cirrhosis Collaborators, 2020). There are about 400 million people around the world who are obese or diabetic. Obesity and diabetes are linked to non-alcoholic fatty liver disease (NAFLD) as well as HCC. Almost two billion people throughout the world partake in the consumption of alcoholic beverages, of which more than seventy-five million have been identified as suffering from alcohol use disorders and are at risk for alcohol-related liver injury (Crabb et al., 2020; Singal et al., 2021; Nouredin et al., 2015). The prevalence of viral hepatitis remains high all over the world, despite the fact that drug-induced liver injury is becoming an increasingly common major cause of acute hepatitis (Devarbhavi, 2012; Manka et al., 2016). These statistics are disturbing; nevertheless, they also present a great opportunity to improve public health, as the vast majority of liver diseases may be avoided by making healthier choices in lifestyle (Das et al., 2022).

In developed countries, the leading causes of chronic liver disease (also known as CLD) include alcoholic liver disease, NFALD, and chronic viral hepatitis (hepatitis B and C) (Cheemerla et al., 2021). Damage to the liver, including inflammation, fibrosis, and the

death of liver cells (hepatocytes), can occur as a direct result of chronic and repetitive assaults, which are the fundamental reason why CLDs arise. Hepatic damage can be caused by a wide variety of factors, including viral infections, exposure to toxic substances, excessive alcohol intake, metabolic abnormalities, and many others (Bataller et al., 2005). Damage is the first step in a process that is followed by inflammation, fibrosis, and compensatory hepatocyte hyperplasia on the way to cirrhosis, which is the last stage of the disease. Cirrhosis and CLDs, almost always end up in HCC, which is the third most lethal form of malignancy in the world (McGlynn et al., 2015).

When the liver metabolises a variety of potentially dangerous substances, reactive oxygen species (ROS) are formed. These ROS are what cause damage to the hepatocytes, which in turn causes damage to the liver (Li et al., 2015). In addition, in reaction to oxidative stress, Kupffer cells will release IL-6 and TNF- α which are prominent inflammatory cytokines. They cause cells to bloat up and eventually die. ROS is responsible for the promotion of lipid peroxidation in hepatic stellate cells. When hepatic stellate cells are damaged, the damage to the liver is compounded by the secretion of more collagen (Slevin et al. 2020; Koyama et al., 2017; Lee et al., 2011; Gandhi, 2012). In addition to causing liver damage through the induction of irreversible alterations to lipids, proteins, and nucleic acids, oxidative stress also encourages several pathogenic pathways through the regulation of gene and protein expressions. It's probable that this factor contributed to the development of liver troubles in the first place. As a result of this, oxidative stress is now recognised as a pathogenic mechanism that plays a vital part in the aetiology and progression of a wide variety of CLDs (Cicho-Lach et al., 2014; Arroyave-Ospina et al., 2021). In addition to this, it has been proposed that there are intricate relationships between the factors that cause disease, inflammation, free radicals, and immune responses (Muriel, 2009). In annexation, the systemic oxidative stress that is caused by liver disease can have a detrimental effect on other organs as well, including the brain and the kidneys (Sharifi-Rad et al., 2020). Although while numerous therapeutic approaches have been created over the course of time in order to cure a variety of liver diseases, these approaches have not shown a great deal of promise in curing CLDs, particularly because they produce side effects, which continue to be a big concern. Hence formulations that are based on natural products are receiving an increasing amount of attention from researchers in the scientific community for the therapeutic management of CLDs.

1.2. High-risk CLDs

1.2.1. Non-cancerous CLDs

In non-cancerous CLDs, the production of clotting factors and other related proteins, the detoxification of harmful metabolites, and the elimination of bile from body gradually

decrease (Ozougwu, 2017). CLDs, are distinguished by a recurrent cycle of inflammation, tissue loss, and regeneration in the liver parenchyma, which ultimately results in fibrosis and cirrhosis. Cirrhosis is the scarring of the liver caused by fibrosis (Figure 1.1). (Tanaka et al., 2016). Alcoholism, NAFLD, chronic viral hepatitis, genetic susceptibility, and drug induction are all common causes of CLDs (Nagaratnam et al., 2017). The final stage of non-malignant CLDs is called cirrhosis, and it is responsible for the disintegration of the architecture of the liver, the development of many nodules, the remodelling of blood vessels, the creation of new blood vessels (neo-angiogenesis), and the deposition of extracellular matrix (Borrello et al., 2022). Hepatic stem cells are necessary for parenchymal regeneration; however, the molecular process of cirrhosis is the recruitment of stellate cells and fibroblasts that promote fibrosis (Kisseleva et al., 2021; Zhou et al., 2014). Fatigue, anorexia, and weight loss are examples of nonspecific signs and symptoms of CLDs; however, they might be made worse by the presence of comorbidities. Hepatocellular insufficiency and portal hypertension are both conditions that can have devastating effects. A decompensated chronic liver disease can present itself as any of the symptoms listed above (Nusrat et al., 2014; Volk et al., 2012). In the vast majority of cases, a diagnosis of CLD can be arrived at using a mix of clinical examinations, both invasive and non-invasive diagnostic procedures, and diagnostic testing (Kang et al., 2017). In view of the fact that the progression of symptoms and issues should be slowed or stopped entirely with the help of treatment, it is necessary to employ an all-encompassing approach. In general, CLD is treated by addressing the underlying causes of the disease, managing portal hypertension, and customising treatment to the individual patient (Wiegand et al., 2013).

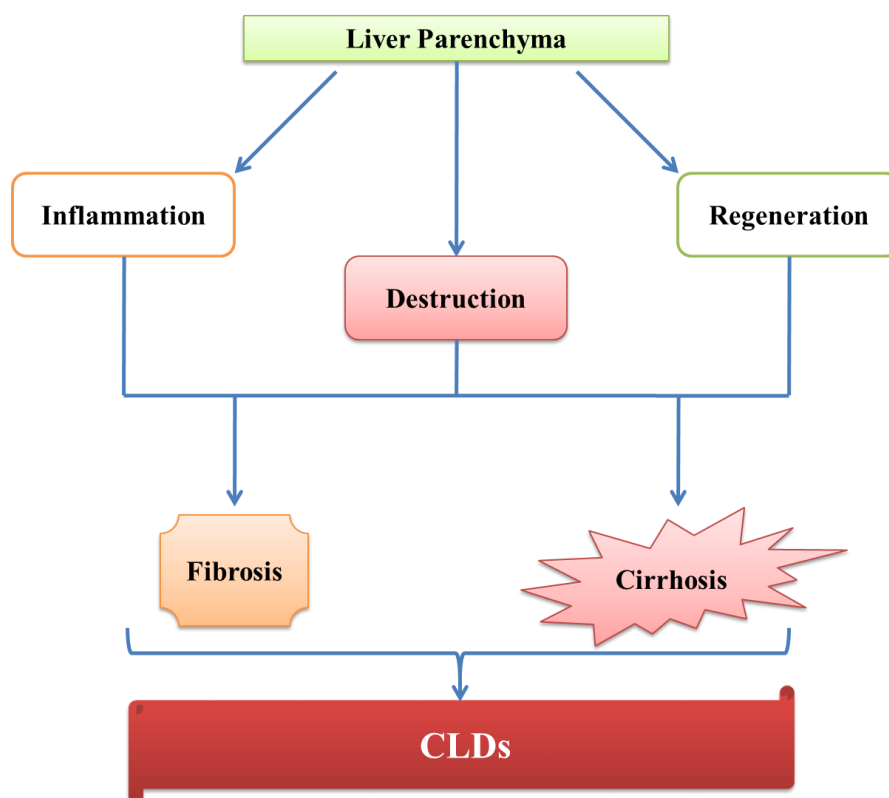


Figure 1.1. The basic mechanism of developing CLDs.

1.2.2. HCC

The incidence of liver cancer has skyrocketed in recent decades, propelling it to the position of being the second biggest cause of cancer-related casualties globally. It has been discovered that HCC is responsible for between 85 to 90 % of all occurrences of liver cancer diagnosed in adults (Chidambaranathan-Reghupaty et al., 2021). The development of HCC has been related to cirrhosis on a global scale, and more than 80 % of tumours have a history of chronic hepatitis or cirrhosis. The most common causes of HCC are infections with the hepatitis B and C viruses, NAFLD, alcoholism, and dietary carcinogens such as aflatoxins and nitrosamines. This is what the findings of a study by Lin and colleagues (2020) show. It is vital to combine both radiological imaging and research on quantification of serological markers in order to have an extensive screening strategy for HCC as both of these methods are widely used to detect cancer. Radiological examinations are the more non-invasive choice of the two options; hence, they are the one to choose. Some of the radiological diagnostics that are used for monitoring patients the most frequently include computed tomography (CT), multiphase computed tomography (CT), and magnetic resonance imaging (MRI) with contrast. The serum marker known as alpha-fetoprotein, or AFP, has been utilised in the process of diagnosing HCC. The usually accepted upper limit of normal is 20 ng/mL, which is based on the fact that excessive AFP levels in otherwise healthy people are quite

uncommon. Individuals who have head and neck cancer also have a higher percentage of alpha-fetoprotein in their bodies that is reactive to lens culinaris agglutinin (AFP-L3). Malignant hepatocytes are responsible for the production of a serological marker known as des- γ -carboxy prothrombin (DCP), which has a specificity of 91%. These three diagnostic markers for HCC have the greatest diagnostic accuracy when utilised in concert with one another (Bialecki et al., 2005; Sherman, 2010). Even though there are numerous common therapeutic alternatives, the only two options that can result in a full recovery are orthotopic liver transplantation (OLT), also known as surgical excision, and surgical removal of the affected area. Some of the additional treatment possibilities include radiofrequency/microwave ablation, percutaneous ethanol injection, cryoablation, radiation therapy, systemic chemotherapy along with drugs that are targeted at receptor and molecular level. It is important to keep in mind that the characteristics of the tumour, such as its size, location, extrahepatic spread, and baseline liver function, play a considerable effect in defining the treatment course (Crissien et al., 2014; Bruix et al., 2011; de Lope et al., 2012).

1.3. Challenges associated with the treatment of liver diseases

Even though more advanced treatment plans have been developed over time for the treatment of various liver diseases, they are not particularly successful and satisfactory in treating CLDs without causing side effects, which is still a major cause for concern. Those who use the therapeutic medications that are already on the market have reported experiencing a variety of negative side effects, including hepatotoxicity, medication resistance, and relapses. As a result, there is a need for an improved therapeutic efficacy as well as a safer profile in the treatment of this ailment (Senapati et al., 2018; Abbas et al., 2018). As a result of this, the concept of making use of bioactive substances found in nature as prospective therapeutic agents for the treatment of CLDs such as HCC has surfaced (George et al., 2021; Calvani et al., 2020; Sofowora et al., 2013; Teodoro, 2019). Bioactive components in fruits, vegetables and spices that have shown promise in lowering CLDs and HCC in pre-clinical animal models and in high-risk populations, constitute the foundation of this strategy (Wang et al., 2012; Choudhari et al., 2020; Liu, 2013; Kaefer et al., 2008).

1.4. Treatments of CLDs and HCC using naturally occurring plant metabolites

People from a wide variety of cultural backgrounds have been turning to natural remedies for the prevention and treatment of a wide array of liver problems for thousands upon thousands of years (Dhiman et al., 2005). The use of natural phytochemicals in the treatment of illness has received a lot of attention as of late. There has been a lot of buzz about the medicinal potential of natural products in recent years, especially in regards to

liver pathologies (Hong et al, 2015). In the pharmaceutical business, the research of natural phytoconstituents as potential treatments for cancer and other diseases is becoming an increasingly important area of focus (Singh et al., 2016). Phyllanthin has been shown to be effective in treating chronic hepatitis B (Yuandani et al., 2013), ellagic acid has been shown to be effective in treating hepatic fibrosis (Liu et al., 2021), and glycyrrhizin has been shown to be effective in treating chronic viral hepatitis. These are a few examples of phytochemicals that have shown promise in (Sato et al., 1996). According to the findings of various pieces of study, flavonoids are an effective treatment option for fatty liver diseases caused by both alcohol and non-alcoholic beverages (Pisonero-Vaquero et al., 2015). (Zhao et al., 2018). Because of their one-of-a-kind make-up and activities, which have a beneficial effect on the liver on their own, these compounds are highly prized for the antioxidant characteristics that they possess. These compounds have the potential to serve as primary compounds for further development as hepatoprotective medicines in experimental settings due to the demonstrated antioxidant, antiviral, and anticarcinogenic as well as hepatoprotective action that they have. Additionally, these compounds have low systemic side effects (Ali et al., 2018).

Treatment options for HCC include chemotherapy, immunotherapy, and adjuvant therapy; however, these treatments all come with their own set of undesirable side effects (Raza et al., 2014). As rates of medicine resistance and toxicity continue to rise, these alternate forms of treatment are becoming less useful. Many food sources have been demonstrated to have components that help prevent and treat HCC, according to a number of studies in the scientific community globally. Some examples include asparagus, black currants, strawberries, plums, grapes, pomegranates, tomatoes, turmeric, garlic, ginger and many more (Zhou et al., 2016). Curcumin, myricetin, resveratrol, quercetin (Qr), silibinin, lycopene, emodin, caffeine, and phloretin are some of the phytochemicals that have demonstrated potential for use in the treatment of HCC. Recent investigations have showed that 60% of the anticancer medications that are currently in use come from substances that occur naturally in the environment (Abdel-Hamid et al., 2018). Naturally occurring bioactives may help to prevent the development and progression of liver cancer by doing a plethora of things, including blocking oxidative stress and chronic inflammation, impeding the growth of tumours and metastases, protecting against liver carcinogens, and inhibiting the progression of tumours and metastases (Zubair et al., 2017). In addition to this, they induce the yield of reactive oxygen species (ROS), which leads to the death of cancer cells, and they have the potential to be used as a chemotherapeutic agent due to the prooxidant chemistry that they exhibit.

1.5. Role of flavonoids in liver ailments

1.5.1. Flavonoids in CLDs

The management of CLDs is a real challenge but the consumption of flavonoid-enriched foods could at least offer prophylactic roles. The flavonoid-containing foods are not only abundant in the market but also exhibit promise against CLDs (Simón et al., 2020). Emerging evidence has revealed that flavonoids can ameliorate hepatic injury by suppressing inflammation, fibrosis, and apoptosis, thus preventing cirrhosis in the setting of CLDs. In addition, flavonoids are gaining more interest due to their low toxicity and safety profile (Cory et al., 2018). In addition to their innate capacity for radical scavenging and antioxidant activity, flavonoids are able to demonstrate hepatoprotective benefits in the context of CLDs as a result of their interaction with a wide variety of signaling pathways linked to hepatic apoptosis, inflammation and fibrosis involving protein kinase C (PKC), mitogen-activated protein kinases (MAPKs), and mammalian target of rapamycin (mTOR), phosphatidylinositol 3-kinase (PI3K), protein kinase B (Akt), transforming growth factor beta (TGF β), suppressor of mothers against decapentaplegic (SMAD), and NF- κ B-light-chain enhancer of activated B cells and regulation of the actions that are a consequence of these interactions. (Sun et al., 2019). Flavonoids like epigallocatechin-3-gallate, epicatechin, icariin, morin, naringenin, silymarin, Qr, puerarin, apigenin (API), etc. exhibited excellent hepatoprotective effects in different preclinical studies (Saha et al., 2019; Rudrapal et al., 2022). Thus, these plant-derived antioxidant compounds may exhibit prospects in attenuating chronic liver damage and would open new ambition in the treatment of different CLDs (Guan et al., 2015).

1.5.2. Flavonoids against HCC

In the area of cancer therapy and control, the application of phytochemicals derived from food as a component of chemopreventive techniques is acquiring an ever-increasing amount of significance. Because HCC develops in an inflammatory milieu that is persistent over time, preventing hepatocarcinogenesis by the consumption of bioactive phytochemicals on a consistent basis through diet would be protective against the development of the disease. It is already common knowledge that flavonoids prevent cancer, especially head and neck cancer (HCC). Because of their high level of safety and the abundance of flavonoids that can be found in vegetables and fruits that are regularly eaten, flavonoids are an excellent choice for chemoprevention and chemo-sensitization in the treatment of chronic diseases. Flavonoids have been shown to be effective against cancer in a variety of different ways. These include the scavenging of free radicals, the stopping of the cell cycle, the stopping of uncontrolled angiogenesis, the induction of apoptosis (via the chemistry of prooxidants), and more (Figure 1.2). Myricetin, found in

many natural sources has been reported to have an anti-HCC activity in vitro by decreasing cell growth and producing cell cycle arrest during the G2/M phase in Hep3B and HepG2 cells which reduce the development of HCC cells thereby presenting a potential new treatment method for treating this malignancy by suppressing the expression of membrane associated ring-CH-type finger 1, also known as MARCH1 (Yang et al., 2021); naringenin effectively subdued N-nitrosodiethylamine (NDEA)-induced hepatocarcinogenesis in rat model by regulating enzymes responsible for xenobiotic-metabolizing, diminishing levels of liver marker enzymes and lipid peroxidation (Arul et al., 2013); Qr promotes apoptosis in hepatoma cell line through amendment of PI3K/ERK signalling pathways and caspase-3 activation (Granado-Serrano et al., 2006); API was found to inhibit the in vivo tumor growth in a xenograft mice model through H19-mediated wingless-related integration site (Wnt)/ β -catenin signalling regulatory axis thereby making it a potential approach in treatment of HCC (Pan et al., 2021); luteolin exerted therapeutic effect by altering the tissue damaging enzymes and the enzymatic antioxidants and restoring the damaged histoarchitecture of diethyl nitrosamine-treated rat liver (Balamurugan et al., 2012). Emerging evidence shows both the chemopreventive and chemotherapeutic effects of polyphenols present in tea. Reportedly, the phenolic fraction of tea inhibits the relocation of HCC cells. It has been shown that tea polyphenols hinder carcinogenesis of mouse liver by modulating the Wnt/ β -catenin signalling pathway. Further, in the carcinogenesis model of rat liver induced by dimethylaminoazobenzene, it has been found that polyphenon-B, a polyphenol found in black tea, has a huge potential in combating liver disorders by regulating different molecular markers (Murugan et al., 2009). Hepatoma cells that were treated with an extract of polyphenols found in mulberry leaves exhibited a suppression of the AMPK/PI3K/Akt signalling pathway (Yang et al., 2012). In hepatoma cultures, it has been demonstrated that the polyphenols present in pomegranate peel can both suppress the growth of tumours and accelerate cell death (Song et al., 2016). These scientific findings presented here lead to the conclusion that some flavonoids may have an anticancer effect on HCC.

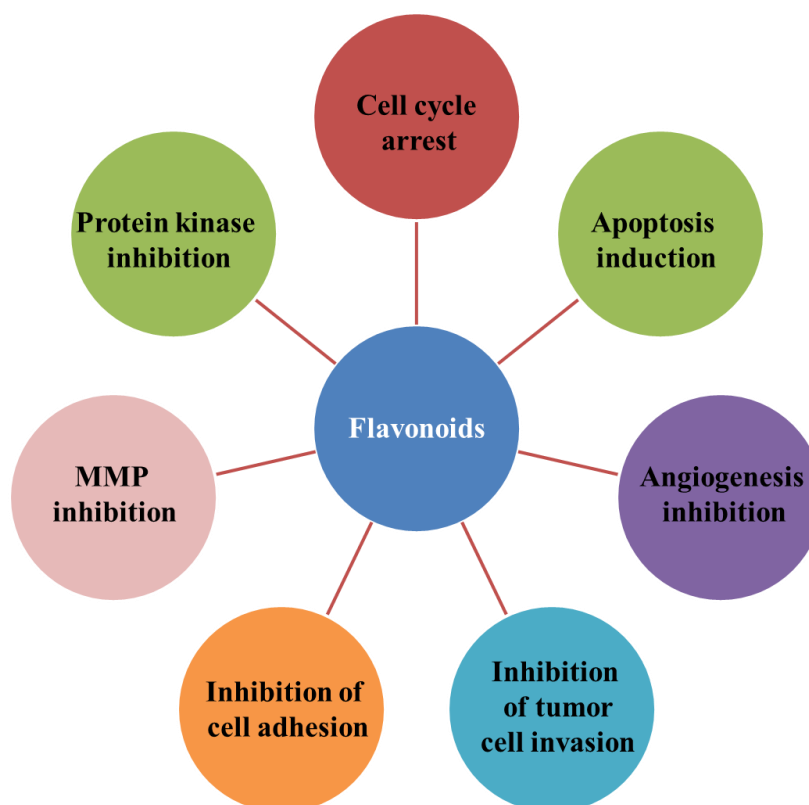


Figure 1.2. Anticancer mechanism of flavonoids against HCC.

1.6. Drawback of using flavonoids as a therapeutic option

The effectiveness of plant flavonoids as a treatment for disease, notably cancer, has increased as a result of a number of advances that have taken place during the past two decades. The extensive use of flavonoids in the therapy of cancer has a number of challenges, including low water solubility, low bioavailability, poor stability, and insufficient administration of targeted drugs. Many flavonoids were unable to demonstrate their therapeutic value due to unexpectedly altered clearance, inadequate absorption after dosing, low efficacy, and/or unexpected side effects (Kopustinskiene et al., 2020).

Various factors contribute to the low bioavailability of flavonoids

Low water solubility

Flavonoid as free aglycones have low solubility in an aqueous medium, which lead to low absorption and hence low bioavailability (Thilakarathna et al., 2013; Zhao et al., 2019).

Effect of molecular weight and structure

Whenever it comes to how well a chemical is absorbed, the molecular weight of the molecule plays a significant influence. The bioavailability of flavonoids with a high molecular weight decreases significantly. According to research by D'Archivio et al. 2010

and Scalbert et al. 2000, the chemical structure and isomeric arrangement of the bioactive dietary components have an effect on how well they are absorbed.

Degradation at low pH

Under the influence of the acidic environment in the stomach, oligomeric flavonoids are hydrolyzed into monomers and dimers. The dimerization leads to reduce the bioavailability of flavonoids (Kumar et al., 2013).

Low bio-accessibility in the food matrix

Flavonoids are present in a complex textured food matrix; hence it hampers bioavailability. The amount of food matrix results in physiological changes in the gastrointestinal tract, which have an impact on the bio-accessibility of digested compounds. (Kamiloglu et al., 2021; Palafox-Carlos et al., 2011).

Metabolic conversion

The primary routes for the hepatic metabolism of ingested polyphenols occur through phase I hydroxylation chemistry of the aromatic hydrocarbon rings followed by phase II metabolism via different conjugating enzymes like uridine-5-diphospho (UDP)-glucuronosyltransferase, glutathione S-transferase (GST), and catechol-O-methyltransferase (Liu et al., 2007; Pandey et al., 2009; Cassidy et al., 2017; Baky et al., 2022). Because of these interactions, the kidneys are in a position to rapidly flush away the more water-soluble flavonoid metabolites.

Metabolism by colonic microflora

Colonic microflora can tamper with the chemical structure of the flavonoids. Flavonoids that are not absorbed very well in the small intestine make their way to the large intestine, where colonic bacteria transform them to simpler phenolic acids, hence lowering the bioavailability of the parent molecule (Serra et al., 2012; Rechner et al., 2004).

Poor intestinal absorption

Microbial enzymes present in the human gastrointestinal tract could influence the absorption of flavonoids. In the colon, the transmembrane enzyme lactase phlorizin hydrolase acts on a wide variety of flavonoid glycosides, turning them into the less soluble free aglycones. These free aglycones can only reach the bloodstream by passively diffusing past the epithelium and into the bloodstream. The sugar moiety that is present in flavonoid glycosides have a significant role in determining the bioavailability and absorption of flavonoids (Kawabata et al, 2019).

1.7. Requirements for novel formulations

1.7.1. Requirements for novel drug delivery systems for phytoconstituents

Naturally occurring small molecules have limited clinical applications due to their complicated nature, large dosages, poor absorption, and dose recurrence (Moradi et al.,

2020). Whenever a therapeutic molecule is provided via a novel drug delivery system (NDDS), the bioavailability of the drug is enhanced. This is because the requirement for frequent dosing is minimised, as are changes in the dose. In addition, the bioavailability of the drug is raised. There have been a number of studies that have investigated the possible advantages of NDDS in phytopharmaceuticals, and there is currently a wide variety of phytoconstituent formulations that are available for purchase in markets all over the world (Ansari et al., 2012; Kumari et al., 2022). Because of a variety of circumstances, the use of traditional herbal extracts is not an acceptable method of drug administration for herbal treatments; instead, novel drug delivery strategies are required (Devi et al., 2010).

- To increase the bioavailability of the naturally occurring constituents and to convey high concentrations of medications to the site of action.
- By delivering the medication in extremely fine particles, one of the objectives is to hasten the process by which it is absorbed into the bloodstream.
- To accomplish the impact that seems to last at the locations for a long time, leading to enhanced permeability and retention (EPR), i.e., better permeation through the barriers due to the reduced particle size, and retention because of insufficient lymphatic outflow.
- To use innovative carrier systems that demonstrate passive targeting to the diseased site without the inclusion of a specific ligand moiety, thereby ensuring localised delivery to the liver and other sites of interest.
- To reduce adverse unwanted consequences arising due to ingestion of medications.
- To reduce pharmacological doses in formulations and creating standardised dosage forms.
- To protect the therapeutic molecules from being broken down in the gastrointestinal tract and increase their stability.

Recently, there has been growing enthusiasm for the advancement of NDDS for phytoconstituents. The innovative drug carriers would satisfy two requirements. To begin, it is believed to dispense the medication during the course of the treatment at a pace that is based on the requirements of the body. In addition to this, it should be able to direct the active component of the herbal medication to the target area in which it is required. Conventional dosing methods, such as delayed-release dosing methods, do not meet these benchmarks. The development of new dosage forms for naturally occurring substances can be of great use in formulation research in a number of different ways. They include increased solubility and bioavailability, pharmacological efficacy, protection from toxicity, stability, tissue macrophage distribution, prolonged administration, protection from physical and chemical degradation, and more. Further advantages include these as

well. These are just some of the advantages that can be gained from this type of research. In this regard, formulation scientists have paid close attention to the various nanoparticles (NPs), such as lipid NPs, polymeric NPs, nanoliposomes, nanoemulsion, etc. because of their advantages over other NDDS in overturning biopharmaceutical and pharmacokinetic constraints and enhancing the therapeutic efficacy and compliance of naturally derived small molecules. Accordingly, improving the action and resolving difficulties with plant ingredients could be accomplished in the future by using NDDS including nanosized formulations of naturally occurring small compounds, such as flavonoids (Patra et al., 2018; Zhang et al., 2021; Ajazuddin et al., 2010).

1.7.2. NPs: novel formulations with significant promise

NPs and nanotechnology are becoming increasingly significant in the medical field, particularly in the areas of disease diagnosis and therapy. Nanomaterials, which are materials that have dimensions at the nanoscale level, can be comprehensively categorised as either naturally occurring or synthetically made using cutting edge technology. Adaptability of "designed" nanomaterials, on the other hand, has attracted a lot of attention in recent years. Newcomers to the field of nanotechnology may have a tough time selecting a nanocarrier system and the potential applications for such a system, despite the fact that nanotechnology has achieved significant advancements in research and development. There are a number of key challenges that must be overcome in order for effective drug delivery systems to be developed, including regulated drug release, targeted or particulated drug delivery, and the avoidance of opsonization. As a result of this, we discuss the alternative routes that pharmaceuticals can take to reach their targets, the significance of manufacturing drug-loaded nanocarriers, and the different ways that drug solubility and bioavailability can be improved. In addition to this, the effects of biological and other types of barriers on drug transport, as well as the many different methods of nanocarrier distribution, are investigated in various research studies (Yetisgin et al., 2020; Jeevanandam et al. 2018).

Nanoscale materials are characterised by the fact that they have advantages in terms of surface area to total volume. NPs can be found essentially important in a wide number of fields, ranging from agriculture to medicine. NPs are undergoing development to make them more useful in a wide variety of medical applications, such as the delivery of drugs, the diagnosis of illnesses, and the engineering of tissue. NPs have the ability to transport traditional drugs, as well as recombinant proteins, vaccines, and nucleotides, in a more effective manner than other standard delivery methods (Yu et al., 2016). The production of NPs can make use of a wide variety of components, including lipids, proteins, synthetic and natural polymers, and metals (Murthy, 2007). NPs can encapsulate or covalently

conjugate hydrophobic medicines, so improving their solubility in water and making them more suitable for use as drug delivery vehicles. They can also encapsulate hydrophilic medicines or biomacromolecules such as proteins, peptides, or nucleic acids in order to improve their in vivo stability, increase their blood circulation time, and promote transmembrane distribution. These three benefits are achieved by increasing the amount of time that the medicine spends circulating in the blood. Due to the fact that they are so small, nanoparticles, or NPs, have the potential to greatly reduce the off-target effects that are caused by chemotherapy (Golombek et al., 2018) and utilizing the EPR effect target tumors. An appropriate foundation can be provided by NPs that have a large surface area, extended circulation duration, and great stability. These characteristics make them well suited for highly selective and sensitive molecular imaging. They are able to accomplish this by transporting the imaging probe or contrast chemical to the tissues or cells of interest (Siafaka et al., 2021). Grafting a variety of ligands or antibodies onto the surface of NPs makes it possible to accomplish targeting that is both more selective and more effective. On the other hand, the structure of certain NPs makes them helpful for imaging or therapeutic applications. This is particularly true for inorganic NPs that possess attractive optical properties. Gold NPs and superparamagnetic iron-oxide NPs are able to provide the imaging contrast themselves, which enables multimodal imaging. NPs also have the ability to mediate photothermal treatment by turning light into thermal energy (Vines et al., 2019). Figure 1.3 highlights the benefits of nanoparticles, including their ability to increase the bioavailability of active pharmaceutical ingredients by increasing their aqueous solubility; prolong the time the drug spends in the body by extending its half-life for clearance and increasing its specificity for the receptors and direct the drug to a specific site in the body, thereby minimizing the dosage regimen and the untoward side effects of the medication. When it comes to the delivery of drugs, NPs excel due to the many desirable properties that they possess. Some of these qualities include the capability of combining hydrophilic and hydrophobic molecules, rendering improved stability, drug loading capacity as well as the adaptability to be ingested orally, applied topically or breathed in, however these are just a few examples.

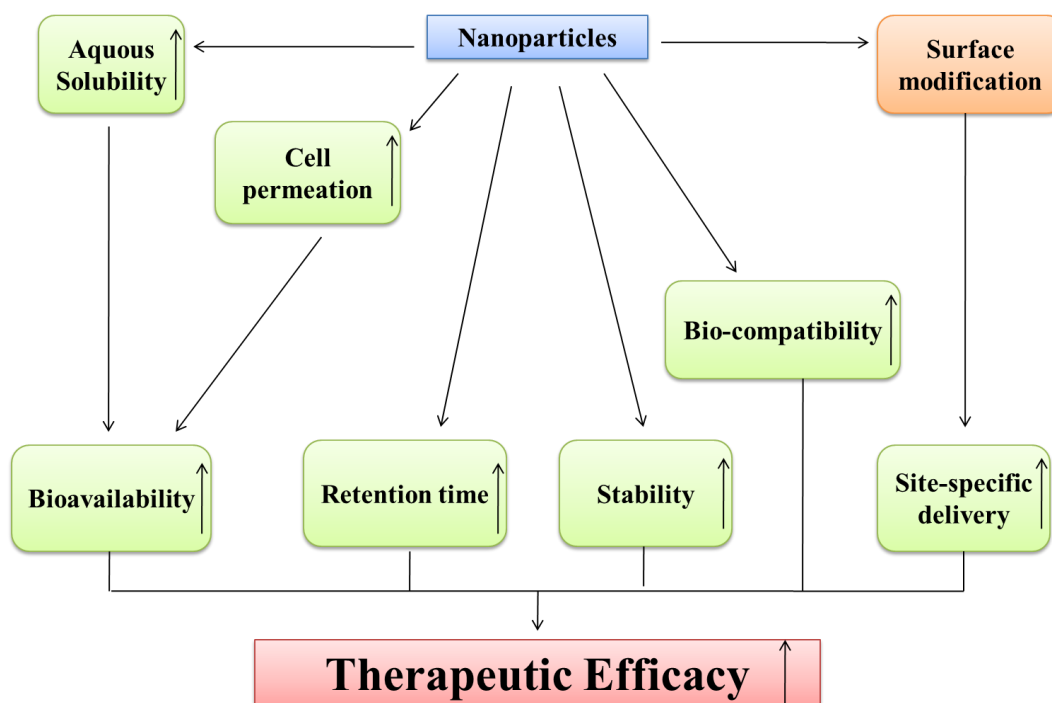


Figure 1.3. Advantages of NPs formulation

1.7.2.1. Polymeric NPs

Since of their improved bioavailability, solubility, and retention time, the therapeutic efficacy of bioactive substances can frequently be improved by encapsulating them in biodegradable polymeric NPs (Mahapatro et al., 2011; Castro et al., 2022). Nanoencapsulation has shown the potential to maximize the therapeutic potential, target specificity, tolerability, and therapeutic index of a poorly soluble drug. Non-specific adverse effects have also been demonstrated to be decreased by nanoencapsulation (Chenthamara et al., 2019). Synthetic polymers are more frequently used in formulating polymeric NPs over natural polymers because of their purity, uniformity, and crosslinking issues. The most prevalent kinds of polymer include poly(lactic acid) (PLA), poly(glycolic acid) (PGA), and copolymers such poly(lactide-co-glycolide) (PLGA). These synthetic polymers are distinguished by their biocompatibility as well as their natural biodegradation pathways. Adjusting the ratio of PLA to PGA has an effect on the rate of degradation, which in turn has an effect on the rate at which the medication is released. Nanoparticle formulations can also make use of polymers such as poly-alkyl-cyano-acrylates (PAC), poly-caprolactone (PCL), chitosan, and gelatin, as well as other polymers with a comparable structure (Kumari et al., 2010). Targeting abilities of polymeric NPs are affected by a number of factors, including size, zeta potential, surface modification, and release kinetics (Zielińska et al., 2020; Begines et al., 2020).

1.7.2.2. Successes of flavonoid-loaded polymeric NPs in combating against CLDs and HCC

Detoxification, protein synthesis, and the creation of biochemicals for sustaining life are just a few of the many important functions that the liver is responsible for doing. Those who have CLDs such as viral hepatitis, liver cirrhosis, or HCC typically undergo treatment for an extended period of time using pharmaceuticals or natural treatments are in need for serious consideration as these conditions are a major threat to life. Flavonoids, in particular, have been discussed earlier in this chapter as possessing potential hepatoprotective effects; nevertheless, their poor pharmacokinetic and biopharmaceutical characteristics severely restrict their therapeutic usefulness. To overcome these limitations, polymeric NPs provide the desired attributes as it was discussed in previous sections. The successes of flavonoid-loaded polymeric NPs are discussed hereunder. Naringenin-loaded polymeric NPs served as effective nanoplatforams for successful oral delivery of naringenin against aflatoxin B1-induced HCC (Wang et al., 2022). Eudragit NPs loaded with naringenin improved the bioavailability of naringenin and demonstrated high hepatoprotective potential against CCl₄-induced chronic liver failure in rats (Yen et al., 2009). API-loaded polymeric NPs demonstrated better bioavailability and successfully cured chemically induced HCC in murine models (Bhattacharya et al., 2018; Ganguly et al., 2021). Qr NPs prepared by the nanoprecipitation technique demonstrated significant hepatocellular protection against the cytotoxic effects of aflatoxin-B1 in vivo (Eftekhari et al., 2018). Nanocapsulated Qr demonstrated remarkable therapeutic prowess against arsenic-induced chronic liver damage in an animal model (Ghosh et al., 2009). Using an emulsification technique, Kazmi and colleagues (2021) formulated kaempferol-loaded NPs which exhibited excellent antioxidant and hepatoprotective effects in CdCl₂-induced HCC in rats. Rutin-loaded PLGA NPs were found to exhibit significant protective activity against HCC evidenced by improvement in hepatic and hematological biochemical markers (Pandey et al., 2018). Considering the superiority of flavonoid-loaded polymeric NPs in improving pharmacokinetic and biopharmaceutical behaviours over free flavonoid, the subsequent research aimed to formulate flavonoid-loaded polymeric NPs to achieve better therapeutic efficacy against CLDs and HCC.

1.8. Nuclear scintigraphy: A non-invasive imaging modality

1.8.1. Roles of nuclear scintigraphy

Patients are given radioactive tracer compounds by injection as part of the nuclear scintigraphy process. These compounds (such as technetium, iodine, thallium, gallium, xenon, and krypton) can be localised to a particular organ or tissue. The radioactive decay

of these substances is detected by a gamma camera, which then creates two-dimensional images that can be used to investigate whether or not the functioning of a specific organ system or tissue is normal or dysfunctional (Brawner et al., 1993; Snyder et al., 2021). By monitoring how the radionuclide behaves inside the body during a nuclear scan, medical professionals are able to examine and diagnose a variety of conditions, including tumours, infections, hematomas, organ enlargement, and cysts, amongst others. Nuclear imaging is another tool that can be utilised to assess organ function and blood flow (Sharp et al., 1986; Heymann, et al., 1977; Werner et al., 2022). "Hot spots" are areas of a radioactive accumulation site that have been identified as having the highest amounts of the radioactive tracer substance. A region that does not accumulate the radionuclide and, as a result, appears to be pale in the scanned image is referred to as a "cold spot." Among the many examples of routine imaging procedures are scans of the heart (Underwood et al., 2004; Berman et al., 2006; Hanna et al., 2020), brain (Jones et al., 1974; Wieler et al., 1993), and kidneys (Taylor et al., 1995), thyroid (Broome, 2006), bone (Merrick, 1989; Buckley et al., 2007), gallium (Vorster et al., 2022).

The United States Food and Drug Administration (USFDA) has given its approval to the utilisation of a variety of radioactive isotopes in the medical field; nonetheless, technetium-99m (^{99m}Tc) has been the subject of the most extensive use due to the imaging and diagnostic capabilities it possesses. ^{99m}Tc is the radioactive isotope tracer that is most commonly used for SPECT imaging of the central nervous system, the skeletal system, the thyroid, the heart, the gall bladder, the liver, the spleen, the bone marrow, the salivary and lachrymal glands, the blood pool and sentinel lymph nodes. In the year 1938, ^{99m}Tc was first isolated from decaying molybdenum-99 (Mo-99) as a result of the research that was being done at the time. ^{99m}Tc is a more preferred radionuclide than other nuclear agents both due to the fact that its radioactive half-life is only six hours, which is significantly less than that of other nuclear agents, and due to the fact that it does not explicitly target a major organ. Due to the fact that ^{99m}Tc has such a short half-life, the patient will be subjected to a lower total radiation dose as well as exposure time (Papagiannopoulou, 2017; Kane et al., 2021). Numerous different nuclear imaging systems that do not require the patient to undergo any kind of invasive procedure have been developed. In the 1970s, ^{131}I -rose bengal was first offered to the market, and it quickly established itself as a leading agent in the field of hepatobiliary scintigraphy (HBS) (Nordyke, 1972). The radioactive isotope ^{131}I -rose bengal is removed from the bloodstream by hepatocytes, which subsequently pass it on to the biliary system for excretion. Due to the fact that Rose Bengal had poor imaging capabilities, it had to be phased out of use. Regrettably, this was necessary because of rose bengal's slow hepatic

clearance and high β -radiation levels, both of which limited the quantity of radiation that could be safely supplied leading to substandard imaging outputs. Because of its superior physical qualities, ^{99m}Tc is a more desirable isotope for scintigraphy than other isotopes. As a result, several ^{99m}Tc -labelled agents have been developed, such as ^{99m}Tc -sulphur colloid, ^{99m}Tc -galactosyl human serum albumin, and derivatives of ^{99m}Tc -iminodiacetic acid. Nevertheless, liver reticuloendothelial cell function can be visualised with ^{99m}Tc -sulphur colloid scintigraphy since it is based on the principle of phagocytosis. Using the latter two radiopharmaceuticals, one is able to evaluate hepatocyte function (Doonan, 2020; Ziessman, 2014; Iida et al., 2022).

1.8.2. Liver scintigraphic imaging

Radiopharmaceuticals that are used in liver imaging can be separated into two main types according to the physiological roles that they have. One group focuses on the hepatocytes and biliary ducts, while another investigates the phagocytic role of the Kupffer cells in the liver. The first category consists of lipophilic compounds that have been radioactively tagged, and the second category consists of labelled colloids. Imaging of the liver and biliary system is a common application for ^{99m}Tc -labeled derivatives (^{99m}Tc -DISIDA and ^{99m}Tc -mebrofenin) of iminodiacetic acid (IDA). Hepatocytes are responsible for the absorption of tracer molecules, which then traverse through the bile duct and gallbladder before being excreted into the intestine. Urinary excretion of the radioactive dose that was administered through injection is quite a low fraction of the dose. When the alkyl chain that is attached to the benzene ring of IDA moiety making it longer, two things happen: first, hepatobiliary extraction goes up, and second, renal excretion goes down. In situations in which bilirubin concentrations are extremely high (over 20-30 mg/100 ml), IDA derivatives face a stiff competition from bilirubin, which results in impaired imaging. Imaging agents for the hepatobiliary system include ^{99m}Tc -DISIDA (Hepatolite) and ^{99m}Tc -mebrofenin (Choletec) (Okuda et al., 1986; Krishnamurthy et al., 1990; Labeur et al., 2020; Serenari et al., 2021). Patients who have been fasting for four to six hours get an intravenous injection containing around 3 to 5 mCi (111 to 185 megabecquerels) dose of ^{99m}Tc -IDA derivatives. The scintillation camera that has been coupled with the low-energy parallel hole collimator takes serial scintiphotos every five minutes for the first half an hour, and then at 45- and 60-minutes time points. Cholescintigraphy is the term that has been given to describe this method. Each image contains depictions of the hepatic and jejunal structures in their entirety (Hopfer et al., 2011). Healthy subjects, will be able to visualize their gallbladder at 30 min post injection mainly because the liver clears the radioactivity quickly. In the event if none of the aforementioned can be seen in one to one and a half hours, radio technologists

continue to take scinti-images every hour for up to four hours. An active transport mechanism, which comprises hepatic extraction, hepatocyte binding and storage, as well as excretion into the biliary canaliculi, is responsible for the elimination of ^{99m}Tc -IDA derivatives from the body (Ramaswamy et al., 2004). Cholescintigraphy using ^{99m}Tc -IDA derivatives can be used to differentiate between acute and chronic cholecystitis. This can be accomplished with the help of the procedure (Freitas, 1982). ^{99m}Tc -sulphur colloid is the kind of substance that most commonly gets used for imaging the liver (Ramaswamy et al., 2004). The liver's absorption capacity of the radioactive colloid is at its maximum for 20 minutes and phagocytes have the property of flushing colloids from the physiological system. The spleen amasses between 5% to 10% of the colloidal particles, while the bone marrow stores the remaining portion of the particles whereas the liver accrues between 85% to 95% of the colloidal particles. Since the phagocytes in the liver always accumulate the majority of the radioactive colloids, the ^{99m}Tc -radioactive colloid has a half-life that is very similar to that of the radioactive nuclei itself. It is necessary to perform a liver flow study in order to investigate the vascularity of liver tumours and abscesses (Willyard et al., 2022; Chacko et al., 2009). Since nuclear scintigraphic imaging is a useful tool to determine the *in vivo* condition of HCC, as well as to perceive the drug action, thus this technique has been used in this research to perceive the effect of the developed drug formulations against chemical-induced chronic liver damage and HCC.

1.9. Aim & Objectives

This research aimed to develop and optimize an effective drug delivery system (PLGA NPs formulation) of Qr and API to improve their therapeutic effect against non-cancerous CLDs and HCC, respectively. The therapeutic effects of the nanoformulations have been assayed by employing suitable *in vitro* and *in vivo* models and compared with the free flavonoids. Special attention has been on non-invasive liver scintigraphic analysis using ^{99m}Tc -labeled sulphur colloid and mebrotfenin to reveal the hepatoprotective efficacy of the selected flavonoids and their respective formulations.

Chapter 2

Literature review

Contents

- 2.1. Quercetin (Qr)
 - 2.1.1. Physicochemical characteristics
 - 2.1.2. Biological activities of Qr
 - 2.1.3. Bioavailability of Qr
 - 2.1.4. Nanoformulations of Qr: A potential solution to its poor bioavailability
- 2.2. Apigenin (API)
 - 2.2.1. Physicochemical characteristics
 - 2.2.2. Biological activities of API
 - 2.2.3. Bioavailability of API
 - 2.2.4. API nanoformulations: A way to overcome its bioavailability issues
- 2.3. PLGA
 - 2.3.1. Solubility
 - 2.3.2. Molecular weight
 - 2.3.3. Crystallinity
 - 2.3.4. Thermal stability and storage
 - 2.3.5. Degradation
 - 2.3.6. Elimination
 - 2.3.7. Biomedical applications of PLGA

2. Literature Review

2.1. Quercetin (Qr)

Qr is a flavonoid that is abundant in various vegetables, fruits, and beverages (Anand David et al., 2016). In plants, Qr is usually found as glycosides, ethers, prenylated derivatives, sulphates, or as a free aglycone. The forms of Qr have a significant impact on their absorption and pharmacokinetic behaviours (Hollman 2004; Murota et al., 2003; Kawabata et al., 2015). Qr has attracted increasing attention due to its multimodal therapeutic attributes (D'Andrea et al., 2015) Qr has gained attention as a prospective nutraceutical by the pharmaceutical industries due to its potential health benefits.

The oxygen atom at position 1 of the molecule of Qr is basic and can cause the formation of salts that are strong acids due to the presence of the keto-carbonyl group (Figure 2.1). The molecular structure of Qr demonstrates that it is a typical flavonoid due to the presence of five hydroxyl groups, two benzene rings (A and B), and a pyrene ring comprising of oxygen (C). It possesses a C2=C3 double bond, a 4-carbonyl group, two hydroxyl groups in the A ring, and two hydroxyl groups in the B ring. Moreover, it possesses two hydroxyl groups in the A ring. Qr has significant antioxidant action because it has a phenolic hydroxyl group and double bonds. Its anti-oxidant and anti-inflammatory outcomes have been linked to the treatment and prevention of a wide range of diseases and conditions, including cancer. (Magar et al., 2020; Salehi et al., 2020).

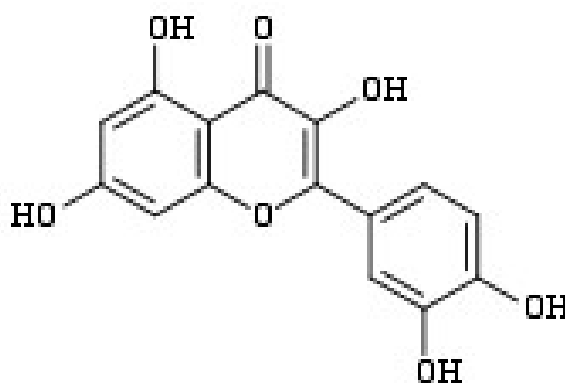


Figure 2.1. Structure of Qr

2.1.1. Physicochemical characteristics

Mol. Formula: C₁₅H₁₀O₇

Mol. Weight: 302.23

IUPAC Name: 2-(3,4-dihydroxyphenyl)-3,5,7-trihydroxychromen-4-one

Solubility: Qr molecule is lipophilic chemical that has moderate solubility in ethanol but a high solubility in dimethyl sulfoxide. Despite this, its solubility in water is not particularly high (Vinayak et al., 2019).

2.1.2. Biological activities of Qr

Qr is an important bioactive compound with an array of medicinal properties (Figure 2.1) and is widely researched globally. Some of the research enumerating its therapeutic potential is outlined hereunder.

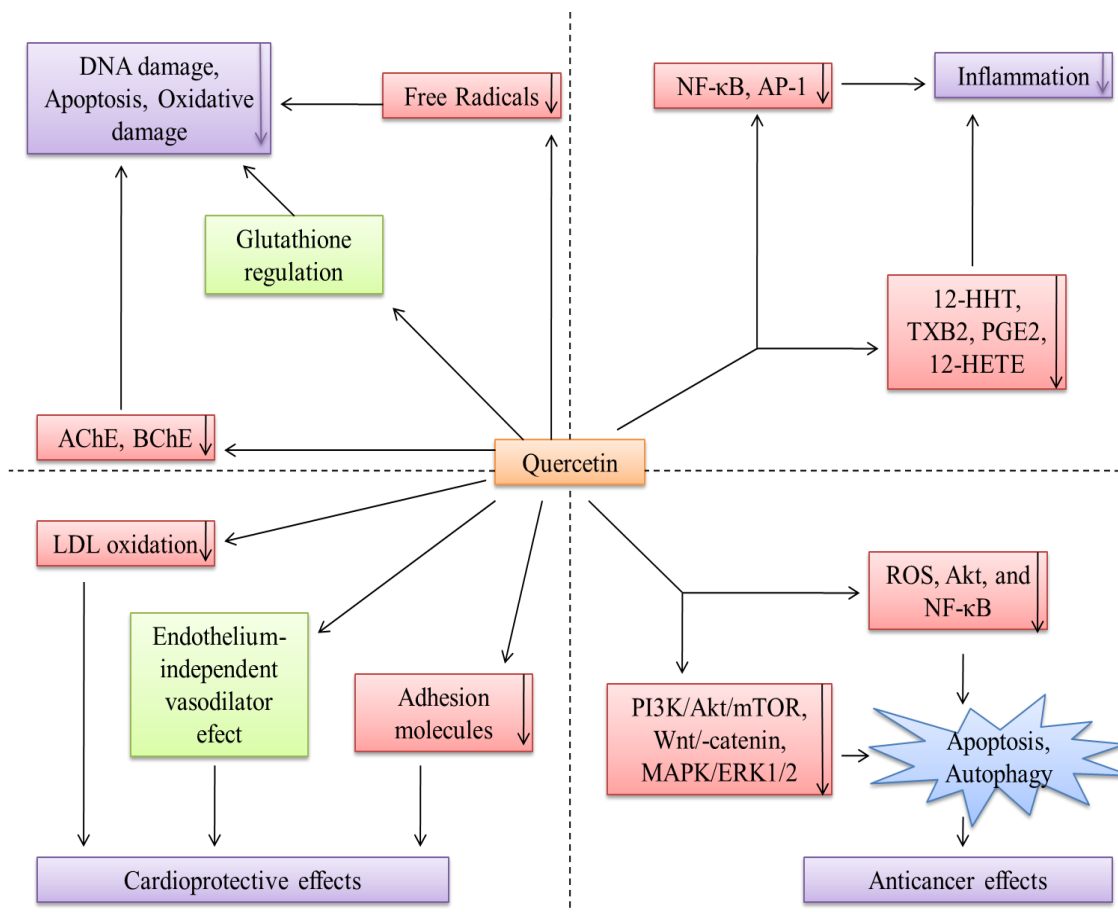


Figure 2.2. The therapeutic mechanism of Qr

2.1.2.1 Antioxidant activities

The antioxidant effects of Qr have been widely explored and discussed (Xu et al., 2019; Boots et al., 2008). Qr, a naturally occurring ROS scavenger, can neutralize hydrogen peroxide, superoxide anion, and hydroxyl radicals, which are associated with various disease pathophysiology (Khan et al., 2016). Additionally, it has the ability to scavenge highly damaging RNS, such as peroxynitrite, which contributes to its positive impacts on health. It can simultaneously increase the body's capacity for redox defence by regulating glutathione levels (Xu et al., 2019). Zhang and colleagues (2011) investigated the impact

of Qr on the generation of ROS and NO in human THP-1 acute monocytic leukaemia cells stimulated by LPS. Their findings clearly demonstrate a higher reducing potential of Qr and consequently greater antioxidant properties. Through theoretical and practical research, Song and colleagues (2020) concluded that Qr can shield free radical-provoked DNA damage. Qr is also capable to prevent of free radical-mediated ailments by suppressing DNA glycation (Sengupta et al., 2006).

2.1.2.2. Anti-inflammatory activity

Qr, like other flavonoids, exhibits significant anti-inflammatory properties and thus could attribute potential therapeutic benefits against a variety of disease etiologies. Qr can suppress TNF- α -induced inflammation by suppressing NF- κ B and AP-1 activation in human umbilical vein endothelial cells, which could open a new avenue in the management of coronary heart diseases (Chen et al., 2020). It can also suppress TNF- α -induced MMP-9 activation in GES-1 cell line via inhibiting TNFR/c-Src /ERKs /c-Fos /NF- κ B activation (Hsieh et al., 2022). In addition, it is capable to attenuate TNF- α -induced ICAM-1 activation in human retinal pigment epithelial cells (Cheng et al., 2019). Zhang and colleagues (2022) indicated that it can target PI3K/Akt signalling to exert an anti-inflammatory mechanism in LPS- motivated RAW264.7 cells. Qr also showed therapeutic promise to alleviate atopic dermatitis-like skin lesions mediated through anti-inflammatory attributes (Hou et al., 2019). Chen and colleagues (2016) mentioned the anti-inflammatory properties of Qr against inflammation-provoked pathogenesis in obesity and type 2 diabetes. The anti-inflammatory properties of Qr could also be beneficial in the management of rheumatoid arthritis (Costa et al., 2021).

2.1.2.3. Antidiabetic activity

An increasing body of information demonstrates the antidiabetic potential of Qr (Chen et al., 2016; Bule et al., 2019; Salehi et al., 2020; Nie et al, 2021). The antidiabetic mechanisms of Qr include improving insulin sensitivity, activating glycogenesis, and reducing insulin resistance (Jiao et al., 2022). Qr has been shown to reciprocate glucose metabolism disorder by activating Sirtuin 1/Akt signaling pathway (Peng et al., 2017). Accumulating evidence reveals that Qr can protect pancreatic beta cells from oxidative stress- and inflammation-induced injuries and restores optimum insulin output (Kim et al., 2007; Youl et al., 2010; Carrasco-Pozo et al., 2016; Vessal et al., 2003). In addition, Qr has also been noted as α -glucosidase and α -amylase inhibitor which aids in combating type 2 diabetes mellitus (Meng et al., 2016; Ansari et al., 2022).

Qr also exhibited therapeutic promise against diabetic complications. It shows therapeutic effectiveness against diabetes-provoked oxidative liver injury by suppressing CYP2E1. (Maksymchuk et al., 2017). It is equally effective against diabetic nephropathy by

reducing diabetes-induced oxidative stress and inflammation in renal cells (Chen et al., 2013; Elbe et al., 2015). According to a recent study, Qr demonstrates its effectiveness against high glucose-induced retinal neovascularization by inhibiting NLRP3 inflammasome and autophagy and showing promise as a potential treatment for diabetic retinopathy (Li et al., 2021).

2.1.2.4. Neuroprotective Activity

The neuroprotective effects of Qr against oxidative stress to combat paediatric neurological disorders like CNS tumors, ASD and attention-deficit/hyperactivity disorder have been revealed (Alvarez-Arellano et al., 2020). When it comes to neurodegenerative illnesses like Alzheimer's disease, Qr shields neurons from oxidative damage and prevents the accumulation of amyloid-beta ($A\beta$) fibrils (Khan et al., 2019). Qr also exhibits therapeutic potential against epilepsy by controlling neurotransmitters and ion channels, ameliorating oxidative stress and downregulating neuroinflammation (Akyuz et al., 2021). Scientific evidence showed that Qr induces neuroprotective effects by endorsing Nrf-2/ARE activation and triggering PON2, an antioxidant/anti-inflammatory enzyme as well as to activate Sirtuin 1 (Costa et al., 2016; Grewal et al., 2021).

2.1.2.5. Hepatoprotective activity

Qr exhibits hepatoprotective effects against a variety of xenobiotic-induced hepatotoxicity. It has been revealed to reciprocate hepatotoxicity through anti-inflammatory, anti-apoptotic and anti-oxidant mechanisms (Miltonprabu et al., 2017; Pingili et al., 2020). Qr predominantly down-regulates different pro-inflammatory mediators and enzymes involved in hepatotoxicities, like $TNF-\alpha$, $IL-1\beta$, COX-2 and iNOS. In search for anti-apoptotic mechanisms, it has been found to suppress NF- κB /p53/PPAR- α /PI3K/Akt pathways in normal liver cells. It has the ability to reduce lipid accumulation, restore SOD, CAT, and GSH levels, and lower total cholesterol and triglyceride levels in livers, all of which make it an attractive candidate for use as a therapeutic agent. Qr may be an effective treatment for T2D-induced NAFLD (Yang et al., 2019). In addition, it simultaneously activates the FXR-1 and TGPCR-5 signalling mechanism to exert hepatoprotective mechanisms against T2D-induced NAFLD (Yang et al., 2019). Qr also showed its effectiveness against HCC progression by modulating cell apoptosis, migration, invasion, and autophagy (Wu et al., 2019).

2.1.2.6. Cardioprotective activity

Qr can be useful against a variety of cardiovascular complications. A growing body of evidence proposed that Qr attenuates heart-related complications through suppression of LDL oxidation, inhibition of adhesion molecules and inflammatory markers, endothelium-independent vasodilator activities, and the shielding effect on NO and

endothelial function under redox insult (Patel et al., 2018; Ferenczyova et al., 2020). In an experimental research model of myocardial ischemia/reperfusion damage, Qr showed cardioprotective effects evidenced by a reduction of inflammatory reactions and improvement of myocardial contractility along with the involvement of mitochondrial ATP-sensitive potassium channels and NO system (Liu et al., 2021). The cardioprotective effects of Qr against ischemia/reperfusion injury have been revealed to be achieved by suppressing Src kinase, STAT3, caspases, Bax, intracellular ROS production, and inflammation factor and activating inducible MnSOD expression (Chen et al., 2013).

2.1.2.7. Nephroprotective activity

A large number of studies by different research groups has established the nephroprotective potential of Qr (Chen et al., 2022; Alasmari, 2021; Diniz et al., 2020). Qr offers renal protection against radiation-induced kidney damage through a radioprotective mechanism (Baran et al., 2022). Qr has been shown to minimize acute renal injury and apoptosis by inhibiting HIF-1 α on lncRNA NEAT1/HMGB1 signalling pathway (Luo et al., 2022). Qr limits fibroblast activation and kidney fibrosis by inhibiting the mTOR/ β -catenin activation paving a way for the management of chronic kidney diseases (Ren et al., 2016). A study by Cao and colleagues (2018) reported that Qr is able to mitigate TGF- β induced renal fibrosis. In an in vitro assay of chronic kidney disease, Qr protects mesangial cells via anti-inflammatory, antioxidant, and anti-fibrotic effects showing its effectiveness against chronic kidney diseases (Widowati et al., 2022). In addition, Qr has been found to be effective against obstructive nephropathy (Wang et al., 2023) and lupus nephritis (Chen et al., 2022). Qr also exhibits protective roles against off-target nephrotoxicity caused by different therapeutic drugs, such as valproic acid and cisplatin (Sanchez-Gonzalez et al., 2011; Chaudhary et al., 2015).

2.1.2.8. Anticancer activity

Qr's anti-tumor activities arise from its ability to alter cell cycle progression, suppress cell proliferation, promote apoptosis, halt angiogenesis, metastatic progression, and regulate autophagy (Tang et al., 2020). The anticancer effects of Qr lie in its ability to endorse cell death, apoptosis, and autophagy by interfering with PI3K/mTOR, Wnt/ β -catenin and MAPK signaling pathways. It can also inhibit metastasis by suppressing VEGF and MMPs. Reyes-Farias and colleagues (2019) discussed that Qr exhibits an anticancer effect through inhibition of the anabolic metabolism causing a negative energy state in cancer cells. Numerous researches, including Rauf et al. (2018), Reyes-Farias et al. (2019), and Özsoy Gokbilen et al. (2022), have shown that Qr exerts pro-apoptotic effects on tumour cells. The chemopreventive role of Qr has also been explored. It is shown to

exhibit chemopreventive mechanisms through antioxidant and anti-inflammatory mechanisms along with the involvement of different signal transduction pathways involved in carcinogenesis pathways (Ward et al., 2018; Lin et al., 2020; Özsoy Gökbilen et al., 2022).

2.1.2.9. Antimicrobial activity

Qr exhibits significant antimicrobial ramifications on both Gram-positive and Gram-negative bacteria along with fungi (Qi et al., 2022; Nguyen et al., 2022; Jaisinghani, 2017). The prominent antibacterial effect of Qr on various strains of bacteria including *Streptococcus mutans*, *Streptococcus sobrinus*, *Streptococcus sanguis*, *Actinobacillus actinomycetemocomitans*, *Prevotella intermedia*, *Staphylococcus aureus* and *Pseudomonas aeruginosa* has been revealed (Shu et al., 2011; Jaisinghani, 2017). Qr showed equal effectiveness against both methicillin-resistant and methicillin-sensitive *Staphylococcus aureus* as well as standard *Enterococcus* species (Li et al., 2012). Qr has also been found to impede biofilm formation by *Vibrio parahaemolyticus* and *Staphylococcus epidermidis* (Mu et al., 2021; Roy et al., 2022). Research has proposed that Qr can also be utilized as a substitute for antibiotics due to its promising bactericidal effect (Wang et al., 2018).

Qr also exhibits a potential antifungal effect against *Aspergillus fumigatus* by the downregulation of TLR-4, TLR-2 and HMGB1 (Yin et al., 2021). It has been shown to induce apoptosis in *Aspergillus niger* and *Candida albicans* by endorsing mitochondrial dysfunction (Abd-Allah et al., 2015; Kwun et al., 2020). Qr also displays effectiveness against fluconazole-resistant vulvovaginal candidiasis by inhibiting biofilm formation and fungal load in vaginal mucosa (Gao et al., 2016).

2.1.2.10. Antiviral activities

Flaviviridae, Orthomyxoviridae, Coronaviridae, Retroviridae, Picornaviridae and Filoviridae are just some of the virus families that have been found to be vulnerable to the antiviral effects of Qr. Other virus families include Retroviridae, Picornaviridae, Pneumoviridae (Di Petrillo et al., 2021). Qr has been revealed to inhibit the replication of human Herpesvirus by suppressing viral IE-genes (Kim et al., 2020). According to a recent theoretical study by Derosa and colleagues (2021), Qr may be able to block 3CLpro and PL pro, thus could prevent SARS-CoV-2 replication and may be used as a therapeutic intervention against SARS-CoV-2 infection. In the early stages of influenza infection, Qr showed an inhibitory impact, proposing that it may be useful in the management of Influenza virus infections (Wu et al., 2015).

2.1.3. Bioavailability of Qr

Due to its short biological half-life, high first-pass metabolism in the liver, poor permeability, and instability in the physiological medium of the stomach and intestines, Qr has a low oral bioavailability. As a consequence, both its ability to effectively treat patients and their willingness to comply with treatment are weakened (Cai et al., 2013; Gao et al., 2010; Guo et al., 2015; Murota et al., 2018).

2.1.4. Nanoformulations of Qr: A potential solution to its poor bioavailability

By increasing solubility, stability in a biological system, bioavailability, and cellular absorption, NPs provide a viable platform for therapeutic delivery of poorly soluble chemicals like Qr. Targeted delivery of medications in a single dose is just one of the many applications for synthetic nanoparticles. Over the years, different polymeric and lipid NPs of Qr have been formulated by different research groups around the world to achieve better therapeutic efficacy and compliance.

The neuroprotective impact of Qr-loaded solid lipid NPs (mean particle size 200 nm) was observed to be enhanced in Alzheimer's disease when compared to free Qr (Pinheiro et al., 2020). Qr-loaded PLGA NPs have been found to improve the anti-glioma effect by improving cellular uptake of Qr by C6 glioma cells (Ersoz et al., 2020). Qr-loaded chitosan NPs synthesized by ionic gelation method demonstrated excellent wound healing potential in a rat model by modulation of cytokines (Choudhary et al., 2020). Qr-loaded silk fibroin NPs showed improved intestinal anti-inflammatory effects over free Qr in an experimental model of mouse colitis (Diez-Echave et al., 2021). Qr-loaded silver NPs formulated within hydrogel matrices using carbopol-934 and *Aloe vera* exhibited remarkable curative effects in diabetic and burn wounds (Badhwar et al., 2021). Qr-loaded zein NPs prepared by electro-spraying technique significantly improved in vitro bioavailability of Qr to greater than 3 folds (Rodríguez-Félix et al., 2019). Lactobionic acid-coupled Qr-loaded in organically designed silica NPs have been shown to improve hepatoprotective effect compared to free Qr in cyclophosphamide-induced liver injury in rats, which is mediated through active liver targeting by fabricated nanoformulation (Naqvi et al., 2019). PLGA-based NPs of Qr exhibited improved antioxidant and in vivo diuretic activity when compared to pure Qr (Anwer et al., 2016). Qr-loaded PLGA-TPGS NPs have been developed to overturn the low hydrophilicity of Qr and this nanoformulation better skin protective effect against ultraviolet (UV)-B radiation by blocking UV-B-induced dermal inflammation as compared with native Qr (Zhu et al., 2016). Qr-encapsulated in PLGA NPs significantly improved the therapeutic efficacy of Qr against hypoxia-reoxygenation-provoked cardiac injury (Lozano et al., 2019). These observations clearly suggest that Qr nanoformulations improved the therapeutic efficacy

of the drug as compared with free Qr against a variety of diseases, thus opening a prospect to overturn the pharmacokinetic limitations of Qr.

2.2. Apigenin (API)

API is known to be a flavonoid with the chemical formula 4',5,7-trihydroxyflavone in Figure 2.3. (Ali et al., 2017). Its unadulterated form is a needle-like component that is golden in colour and has a low molecular weight (Hostetler et al., 2017; Shukla et al., 2010). When it comes to plants, it is one of those that can be found almost anywhere. Vegetables (such as parsley, celery, onions, and others), fruits (such as oranges and grapes), herbs (such as chamomile, thyme, oregano, and basil, and others), and drinks made from plants (tea, beer, wine, etc.) are also excellent sources of API, particularly in the glycosylated form of these substances. It has been demonstrated that a high concentration of API possesses potent anti-cancer, anti-inflammatory, antimicrobial, and anti-microbial properties.

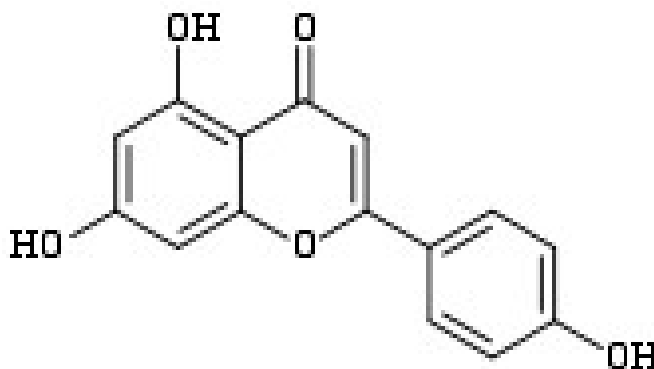


Figure 2.3. Structure of API

2.2.1. Physicochemical characteristics

Mol. Formula: C₁₅H₁₀O₅

Mol. Weight: 270.24

IUPAC Name: 5,7-dihydroxy-2-(4-hydroxyphenyl) chromen-4-one

Solubility: It's almost completely insoluble in water but soluble in hot alcohol moderately. Apart from these API freely solubilizes in dilute potassium hydroxide solution and dimethyl sulfoxide (Brad et al., 2018; Huang et al., 2019).

2.2.2. Biological activities of API

API exhibits immense pharmacological attributes (Figure 2.4). Some of them are outlined in this section.

2.2.2.1. Antioxidant activity

API is a potent antioxidant, which acts by suppressing oxidant enzymes, scavenging free radicals, reinforcing enzymatic and nonenzymatic antioxidants, and chelating metal ions (Kashyap et al. 2022). In preclinical models, API effectively reciprocated disease and

xenobiotic-induced redox insults (Wang et al., 2017; Sahindokuyucu-Kocasari et al., 2021). There is growing evidence that API can increase the potential of antioxidant enzymes such as GPx and SOD, as well as those enzymes involved in aerobic respiration, most notably the mitochondrial respiratory enzyme complexes I, II, and IV (Wang et al., 2020). A possible function in mitochondrial biogenesis is suggested by the upregulation of genes such as ATP5B, mitochondrial transcription factor A, nuclear respiratory factor-1, and pyruvate kinase C1. In addition, API is also involved in reversing oxidative stress-induced pathogenesis by modulating various redox-sensitive signal transduction processes.

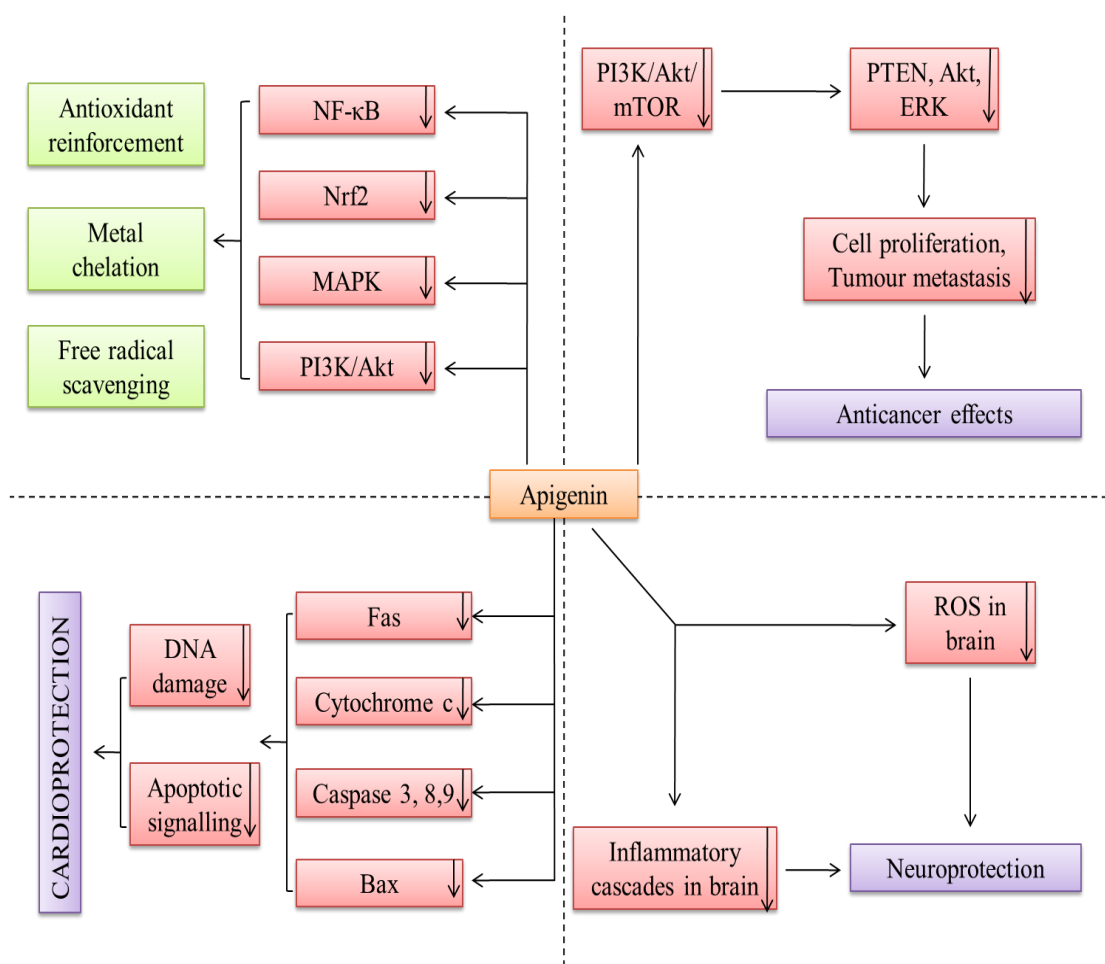


Figure 2.4. The therapeutic mechanism of API.

2.2.2.2. Anti-inflammatory activity

API displays a strong anti-inflammatory action, similar to other flavonoids. API significantly attenuated LPS-induced microglial inflammation and reduced TNF- α and IL-1 β production in BV2 microglia cells by subduing NF- κ B activation and endorsing GSK-3 β /Nrf2/HO-1 signalling (Chen et al., 2020). It also exhibited NF- κ B inhibitory effect in lung tissue of asthmatic mice and exhibited an anti-neutrophil-associated inflammatory

activity (Pang et al., 2019). Cicek and colleagues (2021) reported that API can suppress sepsis-induced lung injury by inhibiting inflammatory cell damage. API was found to suppress the inflammatory response in murine macrophages and rat basophilic leukemia cells by inhibiting NO production, IL-1 β , IL-6 and iNOS expressions, and MAPK phosphorylation (Park et al., 2020).

2.2.2.3. Antidiabetic activity

API exhibits pronounced antidiabetic property due to its anti-gluconeogenic and anti-lipogenic capacities (Bumke-Vogt et al., 2014; Panda et al., 2007). In addition, it is effective in the reversal of insulin resistance and glucose intolerance in type 2 diabetes (Ren et al., 2016). In addition, apigenin can protect pancreatic beta cells from oxidative stress- and inflammation-induced damages (Suh et al., 2012). It is capable of reducing postprandial hyperglycemia (Sahnoun et al., 2018). API shows significant α -glucosidase inhibitory activity, which vouches for its anti-diabetic activity thereby making it a promising drug candidate (Wang et al., 2014; Zeng et al., 2016).

2.2.2.4. Neuroprotective effects

Neuroprotective effect of API has been revealed (Nabavi et al., 2018). API exhibits anticonvulsive effect as well as prevents memory impairments by suppressing neuronal apoptosis (Hashemi et al., 2019). It has been shown to attenuate cerebral ischemia/reperfusion injury by upregulating the PI3K/Akt/Nrf2 pathway (Ling et al., 2020. Fu et al., 2021). Through suppressing NLRP3 and TLR4 overexpression, API also displayed regulatory potency in cellular energy balance and immune system gene expression, and as a result, exhibits antidepressant potential (Bijani et al., 2022). The ability of API to protect Alzheimer's disease neurons by reducing spontaneous Ca²⁺ signal frequency and caspase-3/7-mediated apoptosis demonstrated its neuroprotective action against neurodegenerative diseases (Balez et al., 2016).

2.2.2.5. Hepatoprotective activity

The hepatoprotective activity of API have been revealed by different preclinical studies. It has been reported to attenuate paracetamol-induced acute liver injury by decreasing lipid peroxidation and increasing endogenous antioxidant enzymes (Rašković et al., 2017). In search of hepatoprotective mechanism, API has been found to attenuate paracetamol-induced acute hepatotoxicity by suppressing IL-1 β , STAT3, and caspase-3 activation and regulating Sirtuin 1/p53 axis (Mohamed et al., 2020; Zhao et al, 2020). It can also inhibit CCl₄-induced acute liver injury by attenuating hepatic oxidative stress and inflammation (Yue et al., 2020). In search for the mechanism, it shows to activate c-IAP1 and TRAF 2/3 and inhibit NF- κ B. In another model of CCl₄-induced hepatotoxicity, API inhibits liver fibrosis by restraining the activation of hepatic stellate cells and autophagy by

suppressing TGF- β 1/Smad3 and p38/PPAR α signaling (Ji et al., 2021). In various studies, API exhibited hepatoprotective potential against different xenobiotic-induced liver damages by suppressing hepatic inflammation and redox insults (Ali et al., 2014; Goudarzi et al., 2021; Sahindokuyucu-Kocasari et al., 2021; Al-Amarat et al., 2022)

In a research model of D-GalN/LPS inflicted hepatotoxicity in mice, API exhibited hepatoprotective effect by activating Nrf-2 and PPAR γ expressions and suppressing NF- κ B and TNF- α activation (Zhou et al., 2017). In addition, API inhibits xanthine oxidase and the NLRP3 inflammasome, which, respectively, decreases oxidative stress and inflammation in NAFLD (Lv et al., 2019).

2.2.2.6. Cardioprotective effect

API exhibits cardioprotective effect by inhibiting cardiac apoptosis and autophagy by activating PI3K/AKT/mTOR signaling (Yu et al., 2017). In an in vitro model of xenobiotic-induced cardiotoxicity, API significantly attenuated isoproterenol hydrochloride-induced apoptosis in H9C2 cardiomyoblasts (Thangaiyan et al., 2018). Its cardioprotective mechanism also includes suppression of myocardial SphK1/S1P signalling (Zhang et al., 2015). In an animal model of myocardial infarction, API significantly prevented the hemodynamic disorders by restoring the left ventricular function and reinstating redox balance (Mahajan et al., 2017). API can also protect cardiac cells against anoxia/reoxygenation injury by suppressing cardiomyocyte apoptosis (Chen et al., 2016).

2.2.2.7. Nephroprotective activity

The evidence that API has nephroprotective properties is growing stronger all the time. There is a connection between the renoprotective characteristics of API and the inhibition of CYP2E1, NF- κ B, and MAPK activation. These features, in turn, lower oxidative stress and inflammation (He et al., 2016). By downregulation of CD38 expression, raising the intracellular NAD⁺/NADH ratio, suppressing MAPK activation, and promoting Sirt3-mediated mitochondrial antioxidant enzyme activities, API considerably reduced the kidney lesions that are caused by diabetes in diabetic rats. These effects were seen in tubulointerstitial fibrosis, damage to tubular cells, and expression of pro-inflammatory genes (Ogura et al., 2020). In a mouse model of diabetic nephropathy, API inhibited the MAPK/NF- κ B/TNF- α and MAPK/fibronectin pathways, which resulted in a significant reduction in oxidative stress and fibrosis. Because of this, there was a significant increase in renal function (Malik et al., 2017). In animal models that were treated with API prior to ischemia/reperfusion injury, there was a reversal of renal cell death, as indicated by decreased Bax and caspase 3 expression and in kidney enhanced Bcl-2 activity. This was seen in the kidneys (Wang et al., 2018). Another study found that renal apoptosis caused

by 3-chloro-1, 2-propanediol was significantly inhibited by the compound (Zhong et al., 2018).

2.2.2.8. Anticancer effects

The anticancer potential of API lies in its ability to modulate various cell signaling pathways (Salmani et al., 2017, Madunić et al., 2018, Singh et al., 2019; Rahmani et al., 2022). It has been demonstrated chemopreventive role by supporting tumour suppressor genes, reducing inflammation, preventing angiogenesis, endorsing apoptosis, and arresting the cell cycle. Promising antitumor effects of API in reducing genomic instability and the risks of second malignancies among normal tissues has also been revealed (Moslehi et al., 2023). API is also capable of suppressing the unwanted toxicities of chemotherapeutic agents (Nozhat et al., 2021). API simultaneously exhibits chemotherapeutic role through a prooxidant mechanism and capable to kill cancer cells (Sharma et al., 2019; Yan et al., 2017). Various research groups have explored chemotherapeutic roles of API against cervical (Zhang et al., 2020), pancreatic (Ashrafizadeh et al., 2020), gastric (Kim et al., 2021), prostate (Hnit et al., 2022), and breast (Nabavi et al., 2015) cancers.

2.2.2.9. Antimicrobial properties

Antibacterial activity of API has been well documented (Nayaka et al., 2014; Lee et al., 2018). API has been revealed to exhibit antibacterial effect by endorsing bacterial apoptosis through prooxidant chemistry associated with enhanced production of ROS and RNS (Kim et al., 2020). There is an increasing body of evidence suggesting that API is a novel molecular kind of natural antibiotic with antibacterial activity that works in the reverse manner against quinolone-resistant bacteria (Morimoto et al., 2015). In addition to that, it possessed antifungal qualities and delayed the spread of dangerous fungi that are the underlying cause of skin illnesses (Lee et al., 2018).

2.2.2.10. Antiviral activity

API exhibited antiviral effects against different viruses. It has been shown to inhibit Epstein-Barr virus reactivation by subduing of the promoter functions of two viral IE genes (Wu et al., 2017). Khandelwal and colleagues (2020) reported the antiviral activity of API against the Buffalopox virus. It has shown inhibitory effect on the replication of Hepatitis C virus by inhibiting TRBP phosphorylation in a miR-122-dependent manner (Shibata et al., 2014). It also interferes with the translational activity of the Foot-and-mouth disease virus by inhibiting internal ribosome entry and virus replication (Qian et al., 2015). API can selectively block enterovirus-71 infection by destroying viral RNA relation with hnRNP A1 and A2 (Zhang et al., 2014). In a recent study, Xu and colleagues (2020) revealed that it can attenuate Influenza A virus replication and Influenza A virus-

induced inflammation by inhibiting viral neuraminidase activity and activating RIG-I and IFN expression.

2.2.3. Bioavailability of API

API is categorized as a class II drug by the biopharmaceutics categorization system with low water solubility but strong intestinal membrane permeability (Zhang et al., 2012). The oral bioavailability of API is relatively low because of its low water solubility (Kazi et al., 2020). In addition to the poor solubility, the poor bioavailability of API in part is due to its extensive first-pass metabolism and phase II conjugation by hepatic uridine 5'-diphospho-glucuronosyltransferase and sulfotransferase enzymes (Wu et al., 2011; El Daibani et al., 2020). Despite having multiple therapeutic attributes, the low bioavailability issue largely severely limits its clinical translation.

2.2.4. API nanoformulations: A way to overcome its bioavailability issues

Extensive research has established that API is effective in treating various diseases, however, developing suitable dosage forms has always been a challenge because of its poor pharmacokinetic properties. Utilizing different nanocarriers has successfully addressed these issues and improved the therapeutic efficacy of API. He and colleagues (2021) revealed that API-loaded polymeric NPs showed better therapeutic efficacy against ischemia/reperfusion-triggered renal inflammation by improving the bioavailability of API. API-loaded polymeric NPs exhibited improved biodistribution patterns of the drug in both liver and blood following intravenous administration and the nanoformulation showed better therapeutic efficacy against HCC in vitro and in vivo compared with free API (Bhattacharya et al., 2018). In the treatment of metastatic melanoma of lung, PLGA NPs loaded with API and functionalized with meso-2,3-dimercaptosuccinic acid showed promise when compared to native API (Sen et al., 2021). Xu and colleagues (2021) fabricated a stable API nanosuspension using polyethylene glycol (PEG)-400 employing a green and efficient anti-solvent system, which substantially improved the pharmacokinetic profile of API. API-Fe₂O₃/Fe₃O₄@mSiO₂-hyaluronic acid nanocomposites exhibited improved biocompatibility as well as antitumor efficacy than free API (Liu et al., 2021). API-selenium NPs showed better cytotoxic potential against breast cancer cells in terms of reduction of cell viability and induction of apoptosis than free drug (Al-Otaibi et al., 2022). API-loaded polymer-lipid hybrid NPs formulated using PLGA, phospholipon, and poloxmer-188 also exhibited pronounced cytotoxicity toward breast cancer cells (Kazmi et al., 2022). API-loaded chitosan NPs coated with albumin-folic acid demonstrated increased anticancer activity in vitro on HepG2 cells compared to pure API in terms of onset of apoptosis and arresting the cell cycle (Mabrouk Zayed et al., 2022). API-loaded lipoid-PLGA-TPGS NPs improved the

therapeutic effect of API against colon cancer (Alfaleh et al., 2022). API-carbon nanopowder solid dispersions showed promising results in improving the oral bioavailability and drug safety of API (Ding et al., 2014). The aforementioned observations clearly demonstrate that nanoscale formulations of API improve the therapeutic effects of API by overturning its pharmacokinetic limitations. Surface fabrication and engineering with suitable ligands/groups of API NPs further glorify its therapeutic efficacy and compliance.

2.3. PLGA

PLGA is a synthetic co-polymer of lactic acid and glycolic acid. It is a biodegradable polymer. Since lactic acid being an intermediate metabolite or by-product of carbohydrate metabolism, it is widely distributed in natural sources. Glycolic acid is also found in nature but in a much lesser extent than lactic acid. PLGA degrades in lactate and glycolate (salt forms of lactic acid and glycolic acid, respectively). For targeted drug delivery, ligands can be easily added to and modified on the surface of PLGA (Makadia et al., 2011; Kapoor et al., 2015; Essa et al., 2020). USFDA approved the use of PLGA for drug delivery purposes (Makadia et al., 2011).

Glycolic acid and lactic acid are the two distinct monomer units that are mainly used during the synthesis of PLGA via ring-opening co-polymerization reaction (Gentile et al., 2014). Different forms of PLGA with different molecular weights are synthesized depending on the lactides: glycolides ratio which indicates the percentages of lactic acid and glycolic acid in that particular form of PLGA (Table 2.1).

Table 2.1. List of PLGA polymeric ratios versus molecular weights (Hyon et al., 1997).

Lactide: glycolide ratios	Molecular weights
50:50	30,000-60,000
50:50 (ester terminated)	100,000
50:50 (acid terminated)	25000
65:35	40,000-75000
75:25	66,000-107,000
80:20	200,000
85:15	190,000-240,000

2.3.1. Solubility

The solubility of PLGA depends on the ratio of lactide and glycolide. Higher glycolide concentration (> 50 %) in PLGA increases the lipophilicity of the polymers, making them more soluble in non-polar solvents like acetone, dichloromethane, chloroform, etc.

(Makadia et al., 2011; Kamaly et al., 2016; Garner et al., 2021). In contrast, increase in lactide content within the polymer enhances hydrophilicity of PLGA.

2.3.2. Molecular weight

PLGA polymers have variety of molecular weights depending upon the ratios of lactide and glycolide as shown in Table 2.1.

2.3.3. Crystallinity

The composition of a polymer critically determines its crystallinity. The extent of PLGA crystallinity is inversely related to glycolide content resulting in less chain rearrangement to develop crystalline structures. In contrast, high lactide content enhances the crystallinity of PLGA (Makadia et al., 2011). The crystallinity of PLGA also depends on the molecular weight (Makadia et al., 2011).

2.3.4. Thermal stability and storage

Different forms of PLGA are generally thermostable in absence of moisture. Prolonged heating above 200°C in a nitrogen environment or under vacuum results in the degradation of the polymer. Thus, PLGA should be stored in a cool and dry place in an air-tight container (Gilding et al., 1979; Hines et al., 2013; Liu et al., 2022).

2.3.5. Degradation

The hydrolytic breakdown of ester linkages in PLGA yields lactic acid and glycolic acid. In normal conditions, the average degradation times for PLGA 50/50, 75/25, and 85/15 are 1-2, 4-5, and 5-6 months, respectively (Xu et al., 2017; Elmowafy et al., 2019).

2.3.6. Elimination

PLGA biodegradation yields lactic and glycolic acids. Lactate is eliminated from the body in the form of carbon dioxide (CO₂) and water after undergoing additional metabolic processing through the Krebs cycle. On the other hand, glycolic acid is either expelled unaltered through the urine or travels through the Krebs's cycle to be converted into carbon dioxide and water before being eliminated from the body (Makadia et al., 2011).

2.3.7. Biomedical applications of PLGA

The USFDA approved the use of the biodegradable, biocompatible, and non-toxic polymer PLGA for internal usages (Gentile et al., 2014; Lü et al., 2009). Since 1974, PLGA has been used in the biomedical industry as the brand name of vicryl, and currently being extensively prepared by number of commercial manufacturers (Blasi, 2019). PLGA is frequently used in the development of polymeric NPs because of its safety, biocompatibility, and biodegradability. Here, it serves as an efficient drug carrier for a wide variety of compounds, including chemotherapeutics (Sadat Tabatabaei Mirakabad et al., 2014; Rezvantalab et al., 2018; Chung et al., 2020), genes (Ramezani et al., 2017), proteins (Allahyari et al., 2016), enzymes (Bhatt et al., 2017), antibodies (Jiang et al.,

2021), aptamers (Hashemi et al., 2020). For the production of micron- and submicron-formulations, such as microspheres, microcapsules, NPs, and nanofibers, the polymer PLGA is by far the most popular choice. These formulations are employed in drug delivery systems (Yamaguchi et al., 2002; Bala et al., 2004; Meng et al., 2011; Boltnarova et al., 2021; Su et al., 2021). Table 2.2 provides information regarding the usage of a limited number of drug-loaded PLGA NPs as delivery vehicles for a number of different illnesses

Table 2.2. PLGA nanoparticles developed against different types of diseases

Sl. No.	Drug/ Compounds	Targets	Diseases	References
1	Memantine	Brain targeting using nano-formulation via intranasal route	Alzheimer's disease	Kaur et al., 2022
2	Naringenin	Brain targeting using glutathione and tween-80 coated nanoparticles	Autistic Disorders	Bhandari et al., 2023
3	Baicalin	Brain targeting via intra-nasal route using RVG29 peptide-modified nanoparticles	Cerebral ischemia	Li et. al., 2022
4	Baclofen and Lamotrigine	Brain targeting via intra-nasal administration of nanoparticles	Neuropathic pain	Nigam et. al., 2022
5	Resveratrol	Brain targeting using lactoferrin conjugated nanoparticles	Parkinson's disease	Katila et. al., 2022
6	Rapamycin	Heart targeting via adventitial injection of nanoparticles	Neointimal hyperplasia	Bai et. al., 2022
7	Mesenchymal stromal cell-secreted factors (MSCF)	Heart targeting via intramyocardial injection of nanoparticles	Cardiac repair	Hu et al., 2022
8	Colchicine	Heart targeting using modified-macrophage-membrane-coated nanoparticle system	Atherosclerosis	Li et. al., 2022
9	Celecoxib	Targeting abnormal angiogenesis via parenteral administration of nanoparticles	Cancer and arthritic disease	Alonso-González et. al., 2022

10	Polysaccharide sulfate	Targeting heart via intraperitoneal injection of nanoparticles	Coronary microcirculatory dysfunction	Gao et. al., 2022
11	Docetaxel	Nanoparticles linked to chitosan and folic acid can be used to specifically target cancer cells that have an overexpression of folate receptors.	Cancer	Al-Nemrawi et. al., 2022
12	Genistein	Ovarian cancer drug delivery employing polymer-conjugated lipid (PLGA-PEG-FA) nanoparticles	Ovarian cancer	Patra et al., 2022
13	Trans-cinnamic acid	Targeting tumor via intra peritoneal injection of nanoparticles	Breast cancer	Badawi et al., 2022
14	α -Terpineol	Targeting colon cancer cells using folic acid-chitosan coated nanoparticles	Colon cancer	Rahmati et al., 2022
15	Docetaxel	Targeting prostate cancer cell line using PLGA nanoparticles of different molecular weight.	Prostate cancer	Simitcioglu et al., 2022
16	Nimbolide	Targeting pancreatic Cancer Stem Cells (CSC) using nanoparticles	Pancreatic ductal adenocarcinoma	Singh et al., 2022
17	1,3-Bis[3,5-bis(trifluoromethyl)phenyl]urea	Targeting cariogenic bacterial strain <i>Streptococcus mutans</i> UA159 to combat caries using nanoparticles.	Caries in the human oral cavity	Zhang et al., 2022
18	Curcumin	Targeting different H. pylori strains and gastric cancer cells using nanoparticles	Gastric cancer and H. Pylori infections	Alam et al., 2022
19	Dexamethasone	Delivery of drugs to inflamed tissues and reduce joint inflammation using pegylated nanoparticles	Rheumatoid arthritis	Simón-Vázquez et al., 2022

20	Simvastatin	Pulmonary delivery of nanoparticles using nebulizer for the treatment of subacute paraquat poisoning	Pulmonary fibrosis	Shahabadi et al., 2022
21	Curcumin	To reverse corticosteroid resistance induced by cigarette smoke extract (CSE) using nanoparticle formulation. Treatment for hepatocellular carcinoma that is based on nanoparticles and works by inhibiting acquired resistance produced by P-glycoprotein.	Chronic obstructive pulmonary disease	Chen et al., 2022
22	Sorafenib	Liver cancer targeting using galactosedecorated nanoparticles	Hepatocellular carcinoma	Tang et al., 2022
23	Dalbergin	Treatment of NAFLD using mPEG-PLGA nanoparticles	Non-alcoholic fatty liver disease; Hepatic steatosis	Gautam et al., 2022
24	Rapamycin	Targeting ocular tissues using PEG and cell-penetrating peptides functionalized nanoparticles	Ocular inflammation	Zhao et al., 2020
25	Licochalcone-A			Galindo et al., 2022

Chapter 3

Fabrication of surfactant-free quercetin-loaded PLGA nanoparticles: Evaluation of hepatoprotective efficacy by nuclear scintigraphy

Contents

- 3.1. Introduction
- 3.2. Materials and methods
 - 3.2.1. Materials
 - 3.2.2. Preparation of NPs
 - 3.2.3. Characterization of NPs
 - 3.2.4. In vitro cytotoxicity studies
 - 3.2.5. Confocal laser scanning microscopy
 - 3.2.6. In vivo experiment
 - 3.2.7. Statistical analysis
- 3.3. Results and discussion
 - 3.3.1. Surface morphology, particle size and zeta potential
 - 3.3.2. Drug physical status characterization
 - 3.3.3. In-vitro release profile
 - 3.3.4. Cytotoxicity test
 - 3.3.5. Cellular uptake
 - 3.3.6. In vivo effects
- 3.4. Conclusion

3.1. Introduction

Various natural products have been used in clinical practice as hepatoprotective agents. Among them, flavonoids are considered to be highly efficient against reactive oxygen species by virtue of their antioxidant activities and could be effectively used for the prevention and treatment of various liver ailments. Qr, an important dietary flavonoid present ubiquitously in fruits and vegetables, exhibits promising hepatoprotective activity (Casas-Grajales et al., 2015). Recent years have seen a rise in the number of studies that investigate whether or not Qr therapy could be effective in curing and preventing disease. Qr possesses a wide array of pharmacological activities, e.g. antioxidative (Hu et al., 2015; Seufi et al., 2009), hypolipidemic (Bashir, 2014), ROS scavenging, anti-inflammatory (Boots et al., 2008), antifibrotic (Horton et al., 2013), anti-cancer (Dajas, 2012) and hepatoprotective (Casas-Grajales et al., 2015).

The hepatoprotective efficacy of Qr has been investigated against CCl₄-induced hepatocellular injury (Ma et al., 2015), acrylonitrile-induced hepatotoxicity (Abo-Salem et al., 2011), ethanol-induced liver injury (Kahraman et al., 2012) as well as in diethylnitrosamine induced hepatocarcinoma model in animals (Gupta et al., 2010), wherein it was observed that free radical scavenging, as well as modulation of signalling pathways, are the important therapeutic strategies of the flavonoids. The liver protects our body by detoxifying poisonous chemicals. Chemical-induced liver impurities are associated with oxidative damages and lipid peroxidation leading to liver dysfunction. Qr protects liver cells by enhancing the manufacture of antioxidant enzymes and protective proteins, as well as inhibiting the cancer replicative cell cycle and reducing toxin-induced DNA alterations (Granado-Serrano et al., 2012; Aherne et al., 1999).

Flavones are not commonly used as medicines despite having the potential to be therapeutically beneficial. This is because flavones have a low aqueous solubility in the gastric and intestinal fluids. As a direct result of this, the molecules have a low bioavailability, limited permeability, and undergo substantial first-pass metabolism before entering the systemic circulation. The bioavailability of Qr after oral administration is less than 1% in humans due to its extremely poor hydrophilicity and instability in alkaline medium (Gugler et al., 1975). These problems may be circumvented by entrapping/adsorbing the drug molecules either into liposomes (Wang et al., 2013) or into biodegradable polymeric NPs (Ghosh et al., 2013). A possible method for the delivery of drugs is nanoparticles, which can range in size from 10 to 1000 nm. They have a very high level of biocompatibility and bioavailability, and their peculiar physicochemical and biological properties are a direct result of the fact that they are so small. As nano-encapsulation protects the natural products from fast deterioration and enhances drug

accumulation in tissues of target, it makes it possible to utilise lower doses of the medication while simultaneously reducing the number of unwanted side effects.

Successful nano-encapsulation of Qr on PLA has been achieved by solvent evaporation method to attain sustained delivery of the drug in biological fluids (Pandey et al., 2015). Encapsulating Qr in liposomes (Gang et al., 2012) and chitosan NPs was successful in achieving both an increase in the water solubility of the compound as well as the maintenance of a continuous release of the flavonoids (Zhang et al., 2008). Qr-loaded lecithin-chitosan NPs were formulated for topical administration in order to enhance the level of medicament absorption that occurs in the epidermal layer of the skin (Tan et al., 2011). PLGA, a widely used biodegradable and biocompatible polymer approved by USFDA and European Medical Agency (Danhier et al., 2012), has also been used to encapsulate Qr. There is a rapidly growing interest in this field to use the different molecular weights of PLGA and its copolymers to influence drug release, drug delivery, cellular uptake and biodistribution.

Solvent evaporation, nanoprecipitation, solvent diffusion, salting out, and dialysis are some of the typical procedures that are used to disperse medicines in polymers in order to generate biodegradable NPs from PLGA (Rao et al., 2011). Though solvent evaporation and nanoprecipitation are the most widely accepted methods, they are associated with several problems related to the removal of non-chlorinated organic solvents and surfactants. Inactivation of the medication during the manufacturing process and drug loss during the washing stage both contribute to the low drug loading efficiency (Jeong et al., 2001). To avoid these, the dialysis method has been developed and many workers in this field used this technique for the preparation of liposomes and polymeric micelles. However, the application of this method for the preparation of Qr-NPs has not been reported earlier.

We, in this research, report dialysis method for synthesizing Qr-NPs, which was chosen because it eliminates the need for potentially hazardous surfactants. The prepared NPs were characterized by physicochemical characterization techniques such as FE-SEM, FTIR, and zeta potential measurements. Drug loading, encapsulation efficiency, in vitro drug release studies and particle size measurements by DLS were also performed. In vitro studies were conducted in HepG2 cells to observe the binding efficiency of Qr-loaded NPs using fluorescence microscopy, while cytotoxicity of the formulation was evaluated using an MTT assay to determine the optimum dose. The therapeutic efficacy of the Qr-NPs to combat liver dysfunction was also ascertained by monitoring different biochemical parameters. Finally, the hepatoprotective efficacy of Qr-NPs in CCl₄-induced

hepatocellular degeneration in a rat model was monitored by scintigraphic imaging technique using ^{99m}Tc -labeled sulphur colloid and mebrotfenin.

3.2. Materials and methods

3.2.1. Materials

Qr was procured from Alfa Aesar, Thermo Fisher Chemicals, Waltham, USA. PLGA with L/G molar ratio of 50:50 (PURASORB PDLG 5002A), L/G molar ratio of 75:25 (PURASORB PDLG 7502A) and L/G molar ratio of 85:15 (PURASORB PLG 8531) were kindly gifted by Purac Biomaterials, Amsterdam, Netherlands. Dialysis membranes with molecular weight cutoff 3.5 or 7.5 kDa were bought from Thermo Fischer, Waltham, USA, while membrane of 12-14 kDa was obtained from Hi-Media, Mumbai, India. FITC and DAPI were procured from Sigma Aldrich (St. Louis, MO, USA) and Invitrogen (California, USA), respectively. DMF was purchased from Spectrochem, located in Bombay, India. In addition to it, everything else used in experiment was of an analytical standard. Via the use of 2-butanone extraction of a 5N NaOH solution containing $^{99}\text{MoO}_4^-$ acquired from the Bhabha Atomic Research Centre (Mumbai, India), the $^{99m}\text{TcO}_4^-$ was generated. For the purpose of determining the radioactivity levels of various organs of the body, an ECIL gamma-ray spectrometer was utilised (type GRS23C; Hyderabad, India). A GE Infinia Gamma camera from Chicago, United States was used to scan the animals, and this camera was configured to a Xeleris work station (Chicago, United States).

3.2.2. Preparation of NPs

Qr-NPs were prepared using dialysis method without surfactant. After dissolving Qr (5 mg) in DMF (1 ml), it was added to PLGA (50 mg) that had been previously dissolved in acetone (5 ml). After agitating the preformed solution for 5 minutes on a stirrer, it was added dropwise in 15 ml of distilled water and continued to be stirred. The cloudy solution that was produced instantaneously was introduced in the dialysis tube, and dialysed against an external aqueous phase. The external phase was kept under gentle stirring to aid diffusion and replaced at an interval of 3 to 4 h for a period of 24 h. Because the organic solvent diffused out of the membrane during dialysis and water diffused into it, this led to the precipitation of polymers that self-assembled into spherical NPs that encased the drug. After a period of 24 hours, the contents of the dialysis bag were removed and subjected to centrifugation at 11,500 rpm for a period of 30 minutes (Sorvall RC-5C, Waltham, Massachusetts, United States). The NPs formulated was initially in the shape of a pellet, but it was transformed into a powder through the application of freeze drying. FITC loaded PLGA NP were prepared by utilizing FITC instead of Qr in the same quantity.

3.2.3. Characterization of NPs

3.2.3.1. Determination of NP yield, encapsulation efficiency and loading capacity

Weighing the initial quantity of polymer and drug used to make the Qr-NPs and dividing the result by the total weight was the method that was utilised to calculate the yield percentage. Encapsulation efficiency was calculated by knowing the amount of Qr added initially and the amount of the flavonoids extracted from the drug-loaded NPs. After dissolving NP pellet (2 mg) in acetone (10 ml) and centrifuging the mixture, a concentration of Qr was determined by measuring the amount of UV radiation absorbed at 370 nm with a Shimadzu-1700 spectrophotometer. The encapsulation efficiency and loading efficiency have been calculated.

3.2.3.2. Morphology of NPs

FE-SEM was utilised in order to investigate the morphology of the NPs (Jeol JSM-7600F, Tokyo, Japan). A single drop of NP suspension that was placed on a glass cover slip was dried with the application of freeze-drying for imaging purpose. The dried sample was ion coated with gold (4-5 nm) using a sputter coater (QUORUM Q150T ES, Sussex, United Kingdom) for 40 seconds under vacuum at a current intensity of 40 milliamperes. The sputter coater was located in Sussex, United Kingdom. The acceleration voltage was varied between 2 and 5 kV while the scanning was being done.

3.2.3.3. Drug physical state characterization

The physical status of Qr-NPs was ascertained by measuring the DSC, XRPD and FTIR patterns. Purified dry nitrogen was utilised at a flow rate of 150 ml/min to purge standard aluminium pans for DSC analysis, each of which contained 10 mg of sample material. While monitoring heat flow between 0-400°C, by using a ramp rate of 12°C per minute DSC data was acquired. The DSC instrument, which was a Pyris Diamond TG/DTA manufactured by Perkin Elmer in Singapore, had its temperature and energy scales calibrated with the help of indium powder, which served as the standard reference material. The diffraction patterns of pure Qr, polymer, and Qr-NPs were determined with the help of an X-ray powder diffractometer (XRD-2000, Rigaku, Tokyo, Japan). The CuK α radiation was employed as the X-ray source for the studies (45 kV, 40 mA), and the scanning rate was 1° min⁻¹ across a 2 θ range of 2- 50°. A Fourier transform infrared (FTIR) study was performed using potassium bromide pellets using a Bruker Tensor-27 instrument from Massachusetts, United States. This was done in order to confirm the possibility of a chemical interaction between the flavonoid and the polymer matrix. We scanned PLGA, free Qr, and Qr-NPs between a range of 400 and 4000 cm⁻¹.

3.2.3.4. Particle size and zeta potential analysis

A Zeta Potential analyser (Zeta Plus, Brookhaven Instruments, Holtsville, NY, United States) was used to determine the average particle size of the Qr-NPs as well as their zeta potential. Before conducting an analysis of the particle size, an NP sample that contained 10 mg of the formulation was suspended in 1 ml of deionized water and diluted 10 times again in deionized water. It was possible for us to determine the zeta potential of the drug-encapsulated NPs by first dispersing the sample (1.5 mg) in 1.5 ml of KCl (1 mM). In order to carry out the analysis, the powdered sample was inserted into an optical cuvette that was intended for single-use only. At least three separate analyses were performed on every batch of samples, and the results are presented here as an average.

3.2.3.5. In vitro release studies

A solution of 20 mg of NPs suspended in 4 ml of PBS was put into the dialysis bag (MWCO 12-14 kDa), and positioned in a beaker that contained 400 ml of PBS, the bag was shaken (100 rpm) horizontally while being incubated at 37°C. At regular time intervals, 4 ml of the releasing media was aspirated out and replaced by equal amount of fresh PBS. We were able to calculate the released Qr concentration by UV spectrophotometric analysis at 370 nm. The outcomes of these tests, including their averages, were recorded. A computation and graph were created to show the cumulative percentage of drug release over time.

3.2.4. In vitro cytotoxicity studies

We evaluated the effects of free Qr and Qr-NPs on the viability of the HepG2 cell line using a microplate reader and an MTT assay (GENios, Mannedorf, Switzerland). HepG2 cells were cultured in DMEM at a temperature of 37°C, with a humidity of 90% and a CO₂ concentration of 5%. When the cells were to be harvested, trypsin-EDTA was applied, and the medium was replaced every other day. A 96-well plate had 1×10⁴ cells plated into each well of the plate. The media was changed every other day until a convergence rate of 80% was achieved. At this stage, 100 µl of freshly prepared suspension of free drug (at varied concentrations) and drug encapsulated NPs were added to the growth medium, and was incubated for 24 hours at the same temperature and humidity levels as detailed before. One of the rows of wells in the 96-well plate did not have any NPs added to it so that it could serve as a control. After discarding the media that contained the drug and washing the wells three times with PBS, 10 µl of MTT solution (5 mg/ml in PBS) and 90 µl of medium were added to each well. The wells were then incubated for an additional 4 hours in order to determine the level of cell viability present at each of the indicated time points. When the allotted amount of time had passed for the incubation process, the MTT-containing medium was discarded and replaced with

100 µl of DMSO in order to dissolve the formazan crystals. The absorbance was then measured using a microplate reader at 550 nm. In the control group, we anticipated that one hundred percent of the cells would be able to survive.

3.2.5. Confocal laser scanning microscopy

The confocal laser scanning microscope (Andor spinning disc confocal microscope, UK). was utilised to measure the uptake by the cells. A cell culture plate of 35 mm in diameter contained 1×10^5 HepG2 cells that were cultured on coverslips. When the cells in each dish had reached 80% confluence, the medium was removed and replaced with a FITC-loaded PLGA NP suspension (250 µg/ml). The dishes were then placed in an incubator for two hours. After the incubation one ml of ethanol at a concentration of 70% v/v was added to each petri dish in order to fix the cells at a temperature of -20°C for 15 minutes of incubation. The ethanol solution was discarded, and the dishes were washed three times with PBS before the DAPI solution was applied to stain the nuclei and allowed to remain there for 5 minutes. Cellular internalization was evaluated using confocal laser scanning microscopy.

3.2.6. In vivo experiment

All animal experiment protocols complied with the institutional guidelines and were approved by CPCSEA, Government of India, New Delhi. In a controlled environment with a temperature of $30 \pm 2^\circ\text{C}$, relative humidity of 60-80%, and a light-dark cycle of 12 hours, mature male Swiss Albino rats weighing 120-150 g were kept for seven days with unrestricted access to both food and water. There were a total of 30 animals, with six rodents assigned to each of the five categories. Group I (Normal Control) received subcutaneously (s.c.) single dose of olive oil (1 ml/kg body weight). Group II was given CCl_4 (40% v/v in olive oil, 1 mg/kg body weight) subcutaneously. Animals in group III, IV and V were treated by oral gavage with free drug (0.5 ml suspension of 0.2% Tween 80 aqueous solution containing 8.98 µmol/kg b.w. Qr), empty NPs (0.5 ml suspension) and Qr-NPs (0.5 ml suspension contains 8.98 µmol/kg b.w. Qr), respectively. Two hours after oral feeding of drugs, all animals in groups III to V were injected subcutaneously with CCl_4 (40% v/v, 1 ml/kg b.w.). Twenty-four hours after the CCl_4 challenge, the animals were anaesthetized and sacrificed to collect the blood sample and to collect the liver. A portion of the liver was fixed in 10% formalin to a prepared paraffin section for histological study and the remaining parts were immediately stored at -80°C for other assays.

3.2.6.1. Serum biochemical analysis

After allowing the blood samples to sit for 30 minutes to coagulate, they were centrifuged at 2000 g for 10 minutes at 4°C. The serum that was obtained from this process was then

stored at 4°C until it could be further analyzed. Serum marker enzymes, e.g. SGPT, AP and also serum urea and creatinine were determined in accordance with methods provided by the manufacturers of the commercial kits (Span Diagnostics, Surat, India).

3.2.6.2. Measurement of GSH, catalase, lipid peroxide and SOD in liver homogenate

A portion of liver tissue was homogenized in chilled sodium phosphate buffer (0.1 M, pH 7.4) containing 0.15 M KCl. The homogenate was used for the assessment of levels of oxidative stress markers, e.g. GSH and lipid peroxide, and for the estimation of antioxidant enzyme (catalase) activity.

Estimation of GSH was done as per the reported method (Davila et al. 1991). Briefly, 2 ml of 10% liver homogenate was added to a tube containing a mixture of 5% TCA and 1 mM EDTA solution, gently shaken for 5 min, and centrifuged at 3000 g for 30 min at 4°C. An aliquot of the resultant supernatant was transferred to a tube containing 5 ml of phosphate buffer (0.1 M, pH 8.0) and 0.4 ml DTNB (0.01% in 0.1 M phosphate buffer of pH 8.0), and mixed well. The absorbance of the yellow-coloured solution was measured at 412 nm using a UV-Vis spectrophotometer (Shimadzu 1700, Kyoto, Japan) and plotted on a standard curve obtained from a known GSH concentration to estimate the GSH content in the homogenate.

Catalase estimation was done as per the protocol reported earlier (Mandal et al., 2005) with modifications. Liver homogenate (5 ml, 10%) was subject to centrifugation at 300 g for 15 min at 4 °C; the supernatant was collected after separation of small debris and recentrifuged at 105000 g for 60 min at 4°C. To an aliquot of the supernatant containing the cytosolic fraction, ethanol (10 µl) was added and kept in an ice bath for 30 min before the addition of 10 % Triton X-100 (10 µl). H₂O₂ solution (6 mM) was then added to initiate the enzymatic reaction. After 3 min the reaction was terminated by the addition of H₂SO₄ (6 N). Estimation of the enzyme activity was done by measuring the absorbance at 480 nm after the addition of KMnO₄ solution (0.01 N) to the above mixture. The results were expressed as mM of H₂O₂ decomposed per milligram of protein /min.

The cytosolic fraction of the liver homogenate obtained during catalase estimation was used for measuring SOD activity. To an aliquot (0.2 ml) of the fraction, 1.5 ml of tris cacodylate buffer (pH 8.5, 50 mM), 0.1 ml DTPA (1mM), 0.1 ml catalase (0.2 µM) and 0.1 ml pyrogallol were added and the mixture was kept at room temperature for 90 sec. Absorbance was measured at 420 nm. Estimation of SOD is based on the ability of the enzyme to inhibit the autooxidation of pyrogallol. One unit of enzyme per 2 ml of assay mixture is expressed as the amount of enzyme required to cause 50 % inhibition of pyrogallol auto-oxidation (Marklund et al., 1974).

Lipid peroxides were estimated as per the previously outlined method (Mandal et al., 2005). To an aliquot (0.5 ml) of the supernatant obtained after centrifugation (2000 g for 15 min at 4°C) of liver homogenate, methanol (1.75 ml) and chloroform (3.5 ml) were added successively. The mixture was kept at room temperature for 10 min and centrifuged at 260 g for 5 min at 4°C. The aqueous layer was separated out and the organic layer was evaporated under nitrogen. The residue obtained was dissolved in cyclohexane and the absorbance was noted at 234 nm. Results were expressed as mmole of lipohydroxyperoxide/mg protein.

3.2.6.3. Histopathological analysis

A portion of the liver which was previously fixed in 10% formalin was used for the histopathological analysis. After fixation for 48 h, the liver portion was embedded in a paraffin block and cut into 5 µm thick sections using a manual microtome. The sections were stained using haematoxylin-eosin dye and visualized under a microscope (Leica, Germany) to determine the modifications in liver architecture.

3.2.6.4. Scintigraphic imaging studies

Adult male Swiss Albino rats (b.w. 150-200 g) were divided into three groups (three animals in each group). Each animal of the third group was fed (orally) with Qr-NPs (8.9 µmole Qr/kg body weight), whereas all animals belonging to the first and second groups received 0.5 ml saline orally. Two hours after oral feeding of NPs and saline, all animals in the second and third groups were injected subcutaneously with CCl₄ in olive oil (40% v/v, 1 ml/kg b.w.), whereas animals of the first group received only olive oil (1 ml/kg b.w.). After 24 h, 30 µl (3.7 MBq) of ^{99m}Tc-labeled sulphur colloid (prepared as per the reported method) was administered to each anaesthetized animal through a femoral vein using canula. The animals were placed under a gamma camera and whole-body images were acquired at 30 min post injection. The above scintigraphic experiments in different sets of animals were also carried out using ^{99m}Tc-labeled mebrofenin kit (procured from BRIT India). Radiolabelling with ^{99m}TcO₄⁻ was done according to the instructions provided in the commercial kit. The amount of free pertechnetate in the labelled sulphur colloid and mebrofenin was checked for each preparation by ascending thin layer chromatography (silica gel plates, Merck, New Jersey, United States) using saline and acetone respectively as mobile phase. Any preparation showing more than 5% free pertechnetate was discarded.

3.2.7. Statistical analysis

Statistical analysis was performed with Student's t-test. The p-values of the experimental study results were calculated and found to be < 0.05 which was deemed to be statistically significant.

3.3. Results and discussion

Due to the high antioxidant qualities that it possesses, the natural flavonoid Qr has been under a greater amount of study in recent years. Much study has been conducted on the hepatoprotective impact of flavonoids through several mechanisms of oxidative stress. Moreover, efforts have been made to better protect the liver from oxidative damage by developing appropriate Qr formulations in both liposomal and nanoparticulated forms. Throughout the course of this investigation, the dialysis method was utilised in order to generate Qr-loaded PLGA NPs that were free of surfactant. During the process of dialysis water diffused into the organic solvent inside the dialysis tube and the organic solvent in turn diffused into water outside. The displacement of the organic solvent inside the tube resulted in the precipitation of the polymer as micro- and nano- particles and the drug was encapsulated inside the particles.

Though the technique is simple and effective, so far, no report has been available describing the preparation of Qr-NPs by direct dialysis. Different types of dialysis membranes of MWCO 3.5 kDa, 7 kDa and 12-14 kDa were used. The process was continued for 24 h to remove the solvent completely and a milky suspension was obtained at the end.

3.3.1. Surface morphology, particle size and zeta potential

FE-SEM was done to ascertain the formation of NPs. The particle size was measured by zeta-potential analyzer (Table 3.1). Different grades of polymer as well as dialysis membranes with different ranges of MWCO were used to fabricate formulations of nanoparticulated drug delivery systems of optimum particle size, drug loading capacity and encapsulation efficiency.

Table 3.1. Particle characterization.

Dialysis Membrane (MWCO)	Formulation Codes	PLGA Grade	Size (nm)	PDI	Drug Loading (DL, %)	Encapsulation Efficiency (EE, %)
3.5	S1	50:50	97.1 ± 26	0.211	5.1 ± 2.3	75.1 ± 1.6
	S2	75:25	312.1 ± 15	0.118	4.9 ± 2.8	70.5 ± 3.4
	S3	85:15	278.7 ± 21	0.122	4.6 ± 1.8	54.5 ± 5.2
	S4	50:50	429.6 ± 36	0.210	5.2 ± 2.6	50.2 ± 2.9
7.0	S5	75:25	413.5 ± 25	0.197	5.8 ± 3.4	62.1 ± 5.1
	S6	85:15	424.1 ± 11	0.155	4.2 ± 3.2	51.9 ± 4.3
	S7	50:50	258.5 ± 12	0.072	6.2 ± 4.2	48.5 ± 3.9
12-14	S8	75:25	361.2 ± 26	0.206	3.8 ± 2.5	56.2 ± 5.6
	S9	85:15	118.4 ± 32	0.123	2.9 ± 3.1	42.6 ± 3.3

Each value represents the average ± SD (n = 3).

The particle sizes of batches bearing formulation codes S1 - S3 and S7 - S9 which were fabricated using dialysis membrane of MWCO 3.5 and 12-14 kDa respectively were comparatively less, whereas encapsulation efficiencies were comparatively higher in batches S1 and S2. Encapsulation efficiency of Batch S1 fabricated from PLGA grade 50:50 was highest, while drug loading capacity and mean particle size were also optimum. The polydispersity index parameter was used since it was able to illustrate that the particles had a narrow distribution profile and hence was selected for further study. FE-SEM image (Figure. 3.1A, B) showed smooth spherical shaped particles. Particle size distribution profile analyzed by the zeta potential analyser revealed the size distribution (%) by intensity (Figure. 3.1C). The size distribution pattern determines the route of administration and the drug release behaviour. Small size NPs facilitate tissue penetration in vivo by extravasation. It was discovered that the zeta potentials of the NPs were in the negative region, which was measured to be between -70 and -12 mV. (Figure. 3.1D). This is due to the fact that the carboxylic group of the polymer can be found on the surface of the particle. The measurement of zeta potential is vital which can be used to analyse the stability of colloidal systems as well as the projected destination of NPs in vivo.

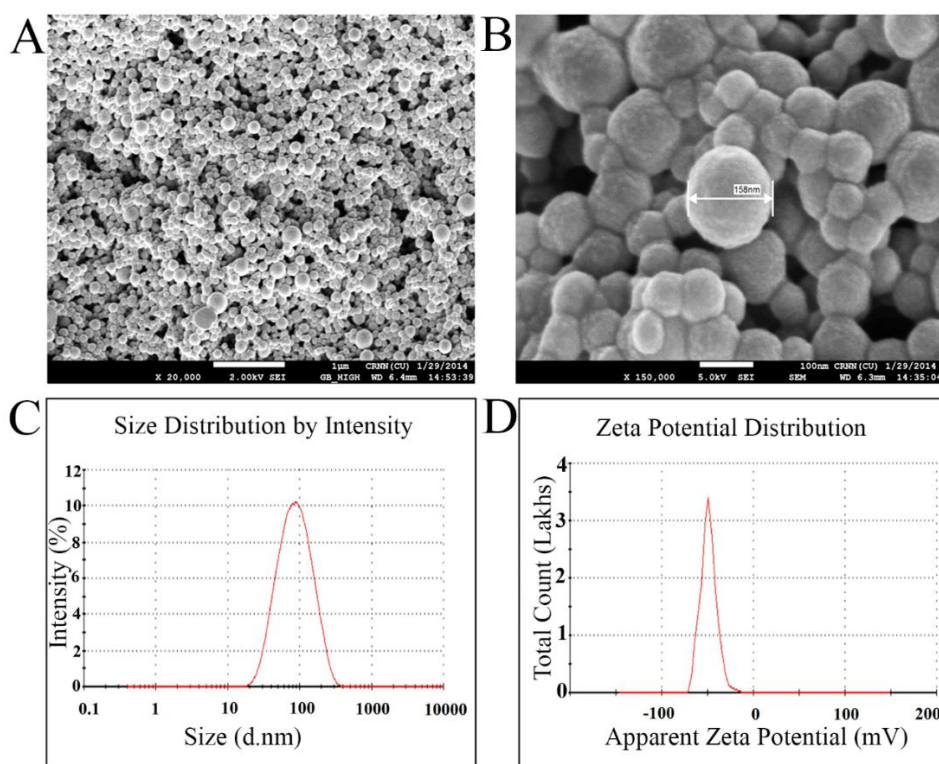


Figure 3.1. FE-SEM images (A and B), particle size distribution profile (C) and zeta potential distribution profile (D) of QR-NPs.

3.3.2. Drug physical status characterization

To learn more about the physical properties of the drug inside the PLGA NPs, we ran DSC, XRD, and FTIR investigations. Figure. 3.2A shows the DSC curves of free Qr,

PLGA, and Qr-NPs. Free Qr showed two endothermic peaks at 118 and 313°C, which are in agreement with the previously reported values. These peaks were not visible in Qr-NPs formulation possibly because the drug loses its crystallinity due to entrapment into NPs. The results of an X-ray powder diffraction experimental data are presented in Figure 3.2B for free Qr, PLGA, and Qr-NPs. A number of distinct peaks characteristic of the crystalline sample were observed in free drug whereas no such peaks were observed in Qr-NPs and in PLGA. This indicates that the free drug gets converted from crystalline to amorphous state due to nanoencapsulation. This finding also corroborates the results obtained from DSC analyses.

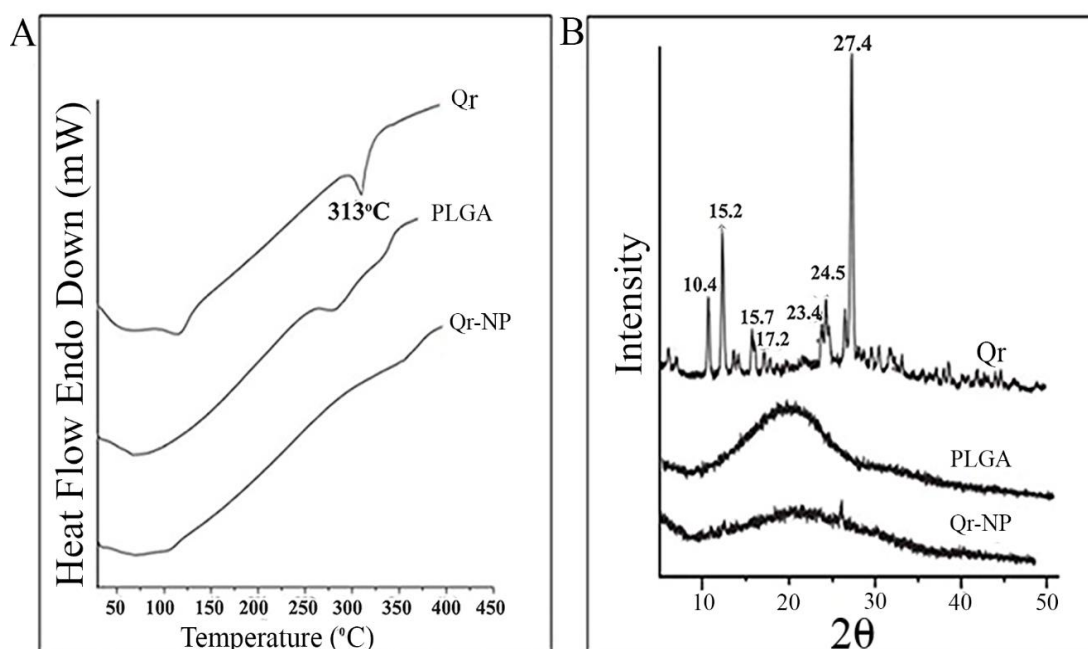


Figure 3.2. DSC thermograms (A), XRD spectra (B) of Qr (free), PLGA and Qr-NPs.

Infrared absorption peaks of Qr, PLGA and Qr-NPs were determined (Figure. 3.3) to confirm nanoencapsulation of the drug. The FTIR spectra of free PLGA showed the characteristic peaks between 2996-2949 cm^{-1} due to $-\text{CH}$, $-\text{CH}_2$, $-\text{CH}_3$ stretching, at 1754 cm^{-1} due to $-\text{C}=\text{O}$ stretching, and at 1271 cm^{-1} for $-\text{C}-\text{O}$ stretching. For Qr the spectrum showed characteristic stretching bands due to $-\text{OH}$ groups (3408 – 3320 cm^{-1}), $-\text{C}=\text{O}$ absorption (1665 cm^{-1}), $-\text{C}=\text{C}$ groups (1609 cm^{-1}), and $-\text{C}-\text{H}$ bending (1456, 1382 cm^{-1}) besides strong $-\text{C}-\text{OH}$ and $-\text{C}-\text{C}$ bending (aromatic) at 1168 cm^{-1} and 1131 cm^{-1} as well as characteristic peaks due to aromatic ring at 1013 cm^{-1} and 821 cm^{-1} . All these results are in agreement with reported values (Wu et al., 2008; Dias et al., 2008). FTIR spectra of Qr-NPs showed slight shifting of $-\text{OH}$ stretching band. This could be due to association of the flavonoid with the polymer through hydrogen bonding. The band at 1759 cm^{-1} ,

which corresponds to $-C=O$ stretching, was broad in nature in Qr-loaded NPs, possibly because of interplay between the carbonyl and carboxyl groups of the polymer.

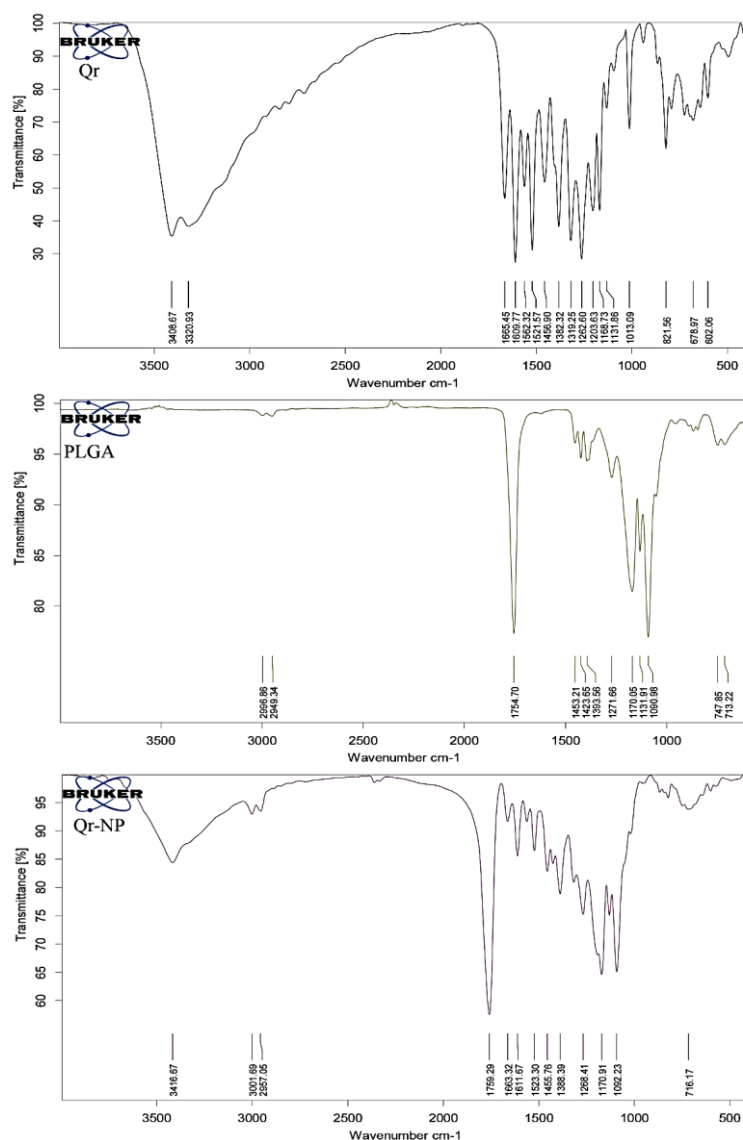


Figure 3.3. FTIR spectra Qr (free), PLGA and Qr-NPs.

3.3.3. In vitro release profile

The cumulative percentage drug release curve of Qr-NPs in PBS may be found displayed in Figure 3.4A. After six days, the graph shows that $69 \pm 4.2\%$ of the free Qr has been released into the free state. The initial burst release ($25 \pm 2.9\%$ during the first 12 hours) may have been the result of the rapid dissolving of drug attached on the surface and positioned near the surface of the NPs, while the subsequent, slower, continuous release at extremely slow rates lasted for almost 6 days. This would imply that the PLGA polymer would deliver the drug in a measured and consistent manner.

3.3.4. Cytotoxicity assessment

In order to determine the cytotoxic effects of free Qr and Qr-NPs on the HepG2 cell line, the vitality of the cells was measured with the MTT test. This test was used to determine whether or not the free Qr and Qr-NPs were able to kill the HepG2 cells (Figure. 3.4B). The study comprised up to a total of 50 hours of observational time. The concentration of NP was determined to be such that the Qr content would fall within the range of plasma levels that could be attained by humans. It was discovered that the cytotoxicity of the NPs that were loaded with the drug was significantly higher than that of the free drug, even when the free drug was given at a concentration that was ten times higher. There was a direct correlation between the residence time of a drug in the system and the level of cytotoxicity it produced. Because of its prolonged release features, the nanoparticulated formulation might have a higher cytotoxicity than its free counterpart.

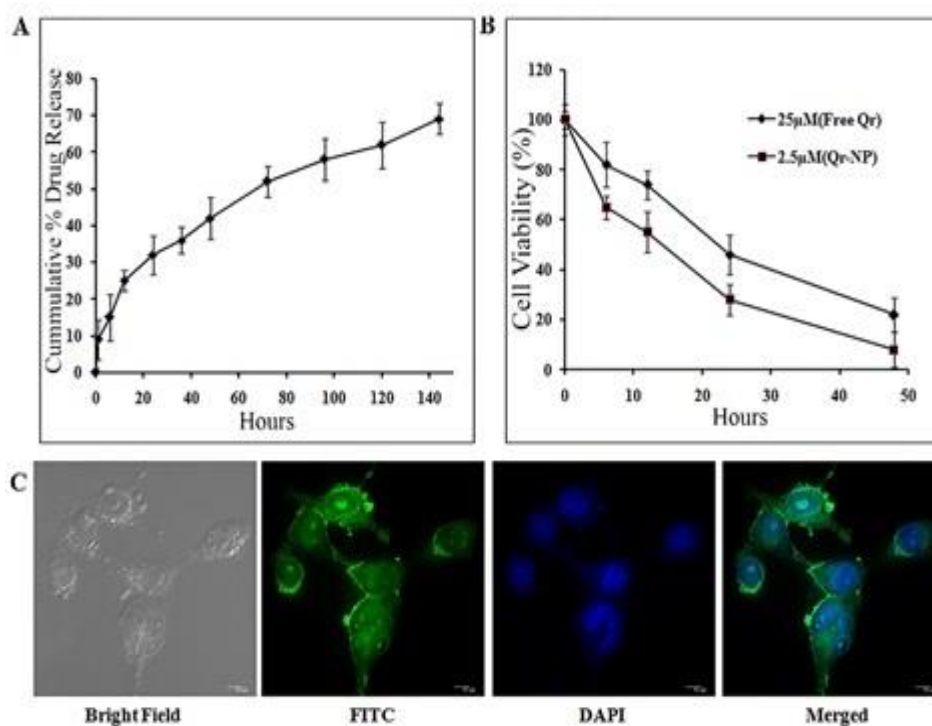


Figure 3.4. In vitro drug release profile of Qr-NPs (A), MTT cytotoxicity studies of free Qr and Qr-NPs against HepG2 cells (B) and fluorescent microscopic images of HepG2 cells treated with FITC-loaded PLGA NPs.

3.3.5. Cellular uptake

Confocal laser scanning microscopy was used to evaluate the cellular uptake efficiency of FITC-loaded PLGA NP suspension in HepG2 cell line. Nucleus staining was performed using DAPI. PLGA NP uptake (green colour) is shown in Figure. 3.4C. The

images show the entrapment of the NPs within the intracellular space. Phagocytosis could be the process by which the cell engulfs the NPs.

3.3.6. In vivo effects

Animal experiments were done to determine the efficacy of the Qr-loaded nanoparticulated formulation. CCl₄ is one of the most commonly used chemicals in experimental study of hepatocellular injury. Oxidative stress occurring due to CCl₄ metabolism plays an important role. Liver damage by CCl₄ increases the membrane permeability and releases the enzymes into circulation, which can be measured in the serum. The levels of ALP and SGPT were increased significantly in CCl₄ treated group. Though treatment with free Qr prior to CCl₄ treatment could not significantly reduce elevated enzyme levels, there was significant restoration of the levels on the administration of Qr-NPs (Table 3.2) before CCl₄ treatment.

Table 3.2. Effect of oral treatment with Qr-NPs on blood serum biochemical parameters in CCl₄-induced acute hepatocellular injury.

Parameters	Normal	CCl ₄ -treated group (A)	A + free Qr treated	A + empty NP treated	A + Qr-NPs treated
AP (unit/l)	298 ± 8.2	721 ± 46.7*	651 ± 6.8	765 ± 12.4	353 ± 14.3*
SGPT (IU/l)	81 ± 11.5	193 ± 13.8*	162 ± 21.3	181 ± 8.9	105 ± 6.5*
Urea (g/l)	0.303 ± 0.12	0.551 ± 0.35*	0.495 ± 0.31	0.501 ± 0.22	0.352 ± 0.25*
Creatinine (mg/l)	16.3 ± 1.2	62.1 ± 3.2*	50.0 ± 3.6	59.8 ± 2.1	23.1 ± 4.2*

Results are expressed as mean ± SD of six animals. CCl₄-treated group was compared with the normal group and Qr-NPs treated group was compared with CCl₄-treated group.

* p < 0.001

After receiving therapy with Qr-NPs, the animals in the study's experimental group saw significant decreases in their serum levels of urea and creatinine (Table 3.2). These studies indicate the protection of structural integrity of hepatocytic cell membrane by nanoformulation of Qr. When compared to the free dug treated groups, the serum creatinine and urea levels of the test group that had been pre-treated with Qr-NPs were much lower than those of the free dug treated groups. In the CCl₄-treated rats, these levels had dramatically increased. However, pre-administration of nanoparticulated Qr caused marked diminutions in the levels of these biomarkers of renal disorder. As kidney is the excretory organ, it might be accumulating some of the bioactive flavonoids offering nephroprotection. The oxidative stress that is brought on by the metabolism of CCl₄ in the liver is what aids in facilitating hepatic fibrogenesis. The poisoning caused by CCl₄ resulted in the loss of structural integrity of cell membranes. In rats that had been inebriated with CCl₄, the content of lipohydroperoxide in the liver homogenates was

significantly higher when contrasted with that of the control group. The treatment with Qr-NP resulted in a significant reduction in these values (Table 3.3).

Table 3.3. Effect of oral treatment with Qr-NPs on GSH, catalase, lipid peroxide and SOD activities of liver in CCl₄-induced acute hepatocellular injury.

Parameters	Normal	CCl ₄ -treated group (A)	A + free Qr treated	A + empty NP treated	A + Qr-NPs treated
Lipohydroperoxide (μmole/mg protein)	1.8 ± 0.25	3.9 ± 0.56*	3.6 ± 0.12	3.4 ± 0.52	2.3 ± 0.09*
Catalase (μmole H ₂ O ₂ reduced/min/mg protein)	9.1 ± 1.2	3.6 ± 0.62*	4.1 ± 0.52	3.8 ± 0.22	8.2 ± 0.12*
GSH (μg/g tissue)	11.3 ± 1.3	4.9 ± 0.65*	6.1 ± 0.32	4.5 ± 0.11	10.2 ± 0.12*
SOD (% auto-oxidation of pyrogallol)	25.43 ± 1.2	9.61 ± 2.4*	11.92 ± 1.8	11.92 ± 1.8	20.58 ± 2.6*

Results are expressed as mean ± SD of six animals. CCl₄ treated group was compared with the normal group and Qr-NPs treated group was compared with CCl₄ treated group.

* p < 0.001

CCl₄ induces oxidative stress, and cells develop several enzymatic and non-enzymatic defences to combat the stress. Catalase and SOD are antioxidant enzymes whereas GSH is the endogenous antioxidant that maintain intracellular redox balance and detoxify reactive oxygen species. CCl₄ induced hepatotoxicity resulted in a significant decrease in SOD, Catalase and GSH levels (Table 3.3). Administration of Qr-NPs provided significant elevation in SOD, Catalase and GSH levels. Qr not only scavenges the free radicals formed due to CCl₄ metabolism but also protects the liver by restoring the levels of various antioxidants by modulating the intracellular signalling systems. Histological examinations of liver sample (Figure. 3.5) also revealed severe liver injury in CCl₄ damaged groups. Liver damage includes gross changes in cellular boundaries, ballooning degeneration and broad infiltration. These changes were markedly reduced by the administration of Qr-NPs before CCl₄ treatment as evidenced by the appearance of normal cellular features with prominent nucleus, absence of ballooning degeneration, minimal cellular infiltration and well brought out central vein as observed in liver section of control groups.

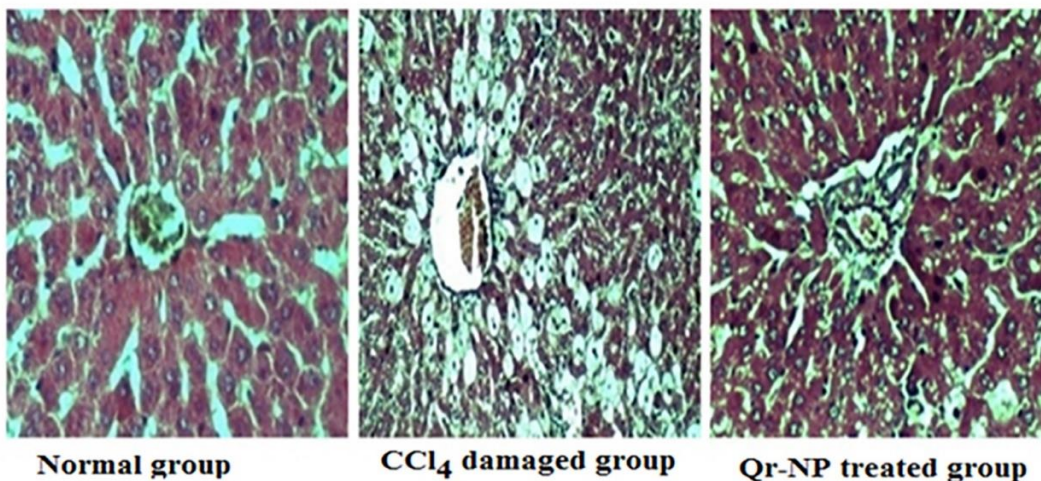


Figure 3.5. Microscopy images of H & E stained liver of rats treated with olive oil (Normal), CCl₄ (damaged) and CCl₄ + Qr-NPs treated.

Hepatoprotective activity of nanoparticulated Qr was further studied on CCl₄ induced acute liver damages (in rat model) by radionuclide scintigraphic studies using ^{99m}Tc-labeled sulphur colloid and ^{99m}Tc-mebrofenin. We thus developed a new probe for the evaluation of hepatoprotective efficacy of nanoparticulated Qr by non-invasive nuclear scintigraphy. ^{99m}Tc-labeled sulphur colloid has been well used for years as liver scintigraphic agent to image the reticulo-endothelial system. This is well documented whereas dynamic ^{99m}Tc-mebrofenin SPECT scan has been used to measure total liver function and diagnose parenchymal disorder. Both the radiopharmaceuticals can delineate normal healthy liver tissue from the damaged one. ^{99m}Tc-sulphur colloid imaging studies were performed in rats of normal, acutely damaged and test groups. The anaesthetized animals were placed anteriorly under gamma camera. An irregularity (or hole) in the liver was seen on scintigraphic images (Figure 3.6A) in the region of reduced assimilation in rats treated with CCl₄. The test group (Qr-NPs treated) saw no sign of this harm.

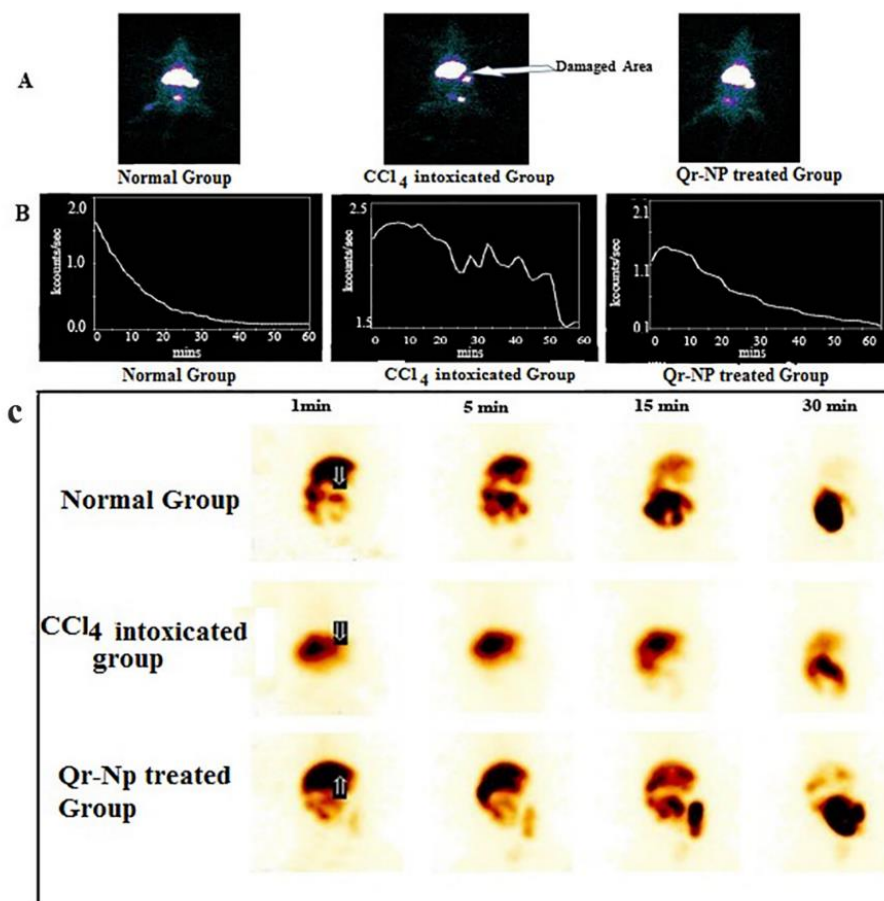


Figure 3.6. (A) Scintigraphic images of ^{99m}Tc-sulphur colloid acquired at 30 min post injection time period of Normal, CCl₄- intoxicated and Qr-NPs treated rats. (B) Hepatobiliary clearance curve and (C) scintigraphic images at different post injection time period of ^{99m}Tc-mebrofenin in Normal, CCl₄- intoxicated and Qr-NPs treated rats.

In dynamic studies with ^{99m}Tc-mebrofenin, the liver was visible very promptly in normal control rats immediately after injection; this was followed by rapid clearance (Figure. 3.6B). In rats treated with CCl₄, there was no change in the amount of ^{99m}Tc-mebrofenin absorbed by the liver; however, the amount of ^{99m}Tc-mebrofenin excreted was dramatically reduced. The pattern of ^{99m}Tc-mebrofenin excretion was moderate in the group that was treated with Qr-NPs; it was neither exceptionally fast nor very sluggish, which indicates that the animals have recovered from their injury. Scintigraphic images (Figure. 3.6C) at different time points (1, 5, 15, and 30 mins) also exhibit liver uptake and excretion of ^{99m}Tc-mebrofenin. At 1 and 5 min, intense activity on the liver was observed in animals of all three groups. However, in normal and NP-treated animals ^{99m}Tc-mebrofenin began to excrete at 5 min, was substantially cleared out at 15 min and was totally cleared at 30 min leaving a shadow of liver. In contrast, the activity retained in the liver up to 15 min in CCl₄-treated group and slowly excreted out. These

studies have demonstrated the utility of non-invasive scintigraphic methods to evaluate the hepatoprotective efficacy of nanoparticulated Qr.

3.4. Conclusion

Various oxidative stresses damage the hepatic cells. Both acute and chronic hepatocellular disorder are very fatal to mankind. During the last two decades the role of Qr has been widely explored for counteracting chemical induced hepatotoxicity. Recent research has led to the development of sophisticated nanoparticulate technology to improve the therapeutic efficacy of bioflavonoids. The present study reports the preparation of Qr-NPs by dialysis method avoiding surfactants and chlorinated solvents. Hepatoprotective efficacy of nanoparticulated Qr has been evaluated noninvasively based on findings of liver scintigraphy by ^{99m}Tc -sulphur colloid and ^{99m}Tc -mebrofenin. Overall, the studies may be considered as starting point for the development of a novel method to monitor the hepatoprotective efficacy of nanoparticulated drug delivery system. This approach is being utilised for monitoring the hepatoprotective efficacy of other nanoparticulated bioflavonoids.

Chapter 4

Apigenin-loaded galactose tailored PLGA nanoparticles: A possible strategy for liver targeting to treat hepatocellular carcinoma

Contents

- 4.1. Introduction
- 4.2. Materials and methods
 - 4.2.1. Materials
 - 4.2.2. Synthesis of GAL-PLGA
 - 4.2.3. Formulation of NPs
 - 4.2.4. Characterization of NPs
 - 4.2.5. In vitro release studies
 - 4.2.6. Stability study
 - 4.2.7. In vitro studies
 - 4.2.8. In vivo studies
 - 4.2.9. Statistical analysis
- 4.3. Results
 - 4.3.1. Structural confirmation of galactosylation of PLGA
 - 4.3.2. Characterization of NPs
 - 4.3.3. Drug loading and encapsulation efficiency
 - 4.3.4. Surface characteristics of NPs
 - 4.3.5. Physicochemical characteristics of NPs
 - 4.3.6. In vitro drug release and kinetic study
 - 4.3.7. In vitro studies
 - 4.3.8. Pharmacokinetic analysis
 - 4.3.9. Antitumor efficacy of NPs in vivo
- 4.4. Discussion

4.1. Introduction

The incidence of hepatocellular carcinoma is one of the leading causes of death from cancer on a global scale (Chakraborty et al., 2020). It is the seventh most common type of cancer found in females and the fifth most common type found in males (Mittal et al., 2013). Over a half-million of newly diagnosed cases of HCC appear per year (Mittal et al., 2013). An extremely poor prognosis worsens the recovery of this disease. Early diagnosis of HCC can have some therapeutic options, such as surgical liver resection, liver transplantation, and chemotherapy (Yang et al., 2019). However, HCC is mostly diagnosed at an advanced stage, where chemotherapy remains the only therapeutic option (Chakraborty et al., 2020). Thus, target-specific delivery of chemotherapeutic agents is a primary therapeutic requirement in its therapeutic management. API is an edible naturally occurring flavonoid that exhibited significant anticancer potential in preclinical studies without imparting toxic effects to normal cells. It is an excellent apoptosis inducer to liver cancer cells and can exhibit significant chemo-preventive and/or tumor-suppressive effects against HCC. API induces apoptosis in liver cancer cells by increasing cellular ROS production mediated through NADPH oxidase activation. In addition, it can inhibit tumor proliferation by inhibiting the cell cycle at G1 and G2/M phases (Imran et al., 2020). cDNA microarray expression analysis revealed that API can regulate 1764 genes in human hepatoma cells (Cai et al., 2011). Suppression of USP-18/IL-4R and Nrf-2/PI3K/Akt signaling and activation of P53/P21/Waf-1 and P38/P21/cyclinD1 pathways were found to be accountable for its chemotherapeutic effect against HCC in different preclinical assays (Imran et al., 2020; Cai et al., 2011; Li et al., 2020). Yet API's poor pharmacokinetic properties greatly restrict its chemotherapeutic potency (Dewanjee et al., 2020). A high level of protein binding and its poor release from the protein-bound form also restricts its chemotherapeutic effectiveness following parenteral delivery (Cao et al., 2011). In these aspects, nanoencapsulation can serve as efficient drug delivery to overturn the aforementioned limitations of free API. PLGA is a USFDA-approved biodegradable and biocompatible polymer. It is feasible to encapsulate medications that have a low solubility in NPs that are based on PLGA. This makes it possible for the medications to extravasate through the vasculature of the tumour due to an increased permeability and retention effect (Acharya et al., 2011). According to Peca et al. (2012), liver cells have a high concentration of asialoglycoprotein receptors, which makes it more likely for those cells to take up polymers that have been galactosylated. Galactose-polymer conjugate offers an amphiphilic structure and during NP formulation, the drug gets encapsulated in the inner hydrophobic core and the outer hydrophilic shell with galactose moieties is available for asialoglycoprotein receptor recognition (Peça et al., 2012). As a result of

this, efforts have been made to develop API-encapsulated galactosylated-PLGA nanoparticles (API-GAL-NPs) so that API can be administered in a manner that is both more effective and more precisely targeted, hence leading to increased therapeutic efficacy in the treatment of HCC. After PLGA had been galactosylated using a straightforward esterification approach, API-GAL-NPs were manufactured using the nanoprecipitation method with GAL-PLGA serving as the polymer. This method was used to create API-GAL-NPs. In order to establish the efficacy of the engineered NPs, tests both in vitro and in vivo were conducted on the particles. When it comes to the efficiency of their respective therapeutic effects, free API and API-NPs were put up against one another.

4.2. Materials and methods

4.2.1. Materials

API was purchased from Otto Chemie Pvt Ltd., Mumbai, India. PLGA with L/G molar ratio of 50:50 (Resomer RG504H) and Kolliphor P188 (Poloxamer 188) were gifted by Evonik India Pvt. Ltd., Mumbai, India and BASF, Mumbai, India, respectively. FITC, DAPI, and acetone were purchased from Sigma Aldrich (St. Louis, Missouri, USA), Invitrogen (California, USA) and Fischer Scientific (Mumbai, India), respectively. HepG2 cells were procured from NCCS, Pune, India. FITC-Annexin V/propidium iodide (PI) double staining assay kit (Catalog No.: 556547) was purchased from BD Biosciences, USA. Primary antibodies p53 (SC #6243), COX-2 (SC #166475), Bcl-2 (SC #7382), BAX (SC #7480), Bcl-xL (SC #8392) and β -Actin (SC # 47778) were obtained from Santa Cruz Biotechnology. Horseradish peroxidase (HRP) conjugated secondary antibody (A9044) was obtained from Sigma-Aldrich, St. Louis, Missouri, USA. ^{99}Mo was procured from Bhabha Atomic Research Centre (Mumbai, India) and 2-butanone extraction of a 5 N NaOH solution of $^{99}\text{MoO}_4^-$ yielded $^{99\text{m}}\text{TcO}_4^-$. All the remaining chemicals used in the experiments were of analytical grade.

4.2.2. Synthesis of GAL-PLGA

Synthesis of GAL-PLGA was carried out as method outlined in earlier research (Peça et al., 2012). To summarize the method, 4 μl of methane sulfonic acid was added to a solution of galactose (1mg/ml) in dry dimethylformamide with continuous stirring for 5 min, to which 200 mg PLGA was added and stirred for 24 h at 60 °C. Ice-cold distilled water was added to it and the synthesized polymer was separated by centrifugation (10000 rpm). Pellet was washed repeatedly with ultrapure water and lyophilized to yield PLGA-galactose conjugate. Galactosylation of PLGA was confirmed by $^1\text{H-NMR}$ spectroscopy (Bruker, DPX 300 MHz NMR Spectrometer, Wissembourg, France) (Peça et al., 2012).

4.2.3. Formulation of NPs

API-GAL-NPs and API-NPs were prepared using nanoprecipitation technique as described by Fessi and colleagues (Fessi et al., 1989). Both the polymer, PLGA or GAL-PLGA, and the drug API, were dissolved in acetone at a concentration of 0.5 mg/ml and 5 mg/ml, respectively. The resulting organic drug-polymer solution was poured into 50 ml ultrapure water containing 250 mg of poloxamer 188 under moderate magnetic stirring. The aqueous phase immediately turned milky due to the formation of NPs. Stirring was continued overnight to evaporate acetone diffused towards the aqueous phase. NPs were then recovered by ultra-centrifugation at 18,000 rpm for 30 min. The pellet thus obtained was washed (3-4 times) using ultrapure water and finally lyophilized to obtain free-flowing powder of NPs. The formulated API-GAL-NPs and API-NPs were stored at 4°C for further use. Fluorescent NPs were prepared following the same protocol by replacing API with FITC (12.5 mg).

4.2.4. Characterization of NPs

4.2.4.1. Particle size distribution and zeta potential analysis

The size distribution, mean particle size, polydispersity index (PDI), and zeta potential of the NPs in the suspension were assessed with the use of a zeta potential analyzer (Zeta Plus, manufactured by Brookhaven Instruments and located in Holtsville, New York, United States) (Baishya et al., 2016).

4.2.4.2. Surface morphology of NPs

FESEM (Jeol JSM-7600 F, Tokyo, Japan) and TEM (FEI, Tecnai G2 SPIRIT Bio Twin, Czech Republic) were utilized for the purpose of analyzing the surface morphology of API-NPs and API-GAL-NPs employing techniques that were previously reported (Baishya et al., 2016).

4.2.4.3. Physicochemical characterization of NPs

Based on a previously established protocols, we used UV-Vis spectroscopy to determine drug loading, encapsulation efficiency, and yield in terms of percentage (Gaonkar et al., 2017). FTIR, differential scanning calorimetry, and X-ray powder diffraction analyses ascertained the physicochemical compatibility between API, polymer, and the other formulation ingredients (Gaonkar et al., 2017).

4.2.5. In vitro release studies

The release of API from API-NPs and API-GAL-NPs in PBS at different time intervals was investigated for 8 days following a cumulative drug release protocol reported elsewhere (Ganguly et al., 2016).

4.2.6. Stability study

Using methods that have been published by Gaonkar and his colleagues, the stability of lyophilized API-NPs and API-GAL-NPs were tested for their size distribution, zeta potential, PDI, drug loading, and encapsulation efficiency after being stored at $4\pm 1^\circ\text{C}$ for 90 days (Gaonkar et al., 2017).

4.2.7. In vitro studies

4.2.7.1. Cell culture

HepG2 cells were cultured in EMEM fortified with 10% FBS and antibiotics solution (Hi-Media, Mumbai, India) and the culture was maintained at 5 % CO₂, 90 % humidity, and 37 °C temperature in an incubator (Ganguly et al., 2016).

4.2.7.2. Cellular uptake studies

In vitro cellular uptake of API-NPs and API-GAL-NPs by HepG2 cells was determined qualitatively and quantitatively by confocal laser scanning microscope (Olympus FluoView FV10i, Olympus, Tokyo, Japan) and flow cytometer (BD LSRFortessa™, BD Biosciences, CA, USA), respectively (Gaonkar et al., 2017). The cellular assimilation of API-GAL-NPs in presence of galactose was determined by blocking studies (Siu et al., 2018).

4.2.7.3. Cytotoxicity studies

An MTT-based colorimetric assay was used to assess the cytotoxic potentials of API, API-NPs, and API-GAL-NPs against HepG2 cells (1×10^4 cells/well) at two different time points (24 and 48 hours) (Ganguly et al., 2016).

4.2.7.4. Apoptosis assay

The apoptotic effects of API, API-NPs, and API-GAL-NPs on HepG2 cells were measured using a FITC-Annexin V/propidium iodide (PI) double staining assay kit (BD Biosciences, NJ, USA) in a flow cytometer (BD LSRFortessa™, BD Biosciences, CA, USA) in accordance with the instructions provided by the manufacturer of the kit.

4.2.8. In vivo studies

4.2.8.1. Pharmacokinetic studies

The pharmacokinetic study of API, API-NPs and API-GAL-NPs were performed in plasma samples collected from Wistar rats following the established protocol by our group (Gaonkar et al., 2017). Briefly, the animals were treated with the aforementioned formulations (equivalent dose of 9.2 μM of API/animal, i.v.) and blood samples were collected at predetermined time points (1, 2, 4, 8, 12, 24 and 48 h) post-administration, and plasma was separated. The samples were then analyzed in Dionex UltiMate 3000 HPLC system (Dionex, Idstein, Germany) using a Hypersil GOLD-C18 column (250 \times 4.6 mm and particle size of 5 μm ; Thermo Scientific™ Hypersil GOLD™, MA, USA)

and eluted with water: acetonitrile: methanol (40:35:25 v/v/v) at a flow rate of 1.0 ml/min. API was detected by UV detection at a wavelength of 340 nm (Sahu et al., 2019). The pharmacokinetic parameters were estimated using PKSolver (A freely available add-in program for pharmacokinetic data analysis in Microsoft Excel). Zhang and colleagues (Zhang et al., 2010) validated PKSolver with respect to other professional PK softwares and established the reliability of this software. Different research groups successfully employed PKSolver to determine pharmacokinetic parameters (Balakumar et al., 2013; Abdelwahab et al., 2021).

4.2.8.2. In vivo antitumor efficacy study

Adult male Wistar rats were randomly divided into five groups (N = 7). Animals in Gr-I (normal control) received three doses of olive oil (0.5 ml/animal). All animals in Gr-II, Gr-III, Gr-IV, and Gr-V received DEN (200 mg/kg b.w. in olive oil, i.p.) three times at an interval of 15 days. Gr-III, Gr-IV, and Gr-V were treated with API, API-NPs, and API-GAL-NPs (equivalent dose of 9.2 μ M of API/animal, i.v.) once a week for 16 weeks, respectively. Gr-I and Gr-II (DEN-treated control) were treated with normal saline (Ghosh et al., 2012). DEN-treated control served as the HCC control group. After 18 weeks, two animals (from each group) from Gr-I, Gr-II, and Gr-V were injected with ^{99m}Tc-labeled sulfur colloid (30 μ l; 3.7 MBq/animal) and ^{99m}Tc-labeled mebrotfenin (50 μ l), and viewed under a gamma camera (Ganguly et al., 2016).

4.2.8.3. Serum enzyme parameters

As described by Ganguly et al., (2016) levels of alanine aminotransferase (ALT), aspartate aminotransferase (ALP), and aspartate aminotransferase (AST) were measured using bioassay kits manufactured by Coral Clinical Systems in Goa, India using protocols outlined by the manufacturers. These kits were used to analyze the enzyme parameters from blood samples taken from animals in both the control group and the treated group.

4.2.8.4. Western blot analysis

In accordance with the established protocol, protein samples were extracted from liver tissues collected from patients participating in a variety of treatment groups (Joardar et al., 2019). To be more specific, 10% SDS-PAGE gel electrophoresis was carried out on the sample proteins (10 μ g), and the proteins that were successfully separated were subsequently loaded onto a nitrocellulose membrane. After being blocked initially, the membrane was then subjected to an incubation with the primary antibody at a temperature of 4°C for an overnight period of 12 hours. After being washed, the membrane was incubated with a secondary antibody that was HRP-conjugated for one hour at room temperature. The immunoblot was developed by an ECL substrate (Millipore, Massachusetts, United States), and the detection was carried out with a ChemiDoc touch

imaging system (Bio-Rad, USA). The amount of protein that was loaded onto the blot was measured using the protein β -actin as a standard. Level 1 of the intensity scale corresponds to the normal control band (Dua et al., 2021). Image Lab was utilised for the purpose of carrying out densitometric analysis (Bio-Rad, USA). Analyses were performed on the levels of expression for P53, Bcl-xL, Bcl-2, and Bax proteins.

4.2.8.5. Gelatin zymography analysis

MMP-9 and MMP-2 activities were measured using gelatin zymography analysis (Sivaramakrishnan et al., 2009). PBS extracts of liver tissue were resolved on an SDS-PAGE gel containing 1 mg/ml gelatin by employing specific conditions that did not involve reduction. After being cleansed, the gels were incubated in a calcium assay solution at 37°C for a period of 24 hours. Finally, it was stained using 0.5% Coomassie blue followed by destaining with methanol:acetic acid:water (4:1:5 v/v/v) until the bands were clearly visible. The zones of gelatinolytic activity appeared as negative staining.

4.2.9. Statistical analysis

For the statistical analysis of the data, version 7.0 of the Graph Pad Prism programme was utilised, and a one-way analysis of variance (ANOVA) followed by a post hoc Dunnett and Sidak test was carried out. After much deliberation, it was agreed that a minimum significance level of $p < 0.05$ was required.

4.3. Results

4.3.1. Structural confirmation of galactosylation of PLGA

The anomeric OH- functional group of galactose reacted with the free -COOH group of PLGA in acidic conditions catalyzed by methane sulfonic acid. This esterification was conducted in DMF media. The conjugation was confirmed by ¹H-NMR spectroscopy (Figure 4.1). ¹H-NMR spectra of PLGA depicted various chemical shifts between 1.57 ppm correspond to methyl proton (-CH₃), 4.82 ppm due to methylene proton (-CH₂), and between 5.22 ppm due to methyne proton (-CH). The chemical shifts were observed in the ¹H-NMR spectra of galactosylated-PLGA, wherein an additional peak at 4.32 ppm appeared due to the galactose unit. The extent of galactosylation can be measured by comparing the relative peak areas of the -CH₃ and -CH₂ of PLGA and peaks of galactose.

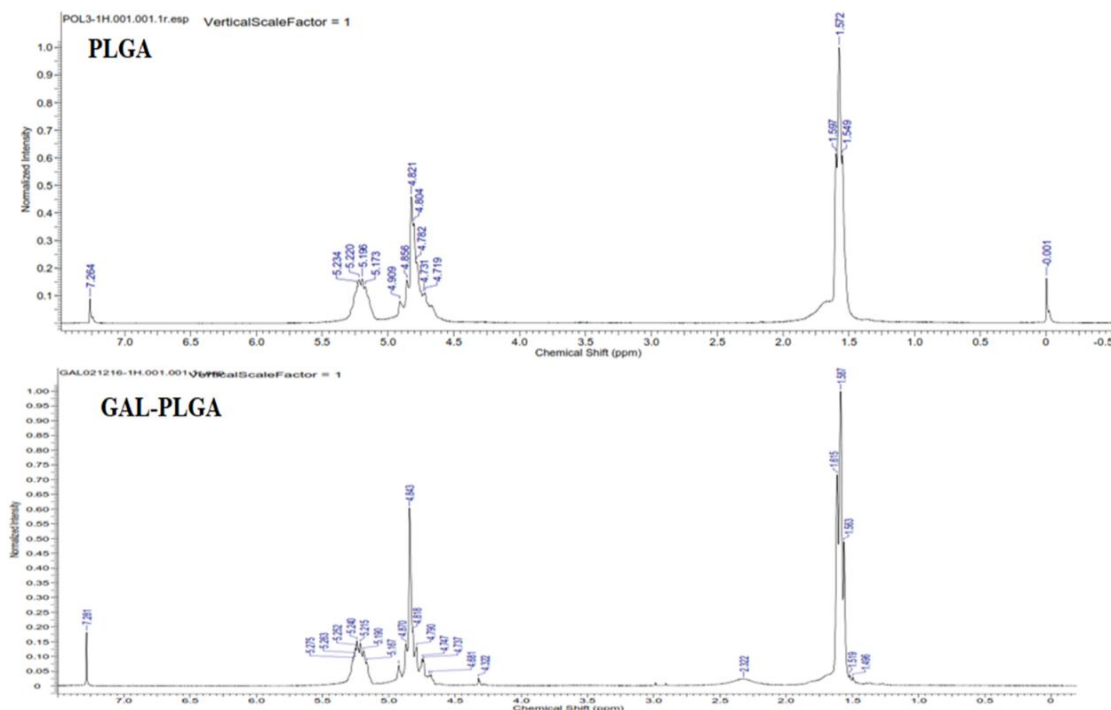


Figure 4.1. $^1\text{H-NMR}$ spectra of PLGA and GAL-PLGA

4.3.2. Characterization of NPs

In order to characterize the NPs that were formulated, measurements were conducted to assess the particle size, the particle size distribution, and the zeta potential. A comparison of API-NPs and API-GAL-NPs revealed that the former displayed a PDI of 0.041 ± 0.004 (Table 1) and a mean particle size of 110.0 nm (Figure 4.2A), while the latter displayed a PDI of 0.059 ± 0.007 (Figure 4.2A) and a mean particle size of 129.0 nm.

Table 4.1. NPs characterization and stability studies

Formulation codes	Initial		After storage at 4°C for 90 days	
	API-NPs	API-GAL-NPs	API-NPs	API-GAL-NPs
PLGA grade	50:50	50:50	-	-
Size (nm)	110.0 ± 25	129.0 ± 16	$122.2 \pm 11.2^{\text{NS}}$	$137.7 \pm 13.8^{\text{NS}}$
Zeta potential (mV)	-25.0 ± 1.3	-14.0 ± 0.9	$-25.8 \pm 1.5^{\text{NS}}$	$-14.7 \pm 0.8^{\text{NS}}$
PDI	0.041 ± 0.004	0.059 ± 0.007	$0.049 \pm 0.018^{\text{NS}}$	$0.079 \pm 0.01^{\text{NS}}$
% Yield	76.3 ± 2.2	70.1 ± 3.5	-N/A-	-N/A-
Drug loading (DL, %)	5.1 ± 0.9	5.3 ± 0.6	$4.9 \pm 0.7^{\text{NS}}$	$5.2 \pm 0.5^{\text{NS}}$
Encapsulation efficiency (EE, %)	70.3 ± 2.6	75.4 ± 1.2	$68.5 \pm 3.1^{\text{NS}}$	$72.8 \pm 2.5^{\text{NS}}$

Results are expressed as mean \pm SD (n = 3). NS represents non-significant. The stability data of each group was statistically compared with the initial data.

Products with low PDI values have particles of a consistent size throughout the formulation. The DLS approach was utilized to arrive at the following conclusions

regarding the average zeta potential of API-NPs and API-GAL-NPs: -25.0 and -14.0 mV, respectively (Figure 4.2B). Due to the galactosylation procedure, the zeta potential of the nanoparticles produced from GAL-PLGA is anticipated to be lower than that of the nanoparticles manufactured from PLGA. The assimilation of NPs by the reticuloendothelial system (RES) in both the liver and the spleen is facilitated by a negative zeta potential. In formulations that were kept at 4°C for 90 days, the particle size, particle distribution index, and zeta potential did not significantly change, which confirmed that the NPs are stable (Table 4.1).

4.3.3. Drug loading and encapsulation efficiency

API-NPs and API-GAL-NPs exhibited ~5.1 and 5.3% w/w of drug loading and ~70.3 and 75.4 % of encapsulation efficiency, respectively (Table 4.1). Drug loading in NPs was optimum; whereas, encapsulation efficiencies were sufficiently high. Galactosylation of PLGA does not affect API entrapment in NPs.

4.3.4. Surface characteristics of NPs

FESEM images of API-NPs and API-GAL-NPs showed that the NPs were spherical in shape, homogeneously, and thickly distributed having a smooth outer surface (Figure 4.2C). TEM images revealed a smooth surface characteristics and entrapment of drug within the NPs (Figure 4.2D). The diameter range of the NPs as obtained from FESEM (60-120 nm) and TEM (85-160 nm) analyses were concurrent with the data obtained in DLS analyses.

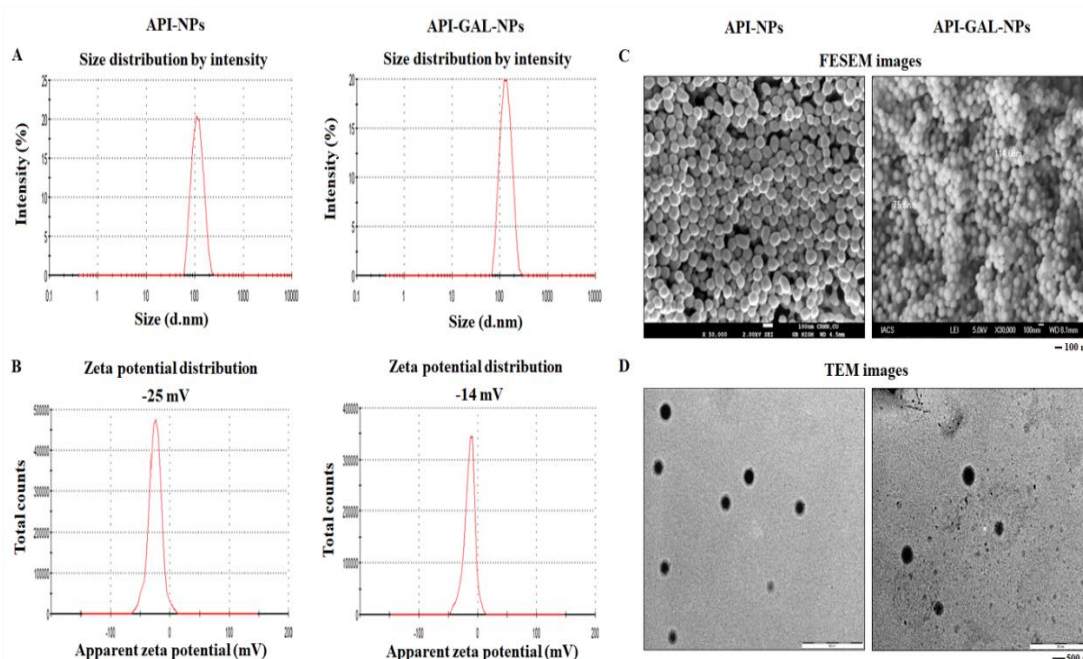


Figure 4.2. Size distribution, zeta potential, and morphology of API-NPs and API-GAL-NPs. (A) Particle size distribution profile, (B) zeta potential distribution pattern, (C) FESEM images, and (D) TEM images.

4.3.5. Physicochemical characteristics of NPs

4.3.5.1. DSC and XRD study

The DSC thermogram of API showed a melting endothermic peak at 359.2°C (Figure 4.3A). PLGA and GAL-PLGA being amorphous did not exhibit any sharp endothermic peak in their respective DSC thermograms. It is likely that the absence of the endothermic peak of API in the corresponding DSC thermograms of API-NPs and API-GAL-NPs is due to the change of API from its crystalline state to its amorphous state during the nano-formulation process. The nanoencapsulation procedure may result in less crystallinity and amorphization in the final formulation, which may contribute to the formulation's increased stability. The outcomes of the XRD investigation provided solid backing for the DSC analysis results that were discussed previously. Due to the fact that API is a crystalline material, the XRD spectrum of the substance displayed peaks that were prominent and easily distinguishable (Figure 4.3B). It was determined that PLGA and GAL-PLGA were amorphous due to the absence of a prominent peak in their XRD spectra (Figure 4.3B). After nanoencapsulation, the disappearance of the API's characteristic peaks in API-NPs and API-GAL-NPs was regarded as evidence that the API had transitioned from a crystalline form to an amorphous state (Figure 4.3B).

4.3.5.2. FTIR spectroscopic analysis

In the FTIR spectrum of the physical mixture, API, PLGA, GAL-PLGA, and poloxamer can all be identified as peaks, albeit with some minor shifts. The characteristic peaks of API at wavenumber 3272.17 cm⁻¹ (assigned to O-H stretching of free -OH group), 1650.97 cm⁻¹ and 1605.89 cm⁻¹ (attributed to C=O stretching of carbonyl function), and a strong band at 1353.84 cm⁻¹ (assigned to the C-O stretching couple with C-C stretching modes) were present. Apart from this, comparatively strong bands at 1556.27 cm⁻¹, 1498.50 cm⁻¹ and 1243.97 cm⁻¹ have been attributed to the aromatic ring stretching vibrations of apigenin. The FTIR spectrum of PLGA and GAL-PLGA showed bands at 2996.86-2949.34 cm⁻¹ region and in 3000.99-2955.41 cm⁻¹ region, respectively representing O-H stretching of hydroxyl function. Similarly, intense C-O stretching band due to the ester function of PLGA and GAL-PLGA appeared at 1754.70 cm⁻¹ and 1759.24 cm⁻¹ respectively. The FTIR spectrum of poloxamer revealed characteristic bands at 2880.52 cm⁻¹ (assigned to aliphatic C-H stretching), 1341.79 cm⁻¹ (attributed to in-plane O-H bending) and 1101.92 cm⁻¹ (assigned to C-O stretching). Physical interactions such as the production of weak hydrogen bonds, the force of attraction exerted by Vander-Waals, dipole-dipole interactions, and other similar phenomena were all contributors to the slight repositioning of the peaks. The presence of distinctive peaks of the API is evidence that

the API did not participate in any chemical reactions with the excipients. This is a corollary to the previous statement.

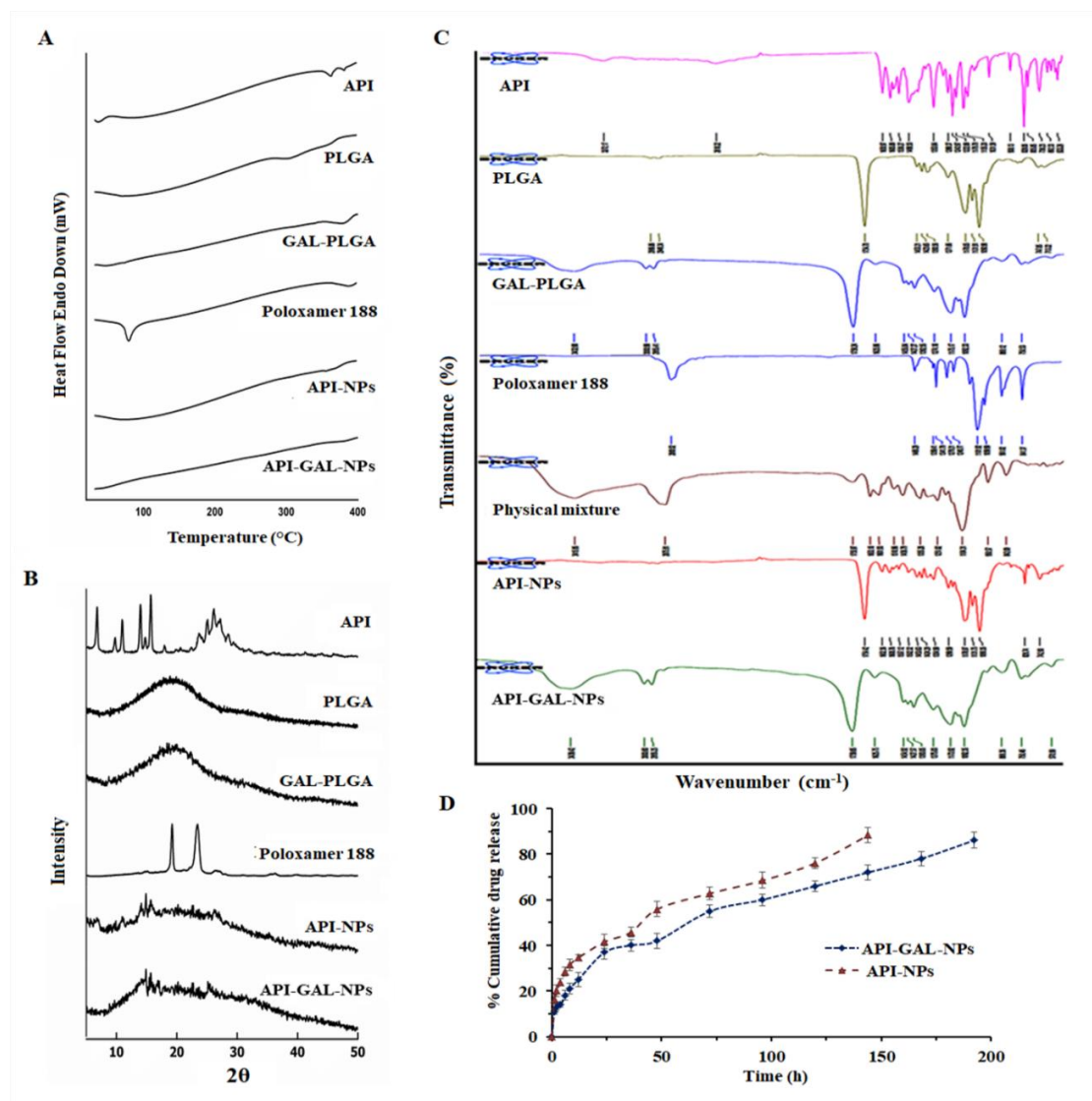


Figure 4.3. (A) DSC thermograms, (B) XRD diffractograms, and (C) FTIR spectra of API, PLGA, GAL-PLGA, POLOXAMER, API-NPs, and API-GAL-NPs. (D) *in vitro* drug release showing cumulative % of drug release of API-NPs and API-GAL-NPs.

4.3.6. *In vitro* drug release and kinetic study

In vitro drug release profile of nanoformulations revealed a biphasic release profile of the formulations as characterized by initial burst release followed by a slow and sustained drug release for about 8 days as depicted in Figure 4.3D. An initial burst release of API (at the end of 8 h) were \square 31.5 % from API-NPs and \square 21 % from API-GAL-NPs. At the end of 8 days, % cumulative drug releases were \square 88 and 86 % from API-NPs and API-GAL-NPs, respectively. When compared to API-NPs, API-GAL-NPs had a slower rate of API release. In addition, there was very little to no change between the drug release profiles of API-NPs and API-GAL-NPs, which indicates that galactosylation did not have any effect on the drug release profile. In addition, the drug release kinetic pattern was

analyzed using the zero-order, first-order, Korsmeyer-Peppas, and Higuchi kinetic models. There are a lot of different values of the regression coefficient (R^2) displayed for the different kinetic models. According to the findings, it would appear that the Higuchi kinetic model is the one that most accurately explains the linearity of both formulations ($R^2 = 0.991$ and 0.994 , respectively, for API-NPs and API-GAL-NPs). The fact that the Fickian drug release mechanism is indicated by the 'n' number in the Korsmeyer-Peppas equation suggests that both formulations share this characteristic.

Table 4.2. Data for various kinetic models for NPs obtained from in vitro drug release studies.

Kinetic models	API-NPs	API-GAL-NPs
Zero order	$y = 0.4904x + 22.323$ $R^2 = 0.8916$	$y = 0.3933x + 16.938$ $R^2 = 0.9251$
First Order	$y = -0.0051x + 1.9152$ $R^2 = 0.9557$	$y = -0.0038x + 1.9422$ $R^2 = 0.9796$
Higuchi	$y = 6.3439x + 9.6685$ $R^2 = 0.9914$	$y = 5.7969x + 3.9925$ $R^2 = 0.9943$
Korsmeyer-Peppas	$y = 0.327x + 1.1938$ $R^2 = 0.9795; n = 0.327$	$y = 0.4088x + 0.9708$ $R^2 = 0.988; n = 0.4088$

4.3.7. In vitro studies

4.3.7.1. Cellular uptake and internalization

The quantitative measurement of cellular uptake behavior of FITC-labelled galactose conjugated (FITC-GAL-NPs) and unconjugated (FITC-NPs) NPs by HepG2 cells were determined at different intervals (15, 30, 60, and 120 min) by flow cytometric analysis (Figure 4.4A and B). The internalization of galactosylated-NPs by the cells was significantly decreased in presence of excess galactose (Figure 4.4C). FITC-GAL-NPs exhibited favorably high cellular internalization relative to FITC-NPs at all the time points (Figure 4.4D). The decrease of internalization of galactosylated-NPs in presence of excess galactose may arise due to competitive inhibition of asialoglycoprotein receptors present on the surface of the HepG2 cells by the excess of galactose. Qualitative analysis by confocal microscopic studies also revealed that the intracellular fluorescence intensity of the cells treated with galactosylated-NPs was stronger than that treated with non-galactosylated one (Figure 4.4E). Thus, galactosylation enhances cellular internalization and may strengthen the biological activity of the formulation.

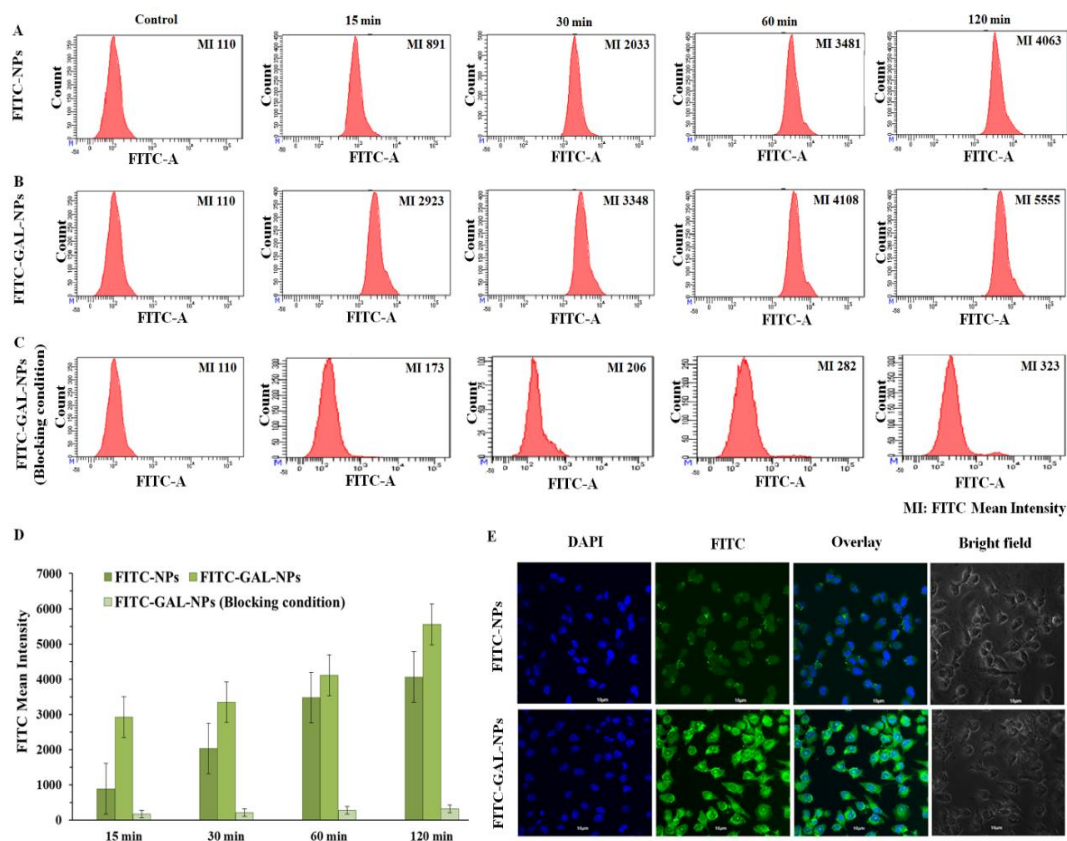


Figure 4.4. In vitro cellular uptake of galactosylated and non-galactosylated NPs in HepG2 cells at different time points. (A) Cellular uptake of FITC-NPs. (B) Cellular uptake of FITC-GAL-NPs. (C) Cellular uptake of FITC-GAL-NPs in the presence of galactose (blocking condition). (D) Histogram representing the cellular uptake of FITC-NPs, FITC-GAL-NPs, and FITC-GAL-NPs (blocking condition) at different time points.

Results are expressed as \pm SD ($n = 3$). (E) Confocal microscopic images representing cellular uptake of FITC-NPs and FITC-GAL-NPs in HepG2 cells at a time interval of 2 h. FITC exhibits green fluorescence and DAPI (nuclear stain) exhibits blue fluorescence.

4.3.7.2. MTT assay

The cytotoxic potentials of free API, API-NPs, and API-GAL-NPs were evaluated at two different time intervals (24 and 48 h) by MTT assay using HepG2-cells (Table 4.3). The concentrations of NPs were selected on the basis of API available to exert the anti-proliferative effect. In both cases API-GAL-NPs exhibited better cytotoxic potential than API-NPs and API-GAL-NPs. After 24 h of incubation, the IC₅₀ value of API-GAL-NPs ($37.1 \pm 3.4 \mu\text{M}$) was significantly ($p < 0.01$) lower than the IC₅₀ values of API-NPs ($77.2 \pm 6.4 \mu\text{M}$) and API ($130.2 \pm 8.9 \mu\text{M}$). The anti-proliferative effect was more pronounced after 48 h of incubation and the corresponding IC₅₀ values of API-GAL-NPs, API-NPs, and API were found to be 60.1 ± 7.1 , 40.2 ± 5.9 , and $15.9 \pm 4.8 \mu\text{M}$, respectively. Better cellular internalization of API-GAL-NPs increased cytotoxic behavior and may attribute better anticancer potential (Figure 4.5A).

Table 4.3. IC₅₀ values of free drug and NPs on HepG2 cells at different time intervals.

Time interval (Hours)	IC ₅₀ Conc. (μM)		
	API	API-NPs	API-GAL-NPs
24	130.2 ± 8.9	77.2 ± 6.4**	37.1 ± 3.4**,#
48	60.1 ± 7.1	40.2 ± 5.9*	15.9 ± 4.8**,#

Results are expressed as mean ± SD (n = 3). *Values significantly (p < 0.05) differed from API-treated group. **Values significantly (p < 0.01) differed from API-treated group. #Values significantly (p < 0.001) differed from API-treated group.

4.3.7.3. Apoptosis study

After treating HepG2 cells (IC₅₀ dosage for 24 h) with API, API-NPs, and API-GAL-NPs, we used a flow cytometric test to determine how effectively free API and each of the formulations induced apoptosis (Figure 4.5B). HepG2 cells subjected to API and showed 8.8% and 4.1% apoptotic cells in early and late phases, respectively. These values were relatively high with API-NPs treatment, which exhibited 22.5% and 10.9 % apoptotic cells at early and late phases, respectively. The apoptotic activity following API-GAL-NPs treatment was highest, which showed 27.9% and 11.3 % of apoptotic cells at early and late phases, respectively. Optimum particle size, sustained release of API from NPs, and promising cytotoxic effect might have resulted in higher apoptotic potentials of API-NPs, which was further intensified in API-GAL-NPs due to improved cellular penetration through asialoglycoprotein receptors.

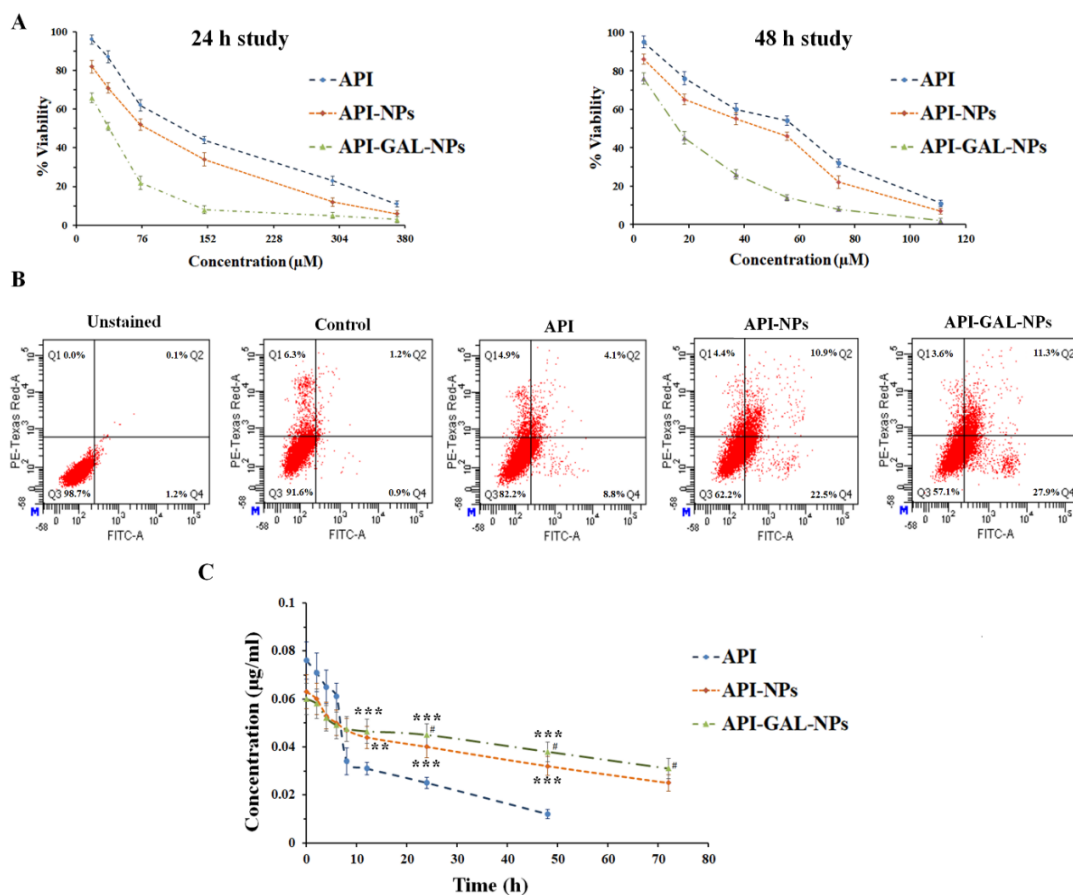


Figure 4.5. (A) Cytotoxic effect of API, API-NPs, and API-GAL-NPs on HepG2 cells at 24 and 48 h measured by MTT assay. (B) Apoptosis induction by API, API-NPs, and API-GAL-NPs to HepG2 cells measured by flow cytometry. (C) Plasma concentration-time profile of API at different time points following API, API-NPs, and API-GAL-NPs treatments. Results are expressed as \pm SD ($n = 3$). **Values significantly ($p < 0.01$) differed from API-treated group. ***Values significantly ($p < 0.001$) differed from API-treated group. #Values significantly ($p < 0.05$) differed from API-NPs-treated group.

4.3.8. Pharmacokinetic analysis

Pharmacokinetic analysis was executed to understand the plasma profile of the drug in experimental rats following treatment with API, API-NPs, and API-GAL-NPs (Table 4.4). Despite an initial high plasma level of API was seen in the free drug-treated group, it was rapidly eliminated (Figure 4.5C). In contrast, both the nanoformulations were capable to restore a steady plasma concentration of API up to 72 h (Figure 4.4C). At 48 h, plasma API concentration remained ~ 2.6 and 2.1 -fold ($p < 0.001$) high in API-GAL-NPs and API-NPs-treated animals as compared to free drug-treated group, respectively. Elimination half-life ($t_{1/2}$) and AUC_{0-t} values of API-GAL-NPs were found to be significantly ($p < 0.001$) higher than API-NPs. Similarly, MRT value of API-GAL-NPs increased by ~ 1.27 -fold ($p < 0.001$) than the value for API-NPs. Drug clearance of API-GAL-NPs is decreased by ~ 1.33 -fold ($p < 0.001$) as compared to API-NPs. All these

parameters indicate that API-GAL-NPs maintained a steady and significantly high level of API in the blood even up to 72 h and could provide better therapeutic efficacy than API and API-NPs.

Table 4.4. Pharmacokinetic data

Parameters	API	API-NPs	API-GAL-NPs
Elimination $t_{1/2}$ (h)	26.60 ± 1.203	70.79 ± 1.105***	92.28 ± 1.225***.#
C_{max} (µg/ml)	0.076 ± 0.0025	0.063 ± 0.0033***	0.060 ± 0.0027***.NS
AUC _{0-t} (µg/ml*h)	1.41 ± 0.051	2.67 ± 0.044***	2.99 ± 0.035***.#
AUC _{0-inf} (µg/ml*h)	1.87 ± 0.031	5.22 ± 0.025***	6.98 ± 0.035***.#
MRT _{0-inf} (h)	33.51 ± 2.114	100.88 ± 2.225***	128.75 ± 2.656***.#
Cl (mg/kg)/(µg/ml)/h	1.33 ± 0.027	0.48 ± 0.015***	0.36 ± 0.012***.#

Pharmacokinetic data where values represent mean ± SD (n =3). ***Values significantly (p < 0.001) differed from API-treated group. #Values significantly (p < 0.001) differed from API-treated group. NS: NS: Non-significant with respect to API-treated group.

4.3.9. Antitumor efficacy of NPs in vivo

4.3.9.1. Efficacy of NPs against DEN-induced HCC

Visible nodules were observed on the liver surface of all animals in DEN-treated group (HCC control), which signified the establishment of HCC in rats caused by DEN treatment. A large number of nodules was developed mostly at the edge of liver parenchyma (Figure 4.6).

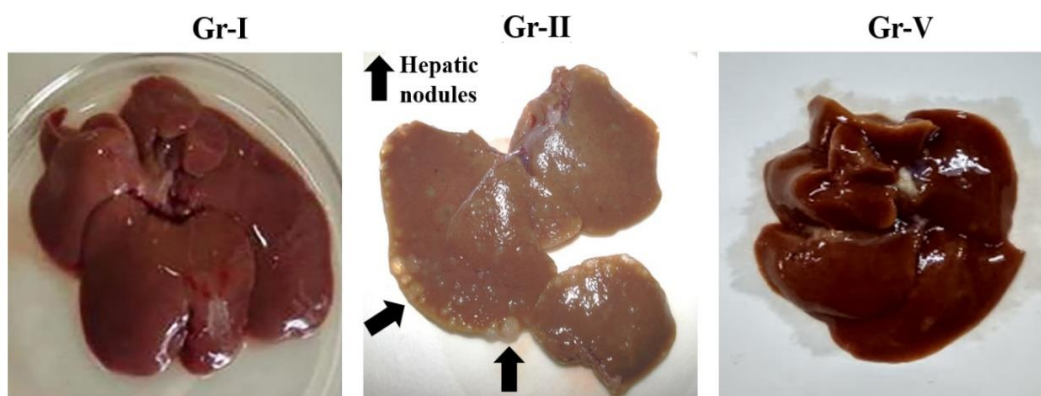


Figure 4.6. Images of the livers in experimental animals. Black arrows represent hepatic nodules developed due to DEN treatment in rat.

It was observed that the average number of nodules were significantly reduced in API-NPs (~1.43-fold; p < 0.01) and API-GAL-NPs (~3.43-fold; p < 0.001) in carcinogenic animals as compared to HCC control group (Table 4.5). However, no remarkable change in nodule number was noticed in API-treated animals. Relative liver weight (RLW) was increased in DEN-treated animals and it was significantly reduced in carcinogenic

animals treated with API-GAL-NPs (~1.32-fold; $p < 0.001$) and API-NPs (~ 1.15-fold; $p < 0.05$) as compared to HCC control rats (Table 4.5).

Table 4.5. Effect of API in free and NP forms on relative liver weight and hepatic nodules in DEN induced hepatocarcinogenic rats.

Experimental groups	Relative liver weight (%) [§]	Total number of hepatic nodules
Gr-I	3.21 ± 0.21	-
Gr-II	4.66 ± 0.52 [#]	79.22 ± 11.50 [#]
Gr-III	4.41 ± 0.16 ^{NS}	82.14 ± 23.24 ^{NS}
Gr-IV	4.04 ± 0.66 [*]	54.78 ± 8.21 ^{**}
Gr-V	3.52 ± 0.32 ^{***}	23.11 ± 4.22 ^{***}

Results are expressed as mean ± SD (n = 5). [#]Values significantly ($p < 0.001$) differed from Gr-I. ^{*}Values significantly ($p < 0.05$) differed from Gr-II. ^{**}Values significantly ($p < 0.01$) differed from Gr-II. ^{***}Values significantly ($p < 0.001$) differed from Gr-II. NS: Non-significant with respect to Gr-II. [§]Relative liver weight = (Liver weight/Final body weight) x 100.

Serum ALP, ALT and AST levels were significantly increased in HCC control animals as compared to normal control group (Table 4.6). However, treatment with API-NPs ($p < 0.01$) and API-GAL-NPs ($p < 0.001$) to carcinogenic rats significantly reduced and ALK, AST, and ALT levels in sera as compared to HCC control animals (Table 4.6). API-treatment though reduced serum ALK, AST, and ALT levels; however, changes remained insignificant as compared to DEN-treated animals (Table 4.6).

Table 4.6. Effect of API and nanoparticulated API on serum enzyme parameters

Parameters	Gr-I	Gr-II	Gr-III	Gr-IV	Gr-V
ALP (KA units)	20.22 ± 1.82	112.04 ± 4.46 [#]	107.09 ± 6.68 ^{NS}	71.01 ± 2.12 ^{**}	32.14 ± 1.14 ^{***}
AST (IU/l)	70.14 ± 2.11	354.92 ± 8.86 [#]	346.50 ± 9.13 ^{NS}	212.33 ± 4.89 ^{**}	86.54 ± 0.65 ^{***}
ALT (IU/l)	30.89 ± 1.65	165.44 ± 9.55 [#]	156.21 ± 7.96 ^{NS}	79.67 ± 2.39 ^{**}	42.37 ± 2.22 ^{***}

Results are expressed as mean ± SD (n = 5). [#]Values significantly ($p < 0.001$) differed from Gr-I. ^{**}Values significantly ($p < 0.01$) differed from Gr-II. ^{***}Values significantly ($p < 0.001$) differed from Gr-II. NS: Non-significant.

4.3.9.2. Histopathological analysis

The effects of API, API-NPs, and API-GAL-NPs on DEN-induced HCC in rats was examined by the histopathological investigation. Haematoxylin-eosin-stained liver

sections collected from the normal control animals (Gr-I) exhibited normal hepatocytes arranged in the cords and the portal tracts also appeared normal.

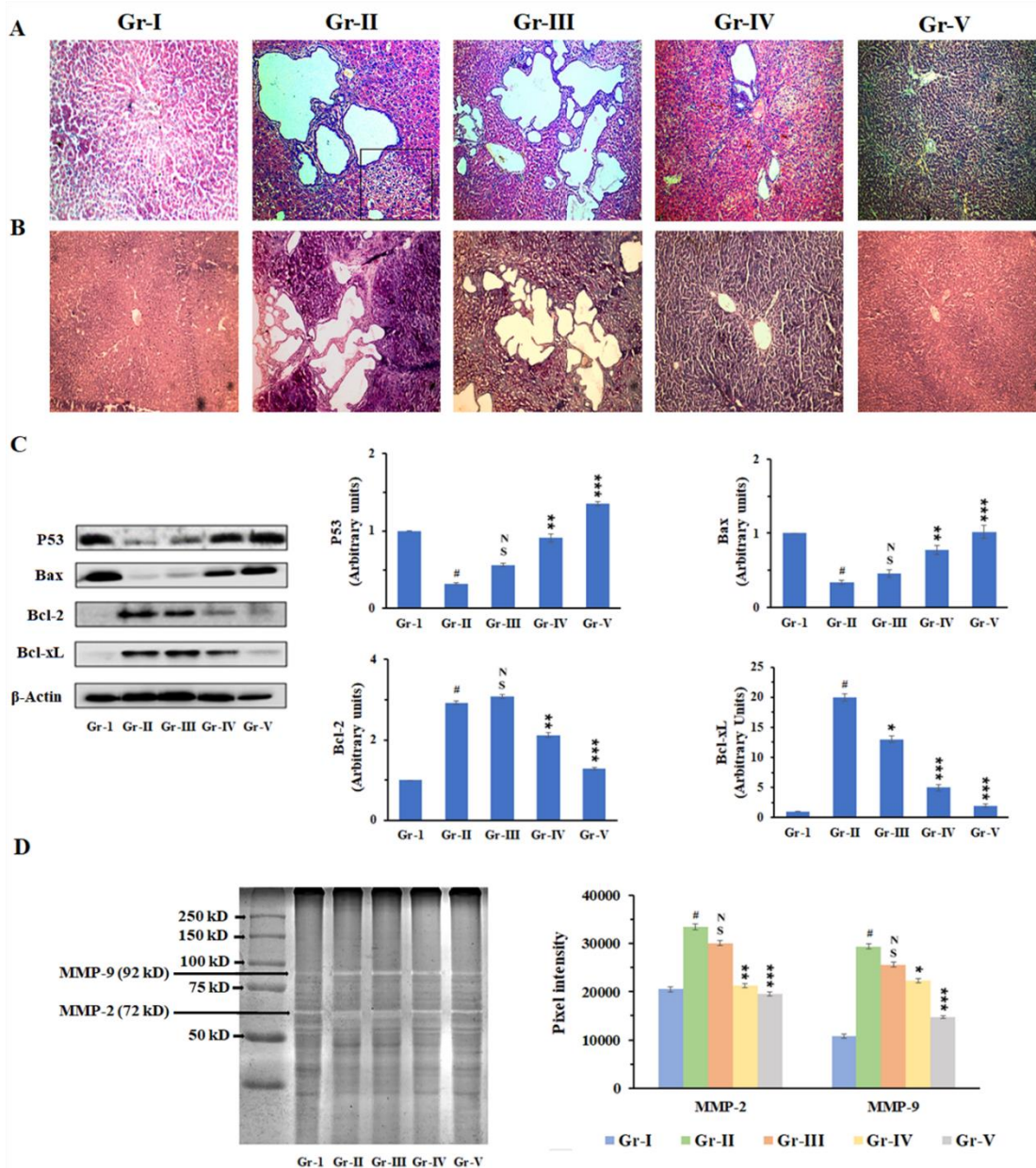


Figure 4.7. (A) Representative photomicrographs of haematoxylin-eosin-stained liver section. (B) Representative photomicrographs of PAS-stained liver section. (C) Western blot analysis expression of different apoptotic proteins and histogram showing their relative expressions in the liver. β -Actin served as a loading control protein. The intensity of the normal control band was assigned 1 (D) Zymogram and histogram showing the effect on MMP-9 and MMP-2 in the liver. Results are expressed as \pm SD ($n = 5$). #Values significantly ($p < 0.001$) differed from Gr-I. **Values significantly ($p < 0.01$) differed from Gr-II. ***Values significantly ($p < 0.001$) differed from Gr-II. NS: Non-significant.

The liver section collected from HCC animals (Gr-II) exhibited scattered lesions with cells of ground-glass opacity, dilated hepatic veins, and loss of normal hepatic

architecture (Figure 4.7A). Cells with the pyknotic nucleus and multinucleated hepatocytes were observed in the HCC control group (Gr-II) with respect to Gr-I. No distinguishable change was observed in the liver sections of API-treated carcinogenic rats (Figure 4.7A). API-NPs treatment in carcinogenic rats demonstrated some improvement in liver architecture and structural integrity; however, dilated hepatic veins and lesions were still evident (Figure 4.7A). In contrast, API-GAL-NPs treatment in carcinogenic rats resulted in perceptible recovery in the liver architecture showing increased cell density with escalated eosinophilic staining and more defined cord structure. Significant reduction in hepatic lesions and abnormal cells was observed in the API-GAL-NPs-treated group (Figure 4.7A). No PAS-positive cells appeared in the PAS-stained liver section collected from normal rats (Gr-I) (Figure 4.7B). However, the liver sample collected from HCC control rats showed an appreciable extent of PAS-positive reaction; whereas, adjacent pale staining of centrilobular hepatocytes indicated an ischemia/reperfusion injury (Figure 4.7B). Free API treatment did not have much effect as the staining intensity was not reduced (Figure 4.7B). API-NPs-treated group (IV) exhibited better results than the free drug-treated group evidenced by the reduction of PAS-positive cells and nodules (Figure 4.7B). API-GAL-NPs treatment in carcinogenic rats caused a significant reduction in the intensity of PAS-positive staining in the cytoplasm with a concomitant reduction in pre-neoplastic nodules, which signified that API-GAL-NPs exhibited better curative effect over API-NPs against HCC in rats (Figure 4.7B).

4.3.9.3. Western blot analysis of apoptosis markers

The therapeutic efficacy of API-GAL-NPs against DEN-induced HCC was further estimated by studying the signaling events involved in apoptotic pathways (Figure 4.7C). In this experiment, a prominent downregulation ($p < 0.001$) was noticed in the expression of P53 and Bax proteins in the livers of HCC control animals. In contrast, API-NPs ($p < 0.01$) and API-GAL-NPs ($p < 0.001$) treatments to carcinogenic rats significantly activated P53 and Bax expression in the liver as compared to HCC control rats. No significant change was seen in the expression of either of the proteins in the liver of API-treated carcinogenic rats. In search of the effects on anti-apoptotic factors, the expressions of Bcl-2 and Bcl-xL were studied in the liver of rats that received different therapy. HCC control animals exhibited significant upregulation ($p < 0.001$) in the expression of Bcl-2 and Bcl-xL in the liver. In contrast, API-NPs ($p < 0.01-0.001$) and API-GAL-NPs ($p < 0.001$) treatments significantly reduced Bcl-2 and Bcl-xL expressions in the liver of carcinogenic animals. API treatment could only suppress ($p < 0.05$) Bcl-xL expressions in

carcinogenic rats. The expression analyses of the apoptotic factors clearly indicated that API-GAL-NPs could induce apoptosis more intensively than API-NPs.

4.3.9.4. Gelatin zymography analysis

Gelatin zymography analysis of liver tissue (Figure 4.7C) exhibited significant downregulation of the expression of MMP-2 ($p < 0.01-0.001$) and MMP-9 ($p < 0.05-0.001$) in API-NPs and API-GAL-NPs treated carcinogenic rats as compared to HCC control animals. However, API-GAL-NPs treatment caused ~1.1 and 1.5-fold intense reduction in hepatic MMP-2 and MMP-9 levels as compared to API-NPs treated group (IV).

4.3.9.5. Evaluation of hepatoprotective efficacy by scintigraphic imaging analysis

The mechanistic evaluations stated above suggested the potential efficacy of API-GAL-NPs to treat DEN-induced HCC in rats, which could be further corroborated with scintigraphic imaging analysis.

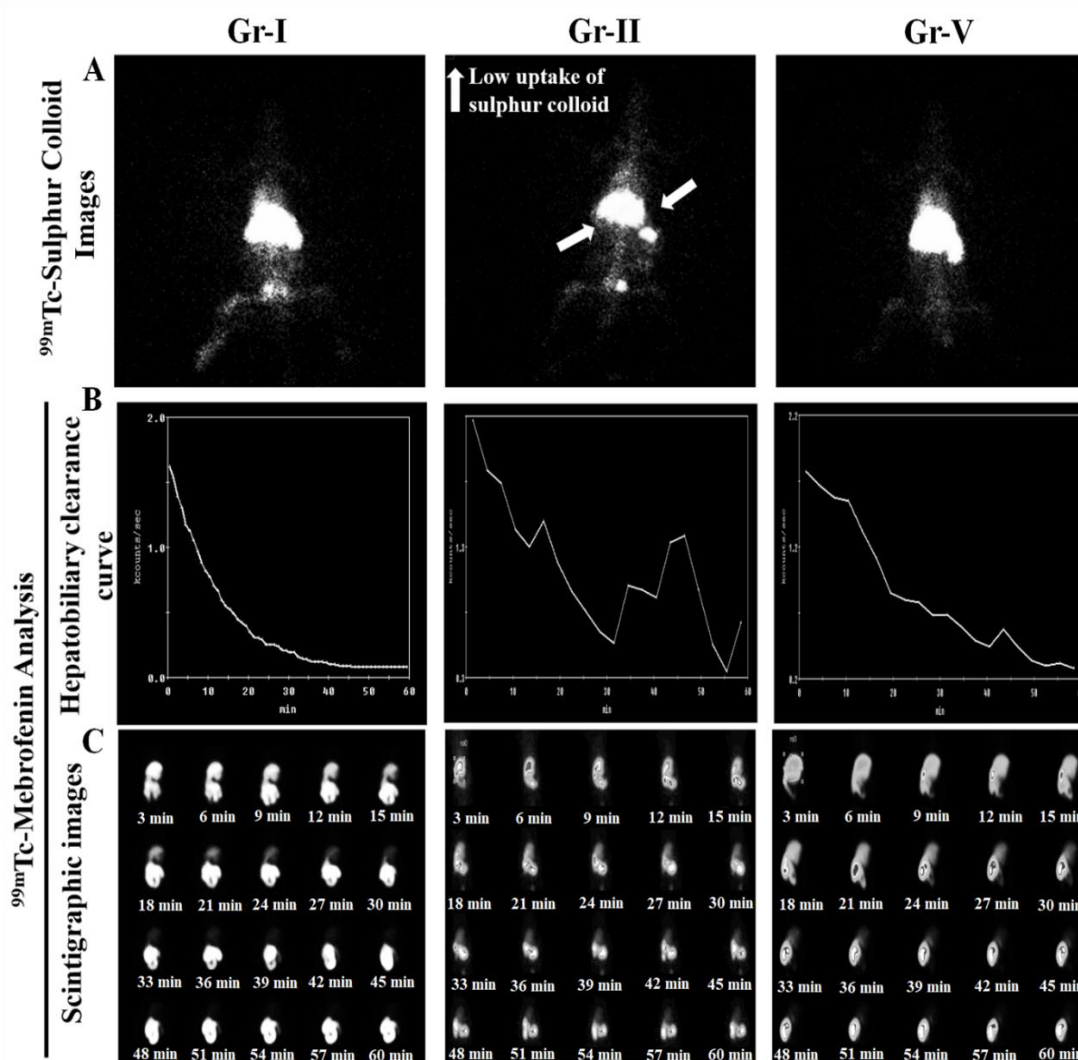


Figure 4.8. Nuclear scintigraphic image analyses of normal (Gr-I), HCC control (Gr-II), and API-GAL-NPs-treated rats (Gr-V). (A) Representative scintigraphic images of

^{99m}Tc-sulphur colloid acquired at 1 h post-injection. (B) Representative hepatobiliary clearance curves of ^{99m}Tc-mebrofenin. (C) Representative scintigraphic images at different post-injection time periods of ^{99m}Tc-mebrofenin. White arrows represented areas of low uptake of sulphur colloids.

The function of hepatic RES was qualitatively assessed using a ^{99m}Tc-labeled sulphur colloid imaging protocol. The anterior view of the scinti-photos revealed that uniform distribution of ^{99m}Tc-sulphur colloid in the liver of normal control animals (Gr-I) indicating good functioning of RES (Figure 4.8A). In contrast, hepatic distribution was discontinuous in HCC control animals (Gr-II) (Figure 4.8A). However, API-GAL-NPs treatment significantly reciprocated hepatic distribution in carcinogenic animals (Gr-V), which signified that RES function could have recovered with API-GAL-NPs treatment (Figure 4.8A). The liver function of the normal, HCC control, and API-GAL-NPs-treated group were also monitored non-invasively by nuclear scintigraphy approach using ^{99m}Tc-labeled mebrofenin. The normal group exhibited immediate liver accumulation following injection of ^{99m}Tc-labeled mebrofenin and rapid excretion. The sharp rise and fall were observed in the curve as generated from the instrument (Figure 4.8B). The nature of the curve was very irregular in HCC control (Gr-II) group representing slow and erratic uptake with sluggish excretion (Figure 4.8B). However, these irregularities in uptake and excretion were relatively reversed following treatment with API-GAL-NPs to carcinogenic animals (Figure 4.8B). The serial images of liver uptake and subsequent clearance for a period of 1 h at 3 min interval was also depicted in Figure 4.8C.

4.4. Discussion

Emerging evidence highlighted the chemo-preventive role of API against various types of cancer including HCC (Imran et al., 2020; Rodríguez-García et al., 2019). It exerts anticancer effects on human liver cancer cells by inhibiting cell growth, arresting cell cycle, and inducing apoptosis without imparting any toxic manifestation to normal liver cells (Chiang et al., 2006). However, a gap exists between in vitro and in vivo observations. Poor solubility in both aqueous and non-aqueous solvents, high metabolic transformation, and high inter-individual variability limit its in vivo effectiveness (Dewanjee et al., 2020). Thus, a much higher in vivo dosing of API is required to achieve a therapeutic effect against HCC in preclinical assays (Singh et al., 2004; Jeyabal et al., 2005). In this aspect, nanoformulation of API can stand as a solution to improve its therapeutic efficacy. Our recent observations showed that API-loaded PLGA NPs can improve the chemopreventive efficacy of API in a murine model of HCC (Bhattacharya et al., 2018), which encouraged us to fabricate API-PLGA-NPs to achieve better therapeutic efficacy of API via active targeting to the liver tissues. Galactose conjugation to NP surface can improve liver targeting as galactose is actively taken up by asialoglycoprotein

receptors which are abundant on the hepatic parenchymal cells (Peça et al., 2012). In this study, we aimed to prepare galactose-tailored API-NPs to improve the therapeutic efficacy of API-NPs against HCC by improving site (liver) specificity.

To prepare galactosylated API-loaded polymeric NPs, polymer (PLGA) was galactosylated by simple esterification reaction (Peça et al., 2012). Galactose conjugation was confirmed by ¹H-NMR spectroscopy (Peça et al., 2012). The galactosylated-PLGA was used to formulate API-loaded galactosylated polymeric NPs by nanoprecipitation technique using poloxamer 188 as a surfactant. In selecting surfactant, poloxamer 188, polyvinyl alcohol, and vitamin E-TPGS were initially tried; however, poloxamer 188 stood optimum and included in this formulation. DSC thermograms, XRD diffractograms, and FTIR spectra indicated that no chemical reaction occurs between API and excipients; however, some physical interactions and changes in physical form (crystalline to amorphous) might be involved in the formation of NPs. API-GAL-NPs were designed to have a spherical shape, a smooth surface, and an average diameter of 129 nm after they were finished. They have a low PDI value, which demonstrates that API-GAL-NPs are made up of particles of a consistent size (Bhattacharya, et al., 2018). As the API-GAL-NPs' zeta potential of -14.0 mV was found to be within the permitted range (-30 mV to +30 mV), it was assumed that the particles would not settle down quickly following intravenous injection. (Bhattacharya, et al., 2018). When kept at a temperature of 4°C, API-GAL-NPs had a drug loading of 5.3% weight-per-weight (w/w), and the NPs were stable for at least 90 days. API-GAL-NPs, demonstrated a considerable amount of API to be released in a short period of time (21% within 8 hours), followed by a cumulative amount of 86% being released in 8 days. The presence of API on the surface of the NPs may result in a quick release of drug at the beginning, whereas the incorporation of drug into the core of the NPs enables a regulated release of drug over the course of time (Das et al., 2015). The diffusion of the drug from the API-GAL-NPs followed the Higuchi kinetics with a high degree of linearity (as determined by the R² values), while the release of API exhibited Fickian behaviour.

FITC-labeled API-GAL-NPs exhibited better cellular uptake by HepG2 cells compared to API and API-NPs. Galactosylation might facilitate intracellular uptake through asialoglycoprotein receptors present on the surface of HepG2 cells (Peça et al., 2012). This has been verified by blocking studies. Asialoglycoprotein receptor-mediated active targeting improved cytotoxic and apoptotic effects of API-GAL-NPs to HepG2 cells over API-NPs. All these findings suggest that improved internalization of API by HCC cells from API-GAL-NPs would potentiate its chemotherapeutic efficacy to combat HCC in vivo. In this report, the in vivo anticancer potential of API-GAL-NPs was compared with

API and API-NPs in DEN-induced HCC in rats. DEN-induced HCC is a well-established murine model of liver carcinoma (Tolba et al., 2015). API-GAL-NPs treatment to carcinogenic rats more effectively reduced the number of nodules and RLW than API-NPs. A gross reduction of nodule number and RLW signifies low incidence of HCC development and/or chemotherapeutic potential of API-GAL-NPs against HCC in rats (Bhattacharya, et al., 2018). Emerging evidence revealed that an increased risk of HCC is conferred by the increased levels of AST, ALT, and ALP in sera (Hann et al, 2012). In this study, HCC control rats exhibited significant elevation in the levels of AST, ALT, and ALP as compared to normal. In contrast, API-NPs and API-GAL-NPs both could significantly reciprocate AST, ALT, and ALP levels in sera of carcinogenic rats; however, API-GAL-NPs exhibited better therapeutic efficacy. Histological examination revealed that API-GAL-NPs could significantly reduce hepatic lesions, abnormal cells, and glycogen deposition in liver and restore hepatic architecture to near-normal status. API-NPs also ameliorated the tissue structure; however, it was not to the expanse of API-GAL-NPs-mediated improvement.

Induction of apoptosis is a primary requirement in chemotherapy (Chakraborty et al., 2020). Bcl-2 family proteins regulate apoptosis through a complex interplay between pro-apoptotic and anti-apoptotic proteins. Pro-apoptotic factors, such as Bax protein promotes apoptosis through mitochondrial stress (Das et al., 2018). In contrast, anti-apoptotic factors of Bcl-2 family, such as Bcl-2 and Bcl-xL inhibit apoptosis via binding to pro-apoptotic proteins (Das et al., 2018). P53, a tumor suppressor protein, can impart pro-apoptotic role and can arrest cell cycle (Das et al., 2018; Aubrey et al., 2018; Takagaki et al., 2005). Emerging evidence established the cross-talk between P53 and Bcl-2 family proteins in human HCC (Chiu et al., 2003). In this study, immunoblotting showed that API-GAL-NPs treatment to carcinogenic animals significantly activated the expression of pro-apoptotic factors (P53 and Bax) and suppressed anti-apoptotic factors (Bcl-2 and Bcl-xL), which signifies induction of apoptosis to the liver in HCC bearing animals. API-NPs also induced apoptosis to the liver of carcinogenic animals, but the extent was much less as compared to API-Gal-NPs. MMP-2 and MMP-9 are involved in epithelial-mesenchymal transition of HCC and play important role in disease progression (Scheau et al., 2019). Gelatin zymography showed that significant up-regulation of MMP-2 and MMP-9 in the livers of DEN-treated rats, which signifies the progression of HCC in rats. In contrast, API-GAL-NPs treatment to carcinogenic animals prevented HCC progression by reducing the levels of MMP-2 and MMP-9 in the livers. API-NPs also reduced hepatic MMP-2 and MMP-9 in carcinogenic animals; however, the extent was much less as compared to API-GAL-NPs. Hepatoprotective efficacy of the nano-formulations was also

evaluated non-invasively by nuclear scintigraphic analyses using ^{99m}Tc-sulphur colloid and ^{99m}Tc-mebrofenin. ^{99m}Tc scintigraphy is a routinely used technique to study hepatobiliary function (Al-Saeedi et al., 2011). In this study, HCC control rats exhibited significant disruption in hepatobiliary function. In contrast, API-GAL-NPs treatment to significantly attenuated hepatocellular degeneration and restored hepatobiliary function to near normal status as observed in both qualitative and quantitative scintigraphic analyses. Apigenin is a naturally occurring molecule with exciting anticancer potential against HCC. However, poor pharmacokinetic and biopharmaceutical features reduce its in vivo therapeutic effect. Earlier report revealed that API-NPs exhibited improved chemotherapeutic effect against HCC over free API via improving pharmacokinetic and biopharmaceutical attributes. In this study, galactose tailoring to API-NPs caused further improvement in therapeutic efficacy over API-NPs, which has been shown to be mediated through active targeting and improved internalization of API by HCC cells. In conclusion, API-GAL-NPs may serve as a novel drug delivery with improved therapeutic efficacy achieved by active liver targeting in the management of HCC in the future.

References

- Abbas Z, Rehman S. An overview of cancer treatment modalities. *Neoplasms*. 2018; 1:139-157. doi: 10.5772/intechopen.76558.
- Abd-Allah WE, Awad HM, AbdelMohsen MM. HPLC analysis of quercetin and antimicrobial activity of comparative methanol extracts of *Shinus molle* L. *Int. J. Curr. Microbiol. Appl. Sci.* 2015;4:550-558.
- Abdel-Hamid NM, Abass SA, Mohamed AA, Muneam Hamid D. Herbal management of hepatocellular carcinoma through cutting the pathways of the common risk factors. *Biomed Pharmacother.* 2018;107:1246-1258. doi: 10.1016/j.biopha.2018.08.104.
- Abdelwahab NS, Morsi A, Ahmed YM, Hassan HM, AboulMagd AM. Ecological HPLC method for analyzing an antidiabetic drug in real rat plasma samples and studying the effects of concurrently administered fenugreek extract on its pharmacokinetics. *RSC Adv.* 2021;11(8):4740-4750. doi: 10.1039/d0ra08836f.
- Abo-Salem OM, Abd-Ellah MF, Ghonaim MM. Hepatoprotective activity of quercetin against acrylonitrile-induced hepatotoxicity in rats. *J Biochem Mol Toxicol.* 2011;25(6):386-392. doi: 10.1002/jbt.20406.
- Acharya S, Sahoo SK. PLGA nanoparticles containing various anticancer agents and tumour delivery by EPR effect. *Adv Drug Deliv Rev.* 2011;63(3):170-183. doi: 10.1016/j.addr.2010.10.008.
- Aherne SA, O'Brien NM. Protection by the flavonoids myricetin, quercetin, and rutin against hydrogen peroxide-induced DNA damage in Caco-2 and Hep G2 cells. *Nutr Cancer.* 1999;34(2):160-166. doi: 10.1207/S15327914NC3402_6.
- Ajazuddin, Saraf S. Applications of novel drug delivery system for herbal formulations. *Fitoterapia.* 2010;81(7):680-689. doi: 10.1016/j.fitote.2010.05.001.
- Akyuz E, Paudel YN, Polat AK, Dundar HE, Angelopoulou E. Enlightening the neuroprotective effect of quercetin in epilepsy: From mechanism to therapeutic opportunities. *Epilepsy Behav.* 2021;115:107701. doi: 10.1016/j.yebeh.2020.107701.
- Alam J, Dilnawaz F, Sahoo SK, Singh DV, Mukhopadhyay AK, Hussain T, Pati S. Curcumin Encapsulated into Biocompatible Co-Polymer PLGA Nanoparticle Enhanced Anti-Gastric Cancer and Anti-Helicobacter Pylori Effect. *Asian Pac J Cancer Prev.* 2022;23(1):61-70. doi: 10.31557/APJCP.2022.23.1.61.
- Al-Amarat W, Abukhalil MH, Alruhaimi RS, Alqhtani HA, Aldawood N, Alfwuaires MA, Althunibat OY, Aladaileh SH, Algefare AI, Alanezi AA, AbouEl-Ezz AM, Ahmeda

References

- AF, Mahmoud AM. Upregulation of Nrf2/HO-1 Signaling and Attenuation of Oxidative Stress, Inflammation, and Cell Death Mediate the Protective Effect of Apigenin against Cyclophosphamide Hepatotoxicity. *Metabolites*. 2022;12(7):648. doi: 10.3390/metabo12070648.
- Alasmari AF. Cardioprotective and nephroprotective effects of quercetin against different toxic agents. *Eur. Rev. Med. Pharmacol. Sci.* 2021; 25:7425-7439. doi: 10.26355/eurrev_202112_27440.
- Alfaleh MA, Hashem AM, Abujamel TS, Alhakamy NA, Kalam MA, Riadi Y, Md S. Apigenin Loaded Lipoid-PLGA-TPGS Nanoparticles for Colon Cancer Therapy: Characterization, Sustained Release, Cytotoxicity, and Apoptosis Pathways. *Polymers (Basel)*. 2022 ;14(17):3577. doi: 10.3390/polym14173577.
- Ali F, Rahul, Naz F, Jyoti S, Siddique YH. Health functionality of apigenin: A review. *International Journal of Food Properties*. 2017;20(6):1197-1238. doi: 10.1080/10942912.2016.1207188.
- Ali F, Rahul, Naz F, Jyoti S, Siddique YH. Protective effect of apigenin against N-nitrosodiethylamine (NDEA)-induced hepatotoxicity in albino rats. *Mutat Res Genet Toxicol Environ Mutagen*. 2014;767:13-20. doi: 10.1016/j.mrgentox.2014.04.006.
- Ali M, Khan T, Fatima K, Ali QUA, Ovais M, Khalil AT, Ullah I, Raza A, Shinwari ZK, Idrees M. Selected hepatoprotective herbal medicines: Evidence from ethnomedicinal applications, animal models, and possible mechanism of actions. *Phytother Res*. 2018; 32(2):199-215. doi: 10.1002/ptr.5957.
- Allahyari M, Mohit E. Peptide/protein vaccine delivery system based on PLGA particles. *Hum Vaccin Immunother*. 2016;12(3):806-828. doi: 10.1080/21645515.2015.1102804.
- Al-Nemrawi NK, Altawabeyeh RM, Darweesh RS. Preparation and Characterization of Docetaxel-PLGA Nanoparticles Coated with Folic Acid-chitosan Conjugate for Cancer Treatment. *J Pharm Sci*. 2022;111(2):485-494. doi: 10.1016/j.xphs.2021.10.034.
- Alonso-González M, Fernández-Carballido A, Quispe-Chauca P, Lozza I, Martín-Sabroso C, Isabel Fraguas-Sánchez A. DoE-based development of celecoxib loaded PLGA nanoparticles: In ovo assessment of its antiangiogenic effect. *Eur J Pharm Biopharm*. 2022;180:149-160. doi: 10.1016/j.ejpb.2022.09.022.
- Al-Otaibi AM, Al-Gebaly AS, Almeer R, Albasher G, Al-Qahtani WS, Abdel Moneim AE. Potential of green-synthesized selenium nanoparticles using apigenin in human

- breast cancer MCF-7 cells. *Environ Sci Pollut Res Int.* 2022;29(31):47539-47548. doi: 10.1007/s11356-022-19166-2.
- Al-Saeedi F, Loutfi I. (99m)Tc sulfur colloid and (99m)Tc mebrofenin hepatobiliary functional liver imaging in normal and diabetic rats. *Med Princ Pract.* 2011;20(2):129-132. doi: 10.1159/000321216.
- Alvarez-Arellano L, Salazar-García M, Corona JC. Neuroprotective Effects of Quercetin in Pediatric Neurological Diseases. *Molecules.* 2020;25(23):5597. doi: 10.3390/molecules25235597.
- Anand David AV, Arulmoli R, Parasuraman S. Overviews of Biological Importance of Quercetin: A Bioactive Flavonoid. *Pharmacogn Rev.* 2016;10(20):84-89. doi: 10.4103/0973-7847.194044.
- Ansari P, Choudhury ST, Seidel V, Rahman AB, Aziz MA, Richi AE, Rahman A, Jafrin UH, Hannan JMA, Abdel-Wahab YHA. Therapeutic Potential of Quercetin in the Management of Type-2 Diabetes Mellitus. *Life (Basel).* 2022;12(8):1146. doi: 10.3390/life12081146.
- Ansari SH, Islam F, Sameem M. Influence of nanotechnology on herbal drugs: A Review. *J Adv Pharm Technol Res.* 2012;3(3):142-146. doi: 10.4103/2231-4040.101006.
- Anwer MK, Al-Mansoor MA, Jamil S, Al-Shdefat R, Ansari MN, Shakeel F. Development and evaluation of PLGA polymer-based nanoparticles of quercetin. *Int J Biol Macromol.* 2016;92:213-219. doi: 10.1016/j.ijbiomac.2016.07.002.
- Arroyave-Ospina JC, Wu Z, Geng Y, Moshage H. Role of Oxidative Stress in the Pathogenesis of Non-Alcoholic Fatty Liver Disease: Implications for Prevention and Therapy. *Antioxidants (Basel).* 2021;10(2):174. doi: 10.3390/antiox10020174.
- Arul D, Subramanian P. Inhibitory effect of naringenin (citrus flavonone) on N-nitrosodiethylamine induced hepatocarcinogenesis in rats. *Biochem Biophys Res Commun.* 2013;434(2):203-209. doi: 10.1016/j.bbrc.2013.03.039.
- Ashrafizadeh M, Bakhoda MR, Bahmanpour Z, Ilkhani K, Zarrabi A, Makvandi P, Khan H, Mazaheri S, Darvish M, Mirzaei H. Apigenin as Tumor Suppressor in Cancers: Biotherapeutic Activity, Nano delivery, and Mechanisms with Emphasis on Pancreatic Cancer. *Front Chem.* 2020;8:829. doi: 10.3389/fchem.2020.00829.

References

- Aubrey BJ, Kelly GL, Janic A, Herold MJ, Strasser A. How does p53 induce apoptosis and how does this relate to p53-mediated tumour suppression? *Cell Death Differ.* 2018;25(1):104-113. doi: 10.1038/cdd.2017.169.
- Badawi NM, Attia YM, El-Kersh DM, Hammam OA, Khalifa MKA. Investigating the Impact of Optimized Trans-Cinnamic Acid-Loaded PLGA Nanoparticles on Epithelial to Mesenchymal Transition in Breast Cancer. *Int J Nanomedicine.* 2022;17:733-750. doi: 10.2147/IJN.S345870.
- Badhwar R, Mangla B, Neupane YR, Khanna K, Popli H. Quercetin loaded silver nanoparticles in hydrogel matrices for diabetic wound healing. *Nanotechnology.* 2021;32(50):505102. doi: 10.1088/1361-6528/ac2536.
- Bai H, Wu H, Zhang L, Sun P, Liu Y, Xie B, Zhang C, Wei S, Wang W, Li J. Adventitial injection of HA/SA hydrogel loaded with PLGA rapamycin nanoparticle inhibits neointimal hyperplasia in a rat aortic wire injury model. *Drug Deliv Transl Res.* 2022;12(12):2950-2959. doi: 10.1007/s13346-022-01158-x.
- Baishya R, Nayak DK, Kumar D, Sinha S, Gupta A, Ganguly S, Debnath MC. Ursolic Acid Loaded PLGA Nanoparticles: in vitro and in vivo Evaluation to Explore Tumor Targeting Ability on B16F10 Melanoma Cell Lines. *Pharm Res.* 2016;33(11):2691-2703. doi: 10.1007/s11095-016-1994-1.
- Baky MH, Elshahed M, Wessjohann L, Farag MA. Interactions between dietary flavonoids and the gut microbiome: a comprehensive review. *Br J Nutr.* 2022;128(4):577-591. doi: 10.1017/S0007114521003627.
- Bala I, Hariharan S, Kumar MN. PLGA nanoparticles in drug delivery: the state of the art. *Crit Rev Ther Drug Carrier Syst.* 2004;21(5):387-422. doi: 10.1615/critrevtherdrugcarriersyst.v21.i5.20.
- Balakumar K, Raghavan CV, Selvan NT, Prasad RH, Abdu S. Self-nanoemulsifying drug delivery system (SNEDDS) of rosuvastatin calcium: design, formulation, bioavailability and pharmacokinetic evaluation. *Colloids Surf B Biointerfaces.* 2013;112:337-343. doi: 10.1016/j.colsurfb.2013.08.025.
- Balamurugan K, Karthikeyan J. Evaluation of Luteolin in the Prevention of N-nitrosodiethylamine-induced Hepatocellular Carcinoma Using Animal Model System. *Indian J Clin Biochem.* 2012; 27(2):157-163. doi: 10.1007/s12291-011-0166-7.
- Balez R, Steiner N, Engel M, Muñoz SS, Lum JS, Wu Y, Wang D, Vallotton P, Sachdev P, O'Connor M, Sidhu K, Münch G, Ooi L. Neuroprotective effects of apigenin against

inflammation, neuronal excitability and apoptosis in an induced pluripotent stem cell model of Alzheimer's disease. *Sci Rep.* 2016;6:31450. doi: 10.1038/srep31450.

Baran M, Yay A, Onder GO, Canturk Tan F, Yalcin B, Balcioglu E, Yıldız OG. Hepatotoxicity and renal toxicity induced by radiation and the protective effect of quercetin in male albino rats. *Int J Radiat Biol.* 2022;98(9):1473-1483. doi: 10.1080/09553002.2022.2033339.

Bashir SO. Hepatoprotective role for quercetin in diabetic rats: hypolipidemic and antioxidant effects. *Med. J. Cairo. Univ.* 2014; 82:169-178.

Bataller R, Brenner DA. Liver fibrosis. *J Clin Invest.* 2005;115(2):209-218. doi: 10.1172/JCI24282.

Begines B, Ortiz T, Pérez-Aranda M, Martínez G, Merinero M, Argüelles-Arias F, Alcudia A. Polymeric Nanoparticles for Drug Delivery: Recent Developments and Future Prospects. *Nanomaterials (Basel).* 2020;10(7):1403. doi: 10.3390/nano10071403.

Berman DS, Hachamovitch R, Shaw LJ, Friedman JD, Hayes SW, Thomson LE, Fieno DS, Germano G, Slomka P, Wong ND, Kang X, Rozanski A. Roles of nuclear cardiology, cardiac computed tomography, and cardiac magnetic resonance: assessment of patients with suspected coronary artery disease. *J Nucl Med.* 2006;47(1):74-82.

Bhandari R, Paliwal JK, Kuhad A. Enhanced Bioavailability and Higher Uptake of Brain-Targeted Surface Engineered Delivery System of Naringenin developed as a Therapeutic for Autism Spectrum Disorder. *Curr Drug Deliv.* 2023;20(2):158-182. doi: 10.2174/1567201819666220303101506.

Bhatt PC, Verma A, Al-Abbasi FA, Anwar F, Kumar V, Panda BP. Development of surface-engineered PLGA nanoparticulate-delivery system of Tet1-conjugated nattokinase enzyme for inhibition of A β 40 plaques in Alzheimer's disease. *Int J Nanomedicine.* 2017;12:8749-8768. doi: 10.2147/IJN.S144545.

Bhattacharya S, Mondal L, Mukherjee B, Dutta L, Ehsan I, Debnath MC, Gaonkar RH, Pal MM, Majumdar S. Apigenin loaded nanoparticle delayed development of hepatocellular carcinoma in rats. *Nanomedicine.* 2018;14(6):1905-1917. doi: 10.1016/j.nano.2018.05.011.

Bialecki ES, Di Bisceglie AM. Diagnosis of hepatocellular carcinoma. *HPB (Oxford).* 2005;7(1):26-34. doi: 10.1080/13651820410024049.

References

- Bijani S, Dizaji R, Sharafi A, Hosseini MJ. Neuroprotective Effect of Apigenin on Depressive-Like Behavior: Mechanistic Approach. *Neurochem Res.* 2022 ;47(3):644-655. doi: 10.1007/s11064-021-03473-0.
- Blasi P. Poly (lactic acid)/poly (lactic-co-glycolic acid)-based microparticles: An overview. *J.Pharm. Investig.* 2019;49(4):337-346. doi: 10.1007/s40005-019-00453-z.
- Boltnarova B, Kubackova J, Skoda J, Stefela A, Smekalova M, Svacinova P, Pavkova I, Dittrich M, Scherman D, Zbytovska J, Pavek P, Holas O. PLGA Based Nanospheres as a Potent Macrophage-Specific Drug Delivery System. *Nanomaterials (Basel).* 2021;11(3):749. doi: 10.3390/nano11030749.
- Boots AW, Haenen GR, Bast A. Health effects of quercetin: from antioxidant to nutraceutical. *Eur J Pharmacol.* 2008;585(2-3):325-37. doi: 10.1016/j.ejphar.2008.03.008.
- Borrello MT, Mann D. Chronic liver diseases: From development to novel pharmacological therapies: IUPHAR Review 37. *Br J Pharmacol.* 2022. doi: 10.1111/bph.15853. Epub ahead of print.
- Brad K, Zhang Y. Study on Extraction and Purification of Apigenin and the Physical and Chemical Properties of Its Complex with Lecithin. *Pharmacogn Mag.* 2018;14(54):203-206. doi: 10.4103/pm.pm_159_17.
- Brawner Jr WR, Daniel GB. Nuclear imaging. *Veterinary Clinics of North America: Small Animal Practice.* 1993;23(2):379-98. doi: 10.1016/S0195-5616(93)50033-5.
- Broome MR. Thyroid scintigraphy in hyperthyroidism. *Clin Tech Small Anim Pract.* 2006;21(1):10-16. doi: 10.1053/j.ctsap.2005.12.002.
- Bruix J, Sherman M; American Association for the Study of Liver Diseases. Management of hepatocellular carcinoma: an update. *Hepatology.* 2011;53(3):1020-1022. doi: 10.1002/hep.24199.
- Buckley O, O'Keeffe S, Geoghegan T, Lyburn ID, Munk PL, Worsley D, Torreggiani WC. ^{99m}Tc bone scintigraphy superscans: a review. *Nucl Med Commun.* 2007;28(7):521-527. doi: 10.1097/MNM.0b013e3281744440.
- Bule M, Abdurahman A, Nikfar S, Abdollahi M, Amini M. Antidiabetic effect of quercetin: A systematic review and meta-analysis of animal studies. *Food Chem Toxicol.* 2019;125:494-502. doi: 10.1016/j.fct.2019.01.037.
- Bumke-Vogt C, Osterhoff MA, Borchert A, Guzman-Perez V, Sarem Z, Birkenfeld AL, Bähr V, Pfeiffer AF. The flavones apigenin and luteolin induce FOXO1 translocation but

- inhibit gluconeogenic and lipogenic gene expression in human cells. *PLoS One*. 2014;9(8): e104321. doi: 10.1371/journal.pone.0104321.
- Cai J, Zhao XL, Liu AW, Nian H, Zhang SH. Apigenin inhibits hepatoma cell growth through alteration of gene expression patterns. *Phytomedicine*. 2011;18(5):366-373. doi: 10.1016/j.phymed.2010.08.006.
- Cai X, Fang Z, Dou J, Yu A, Zhai G. Bioavailability of quercetin: problems and promises. *Curr Med Chem*. 2013;20(20):2572-2582. doi: 10.2174/09298673113209990120.
- Calvani M, Pasha A, Favre C. Nutraceutical Boom in Cancer: Inside the Labyrinth of Reactive Oxygen Species. *Int J Mol Sci*. 2020;21(6):1936. doi: 10.3390/ijms21061936.
- Cao H, Chen L, Xiao J. Binding Citrus flavanones to human serum albumin: effect of structure on affinity. *Mol Biol Rep*. 2011;38(4):2257-2262. doi: 10.1007/s11033-010-0356-z.
- Cao Y, Hu J, Sui J, Jiang L, Cong Y, Ren G. Quercetin is able to alleviate TGF- β -induced fibrosis in renal tubular epithelial cells by suppressing miR-21. *Exp Ther Med*. 2018;16(3):2442-2448. doi: 10.3892/etm.2018.6489.
- Carrasco-Pozo C, Tan KN, Reyes-Farias M, De La Jara N, Ngo ST, Garcia-Diaz DF, Llanos P, Cires MJ, Borges K. The deleterious effect of cholesterol and protection by quercetin on mitochondrial bioenergetics of pancreatic β -cells, glycemic control and inflammation: In vitro and in vivo studies. *Redox Biol*. 2016;9:229-243. doi: 10.1016/j.redox.2016.08.007.
- Casas-Grajales S, Muriel P. Antioxidants in liver health. *World J Gastrointest Pharmacol Ther*. 2015;6(3):59-72. doi: 10.4292/wjgpt.v6.i3.59.
- Cassidy A, Minihane AM. The role of metabolism (and the microbiome) in defining the clinical efficacy of dietary flavonoids. *Am J Clin Nutr*. 2017;105(1):10-22. doi: 10.3945/ajcn.116.136051.
- Castro KC, Costa JM, Campos MG. Drug-loaded polymeric nanoparticles: a review. *Int J Polym Mater Polym Biomater*. 2022;71(1):1-3. doi: 10.1080/00914037.2020.1798436.
- Chacko AK, Shah RB, Chacko JA. Emergency Nuclear Radiology. Soto JA, Lucey BC (Eds). In: *The Requisites, Emergency Radiology*, Mosby, Missouri, United States 2009, pp. 361-383, ISBN 9780323054072, (<https://www.sciencedirect.com/science/article/pii/B9780323054072000129>).

References

- Chakraborty S, Dlie ZY, Chakraborty S, Roy S, Mukherjee B, Besra SE, Dewanjee S, Mukherjee A, Ojha PK, Kumar V, Sen R. Aptamer-Functionalized Drug Nanocarrier Improves Hepatocellular Carcinoma toward Normal by Targeting Neoplastic Hepatocytes. *Mol Ther Nucleic Acids*. 2020;20:34-49. doi: 10.1016/j.omtn.2020.01.034.
- Chaudhary S, Ganjoo P, Raiusddin S, Parvez S. Nephroprotective activities of quercetin with potential relevance to oxidative stress induced by valproic acid. *Protoplasma*. 2015;252(1):209-217. doi: 10.1007/s00709-014-0670-8.
- Cheemerla S, Balakrishnan M. Global Epidemiology of Chronic Liver Disease. *Clin Liver Dis (Hoboken)*. 2021;17(5):365-370. doi: 10.1002/cld.1061.
- Chen C, He H, Luo Y, Zhou M, Yin D, He M. Involvement of Bcl-2 Signal Pathway in the Protective Effects of Apigenin on Anoxia/Reoxygenation-induced Myocardium Injury. *J Cardiovasc Pharmacol*. 2016;67(2):152-163. doi: 10.1097/FJC.0000000000000331.
- Chen HY, Chiang YF, Hong YH, Shieh TM, Huang TC, Ali M, Chang HY, Wang KL, Hsia SM. Quercetin Ameliorates Renal Injury and Pyroptosis in Lupus Nephritis through Inhibiting IL-33/ST2 Pathway In Vitro and In Vivo. *Antioxidants (Basel)*. 2022;11(11):2238. doi: 10.3390/antiox11112238.
- Chen P, Chen J, Zheng Q, Chen W, Wang Y, Xu X. Pioglitazone, extract of compound Danshen dripping pill, and quercetin ameliorate diabetic nephropathy in diabetic rats. *J Endocrinol Invest*. 2013;36(6):422-427. doi: 10.3275/8763.
- Chen P, Huo X, Liu W, Li K, Sun Z, Tian J. Apigenin exhibits anti-inflammatory effects in LPS-stimulated BV2 microglia through activating GSK3 β /Nrf2 signaling pathway. *Immunopharmacol Immunotoxicol*. 2020;42(1):9-16. doi: 10.1080/08923973.2019.1688345.
- Chen S, Jiang H, Wu X, Fang J. Therapeutic Effects of Quercetin on Inflammation, Obesity, and Type 2 Diabetes. *Mediators Inflamm*. 2016;2016:9340637. doi: 10.1155/2016/9340637.
- Chen T, Zhang X, Zhu G, Liu H, Chen J, Wang Y, He X. Quercetin inhibits TNF- α induced HUVECs apoptosis and inflammation via downregulating NF-kB and AP-1 signaling pathway in vitro. *Medicine (Baltimore)*. 2020;99(38):e22241. doi: 10.1097/MD.00000000000022241.
- Chen X, Wang D, Guo X, Li X, Ye W, Qi Y, Gu W. Curcumin-Loaded mPEG-PLGA Nanoparticles Attenuates the Apoptosis and Corticosteroid Resistance Induced by

- Cigarette Smoke Extract. *Front Pharmacol.* 2022;13:824652. doi: 10.3389/fphar.2022.824652.
- Chen YQ, Chen HY, Tang QQ, Li YF, Liu XS, Lu FH, Gu YY. Protective effect of quercetin on kidney diseases: From chemistry to herbal medicines. *Front Pharmacol.* 2022;13:968226. doi: 10.3389/fphar.2022.968226.
- Chen YW, Chou HC, Lin ST, Chen YH, Chang YJ, Chen L, Chan HL. Cardioprotective Effects of Quercetin in Cardiomyocyte under Ischemia/Reperfusion Injury. *Evid Based Complement Alternat Med.* 2013;2013:364519. doi: 10.1155/2013/364519
- Cheng SC, Wu YH, Huang WC, Pang JS, Huang TH, Cheng CY. Anti-inflammatory property of quercetin through downregulation of ICAM-1 and MMP-9 in TNF- α -activated retinal pigment epithelial cells. *Cytokine.* 2019;116:48-60. doi: 10.1016/j.cyto.2019.01.001.
- Chenthamara D, Subramaniam S, Ramakrishnan SG, Krishnaswamy S, Essa MM, Lin FH, Qoronfleh MW. Therapeutic efficacy of nanoparticles and routes of administration. *Biomater Res.* 2019;23:20. doi: 10.1186/s40824-019-0166-x.
- Chiang LC, Ng LT, Lin IC, Kuo PL, Lin CC. Anti-proliferative effect of apigenin and its apoptotic induction in human Hep G2 cells. *Cancer Lett.* 2006;237(2):207-214. doi: 10.1016/j.canlet.2005.06.002.
- Chidambaranathan-Reghupaty S, Fisher PB, Sarkar D. Hepatocellular carcinoma (HCC): Epidemiology, etiology and molecular classification. *Adv Cancer Res.* 2021;149:1-61. doi: 10.1016/bs.acr.2020.10.001.
- Chiu CT, Yeh TS, Hsu JC, Chen MF. Expression of Bcl-2 family modulated through p53-dependent pathway in human hepatocellular carcinoma. *Dig Dis Sci.* 2003;48(4):670-676. doi: 10.1023/a:1022816204831.
- Choudhari AS, Mandave PC, Deshpande M, Ranjekar P, Prakash O. Phytochemicals in Cancer Treatment: From Preclinical Studies to Clinical Practice. *Front Pharmacol.* 2020;10:1614. doi: 10.3389/fphar.2019.01614.
- Choudhary A, Kant V, Jangir BL, Joshi VG. Quercetin loaded chitosan tripolyphosphate nanoparticles accelerated cutaneous wound healing in Wistar rats. *Eur J Pharmacol.* 2020;880:173172. doi: 10.1016/j.ejphar.2020.173172.
- Chung K, Ullah I, Kim N, Lim J, Shin J, Lee SC, Jeon S, Kim SH, Kumar P, Lee SK. Intranasal delivery of cancer-targeting doxorubicin-loaded PLGA nanoparticles arrests

References

- glioblastoma growth. *J Drug Target.* 2020;28(6):617-626. doi: 10.1080/1061186X.2019.1706095.
- Cicek M, Unsal V, Doganer A, Demir M. Investigation of oxidant/antioxidant and anti-inflammatory effects of apigenin on apoptosis in sepsis-induced rat lung. *J Biochem Mol Toxicol.* 2021;35(5):e22743. doi: 10.1002/jbt.22743.
- Cichoż-Lach H, Michalak A. Oxidative stress as a crucial factor in liver diseases. *World J Gastroenterol.* 2014;20(25):8082-8091. doi: 10.3748/wjg.v20.i25.8082.
- Cory H, Passarelli S, Szeto J, Tamez M, Mattei J. The Role of Polyphenols in Human Health and Food Systems: A Mini-Review. *Front Nutr.* 2018;5:87. doi: 10.3389/fnut.2018.00087.
- Costa ACF, de Sousa LM, Dos Santos Alves JM, Goes P, Pereira KMA, Alves APNN, Vale ML, Gondim DV. Anti-inflammatory and Hepatoprotective Effects of Quercetin in an Experimental Model of Rheumatoid Arthritis. *Inflammation.* 2021;44(5):2033-2043. doi: 10.1007/s10753-021-01479-y.
- Costa LG, Garrick JM, Roquè PJ, Pellacani C. Mechanisms of Neuroprotection by Quercetin: Counteracting Oxidative Stress and More. *Oxid Med Cell Longev.* 2016; 2016:2986796. doi: 10.1155/2016/2986796.
- Crabb DW, Im GY, Szabo G, Mellinger JL, Lucey MR. Diagnosis and Treatment of Alcohol-Associated Liver Diseases: 2019 Practice Guidance From the American Association for the Study of Liver Diseases. *Hepatology.* 2020;71(1):306-333. doi: 10.1002/hep.30866.
- Crissien AM, Frenette C. Current management of hepatocellular carcinoma. *Gastroenterol Hepatol (N Y).* 2014;10(3):153-161.
- Dajas F. Life or death: neuroprotective and anticancer effects of quercetin. *J Ethnopharmacol.* 2012;143(2):383-396. doi: 10.1016/j.jep.2012.07.005.
- D'Andrea G. Quercetin: A flavonol with multifaceted therapeutic applications? *Fitoterapia.* 2015;106:256-271. doi: 10.1016/j.fitote.2015.09.018.
- Danhier F, Ansorena E, Silva JM, Coco R, Le Breton A, Prétat V. PLGA-based nanoparticles: an overview of biomedical applications. *J Control Release.* 2012;161(2):505-522. doi: 10.1016/j.jconrel.2012.01.043.

- D'Archivio M, Filesi C, Vari R, Scazzocchio B, Masella R. Bioavailability of the polyphenols: status and controversies. *Int J Mol Sci.* 2010;11(4):1321-1342. doi: 10.3390/ijms11041321.
- Das PJ, Paul P, Mukherjee B, Mazumder B, Mondal L, Baishya R, Debnath MC, Dey KS. Pulmonary Delivery of Voriconazole Loaded Nanoparticles Providing a Prolonged Drug Level in Lungs: A Promise for Treating Fungal Infection. *Mol Pharm.* 2015;12(8):2651-2664. doi: 10.1021/acs.molpharmaceut.5b00064.
- Das R, Mitra S, Tareq AM, Emran TB, Hossain MJ, Alqahtani AM, Alghazwani Y, Dhama K, Simal-Gandara J. Medicinal plants used against hepatic disorders in Bangladesh: A comprehensive review. *J Ethnopharmacol.* 2022;282:114588. doi: 10.1016/j.jep.2021.114588.
- Das S, Joardar S, Manna P, Dua TK, Bhattacharjee N, Khanra R, Bhowmick S, Kalita J, Saha A, Ray S, De Feo V, Dewanjee S. Carnosic Acid, a Natural Diterpene, Attenuates Arsenic-Induced Hepatotoxicity via Reducing Oxidative Stress, MAPK Activation, and Apoptotic Cell Death Pathway. *Oxid Med Cell Longev.* 2018;2018:1421438. doi: 10.1155/2018/1421438.
- Davila JC, Davis PJ, Acosta D. Changes in glutathione and cellular energy as potential mechanisms of papaverine-induced hepatotoxicity in vitro. *Toxicol Appl Pharmacol.* 1991;108(1):28-36. doi: 10.1016/0041-008x(91)90265-g.
- de Lope CR, Tremosini S, Forner A, Reig M, Bruix J. Management of HCC. *J Hepatol.* 2012;56 Suppl 1:S75-87. doi: 10.1016/S0168-8278(12)60009-9.
- Derosa G, Maffioli P, D'Angelo A, Di Pierro F. A role for quercetin in coronavirus disease 2019 (COVID-19). *Phytother Res.* 2021;35(3):1230-1236. doi: 10.1002/ptr.6887
- Devarbhavi H. An Update on Drug-induced Liver Injury. *J Clin Exp Hepatol.* 2012;2(3):247-259. doi: 10.1016/j.jceh.2012.05.002.
- Devi VK, Jain N, Valli KS. Importance of novel drug delivery systems in herbal medicines. *Pharmacogn Rev.* 2010;4(7):27-31. doi: 10.4103/0973-7847.65322.
- Dewanjee S, Chakraborty P, Mukherjee B, De Feo V. Plant-Based Antidiabetic Nanoformulations: The Emerging Paradigm for Effective Therapy. *Int J Mol Sci.* 2020;21(6):2217. doi: 10.3390/ijms21062217.
- Dhiman RK, Chawla YK. Herbal medicines for liver diseases. *Dig Dis Sci.* 2005;50(10):1807-1812. doi: 10.1007/s10620-005-2942-9.

References

- Di Petrillo A, Orrù G, Fais A, Fantini MC. Quercetin and its derivatives as antiviral potentials: A comprehensive review. *Phytother Res.* 2022;36(1):266-278. doi: 10.1002/ptr.7309.
- Dias K, Nikolaou S, De Giovani WF. Synthesis and spectral investigation of Al(III) catechin/beta-cyclodextrin and Al(III) quercetin/beta-cyclodextrin inclusion compounds. *Spectrochim Acta A Mol Biomol Spectrosc.* 2008;70(1):154-161. doi: 10.1016/j.saa.2007.07.022.
- Diez-Echave P, Ruiz-Malagón AJ, Molina-Tijeras JA, Hidalgo-García L, Vezza T, Cenis-Cifuentes L, Rodríguez-Sojo MJ, Cenis JL, Rodríguez-Cabezas ME, Rodríguez-Nogales A, Gálvez J, Lozano-Pérez AA. Silk fibroin nanoparticles enhance quercetin immunomodulatory properties in DSS-induced mouse colitis. *Int J Pharm.* 2021;606:120935. doi: 10.1016/j.ijpharm.2021.120935.
- Ding SM, Zhang ZH, Song J, Cheng XD, Jiang J, Jia XB. Enhanced bioavailability of apigenin via preparation of a carbon nanopowder solid dispersion. *Int J Nanomedicine.* 2014;9:2327-2333. doi: 10.2147/IJN.S60938.
- Diniz LRL, Souza MTS, Duarte ABS, Sousa DP. Mechanistic Aspects and Therapeutic Potential of Quercetin against COVID-19-Associated Acute Kidney Injury. *Molecules.* 2020;25(23):5772. doi: 10.3390/molecules25235772.
- Doonan M. Hepatobiliary Imaging. *J Nucl Med Technol.* 2020;48(4):304-310. doi: 10.2967/jnmt.120.257436.
- Dua TK, Joardar S, Chakraborty P, Bhowmick S, Saha A, De Feo V, Dewanjee S. Myricitrin, a Glycosyloxyflavone in *Myrica esculenta* Bark Ameliorates Diabetic Nephropathy via Improving Glycemic Status, Reducing Oxidative Stress, and Suppressing Inflammation. *Molecules.* 2021;26(2):258. doi: 10.3390/molecules26020258.
- Eckelman WC. Unparalleled contribution of technetium-99m to medicine over 5 decades. *JACC Cardiovasc Imaging.* 2009;2(3):364-368. doi: 10.1016/j.jcmg.2008.12.013.
- Eftekhari A, Ahmadian E, Panahi-Azar V, Hosseini H, Tabibiazar M, Maleki Dizaj S. Hepatoprotective and free radical scavenging actions of quercetin nanoparticles on aflatoxin B1-induced liver damage: in vitro/in vivo studies. *Artif Cells Nanomed Biotechnol.* 2018;46(2):411-420. doi: 10.1080/21691401.2017.1315427.
- El Daibani AA, Xi Y, Luo L, Mei X, Zhou C, Yasuda S, Liu MC. Sulfation of hesperetin, naringenin and apigenin by the human cytosolic sulfotransferases: a comprehensive analysis. *Nat Prod Res.* 2020;34(6):797-803. doi: 10.1080/14786419.2018.1503264.

- Elbe H, Vardi N, Esrefoglu M, Ates B, Yologlu S, Taskapan C. Amelioration of streptozotocin-induced diabetic nephropathy by melatonin, quercetin, and resveratrol in rats. *Hum Exp Toxicol.* 2015;34(1):100-113. doi: 10.1177/0960327114531995.
- Elmowafy EM, Tiboni M, Soliman ME. Biocompatibility, biodegradation and biomedical applications of poly (lactic acid)/poly (lactic-co-glycolic acid) micro and nanoparticles. *J.Pharm. Investig.* 2019;49(4):347-380. doi: 10.1007/s40005-019-00439-x.
- Ersoz M, Erdemir A, Derman S, Arasoglu T, Mansuroglu B. Quercetin-loaded nanoparticles enhance cytotoxicity and antioxidant activity on C6 glioma cells. *Pharm Dev Technol.* 2020;25(6):757-766. doi: 10.1080/10837450.2020.1740933.
- Essa D, Kondiah PPD, Choonara YE, Pillay V. The Design of Poly(lactide-co-glycolide) Nanocarriers for Medical Applications. *Front Bioeng Biotechnol.* 2020;8:48. doi: 10.3389/fbioe.2020.00048.
- Ferenczyova K, Kalocayova B, Bartekova M. Potential Implications of Quercetin and its Derivatives in Cardioprotection. *Int J Mol Sci.* 2020;21(5):1585. doi: 10.3390/ijms21051585.
- Fessi HP, Puisieux F, Devissaguet JP, Ammoury N, Benita S. Nanocapsule formation by interfacial polymer deposition following solvent displacement. *Int. J. Pharm.* 1989;55(1):R1-4. doi: 10.1016/0378-5173(89)90281-0.
- Freitas JE. Cholescintigraphy in acute and chronic cholecystitis. *Semin Nucl Med.* 1982;12(1):18-26. doi: 10.1016/s0001-2998(82)80026-3.
- Fu C, Zheng Y, Lin K, Wang H, Chen T, Li L, Huang J, Lin W, Zhu J, Li P, Fu X, Lin Z. Neuroprotective effect of apigenin against hypoxic-ischemic brain injury in neonatal rats via activation of the PI3K/Akt/Nrf2 signaling pathway. *Food Funct.* 2021;12(5):2270-2281. doi: 10.1039/d0fo02555k.
- Galindo R, Sánchez-López E, Gómara MJ, Espina M, Ettcheto M, Cano A, Haro I, Camins A, García ML. Development of Peptide Targeted PLGA-PEGylated Nanoparticles Loading Licochalcone-A for Ocular Inflammation. *Pharmaceutics.* 2022; 14(2):285. doi: 10.3390/pharmaceutics14020285.
- Gandhi CR. Oxidative Stress and Hepatic Stellate Cells: A PARADOXICAL RELATIONSHIP. *Trends Cell Mol Biol.* 2012;7:1-10.

References

- Gang W, Jie WJ, Ping ZL, Ming du S, Ying LJ, Lei W, Fang Y. Liposomal quercetin: evaluating drug delivery in vitro and biodistribution in vivo. *Expert Opin Drug Deliv.* 2012;9(6):599-613. doi: 10.1517/17425247.2012.679926.
- Ganguly S, Dewanjee S, Sen R, Chattopadhyay D, Ganguly S, Gaonkar R, Debnath MC. Apigenin-loaded galactose tailored PLGA nanoparticles: A possible strategy for liver targeting to treat hepatocellular carcinoma. *Colloids Surf B Biointerfaces.* 2021;204:111778. doi: 10.1016/j.colsurfb.2021.111778.
- Ganguly S, Gaonkar RH, Sinha S, Gupta A, Chattopadhyay D, Chattopadhyay S, Sachdeva SS, Ganguly S, Debnath MC. Fabrication of surfactant-free quercetin-loaded PLGA nanoparticles: evaluation of hepatoprotective efficacy by nuclear scintigraphy. *J. Nanopart Res.* 2016;18(7):196. doi: 10.1007/s11051-016-3504-0.
- Gao M, Wang H, Zhu L. Quercetin Assists Fluconazole to Inhibit Biofilm Formations of Fluconazole-Resistant *Candida Albicans* in In Vitro and In Vivo Antifungal Managements of Vulvovaginal Candidiasis. *Cell Physiol Biochem.* 2016;40(3-4):727-742. doi: 10.1159/000453134.
- Gao S, Hu M. Bioavailability challenges associated with development of anti-cancer phenolics. *Mini Rev Med Chem.* 2010;10(6):550-567. doi: 10.2174/138955710791384081.
- Gao W, Liang L. Effect of Polysaccharide Sulfate-Loaded Poly(lactic-co-glycolic acid) Nanoparticles on Coronary Microvascular Dysfunction of Diabetic Cardiomyopathy. *J Biomed Nanotechnol.* 2022;18(2):446-452. doi: 10.1166/jbn.2022.3261.
- Gaonkar RH, Ganguly S, Dewanjee S, Sinha S, Gupta A, Ganguly S, Chattopadhyay D, Chatterjee Debnath M. Garcinol loaded vitamin E TPGS emulsified PLGA nanoparticles: preparation, physicochemical characterization, in vitro and in vivo studies. *Sci Rep.* 2017;7(1):530. doi: 10.1038/s41598-017-00696-6.
- Garner J, Skidmore S, Hadar J, Park H, Park K, Kuk Jhon Y, Qin B, Wang Y. Analysis of semi-solvent effects for PLGA polymers. *Int J Pharm.* 2021;602:120627. doi: 10.1016/j.ijpharm.2021.120627.
- Gautam AK, Kumar P, Maity B, Routholla G, Ghosh B, Chidambaram K, Begum MY, Al Fatease A, Rajinikanth PS, Singh S, Saha S, M R V. Synthesis and appraisal of dalbergin-loaded PLGA nanoparticles modified with galactose against hepatocellular carcinoma: In-vitro, pharmacokinetic, and in-silico studies. *Front Pharmacol.* 2022;13:1021867. doi: 10.3389/fphar.2022.1021867.

- GBD 2017 Cirrhosis Collaborators. The global, regional, and national burden of cirrhosis by cause in 195 countries and territories, 1990-2017: a systematic analysis for the Global Burden of Disease Study 2017. *Lancet Gastroenterol Hepatol.* 2020;5(3):245-266. doi: 10.1016/S2468-1253(19)30349-8.
- Gentile P, Chiono V, Carmagnola I, Hatton PV. An overview of poly(lactic-co-glycolic) acid (PLGA)-based biomaterials for bone tissue engineering. *Int J Mol Sci.* 2014; 15(3):3640-3659. doi: 10.3390/ijms15033640.
- George BP, Chandran R, Abrahamse H. Role of Phytochemicals in Cancer Chemoprevention: Insights. *Antioxidants (Basel).* 2021;10(9):1455. doi: 10.3390/antiox10091455.
- Ghosh A, Ghosh D, Sarkar S, Mandal AK, Thakur Choudhury S, Das N. Anticarcinogenic activity of nanoencapsulated quercetin in combating diethylnitrosamine-induced hepatocarcinoma in rats. *Eur J Cancer Prev.* 2012;21(1):32-41. doi: 10.1097/CEJ.0b013e32834a7e2b.
- Ghosh A, Mandal AK, Sarkar S, Panda S, Das N. Nanoencapsulation of quercetin enhances its dietary efficacy in combating arsenic-induced oxidative damage in liver and brain of rats. *Life Sci.* 2009;84(3-4):75-80. doi: 10.1016/j.lfs.2008.11.001.
- Ghosh A, Sarkar S, Mandal AK, Das N. Neuroprotective role of nanoencapsulated quercetin in combating ischemia-reperfusion induced neuronal damage in young and aged rats. *PLoS One.* 2013;8(4):e57735. doi: 10.1371/journal.pone.0057735.
- Gilding DK, Reed AM. Biodegradable polymers for use in surgery—polyglycolic/poly(lactic acid) homo-and copolymers: 1. *Polymer.* 1979;20(12):1459-1464. doi: 10.1016/0032-3861(79)90009-0.
- Golombek SK, May JN, Theek B, Appold L, Drude N, Kiessling F, Lammers T. Tumor targeting via EPR: Strategies to enhance patient responses. *Adv Drug Deliv Rev.* 2018;130:17-38. doi: 10.1016/j.addr.2018.07.007.
- Goudarzi M, Kalantar M, Sadeghi E, Karamallah MH, Kalantar H. Protective effects of apigenin on altered lipid peroxidation, inflammation, and antioxidant factors in methotrexate-induced hepatotoxicity. *Naunyn Schmiedebergs Arch Pharmacol.* 2021; 394(3):523-531. doi: 10.1007/s00210-020-01991-2.
- Granado-Serrano AB, Martín MA, Bravo L, Goya L, Ramos S. Quercetin induces apoptosis via caspase activation, regulation of Bcl-2, and inhibition of PI-3-kinase/Akt

References

- and ERK pathways in a human hepatoma cell line (HepG2). *J Nutr.* 2006;136(11):2715-2721. doi: 10.1093/jn/136.11.2715.
- Granado-Serrano AB, Martín MÁ, Bravo L, Goya L, Ramos S. Quercetin attenuates TNF-induced inflammation in hepatic cells by inhibiting the NF- κ B pathway. *Nutr Cancer.* 2012;64(4):588-598. doi: 10.1080/01635581.2012.661513.
- Grewal AK, Singh TG, Sharma D, Sharma V, Singh M, Rahman MH, Najda A, Walasek-Janusz M, Kamel M, Albadrani GM, Akhtar MF, Saleem A, Abdel-Daim MM. Mechanistic insights and perspectives involved in neuroprotective action of quercetin. *Biomed Pharmacother.* 2021;140:111729. doi: 10.1016/j.biopha.2021.111729.
- Guan YS, He Q. Plants Consumption and Liver Health. *Evid Based Complement Alternat Med.* 2015;2015:824185. doi: 10.1155/2015/824185.
- Gugler R, Leschik M, Dengler HJ. Disposition of quercetin in man after single oral and intravenous doses. *Eur J Clin Pharmacol.* 1975;9(2-3):229-234. doi: 10.1007/BF00614022.
- Guo Y, Bruno RS. Endogenous and exogenous mediators of quercetin bioavailability. *J Nutr Biochem.* 2015;26(3):201-210. doi: 10.1016/j.jnutbio.2014.10.008.
- Gupta C, Vikram A, Tripathi DN, Ramarao P, Jena GB. Antioxidant and antimutagenic effect of quercetin against DEN induced hepatotoxicity in rat. *Phyther Res.* 2010;24(1):119-128. doi: 10.1002/ptr.2883.
- Hann HW, Wan S, Myers RE, Hann RS, Xing J, Chen B, Yang H. Comprehensive analysis of common serum liver enzymes as prospective predictors of hepatocellular carcinoma in HBV patients. *PLoS One.* 2012;7(10):e47687. doi: 10.1371/journal.pone.0047687.
- Hanna M, Ruberg FL, Maurer MS, Dispenzieri A, Dorbala S, Falk RH, Hoffman J, Jaber W, Soman P, Witteles RM, Grogan M. Cardiac Scintigraphy With Technetium-99m-Labeled Bone-Seeking Tracers for Suspected Amyloidosis: JACC Review Topic of the Week. *J Am Coll Cardiol.* 2020;75(22):2851-2862. doi: 10.1016/j.jacc.2020.04.022.
- Hashemi M, Shamshiri A, Saeedi M, Tayebi L, Yazdian-Robati R. Aptamer-conjugated PLGA nanoparticles for delivery and imaging of cancer therapeutic drugs. *Arch Biochem Biophys.* 2020;691:108485. doi: 10.1016/j.abb.2020.108485.
- Hashemi P, Fahanik Babaei J, Vazifekhah S, Nikbakht F. Evaluation of the neuroprotective, anticonvulsant, and cognition-improvement effects of apigenin in

temporal lobe epilepsy: Involvement of the mitochondrial apoptotic pathway. *Iran J Basic Med Sci.* 2019;22(7):752-758. doi: 10.22038/ijbms.2019.33892.8064.

He H, Peng S, Song X, Jia R, Zou Y, Li L, Yin Z. Protective effect of isoflavones and triterpenoid saponins from pueraria lobata on liver diseases: A review. *Food Sci Nutr.* 2021;10(1):272-285. doi: 10.1002/fsn3.2668.

He X, Li C, Wei Z, Wang J, Kou J, Liu W, Shi M, Yang Z, Fu Y. Protective role of apigenin in cisplatin-induced renal injury. *Eur J Pharmacol.* 2016;789:215-221. doi: 10.1016/j.ejphar.2016.07.003.

He X, Wen Y, Wang Q, Wang Y, Zhang G, Wu J, Li Z, Wen J. Apigenin Nanoparticle Attenuates Renal Ischemia/Reperfusion Inflammatory Injury by Regulation of miR-140-5p/CXCL12/NF- κ B Signaling Pathway. *J Biomed Nanotechnol.* 2021;17(1):64-77. doi: 10.1166/jbn.2021.3010.

Heymann MA, Payne BD, Hoffman JI, Rudolph AM. Blood flow measurements with radionuclide-labeled particles. *Prog Cardiovasc Dis.* 1977;20(1):55-79. doi: 10.1016/s0033-0620(77)80005-4.

Hines DJ, Kaplan DL. Poly(lactic-co-glycolic) acid-controlled-release systems: experimental and modeling insights. *Crit Rev Ther Drug Carrier Syst.* 2013;30(3): 257-276. doi: 10.1615/critrevtherdrugcarriersyst.2013006475.

Hnit SST, Yao M, Xie C, Bi L, Wong M, Liu T, De Souza P, Li Z, Dong Q. Apigenin impedes cell cycle progression at G2 phase in prostate cancer cells. *Discov Oncol.* 2022;13(1):44. doi: 10.1007/s12672-022-00505-1.

Hollman PCH. Absorption, Bioavailability, and Metabolism of Flavonoids. *Pharm Biol.* 2004;42 (sup1):74-83, doi: 10.3109/13880200490893492.

Hong M, Li S, Tan HY, Wang N, Tsao SW, Feng Y. Current Status of Herbal Medicines in Chronic Liver Disease Therapy: The Biological Effects, Molecular Targets and Future Prospects. *Int J Mol Sci.* 2015;16(12):28705-28745. doi: 10.3390/ijms161226126.

Hopfer K, Ziessman H. Nuclear medicine hepatobiliary imaging (cholescintigraphy). *Gastrointest Endosc.* 2011;74(2):375-377. doi: 10.1016/j.gie.2011.06.017.

Horton JA, Li F, Chung EJ, Hudak K, White A, Krausz K, Gonzalez F, Citrin D. Quercetin inhibits radiation-induced skin fibrosis. *Radiat Res.* 2013;180(2):205-215. doi: 10.1667/RR3237.1.

References

- Hostetler GL, Ralston RA, Schwartz SJ. Flavones: Food Sources, Bioavailability, Metabolism, and Bioactivity. *Adv Nutr.* 2017;8(3):423-435. doi: 10.3945/an.116.012948.
- Hou DD, Zhang W, Gao YL, Sun YZ, Wang HX, Qi RQ, Chen HD, Gao XH. Anti-inflammatory effects of quercetin in a mouse model of MC903-induced atopic dermatitis. *Int Immunopharmacol.* 2019;74:105676. doi: 10.1016/j.intimp.2019.105676.
- Hsieh HL, Yu MC, Cheng LC, Chu MY, Huang TH, Yeh TS, Tsai MM. Quercetin exerts anti-inflammatory effects via inhibiting tumor necrosis factor- α -induced matrix metalloproteinase-9 expression in normal human gastric epithelial cells. *World J Gastroenterol.* 2022;28(11):1139-1158. doi: 10.3748/wjg.v28.i11.1139.
- Hu J, Sheng Y, Shi J, Yu B, Yu Z, Liao G. Long Circulating Polymeric Nanoparticles for Gene/Drug Delivery. *Curr Drug Metab.* 2018;19(9):723-738. doi: 10.2174/1389200219666171207120643.
- Hu S, Zhu D, Li Z, Cheng K. Detachable Microneedle Patches Deliver Mesenchymal Stromal Cell Factor-Loaded Nanoparticles for Cardiac Repair. *ACS Nano.* 2022;16(10):15935-15945. doi: 10.1021/acsnano.2c03060.
- Hu XT, Ding C, Zhou N, Xu C. Quercetin protects gastric epithelial cell from oxidative damage in vitro and in vivo. *Eur J Pharmacol.* 2015;754:115-124. doi: 10.1016/j.ejphar.2015.02.007.
- Huang Y, Zhao X, Zu Y, Wang L, Deng Y, Wu M, Wang H. Enhanced Solubility and Bioavailability of Apigenin via Preparation of Solid Dispersions of Mesoporous Silica Nanoparticles. *Iran J Pharm Res.* 2019;18(1):168-182. doi: 10.22037/ijpr.2019.2347.
- Hyon SH, Jamshidi K, Ikada Y. Synthesis of polylactides with different molecular weights. *Biomaterials.* 1997;18(22):1503-1508. doi: 10.1016/s0142-9612(97)00076-8.
- Iida M, Yamamoto Y, Katoh H, Taniguchi N, Abe Y, Kumagai K, Uchinami H. ^{99m}Tc -GSA scintigraphy for assessing the functional volume ratio of the future liver remnant in the routine practice of liver resection. *Surg Open Sci.* 2022;8:1-8. doi: 10.1016/j.sopen.2021.12.001.
- Imran M, Aslam Gondal T, Atif M, Shahbaz M, Batool Qaisarani T, Hanif Mughal M, Salehi B, Martorell M, Sharifi-Rad J. Apigenin as an anticancer agent. *Phytother Res.* 2020;34(8):1812-1828. doi: 10.1002/ptr.6647.
- Jaisinghani RN. Antibacterial properties of quercetin. *Microbiology Research.* 2017;8(1):6877. <https://doi.org/10.4081/mr.2017.6877>.

- Jeevanandam J, Barhoum A, Chan YS, Dufresne A, Danquah MK. Review on nanoparticles and nanostructured materials: history, sources, toxicity and regulations. *Beilstein J Nanotechnol.* 2018;9:1050-1074. doi: 10.3762/bjnano.9.98.
- Jeong YI, Cho CS, Kim SH, Ko KS, Kim SI, Shim YH, Nah JW. Preparation of poly (DL- lactide- co- glycolide) nanoparticles without surfactant. *J Appl Polym Sci.* 2001;80(12):2228-2236. doi: 10.1002/app.1326.
- Jeyabal PV, Syed MB, Venkataraman M, Sambandham JK, Sakthisekaran D. Apigenin inhibits oxidative stress-induced macromolecular damage in N-nitrosodiethylamine (NDEA)-induced hepatocellular carcinogenesis in Wistar albino rats. *Mol Carcinog.* 2005;44(1):11-20. doi: 10.1002/mc.20115.
- Ji J, Yu Q, Dai W, Wu L, Feng J, Zheng Y, Li Y, Guo C. Apigenin Alleviates Liver Fibrosis by Inhibiting Hepatic Stellate Cell Activation and Autophagy via TGF- β 1/Smad3 and p38/PPAR α Pathways. *PPAR Res.* 2021;2021:6651839. doi: 10.1155/2021/6651839.
- Jiang G, Huang Z, Yuan Y, Tao K, Feng W. Intracellular delivery of anti-BCR/ABL antibody by PLGA nanoparticles suppresses the oncogenesis of chronic myeloid leukemia cells. *J Hematol Oncol.* 2021;14(1):139. doi: 10.1186/s13045-021-01150-x.
- Jiao Y, Williams A, Wei N. Quercetin ameliorated insulin resistance via regulating METTL3-mediated N6-methyladenosine modification of PRKD2 mRNA in skeletal muscle and C2C12 myocyte cell line. *Nutr Metab Cardiovasc Dis.* 2022;32(11):2655-2668. doi: 10.1016/j.numecd.2022.06.019.
- Joardar S, Dewanjee S, Bhowmick S, Dua TK, Das S, Saha A, De Feo V. Rosmarinic Acid Attenuates Cadmium-Induced Nephrotoxicity via Inhibition of Oxidative Stress, Apoptosis, Inflammation and Fibrosis. *Int J Mol Sci.* 2019;20(8):2027. doi: 10.3390/ijms20082027.
- Jones AE, Frankel RS, Di Chiro G, Johnston GS. Brain scintigraphy with 99mTc pertechnetate, 99mTc polyphosphate, and 67Ga citrate. *Radiology.* 1974;112(1):123-129. doi: 10.1148/112.1.123.
- Kaefer CM, Milner JA. The role of herbs and spices in cancer prevention. *J Nutr Biochem.* 2008;19(6):347-61. doi: 10.1016/j.jnutbio.2007.11.003.
- Kahraman A, Çakar H, Köken T. The protective effect of quercetin on long-term alcohol consumption-induced oxidative stress. *Mol Biol Rep.* 2012;39(3):2789-2794. doi: 10.1007/s11033-011-1037-2.

References

- Kamaly N, Yameen B, Wu J, Farokhzad OC. Degradable Controlled-Release Polymers and Polymeric Nanoparticles: Mechanisms of Controlling Drug Release. *Chem Rev.* 2016;116(4):2602-2663. doi: 10.1021/acs.chemrev.5b00346.
- Kamiloglu S, Tomas M, Ozdal T, Capanoglu E. Effect of food matrix on the content and bioavailability of flavonoids. *Trends in Food Science & Technology.* 2021;117:15-33. doi.org/10.1016/j.tifs.2020.10.030.
- Kane SM, Davis DD. Technetium-99m. InStatPearls [Internet] 2021 Sep 22. StatPearls Publishing. Available from: <https://www.ncbi.nlm.nih.gov/books/NBK559013/>
- Kang JS, Lee MH. Noninvasive diagnostic and prognostic assessment tools for liver fibrosis and cirrhosis in patients with chronic liver disease. Tsoulfas G (Ed). In: *Liver Cirrhosis-Update and Current Challenges* 2017. Intech Open. doi:10.5772/intechopen.68317. Available from: <http://dx.doi.org/10.5772/intechopen.68317>.
- Kapoor DN, Bhatia A, Kaur R, Sharma R, Kaur G, Dhawan S. PLGA: a unique polymer for drug delivery. *Ther Deliv.* 2015;6(1):41-58. doi: 10.4155/tde.14.91.
- Kashyap P, Shikha D, Thakur M, Aneja A. Functionality of apigenin as a potent antioxidant with emphasis on bioavailability, metabolism, action mechanism and in vitro and in vivo studies: A review. *J Food Biochem.* 2022;46(4):e13950. doi: 10.1111/jfbc.13950.
- Katila N, Duwa R, Bhurtel S, Khanal S, Maharjan S, Jeong JH, Lee S, Choi DY, Yook S. Enhancement of blood-brain barrier penetration and the neuroprotective effect of resveratrol. *J Control Release.* 2022;346:1-19. doi: 10.1016/j.jconrel.2022.04.003.
- Kaur A, Nigam K, Tyagi A, Dang S. A Preliminary Pharmacodynamic Study for the Management of Alzheimer's Disease Using Memantine-Loaded PLGA Nanoparticles. *AAPS PharmSciTech.* 2022;23(8):298. doi: 10.1208/s12249-022-02449-9.
- Kawabata K, Mukai R, Ishisaka A. Quercetin and related polyphenols: new insights and implications for their bioactivity and bioavailability. *Food Funct.* 2015;6(5):1399-1417. doi: 10.1039/c4fo01178c.
- Kawabata K, Yoshioka Y, Terao J. Role of Intestinal Microbiota in the Bioavailability and Physiological Functions of Dietary Polyphenols. *Molecules.* 2019;24(2):370. doi: 10.3390/molecules24020370.

- Kazi M, Alhajri A, Alshehri SM, Elzayat EM, Al Meanazel OT, Shakeel F, Noman O, Altamimi MA, Alanazi FK. Enhancing Oral Bioavailability of Apigenin Using a Bioactive Self-Nanoemulsifying Drug Delivery System (Bio-SNEDDS): In Vitro, In Vivo and Stability Evaluations. *Pharmaceutics*. 2020;12(8):749. doi: 10.3390/pharmaceutics12080749.
- Kazmi I, Al-Abbasi FA, Afzal M, Altayb HN, Nadeem MS, Gupta G. Formulation and Evaluation of Kaempferol Loaded Nanoparticles against Experimentally Induced Hepatocellular Carcinoma: In Vitro and In Vivo Studies. *Pharmaceutics*. 2021;13(12):2086. doi: 10.3390/pharmaceutics13122086.
- Kazmi I, Al-Abbasi FA, Imam SS, Afzal M, Nadeem MS, Altayb HN, Alshehri S. Formulation and Evaluation of Apigenin-Loaded Hybrid Nanoparticles. *Pharmaceutics*. 2022;14(4):783. doi: 10.3390/pharmaceutics14040783.
- Khan F, Niaz K, Maqbool F, Ismail Hassan F, Abdollahi M, Nagulapalli Venkata KC, Nabavi SM, Bishayee A. Molecular Targets Underlying the Anticancer Effects of Quercetin: An Update. *Nutrients*. 2016;8(9):529. doi: 10.3390/nu8090529.
- Khan H, Ullah H, Aschner M, Cheang WS, Akkol EK. Neuroprotective Effects of Quercetin in Alzheimer's Disease. *Biomolecules*. 2019;10(1):59. doi: 10.3390/biom10010059.
- Khandelwal N, Chander Y, Kumar R, Riyesh T, Dedar RK, Kumar M, Gulati BR, Sharma S, Tripathi BN, Barua S, Kumar N. Antiviral activity of Apigenin against buffalopox: Novel mechanistic insights and drug-resistance considerations. *Antiviral Res*. 2020;181:104870. doi: 10.1016/j.antiviral.2020.104870.
- Kim CH, Kim JE, Song YJ. Antiviral Activities of Quercetin and Isoquercitrin Against Human Herpesviruses. *Molecules*. 2020;25(10):2379. doi: 10.3390/molecules25102379.
- Kim EK, Kwon KB, Song MY, Han MJ, Lee JH, Lee YR, Lee JH, Ryu DG, Park BH, Park JW. Flavonoids protect against cytokine-induced pancreatic beta-cell damage through suppression of nuclear factor kappaB activation. *Pancreas*. 2007;35(4):e1-e9. doi: 10.1097/mpa.0b013e31811ed0d2.
- Kim S, Woo ER, Lee DG. Apigenin promotes antibacterial activity via regulation of nitric oxide and superoxide anion production. *J Basic Microbiol*. 2020;60(10):862-872. doi: 10.1002/jobm.202000432.

References

- Kim TW, Lee HG. Apigenin Induces Autophagy and Cell Death by Targeting EZH2 under Hypoxia Conditions in Gastric Cancer Cells. *Int J Mol Sci.* 2021;22(24):13455. doi: 10.3390/ijms222413455.
- Kisseleva T, Brenner D. Molecular and cellular mechanisms of liver fibrosis and its regression. *Nat Rev Gastroenterol Hepatol.* 2021;18(3):151-166. doi: 10.1038/s41575-020-00372-7.
- Kopustinskiene DM, Jakstas V, Savickas A, Bernatoniene J. Flavonoids as Anticancer Agents. *Nutrients.* 2020;12(2):457. doi: 10.3390/nu12020457.
- Koyama Y, Brenner DA. Liver inflammation and fibrosis. *J Clin Invest.* 2017;127(1):55-64. doi: 10.1172/JCI88881.
- Krishnamurthy GT, Turner FE. Pharmacokinetics and clinical application of technetium 99m-labeled hepatobiliary agents. *Semin Nucl Med.* 1990;20(2):130-149. doi: 10.1016/s0001-2998(05)80166-7.
- Kumar S, Pandey AK. Chemistry and biological activities of flavonoids: an overview. *Scientific World Journal.* 2013;2013:162750. doi: 10.1155/2013/162750.
- Kumari A, Yadav SK, Yadav SC. Biodegradable polymeric nanoparticles based drug delivery systems. *Colloids Surf B Biointerfaces.* 2010;75(1):1-18. doi: 10.1016/j.colsurfb.2009.09.001.
- Kumari S, Goyal A, Garg M. Phytoconstituents Based Novel Nano-Formulations: An Approach. *ECS Transactions.* 2022;107(1):7365. doi: 10.1149/10701.7365ecst.
- Kwun MS, Lee DG. Quercetin-induced yeast apoptosis through mitochondrial dysfunction under the accumulation of magnesium in *Candida albicans*. *Fungal Biol.* 2020;124(2):83-90. doi: 10.1016/j.funbio.2019.11.009.
- Labeur TA, Cieslak KP, Van Gulik TM, Takkenberg RB, van der Velden S, Lam MGEH, Klumpen HJ, Bennink RJ, van Delden OM. The utility of 99mTc-mebrofenin hepatobiliary scintigraphy with SPECT/CT for selective internal radiation therapy in hepatocellular carcinoma. *Nucl Med Commun.* 2020;41(8):740-749. doi: 10.1097/MNM.0000000000001224.
- Lee H, Woo ER, Lee DG. Apigenin induces cell shrinkage in *Candida albicans* by membrane perturbation. *FEMS Yeast Res.* 2018;18(1):1-9. doi: 10.1093/femsyr/foy003.
- Lee UE, Friedman SL. Mechanisms of hepatic fibrogenesis. *Best Pract Res Clin Gastroenterol.* 2011;25(2):195-206. doi: 10.1016/j.bpg.2011.02.005.

- Li K, Xing S, Wang M, Peng Y, Dong Y, Li X. Anticomplement and antimicrobial activities of flavonoids from *Entada phaseoloides*. *Nat Prod Commun*. 2012;7(7):867-871.
- Li R, Chen L, Yao GM, Yan HL, Wang L. Effects of quercetin on diabetic retinopathy and its association with NLRP3 inflammasome and autophagy. *Int J Ophthalmol*. 2021;14(1):42-49. doi: 10.18240/ijo.2021.01.06.
- Li S, Hong M, Tan HY, Wang N, Feng Y. Insights into the Role and Interdependence of Oxidative Stress and Inflammation in Liver Diseases. *Oxid Med Cell Longev*. 2016;2016:4234061. doi: 10.1155/2016/4234061.
- Li S, Tan HY, Wang N, Zhang ZJ, Lao L, Wong CW, Feng Y. The Role of Oxidative Stress and Antioxidants in Liver Diseases. *Int J Mol Sci*. 2015;16(11):26087-26124. doi: 10.3390/ijms161125942.
- Li SD, Huang L. Stealth nanoparticles: high density but sheddable PEG is a key for tumor targeting. *J Control Release*. 2010;145(3):178-181. doi: 10.1016/j.jconrel.2010.03.016.
- Li X, Li S, Ma C, Li T, Yang L. Preparation of baicalin-loaded ligand-modified nanoparticles for nose-to-brain delivery for neuroprotection in cerebral ischemia. *Drug Deliv*. 2022;29(1):1282-1298. doi: 10.1080/10717544.2022.2064564.
- Li Y, Che J, Chang L, Guo M, Bao X, Mu D, Sun X, Zhang X, Lu W, Xie J. CD47- and Integrin $\alpha 4/\beta 1$ -Comodified-Macrophage-Membrane-Coated Nanoparticles Enable Delivery of Colchicine to Atherosclerotic Plaque. *Adv Healthc Mater*. 2022;11(4):e2101788. doi: 10.1002/adhm.202101788.
- Li Y, Cheng X, Chen C, Huijuan W, Zhao H, Liu W, Xiang Z, Wang Q. Apigenin, a flavonoid constituent derived from *P. villosa*, inhibits hepatocellular carcinoma cell growth by CyclinD1/CDK4 regulation via p38 MAPK-p21 signaling. *Pathol Res Pract*. 2020;216(1):152701. doi: 10.1016/j.prp.2019.152701.
- Li Y, Yao J, Han C, Yang J, Chaudhry MT, Wang S, Liu H, Yin Y. Quercetin, Inflammation and Immunity. *Nutrients*. 2016;8(3):167. doi: 10.3390/nu8030167.
- Lin L, Yan L, Liu Y, Qu C, Ni J, Li H. The Burden and Trends of Primary Liver Cancer Caused by Specific Etiologies from 1990 to 2017 at the Global, Regional, National, Age, and Sex Level Results from the Global Burden of Disease Study 2017. *Liver Cancer*. 2020;9(5):563-582. doi: 10.1159/000508568.

References

- Lin R, Piao M, Song Y, Liu C. Quercetin Suppresses AOM/DSS-Induced Colon Carcinogenesis through Its Anti-Inflammation Effects in Mice. *J Immunol Res.* 2020; 2020:9242601. doi: 10.1155/2020/9242601.
- Ling C, Lei C, Zou M, Cai X, Xiang Y, Xie Y, Li X, Huang D, Wang Y. Neuroprotective effect of apigenin against cerebral ischemia/reperfusion injury. *J Int Med Res.* 2020;48(9):300060520945859. doi: 10.1177/0300060520945859.
- Liu G, McEnnis K. Glass Transition Temperature of PLGA Particles and the Influence on Drug Delivery Applications. *Polymers (Basel).* 2022;14(5):993. doi: 10.3390/polym14050993.
- Liu R, Rong G, Liu Y, Huang W, He D, Lu R. Delivery of apigenin-loaded magnetic Fe₂O₃/Fe₃O₄@mSiO₂ nanocomposites to A549 cells and their antitumor mechanism. *Mater Sci Eng C Mater Biol Appl.* 2021;120:111719. doi: 10.1016/j.msec.2020.111719.
- Liu RH. Health-promoting components of fruits and vegetables in the diet. *Adv Nutr.* 2013;4(3):384S-392S. doi: 10.3945/an.112.003517.
- Liu X, Gao X, Li H, Li Z, Wang X, Zhang L, Wang B, Chen X, Meng X, Yu J. Ellagic acid exerts anti-fibrotic effects on hypertrophic scar fibroblasts via inhibition of TGF- β 1/Smad2/3 pathway. *Applied Biological Chemistry.* 2021;64:67. doi: 10.1186/s13765-021-00641-2.
- Liu Y, Song Y, Li S, Mo L. Cardioprotective Effect of Quercetin against Ischemia/Reperfusion Injury Is Mediated Through NO System and Mitochondrial K-ATP Channels. *Cell J.* 2021;23(2):184-190. doi: 10.22074/cellj.2021.7183.
- Liu Z, Hu M. Natural polyphenol disposition via coupled metabolic pathways. *Expert Opin Drug Metab Toxicol.* 2007;3(3):389-406. doi: 10.1517/17425255.3.3.389.
- Lozano O, Lázaro-Alfaro A, Silva-Platas C, Oropeza-Almazán Y, Torres-Quintanilla A, Bernal-Ramírez J, Alves-Figueiredo H, García-Rivas G. Nanoencapsulated Quercetin Improves Cardioprotection during Hypoxia-Reoxygenation Injury through Preservation of Mitochondrial Function. *Oxid Med Cell Longev.* 2019;2019:7683051. doi: 10.1155/2019/7683051.
- Lü JM, Wang X, Marin-Muller C, Wang H, Lin PH, Yao Q, Chen C. Current advances in research and clinical applications of PLGA-based nanotechnology. *Expert Rev Mol Diagn.* 2009;9(4):325-341. doi: 10.1586/erm.09.15.

- Luo M, Liu Z, Hu Z, He Q. Quercetin improves contrast-induced acute kidney injury through the HIF-1 α /lncRNA NEAT1/HMGB1 pathway. *Pharm Biol.* 2022;60(1):889-898. doi: 10.1080/13880209.2022.2058558.
- Lv Y, Gao X, Luo Y, Fan W, Shen T, Ding C, Yao M, Song S, Yan L. Apigenin ameliorates HFD-induced NAFLD through regulation of the XO/NLRP3 pathways. *J Nutr Biochem.* 2019;71:110-121. doi: 10.1016/j.jnutbio.2019.05.015.
- Ma JQ, Li Z, Xie WR, Liu CM, Liu SS. Quercetin protects mouse liver against CCl₄ - induced inflammation by the TLR2/4 and MAPK/NF- κ B pathway. *Int Immunopharmacol.* 2015;28(1):531-539. doi: 10.1016/j.intimp.2015.06.036.
- Mabrouk Zayed MM, Sahyon HA, Hanafy NAN, El-Kemary MA. The Effect of Encapsulated Apigenin Nanoparticles on HePG-2 Cells through Regulation of P53. *Pharmaceutics.* 2022;14(6):1160. doi: 10.3390/pharmaceutics14061160.
- Madunić J, Madunić IV, Gajski G, Popić J, Garaj-Vrhovac V. Apigenin: A dietary flavonoid with diverse anticancer properties. *Cancer Lett.* 2018;413:11-22. doi: 10.1016/j.canlet.2017.10.041.
- Magar RT, Sohng JK. A Review on Structure, Modifications and Structure-Activity Relation of Quercetin and Its Derivatives. *J Microbiol Biotechnol.* 2020;30(1):11-20. doi: 10.4014/jmb.1907.07003.
- Mahajan UB, Chandrayan G, Patil CR, Arya DS, Suchal K, Agrawal YO, Ojha S, Goyal SN. The Protective Effect of Apigenin on Myocardial Injury in Diabetic Rats mediating Activation of the PPAR- γ Pathway. *Int J Mol Sci.* 2017;18(4):756. doi: 10.3390/ijms18040756.
- Mahapatro A, Singh DK. Biodegradable nanoparticles are excellent vehicle for site directed in-vivo delivery of drugs and vaccines. *J Nanobiotechnology.* 2011;9:55. doi: 10.1186/1477-3155-9-55.
- Makadia HK, Siegel SJ. Poly Lactic-co-Glycolic Acid (PLGA) as Biodegradable Controlled Drug Delivery Carrier. *Polymers (Basel).* 2011;3(3):1377-1397. doi: 10.3390/polym3031377.
- Maksymchuk O, Shysh A, Rosohatska I, Chashchyn M. Quercetin prevents type 1 diabetic liver damage through inhibition of CYP2E1. *Pharmacol Rep.* 2017;69(6):1386-1392. doi: 10.1016/j.pharep.2017.05.020.

References

- Malik S, Suchal K, Khan SI, Bhatia J, Kishore K, Dinda AK, Arya DS. Apigenin ameliorates streptozotocin-induced diabetic nephropathy in rats via MAPK-NF- κ B-TNF- α and TGF- β 1-MAPK-fibronectin pathways. *Am J Physiol Renal Physiol*. 2017;313(2): F414-F422. doi: 10.1152/ajprenal.00393.2016.
- Mandal AK, Das N. Sugar coated liposomal flavonoid: a unique formulation in combating carbontetrachloride induced hepatic oxidative damage. *J Drug Target*. 2005;13(5):305-315. doi: 10.1080/10611860500230278.
- Manka P, Verheyen J, Gerken G, Canbay A. Liver Failure due to Acute Viral Hepatitis (A-E). *Visc Med*. 2016;32(2):80-85. doi: 10.1159/000444915.
- Marklund S, Marklund G. Involvement of the superoxide anion radical in the autoxidation of pyrogallol and a convenient assay for superoxide dismutase. *Eur J Biochem*. 1974;47(3):469-474. doi: 10.1111/j.1432-1033.1974.tb03714.x.
- McGlynn KA, Petrick JL, London WT. Global epidemiology of hepatocellular carcinoma: an emphasis on demographic and regional variability. *Clin Liver Dis*. 2015;19(2):223-238. doi: 10.1016/j.cld.2015.01.001.
- Meng Y, Su A, Yuan S, Zhao H, Tan S, Hu C, Deng H, Guo Y. Evaluation of Total Flavonoids, Myricetin, and Quercetin from *Hovenia dulcis* Thunb. As Inhibitors of α -Amylase and α -Glucosidase. *Plant Foods Hum Nutr*. 2016;71(4):444-449. doi: 10.1007/s11130-016-0581-2.
- Meng ZX, Xu XX, Zheng W, Zhou HM, Li L, Zheng YF, Lou X. Preparation and characterization of electrospun PLGA/gelatin nanofibers as a potential drug delivery system. *Colloids Surf B Biointerfaces*. 2011;84(1):97-102. doi: 10.1016/j.colsurfb.2010.12.022.
- Merrick MV. Bone scintigraphy--an update. *Clin Radiol*. 1989;40(3):231-232. doi: 10.1016/s0009-9260(89)80178-3.
- Mikuš P, Melník M, Forgáčsová A, Krajčiová D, Havránek E. Gallium compounds in nuclear medicine and oncology. *Main Group Metal Chemistry*. 2014;37(3-4):53-65. doi: 10.1515/mgmc-2014-0009.
- Miltonprabu S, Tomczyk M, Skalicka-Woźniak K, Rastrelli L, Daglia M, Nabavi SF, Alavian SM, Nabavi SM. Hepatoprotective effect of quercetin: From chemistry to medicine. *Food Chem Toxicol*. 2017;108(Pt B):365-374. doi: 10.1016/j.fct.2016.08.034.

- Mittal S, El-Serag HB. Epidemiology of hepatocellular carcinoma: consider the population. *J Clin Gastroenterol.* 2013;47Suppl(0):S2-S6. doi: 10.1097/MCG.0b013e3182872f29.
- Mohamed WR, Kotb AS, Abd El-Raouf OM, Mohammad Fikry E. Apigenin alleviated acetaminophen-induced hepatotoxicity in low protein-fed rats: Targeting oxidative stress, STAT3, and apoptosis signals. *J Biochem Mol Toxicol.* 2020;34(5):e22472. doi: 10.1002/jbt.22472.
- Moradi SZ, Momtaz S, Bayrami Z, Farzaei MH, Abdollahi M. Nanoformulations of Herbal Extracts in Treatment of Neurodegenerative Disorders. *Front Bioeng Biotechnol.* 2020;8:238. doi: 10.3389/fbioe.2020.00238.
- Morimoto Y, Baba T, Sasaki T, Hiramatsu K. Apigenin as an anti-quinolone-resistance antibiotic. *Int J Antimicrob Agents.* 2015;46(6):666-673. doi: 10.1016/j.ijantimicag.2015.09.006.
- Moslehi M, Rezaei S, Talebzadeh P, Ansari MJ, Jawad MA, Jalil AT, Rastegar-Pouyani N, Jafarzadeh E, Taeb S, Najafi M. Apigenin in cancer therapy: Prevention of genomic instability and anticancer mechanisms. *Clin Exp Pharmacol Physiol.* 2023;50(1):3-18. doi: 10.1111/1440-1681.13725.
- Mu Y, Zeng H, Chen W. Quercetin Inhibits Biofilm Formation by Decreasing the Production of EPS and Altering the Composition of EPS in *Staphylococcus epidermidis*. *Front Microbiol.* 2021;12:631058. doi: 10.3389/fmicb.2021.631058.
- Muriel P. Role of free radicals in liver diseases. *Hepatol Int.* 2009;3(4):526-536. doi: 10.1007/s12072-009-9158-6.
- Murota K, Nakamura Y, Uehara M. Flavonoid metabolism: the interaction of metabolites and gut microbiota. *Biosci Biotechnol Biochem.* 2018;82(4):600-610. doi: 10.1080/09168451.2018.1444467.
- Murota K, Terao J. Antioxidative flavonoid quercetin: implication of its intestinal absorption and metabolism. *Arch Biochem Biophys.* 2003;417(1):12-17. doi: 10.1016/s0003-9861(03)00284-4.
- Murthy SK. Nanoparticles in modern medicine: state of the art and future challenges. *Int J Nanomedicine.* 2007;2(2):129-141.

References

- Murugan RS, Vinothini G, Hara Y, Nagini S. Black tea polyphenols target matrix metalloproteinases, RECK, proangiogenic molecules and histone deacetylase in a rat hepatocarcinogenesis model. *Anticancer Res.* 2009;29(6):2301-2305.
- Nabavi SF, Khan H, D'onofrio G, Šamec D, Shirooie S, Dehpour AR, Argüelles S, Habtemariam S, Sobarzo-Sanchez E. Apigenin as neuroprotective agent: Of mice and men. *Pharmacol Res.* 2018;128:359-365. doi: 10.1016/j.phrs.2017.10.008.
- Nabavi SM, Habtemariam S, Daglia M, Nabavi SF. Apigenin and Breast Cancers: From Chemistry to Medicine. *Anticancer Agents Med Chem.* 2015;15(6):728-735. doi: 10.2174/1871520615666150304120643.
- Nagaratnam N, Nagaratnam K, Cheuk G. Chronic Liver Disease. In: *Geriatric Diseases.* Springer, Cham. 2017: doi: 10.1007/978-3-319-32700-6_22-1.
- Naqvi S, Sharma H, Flora SJ. Lactobionic Acid Conjugated Quercetin Loaded Organically Modified Silica Nanoparticles Mitigates Cyclophosphamide Induced Hepatocytotoxicity. *Int J Nanomedicine.* 2019;14:8943-8959. doi: 10.2147/IJN.S218577.
- Nayaka HB, Londonkar RL, Umesh MK, Tukappa A. Antibacterial Attributes of Apigenin, Isolated from *Portulaca oleracea* L. *Int J Bacteriol.* 2014;2014:175851. doi: 10.1155/2014/175851.
- Nguyen TLA, Bhattacharya D. Antimicrobial Activity of Quercetin: An Approach to Its Mechanistic Principle. *Molecules.* 2022;27(8):2494. doi: 10.3390/molecules27082494.
- Nie T, Cooper GJS. Mechanisms Underlying the Antidiabetic Activities of Polyphenolic Compounds: A Review. *Front Pharmacol.* 2021;12:798329. doi: 10.3389/fphar.2021.798329.
- Nigam K, Kaur A, Tyagi A, Manda K, Goswami N, Nematullah M, Khan F, Gabrani R, Gauba P, Dang S. In vitro & in vivo evaluations of PLGA nanoparticle based combinatorial drug therapy for baclofen and lamotrigine for neuropathic pain management. *J Microencapsul.* 2022;39(2):95-109. doi: 10.1080/02652048.2022.2041751.
- Nordyke RA. Metabolic and physiologic aspects of ¹³¹I rose bengal in studying liver function. *Semin Nucl Med.* 1972;2(2):157-166. doi: 10.1016/s0001-2998(72)80069-2.
- Noureddin M, Rinella ME. Nonalcoholic Fatty liver disease, diabetes, obesity, and hepatocellular carcinoma. *Clin Liver Dis.* 2015;19(2):361-379. doi: 10.1016/j.cld.2015.01.012.

- Nozhat Z, Heydarzadeh S, Memariani Z, Ahmadi A. Chemoprotective and chemosensitizing effects of apigenin on cancer therapy. *Cancer Cell Int.* 2021;21(1):574. doi: 10.1186/s12935-021-02282-3.
- Nusrat S, Khan MS, Fazili J, Madhoun MF. Cirrhosis and its complications: evidence-based treatment. *World J Gastroenterol.* 2014;20(18):5442-5460. doi: 10.3748/wjg.v20.i18.5442.
- Ogura Y, Kitada M, Xu J, Monno I, Koya D. CD38 inhibition by apigenin ameliorates mitochondrial oxidative stress through restoration of the intracellular NAD⁺/NADH ratio and Sirt3 activity in renal tubular cells in diabetic rats. *Aging (Albany NY).* 2020;12(12):11325-11336. doi: 10.18632/aging.103410.
- Okuda H, Nunes R, Vallabhajosula S, Strashun A, Goldsmith SJ, Berk PD. Studies of the hepatocellular uptake of the hepatobiliary scintiscanning agent ^{99m}Tc-DISIDA. *J Hepatol.* 1986;3(2):251-259. doi: 10.1016/s0168-8278(86)80035-6.
- Ozougwu JC. Physiology of the liver. *International Journal of Research in Pharmacy and Biosciences.* 2017; 4(8):13-24.
- Özsoy Gökbilen S, Becer E, Vatansever HS. Senescence-mediated anticancer effects of quercetin. *Nutr Res.* 2022;104:82-90. doi: 10.1016/j.nutres.2022.04.007.
- Palafox-Carlos H, Ayala-Zavala JF, González-Aguilar GA. The role of dietary fiber in the bioaccessibility and bioavailability of fruit and vegetable antioxidants. *J Food Sci.* 2011;76(1):R6-R15. doi: 10.1111/j.1750-3841.2010.01957.x.
- Pan FF, Zheng YB, Shi CJ, Zhang FW, Zhang JF, Fu WM. H19-Wnt/ β -catenin regulatory axis mediates the suppressive effects of apigenin on tumor growth in hepatocellular carcinoma. *Eur J Pharmacol.* 2021;893:173810. doi: 10.1016/j.ejphar.2020.173810.
- Panda S, Kar A. Apigenin (4',5,7-trihydroxyflavone) regulates hyperglycaemia, thyroid dysfunction and lipid peroxidation in alloxan-induced diabetic mice. *J Pharm Pharmacol.* 2007;59(11):1543-1548. doi: 10.1211/jpp.59.11.0012.
- Pandey KB, Rizvi SI. Plant polyphenols as dietary antioxidants in human health and disease. *Oxid Med Cell Longev.* 2009;2(5):270-278. doi: 10.4161/oxim.2.5.9498.
- Pandey P, Rahman M, Bhatt PC, Beg S, Paul B, Hafeez A, Al-Abbasi FA, Nadeem MS, Baothman O, Anwar F, Kumar V. Implication of nano-antioxidant therapy for treatment

References

- of hepatocellular carcinoma using PLGA nanoparticles of rutin. *Nanomedicine (Lond)*. 2018;13(8):849-870. doi: 10.2217/nmm-2017-0306.
- Pandey SK, Patel DK, Thakur R, Mishra DP, Maiti P, Haldar C. Anti-cancer evaluation of quercetin embedded PLA nanoparticles synthesized by emulsified nanoprecipitation. *Int J Biol Macromol*. 2015;75:521-529. doi: 10.1016/j.ijbiomac.2015.02.011.
- Pang L, Zou S, Shi Y, Mao Q, Chen Y. Apigenin attenuates PM2.5-induced airway hyperresponsiveness and inflammation by down-regulating NF- κ B in murine model of asthma. *Int J Clin Exp Pathol*. 2019;12(10):3700-3709.
- Papagiannopoulou D. Technetium-99m radiochemistry for pharmaceutical applications. *J Labelled Comp Radiopharm*. 2017;60(11):502-520. doi: 10.1002/jlcr.3531.
- Park CH, Min SY, Yu HW, Kim K, Kim S, Lee HJ, Kim JH, Park YJ. Effects of Apigenin on RBL-2H3, RAW264.7, and HaCaT Cells: Anti-Allergic, Anti-Inflammatory, and Skin-Protective Activities. *Int J Mol Sci*. 2020;21(13):4620. doi: 10.3390/ijms21134620.
- Patel RV, Mistry BM, Shinde SK, Syed R, Singh V, Shin HS. Therapeutic potential of quercetin as a cardiovascular agent. *Eur J Med Chem*. 2018;155:889-904. doi: 10.1016/j.ejmech.2018.06.053.
- Patra A, Satpathy S, Naik PK, Kazi M, Hussain MD. Folate receptor-targeted PLGA-PEG nanoparticles for enhancing the activity of genistein in ovarian cancer. *Artif Cells Nanomed Biotechnol*. 2022;50(1):228-239. doi: 10.1080/21691401.2022.2118758.
- Patra JK, Das G, Fraceto LF, Campos EVR, Rodriguez-Torres MDP, Acosta-Torres LS, Diaz-Torres LA, Grillo R, Swamy MK, Sharma S, Habtemariam S, Shin HS. Nano based drug delivery systems: recent developments and future prospects. *J Nanobiotechnology*. 2018;16(1):71. doi: 10.1186/s12951-018-0392-8.
- Peça IN, Petrova KT, Cardoso MM, Barros MT. Preparation and characterization of polymeric nanoparticles composed of poly (dl-lactide-co-glycolide) and poly (dl-lactide-co-glycolide)-co-poly (ethylene glycol)-10%-Triblock end-capped with a galactose moiety. *React. Funct. Polym*. 2012;72(10):729-735. doi: 10.1016/j.reactfunctpolym.2012.06.019.
- Peng J, Li Q, Li K, Zhu L, Lin X, Lin X, Shen Q, Li G, Xie X. Quercetin Improves Glucose and Lipid Metabolism of Diabetic Rats: Involvement of Akt Signaling and SIRT1. *J Diabetes Res*. 2017;2017:3417306. doi: 10.1155/2017/3417306.

- Pingili RB, Challa SR, Pawar AK, Toleti V, Kodali T, Koppula S. A systematic review on hepatoprotective activity of quercetin against various drugs and toxic agents: Evidence from preclinical studies. *Phytother Res.* 2020;34(1):5-32. doi: 10.1002/ptr.6503.
- Pinheiro RGR, Granja A, Loureiro JA, Pereira MC, Pinheiro M, Neves AR, Reis S. Quercetin lipid nanoparticles functionalized with transferrin for Alzheimer's disease. *Eur J Pharm Sci.* 2020;148:105314. doi: 10.1016/j.ejps.2020.105314.
- Pisonero-Vaquero S, González-Gallego J, Sánchez-Campos S, García-Mediavilla MV. Flavonoids and Related Compounds in Non-Alcoholic Fatty Liver Disease Therapy. *Curr Med Chem.* 2015;22(25):2991-3012. doi: 10.2174/0929867322666150805094940.
- Qi W, Qi W, Xiong D, Long M. Quercetin: Its Antioxidant Mechanism, Antibacterial Properties and Potential Application in Prevention and Control of Toxipathy. *Molecules.* 2022; 27(19):6545. doi: 10.3390/molecules27196545.
- Qian S, Fan W, Qian P, Zhang D, Wei Y, Chen H, Li X. Apigenin restricts FMDV infection and inhibits viral IRES driven translational activity. *Viruses.* 2015;7(4):1613-1626. doi: 10.3390/v7041613.
- Rahmani AH, Alsahli MA, Almatroudi A, Almogbel MA, Khan AA, Anwar S, Almatroodi SA. The Potential Role of Apigenin in Cancer Prevention and Treatment. *Molecules.* 2022;27(18):6051. doi: 10.3390/molecules27186051.
- Rahmati A, Homayouni Tabrizi M, Karimi E, Zarei B. Fabrication and assessment of folic acid conjugated-chitosan modified PLGA nanoparticle for delivery of alpha terpineol in colon cancer. *J Biomater Sci Polym Ed.* 2022;33(10):1289-1307. doi: 10.1080/09205063.2022.2051693.
- Ramaswamy MR, Hawkins RA. Nuclear Medicine Imaging. Editor(s): Johnson LR (Eds). In: *Encyclopedia of Gastroenterology*, Elsevier, 2004, pp. 748-754, ISBN 9780123868602. doi: 10.1016/B0-12-386860-2/00512-8.
- Ramezani M, Ebrahimian M, Hashemi M. Current Strategies in the Modification of PLGA-based Gene Delivery System. *Curr Med Chem.* 2017;24(7):728-739. doi: 10.2174/0929867324666161205130416.
- Rao JP, Geckeler KE. Polymer nanoparticles: Preparation techniques and size-control parameters. *Prog in Polym Sci.* 2011;36(7):887-913. doi: 10.1016/j.progpolymsci.2011.01.001.

References

- Rašković A, Gigov S, Čapo I, Paut Kusturica M, Milijašević B, Kojić-Damjanov S, Martić N. Antioxidative and Protective Actions of Apigenin in a Paracetamol-Induced Hepatotoxicity Rat Model. *Eur J Drug Metab Pharmacokinet.* 2017;42(5):849-856. doi: 10.1007/s13318-017-0407-0.
- Rauf A, Imran M, Khan IA, Ur-Rehman M, Gilani SA, Mehmood Z, Mubarak MS. Anticancer potential of quercetin: A comprehensive review. *Phytother Res.* 2018;32(11):2109-2130. doi: 10.1002/ptr.6155.
- Raza A, Sood GK. Hepatocellular carcinoma review: current treatment, and evidence-based medicine. *World J Gastroenterol.* 2014;20(15):4115-4127. doi: 10.3748/wjg.v20.i15.4115.
- Rechner AR, Smith MA, Kuhnle G, Gibson GR, Debnam ES, Srai SK, Moore KP, Rice-Evans CA. Colonic metabolism of dietary polyphenols: influence of structure on microbial fermentation products. *Free Radic Biol Med.* 2004;36(2):212-225. doi: 10.1016/j.freeradbiomed.2003.09.022.
- Ren B, Qin W, Wu F, Wang S, Pan C, Wang L, Zeng B, Ma S, Liang J. Apigenin and naringenin regulate glucose and lipid metabolism, and ameliorate vascular dysfunction in type 2 diabetic rats. *Eur J Pharmacol.* 2016;773:13-23. doi: 10.1016/j.ejphar.2016.01.002.
- Ren J, Li J, Liu X, Feng Y, Gui Y, Yang J, He W, Dai C. Quercetin Inhibits Fibroblast Activation and Kidney Fibrosis Involving the Suppression of Mammalian Target of Rapamycin and β -catenin Signaling. *Sci Rep.* 2016;6:23968. doi: 10.1038/srep23968.
- Reyes-Farias M, Carrasco-Pozo C. The Anti-Cancer Effect of Quercetin: Molecular Implications in Cancer Metabolism. *Int J Mol Sci.* 2019;20(13):3177. doi: 10.3390/ijms20133177.
- Rezvantalab S, Drude NI, Moraveji MK, Güvener N, Koons EK, Shi Y, Lammers T, Kiessling F. PLGA-Based Nanoparticles in Cancer Treatment. *Front Pharmacol.* 2018;9:1260. doi: 10.3389/fphar.2018.01260.
- Rodríguez-Félix F, Del-Toro-Sánchez CL, Javier Cinco-Moroyoqui F, Juárez J, Ruiz-Cruz S, López-Ahumada GA, Carvajal-Millan E, Castro-Enríquez DD, Barreras-Urbina CG, Tapia-Hernández JA. Preparation and Characterization of Quercetin-Loaded Zein Nanoparticles by Electrospraying and Study of In Vitro Bioavailability. *J Food Sci.* 2019;84(10):2883-2897. doi: 10.1111/1750-3841.14803.

- Rodríguez-García C, Sánchez-Quesada C, J Gaforio J. Dietary Flavonoids as Cancer Chemopreventive Agents: An Updated Review of Human Studies. *Antioxidants* (Basel). 2019;8(5):137. doi: 10.3390/antiox8050137.
- Roy PK, Park SH, Song MG, Park SY. Antimicrobial Efficacy of Quercetin against *Vibrio parahaemolyticus* Biofilm on Food Surfaces and Downregulation of Virulence Genes. *Polymers* (Basel). 2022;14(18):3847. doi: 10.3390/polym14183847.
- Rudrapal M, Khairnar SJ, Khan J, Dukhyil AB, Ansari MA, Alomary MN, Alshabrmi FM, Palai S, Deb PK, Devi R. Dietary Polyphenols and Their Role in Oxidative Stress-Induced Human Diseases: Insights Into Protective Effects, Antioxidant Potentials and Mechanism(s) of Action. *Front Pharmacol.* 2022;13:806470. doi: 10.3389/fphar.2022.806470.
- Sadat Tabatabaei Mirakabad F, Nejati-Koshki K, Akbarzadeh A, Yamchi MR, Milani M, Zarghami N, Zeighamian V, Rahimzadeh A, Alimohammadi S, Hanifehpour Y, Joo SW. PLGA-based nanoparticles as cancer drug delivery systems. *Asian Pac J Cancer Prev.* 2014;15(2):517-535. doi: 10.7314/apjcp.2014.15.2.517.
- Saha P, Talukdar AD, Nath R, Sarker SD, Nahar L, Sahu J, Choudhury MD. Role of Natural Phenolics in Hepatoprotection: A Mechanistic Review and Analysis of Regulatory Network of Associated Genes. *Front Pharmacol.* 2019;10:509. doi: 10.3389/fphar.2019.00509.
- Sahindokuyucu-Kocasari F, Akyol Y, Ozmen O, Erdemli-Kose SB, Garli S. Apigenin alleviates methotrexate-induced liver and kidney injury in mice. *Hum Exp Toxicol.* 2021;40(10):1721-1731. doi: 10.1177/09603271211009964.
- Sahnoun M, Saibi W, Brini F, Bejar S. Apigenin isolated from *A. americana* encodes Human and *Aspergillus oryzae* S2 α -amylase inhibitions: credible approach for antifungal and antidiabetic therapies. *J Food Sci Technol.* 2018;55(4):1489-1498. doi: 10.1007/s13197-018-3065-6.
- Sahu R, Dua TK, Das S, De Feo V, Dewanjee S. Wheat phenolics suppress doxorubicin-induced cardiotoxicity via inhibition of oxidative stress, MAP kinase activation, NF- κ B pathway, PI3K/Akt/mTOR impairment, and cardiac apoptosis. *Food Chem Toxicol.* 2019;125:503-519. doi: 10.1016/j.fct.2019.01.034.
- Salehi B, Machin L, Monzote L, Sharifi-Rad J, Ezzat SM, Salem MA, Merghany RM, El Mahdy NM, Kılıç CS, Sytar O, Sharifi-Rad M, Sharopov F, Martins N, Martorell M, Cho

References

- WC. Therapeutic Potential of Quercetin: New Insights and Perspectives for Human Health. *ACS Omega*. 2020;5(20):11849-11872. doi: 10.1021/acsomega.0c01818.
- Salmani JMM, Zhang XP, Jacob JA, Chen BA. Apigenin's anticancer properties and molecular mechanisms of action: Recent advances and future perspectives. *Chin J Nat Med*. 2017; 15(5):321-329. doi: 10.1016/S1875-5364(17)30052-3.
- Sanchez-Gonzalez PD, Lopez-Hernandez FJ, Perez-Barriocanal F, Morales AI, Lopez-Nova JM. Quercetin reduces cisplatin nephrotoxicity in rats without compromising its anti-tumour activity. *Nephrol Dial Transplant*. 2011;26(11):3484-3495. doi: 10.1093/ndt/gfr195.
- Sato H, Goto W, Yamamura J, Kurokawa M, Kageyama S, Takahara T, Watanabe A, Shiraki K. Therapeutic basis of glycyrrhizin on chronic hepatitis B. *Antiviral Res*. 1996;30(2-3):171-177. doi: 10.1016/0166-3542(96)00942-4.
- Scalbert A, Williamson G. Dietary intake and bioavailability of polyphenols. *J Nutr*. 2000;130(8S Suppl):2073S-2085S. doi: 10.1093/jn/130.8.2073S.
- Scheau C, Badarau IA, Costache R, Caruntu C, Mihai GL, Didilescu AC, Constantin C, Neagu M. The Role of Matrix Metalloproteinases in the Epithelial-Mesenchymal Transition of Hepatocellular Carcinoma. *Anal Cell Pathol (Amst)*. 2019;2019:9423907. doi: 10.1155/2019/9423907.
- Sen R, Ganguly S, Ganguly S, Debnath MC, Chakraborty S, Mukherjee B, Chattopadhyay D. Apigenin-Loaded PLGA-DMSA Nanoparticles: A Novel Strategy to Treat Melanoma Lung Metastasis. *Mol Pharm*. 2021;18(5):1920-1938. doi: 10.1021/acs.molpharmaceut.0c00977.
- Senapati S, Mahanta AK, Kumar S, Maiti P. Controlled drug delivery vehicles for cancer treatment and their performance. *Signal Transduct Target Ther*. 2018;3:7. doi: 10.1038/s41392-017-0004-3.
- Sengupta B, Uematsu T, Jacobsson P, Swenson J. Exploring the antioxidant property of bioflavonoid quercetin in preventing DNA glycation: a calorimetric and spectroscopic study. *Biochem Biophys Res Commun*. 2006;339(1):355-61. doi: 10.1016/j.bbrc.2005.11.019.
- Serenari M, Calabrò D, Bonfiglioli R, Fanti S, Ravaioli M. ^{99m}Tc-Mebrofenin Hepatobiliary Scintigraphy Combined With SPECT/CT to Assess Liver Function in Heterotopic Segmental Liver Transplantation in the Splenic Fossa. *Clin Nucl Med*. 2021;46(6): e332-e335. doi: 10.1097/RLU.0000000000003521.

- Serra A, Macià A, Romero MP, Reguant J, Ortega N, Motilva MJ. Metabolic pathways of the colonic metabolism of flavonoids (flavonols, flavones and flavanones) and phenolic acids. *Food chemistry*. 2012;130(2):383-393. doi: 10.1016/j.foodchem.2011.07.055.
- Seufi AM, Ibrahim SS, Elmaghraby TK, Hafez EE. Preventive effect of the flavonoid, quercetin, on hepatic cancer in rats via oxidant/antioxidant activity: molecular and histological evidences. *J Exp Clin Cancer Res*. 2009;28(1):80. doi: 10.1186/1756-9966-28-80.
- Shahabadi N, Moshiri M, Roohbakhsh A, Imenshahidi M, Hashemi M, Amin F, Yazdian-Robati R, Salmasi Z, Etemad L. A dose-related positive effect of inhaled simvastatin-loaded PLGA nanoparticles on paraquat-induced pulmonary fibrosis in rats. *Basic Clin Pharmacol Toxicol*. 2022;131(4):251-261. doi: 10.1111/bcpt.13771.
- Sharifi-Rad M, Anil Kumar NV, Zucca P, Varoni EM, Dini L, Panzarini E, Rajkovic J, Tsouh Fokou PV, Azzini E, Peluso I, Prakash Mishra A, Nigam M, El Rayess Y, Beyrouthy ME, Polito L, Iriti M, Martins N, Martorell M, Docea AO, Setzer WN, Calina D, Cho WC, Sharifi-Rad J. Lifestyle, Oxidative Stress, and Antioxidants: Back and Forth in the Pathophysiology of Chronic Diseases. *Front Physiol*. 2020;11:694. doi: 10.3389/fphys.2020.00694.
- Sharma A, Ghani A, Sak K, Tuli HS, Sharma AK, Setzer WN, Sharma S, Das AK. Probing into Therapeutic Anti-cancer Potential of Apigenin: Recent Trends and Future Directions. *Recent Pat Inflamm Allergy Drug Discov*. 2019;13(2):124-133. doi: 10.2174/1872213X13666190816160240.
- Sharp PF, Smith FW, Gemmell HG, Lyall D, Evans NT, Gvozdanovic D, Davidson J, Tyrrell DA, Pickett RD, Neirinckx RD. Technetium-99m HM-PAO stereoisomers as potential agents for imaging regional cerebral blood flow: human volunteer studies. *J Nucl Med*. 1986;27(2):171-177.
- Sherman M. Hepatocellular carcinoma: epidemiology, surveillance, and diagnosis. *Semin Liver Dis*. 2010;30(1):3-16. doi: 10.1055/s-0030-1247128.
- Shibata C, Ohno M, Otsuka M, Kishikawa T, Goto K, Muroyama R, Kato N, Yoshikawa T, Takata A, Koike K. The flavonoid apigenin inhibits hepatitis C virus replication by decreasing mature microRNA122 levels. *Virology*. 2014;462-463:42-48. doi: 10.1016/j.virol.2014.05.024.

References

- Shu Y, Liu Y, Li L, Feng J, Lou B, Zhou X, Wu H. Antibacterial activity of quercetin on oral infectious pathogens. *Afr. J. Microbiol. Res.* 2011;5:5358–5361. doi: 10.5897/AJMR11.849.
- Shukla S, Gupta S. Apigenin: a promising molecule for cancer prevention. *Pharm Res.* 2010;27(6):962-978. doi: 10.1007/s11095-010-0089-7.
- Siafaka PI, Okur NÜ, Karantas ID, Okur ME, Gündoğdu EA. Current update on nanoplatforms as therapeutic and diagnostic tools: A review for the materials used as nanotheranostics and imaging modalities. *Asian J Pharm Sci.* 2021;16(1):24-46. doi: 10.1016/j.ajps.2020.03.003.
- Simitcioglu B, Karagoz ID, Ilbasmis-Tamer S, Tamer U. Effect of different molecular weight and terminal group PLGA on docetaxel nanoparticles: characterization and cytotoxic activity of castration-resistant prostate cancer cells. *Pharm Dev Technol.* 2022; 27(7):794-804. doi: 10.1080/10837450.2022.2120004.
- Simón J, Casado-Andrés M, Goikoetxea-Usandizaga N, Serrano-Maciá M, Martínez-Chantar ML. Nutraceutical Properties of Polyphenols against Liver Diseases. *Nutrients.* 2020;12(11):3517. doi: 10.3390/nu12113517.
- Simón-Vázquez R, Tsapis N, Lorscheider M, Rodríguez A, Calleja P, Mousnier L, de Miguel Villegas E, González-Fernández Á, Fattal E. Improving dexamethasone drug loading and efficacy in treating arthritis through a lipophilic prodrug entrapped into PLGA-PEG nanoparticles. *Drug Deliv Transl Res.* 2022;12(5):1270-1284. doi: 10.1007/s13346-021-01112-3.
- Singal AK, Mathurin P. Diagnosis and Treatment of Alcohol-Associated Liver Disease: A Review. *JAMA.* 2021;326(2):165-176. doi: 10.1001/jama.2021.7683.
- Singh D, Khan MA, Siddique HR. Apigenin, A Plant Flavone Playing Noble Roles in Cancer Prevention Via Modulation of Key Cell Signaling Networks. *Recent Pat Anticancer Drug Discov.* 2019;14(4):298-311. doi: 10.2174/1574892814666191026095728.
- Singh D, Mohapatra P, Kumar S, Behera S, Dixit A, Sahoo SK. Nimbolide-encapsulated PLGA nanoparticles induces Mesenchymal-to-Epithelial Transition by dual inhibition of AKT and mTOR in pancreatic cancer stem cells. *Toxicol In Vitro.* 2022;79:105293. doi: 10.1016/j.tiv.2021.105293.
- Singh JP, Selvendiran K, Banu SM, Padmavathi R, Sakthisekaran D. Protective role of Apigenin on the status of lipid peroxidation and antioxidant defense against

- hepatocarcinogenesis in Wistar albino rats. *Phytomedicine*. 2004;11(4):309-314. doi: 10.1078/0944711041495254.
- Singh S, Sharma B, Kanwar SS, Kumar A. Lead Phytochemicals for Anticancer Drug Development. *Front Plant Sci*. 2016;7:1667. doi: 10.3389/fpls.2016.01667.
- Siu FY, Ye S, Lin H, Li S. Galactosylated PLGA nanoparticles for the oral delivery of resveratrol: enhanced bioavailability and in vitro anti-inflammatory activity. *Int J Nanomedicine*. 2018;13:4133-4144. doi: 10.2147/IJN.S164235.
- Sivaramakrishnan V, Niranjali Devaraj S. Morin regulates the expression of NF-kappaB-p65, COX-2 and matrix metalloproteinases in diethylnitrosamine induced rat hepatocellular carcinoma. *Chem Biol Interact*. 2009;180(3):353-359. doi: 10.1016/j.cbi.2009.02.004.
- Slevin E, Baiocchi L, Wu N, Ekser B, Sato K, Lin E, Ceci L, Chen L, Lorenzo SR, Xu W, Kyritsi K, Meadows V, Zhou T, Kundu D, Han Y, Kennedy L, Glaser S, Francis H, Alpini G, Meng F. Kupffer Cells: Inflammation Pathways and Cell-Cell Interactions in Alcohol-Associated Liver Disease. *Am J Pathol*. 2020;190(11):2185-2193. doi: 10.1016/j.ajpath.2020.08.014.
- Snyder E, Banks KP. Hepatobiliary Scintigraphy. [Updated 2021 Jul 26]. In: StatPearls [Internet]. Treasure Island (FL): StatPearls Publishing; 2022. Available from: <https://www.ncbi.nlm.nih.gov/books/NBK538243>.
- Sofowora A, Ogunbodede E, Onayade A. The role and place of medicinal plants in the strategies for disease prevention. *Afr J Tradit Complement Altern Med*. 2013;10(5):210-229. doi: 10.4314/ajtcam.v10i5.2.
- Song B, Li J, Li J. Pomegranate peel extract polyphenols induced apoptosis in human hepatoma cells by mitochondrial pathway. *Food Chem Toxicol*. 2016;93:158-66. doi: 10.1016/j.fct.2016.04.020.
- Song X, Wang Y, Gao L. Mechanism of antioxidant properties of quercetin and quercetin-DNA complex. *J Mol Model*. 2020;26(6):133. doi: 10.1007/s00894-020-04356-x.
- Su Y, Zhang B, Sun R, Liu W, Zhu Q, Zhang X, Wang R, Chen C. PLGA-based biodegradable microspheres in drug delivery: recent advances in research and application. *Drug Deliv*. 2021;28(1):1397-1418. doi: 10.1080/10717544.2021.1938756.

References

- Suh KS, Oh S, Woo JT, Kim SW, Kim JW, Kim YS, Chon S. Apigenin attenuates 2-deoxy-D-ribose-induced oxidative cell damage in HIT-T15 pancreatic β -cells. *Biol Pharm Bull.* 2012;35(1):121-126. doi: 10.1248/bpb.35.121.
- Sun LR, Zhou W, Zhang HM, Guo QS, Yang W, Li BJ, Sun ZH, Gao SH, Cui RJ. Modulation of Multiple Signaling Pathways of the Plant-Derived Natural Products in Cancer. *Front Oncol.* 2019;9:1153. doi: 10.3389/fonc.2019.01153.
- Suresh D, Srinivas AN, Kumar DP. Etiology of Hepatocellular Carcinoma: Special Focus on Fatty Liver Disease. *Front Oncol.* 2020;10:601710. doi: 10.3389/fonc.2020.601710.
- Takagaki N, Sowa Y, Oki T, Nakanishi R, Yogosawa S, Sakai T. Apigenin induces cell cycle arrest and p21/WAF1 expression in a p53-independent pathway. *Int J Oncol.* 2005;26(1):185-189. doi: 10.3892/ijo.26.1.185.
- Tan Q, Liu W, Guo C, Zhai G. Preparation and evaluation of quercetin-loaded lecithin-chitosan nanoparticles for topical delivery. *Int J Nanomedicine.* 2011;6:1621-1630. doi: 10.2147/IJN.S22411.
- Tanaka M, Miyajima A. Liver regeneration and fibrosis after inflammation. *Inflamm Regen.* 2016;36:19. doi: 10.1186/s41232-016-0025-2.
- Tang M, Huang Y, Liang X, Tao Y, He N, Li Z, Guo J, Gui S. Sorafenib-Loaded PLGA-TPGS Nanosystems Enhance Hepatocellular Carcinoma Therapy Through Reversing P-Glycoprotein-Mediated Multidrug Resistance. *AAPS PharmSciTech.* 2022;23(5):130. doi: 10.1208/s12249-022-02214-y.
- Tang SM, Deng XT, Zhou J, Li QP, Ge XX, Miao L. Pharmacological basis and new insights of quercetin action in respect to its anti-cancer effects. *Biomed Pharmacother.* 2020;121:109604. doi: 10.1016/j.biopha.2019.109604.
- Taylor A Jr, Nally JV. Clinical applications of renal scintigraphy. *AJR Am J Roentgenol.* 1995;164(1):31-41. doi: 10.2214/ajr.164.1.7998566.
- Teodoro AJ. Bioactive Compounds of Food: Their Role in the Prevention and Treatment of Diseases. *Oxid Med Cell Longev.* 2019;2019:3765986. doi: 10.1155/2019/3765986.
- Thangaiyan R, Robert BM, Arjunan S, Govindasamy K, Nagarajan RP. Preventive effect of apigenin against isoproterenol-induced apoptosis in cardiomyoblasts. *J Biochem Mol Toxicol.* 2018;32(11):e22213. doi: 10.1002/jbt.22213.

- Thilakarathna SH, Rupasinghe HP. Flavonoid bioavailability and attempts for bioavailability enhancement. *Nutrients*. 2013;5(9):3367-3387. doi: 10.3390/nu5093367.
- Tolba R, Kraus T, Liedtke C, Schwarz M, Weiskirchen R. Diethylnitrosamine (DEN)-induced carcinogenic liver injury in mice. *Lab Anim*. 2015;49(1 Suppl):59-69. doi: 10.1177/0023677215570086.
- Underwood SR, Shaw LJ, Anagnostopoulos C, Cerqueira M, Ell PJ, Flint J, Harbinson M, Kelion A, Al Mohammad A, Prvulovich EM. Myocardial perfusion scintigraphy and cost effectiveness of diagnosis and management of coronary heart disease. *Heart*. 2004;90 Suppl 5(Suppl 5):v34-36. doi: 10.1136/hrt.2003.019133.
- Vessal M, Hemmati M, Vasei M. Antidiabetic effects of quercetin in streptozocin-induced diabetic rats. *Comp Biochem Physiol C Toxicol Pharmacol*. 2003;135C (3):357-364. doi: 10.1016/s1532-0456(03)00140-6.
- Vinayak M, Maurya AK. Quercetin Loaded Nanoparticles in Targeting Cancer: Recent Development. *Anticancer Agents Med Chem*. 2019;19(13):1560-1576. doi: 10.2174/1871520619666190705150214.
- Vines JB, Yoon JH, Ryu NE, Lim DJ, Park H. Gold Nanoparticles for Photothermal Cancer Therapy. *Front Chem*. 2019;7:167. doi: 10.3389/fchem.2019.00167.
- Volk ML, Tocco RS, Bazick J, Rakoski MO, Lok AS. Hospital readmissions among patients with decompensated cirrhosis. *Am J Gastroenterol*. 2012;107(2):247-252. doi: 10.1038/ajg.2011.314.
- Vorster M, Sathekge M. Gallium Imaging of Infection and Inflammation. In Harsini S, Alavi A, Rezaei N. (eds). *Nuclear Medicine and Immunology 2022*; pp. 103-123. Springer, Cham. doi: 10.1007/978-3-030-81261-4_4.
- Wang D, Yang Y, Zou X, Zhang J, Zheng Z, Wang Z. Antioxidant Apigenin Relieves Age-Related Muscle Atrophy by Inhibiting Oxidative Stress and Hyperactive Mitophagy and Apoptosis in Skeletal Muscle of Mice. *J Gerontol A Biol Sci Med Sci*. 2020;75(11):2081-2088. doi: 10.1093/gerona/glaa214.
- Wang G, Wang J, Luo J, Wang L, Chen X, Zhang L, Jiang S. PEG2000-DPSE-coated quercetin nanoparticles remarkably enhanced anticancer effects through induced programmed cell death on C6 glioma cells. *J Biomed Mater Res A*. 2013;101(11):3076-3085. doi: 10.1002/jbm.a.34607.

References

- Wang H, Khor TO, Shu L, Su ZY, Fuentes F, Lee JH, Kong AN. Plants vs. cancer: a review on natural phytochemicals in preventing and treating cancers and their druggability. *Anticancer Agents Med Chem.* 2012;12(10):1281-1305. doi: 10.2174/187152012803833026.
- Wang N, Yi WJ, Tan L, Zhang JH, Xu J, Chen Y, Qin M, Yu S, Guan J, Zhang R. Apigenin attenuates streptozotocin-induced pancreatic β cell damage by its protective effects on cellular antioxidant defense. *In Vitro Cell Dev Biol Anim.* 2017;53(6):554-563. doi: 10.1007/s11626-017-0135-4.
- Wang Q, Wang F, Li X, Ma Z, Jiang D. Quercetin inhibits the amphiregulin/EGFR signaling-mediated renal tubular epithelial-mesenchymal transition and renal fibrosis in obstructive nephropathy. *Phytother Res.* 2023;37(1):111-123. doi: 10.1002/ptr.7599.
- Wang QQ, Cheng N, Yi WB, Peng SM, Zou XQ. Synthesis, nitric oxide release, and α -glucosidase inhibition of nitric oxide donating apigenin and chrysin derivatives. *Bioorg Med Chem.* 2014;22(5):1515-1521. doi: 10.1016/j.bmc.2014.01.038.
- Wang S, Yao J, Zhou B, Yang J, Chaudry MT, Wang M, Xiao F, Li Y, Yin W. Bacteriostatic Effect of Quercetin as an Antibiotic Alternative In Vivo and Its Antibacterial Mechanism In Vitro. *J Food Prot.* 2018;81(1):68-78. doi: 10.4315/0362-028X.JFP-17-214.
- Wang W, Liu Q, Liang X, Kang Q, Wang Z. Protective role of naringin loaded solid nanoparticles against aflatoxin B1 induced hepatocellular carcinoma. *Chem Biol Interact.* 2022;351:109711. doi: 10.1016/j.cbi.2021.109711.
- Wang X, Wang W, Wang JZ, Yang C, Liang CZ. Effect of apigenin on apoptosis induced by renal ischemia/reperfusion injury in vivo and in vitro. *Ren Fail.* 2018;40(1):498-505. doi: 10.1080/0886022X.2018.1497517.
- Ward AB, Mir H, Kapur N, Gales DN, Carriere PP, Singh S. Quercetin inhibits prostate cancer by attenuating cell survival and inhibiting anti-apoptotic pathways. *World J Surg Oncol.* 2018;16(1):108. doi: 10.1186/s12957-018-1400-z.
- Werner RA, Pomper MG, Buck AK, Rowe SP, Higuchi T. SPECT and PET Radiotracers in Renal Imaging. *Semin Nucl Med.* 2022;52(4):406-418. doi: 10.1053/j.semnuclmed.2021.12.003.
- Widowati W, Prahastuti S, Tjokropranoto R, Onggowidjaja P, Kusuma HSW, Afifah E, Arumwardana S, Maulana MA, Rizal R. Quercetin prevents chronic kidney disease on

- mesangial cells model by regulating inflammation, oxidative stress, and TGF- β 1/SMADs pathway. *Peer J.* 2022;10:e13257. doi: 10.7717/peerj.13257.
- Wiegand J, Berg T. The etiology, diagnosis and prevention of liver cirrhosis: part 1 of a series on liver cirrhosis. *Dtsch Arztebl Int.* 2013;110(6):85-91. doi: 10.3238/arztebl.2013.0085.
- Wieler H, Marohl K, Kaiser KP, Klawki P, Frössler H. Tc-99m HMPAO cerebral scintigraphy. A reliable, noninvasive method for determination of brain death. *Clin Nucl Med.* 1993;18(2):104-109. doi: 10.1097/00003072-199302000-00002.
- Willyard CE, Kalathil SC. Nuclear Medicine Liver/Spleen Test. In: *StatPearls [Internet]. Treasure Island (FL): StatPearls Publishing; 2022. Available from: <https://www.ncbi.nlm.nih.gov/books/NBK562325/>*
- World health statistics 2021: monitoring health for the SDGs, sustainable development goals. Geneva: World Health Organization; 2021. Licence: CC BY-NC-SA 3.0 IGO.
- Wu B, Kulkarni K, Basu S, Zhang S, Hu M. First-pass metabolism via UDP-glucuronosyltransferase: a barrier to oral bioavailability of phenolics. *J Pharm Sci.* 2011;100(9):3655-3681. doi: 10.1002/jps.22568.
- Wu CC, Fang CY, Cheng YJ, Hsu HY, Chou SP, Huang SY, Tsai CH, Chen JY. Inhibition of Epstein-Barr virus reactivation by the flavonoid apigenin. *J Biomed Sci.* 2017;24(1):2. doi: 10.1186/s12929-016-0313-9.
- Wu L, Li J, Liu T, Li S, Feng J, Yu Q, Zhang J, Chen J, Zhou Y, Ji J, Chen K, Mao Y, Wang F, Dai W, Fan X, Wu J, Guo C. Quercetin shows anti-tumor effect in hepatocellular carcinoma LM3 cells by abrogating JAK2/STAT3 signaling pathway. *Cancer Med.* 2019;8(10):4806-4820. doi: 10.1002/cam4.2388.
- Wu TH, Yen FL, Lin LT, Tsai TR, Lin CC, Cham TM. Preparation, physicochemical characterization, and antioxidant effects of quercetin nanoparticles. *Int J Pharm.* 2008; 346(1-2):160-168. doi: 10.1016/j.ijpharm.2007.06.036.
- Wu W, Li R, Li X, He J, Jiang S, Liu S, Yang J. Quercetin as an Antiviral Agent Inhibits Influenza A Virus (IAV) Entry. *Viruses.* 2015;8(1):6. doi: 10.3390/v8010006.
- Xu D, Hu MJ, Wang YQ, Cui YL. Antioxidant Activities of Quercetin and Its Complexes for Medicinal Application. *Molecules.* 2019;24(6):1123. doi: 10.3390/molecules24061123.

References

- Xu R, Jiang C, Zhou L, Li B, Hu Y, Guo Y, Xiao X, Lu S. Fabrication of Stable Apigenin Nanosuspension with PEG 400 as Antisolvent for Enhancing the Solubility and Bioavailability. *AAPS PharmSciTech*. 2021;23(1):12. doi: 10.1208/s12249-021-02164-x.
- Xu X, Miao J, Shao Q, Gao Y, Hong L. Apigenin suppresses influenza A virus-induced RIG-I activation and viral replication. *J Med Virol*. 2020;92:3057-3066. doi: 10.1002/jmv.26403.
- Xu Y, Kim CS, Saylor DM, Koo D. Polymer degradation and drug delivery in PLGA-based drug-polymer applications: A review of experiments and theories. *J Biomed Mater Res B Appl Biomater*. 2017;105(6):1692-1716. doi: 10.1002/jbm.b.33648.
- Yamaguchi Y, Takenaga M, Kitagawa A, Ogawa Y, Mizushima Y, Igarashi R. Insulin-loaded biodegradable PLGA microcapsules: initial burst release controlled by hydrophilic additives. *J Control Release*. 2002;81(3):235-249. doi: 10.1016/s0168-3659(02)00060-3.
- Yan X, Qi M, Li P, Zhan Y, Shao H. Apigenin in cancer therapy: anti-cancer effects and mechanisms of action. *Cell Biosci*. 2017;7:50. doi: 10.1186/s13578-017-0179-x.
- Yang H, Yang T, Heng C, Zhou Y, Jiang Z, Qian X, Du L, Mao S, Yin X, Lu Q. Quercetin improves nonalcoholic fatty liver by ameliorating inflammation, oxidative stress, and lipid metabolism in db/db mice. *Phytother Res*. 2019;33(12):3140-3152. doi: 10.1002/ptr.6486.
- Yang JD, Hainaut P, Gores GJ, Amadou A, Plymoth A, Roberts LR. A global view of hepatocellular carcinoma: trends, risk, prevention and management. *Nat Rev Gastroenterol Hepatol*. 2019;16(10):589-604. doi: 10.1038/s41575-019-0186-y.
- Yang TP, Lee HJ, Ou TT, Chang YJ, Wang CJ. Mulberry leaf polyphenol extract induced apoptosis involving regulation of adenosine monophosphate-activated protein kinase/fatty acid synthase in a p53-negative hepatocellular carcinoma cell. *J Agric Food Chem*. 2012;60(27):6891-6898. doi: 10.1021/jf302183x.
- Yang W, Su J, Li M, Li T, Wang X, Zhao M, Hu X. Myricetin Induces Autophagy and Cell Cycle Arrest of HCC by Inhibiting MARCH1-Regulated Stat3 and p38 MAPK Signaling Pathways. *Front Pharmacol*. 2021;12:709526. doi: 10.3389/fphar.2021.709526.
- Yen FL, Wu TH, Lin LT, Cham TM, Lin CC. Naringenin-loaded nanoparticles improve the physicochemical properties and the hepatoprotective effects of naringenin in orally-administered rats with CCl(4)-induced acute liver failure. *Pharm Res*. 2009;26(4):893-902. doi: 10.1007/s11095-008-9791-0.

- Yetisgin AA, Cetinel S, Zuvin M, Kosar A, Kutlu O. Therapeutic Nanoparticles and Their Targeted Delivery Applications. *Molecules*. 2020;25(9):2193. doi: 10.3390/molecules25092193.
- Yin J, Peng X, Lin J, Zhang Y, Zhang J, Gao H, Tian X, Zhang R, Zhao G. Quercetin ameliorates *Aspergillus fumigatus* keratitis by inhibiting fungal growth, toll-like receptors and inflammatory cytokines. *Int Immunopharmacol*. 2021;93:107435. doi: 10.1016/j.intimp.2021.107435.
- Youl E, Bardy G, Magous R, Cros G, Sejalon F, Virsolvy A, Richard S, Quignard JF, Gross R, Petit P, Bataille D, Oiry C. Quercetin potentiates insulin secretion and protects INS-1 pancreatic β -cells against oxidative damage via the ERK1/2 pathway. *Br J Pharmacol*. 2010;161(4):799-814. doi: 10.1111/j.1476-5381.2010.00910.x.
- Yu M, Wu J, Shi J, Farokhzad OC. Nanotechnology for protein delivery: Overview and perspectives. *J Control Release*. 2016;240:24-37. doi: 10.1016/j.jconrel.2015.10.012.
- Yu W, Sun H, Zha W, Cui W, Xu L, Min Q, Wu J. Apigenin Attenuates Adriamycin-Induced Cardiomyocyte Apoptosis via the PI3K/AKT/mTOR Pathway. *Evid Based Complement Alternat Med*. 2017;2017: 2590676. doi: 10.1155/2017/2590676.
- Yuandani, Ilangkovan M, Jantan I, Mohamad HF, Husain K, Abdul Razak AF. Inhibitory Effects of Standardized Extracts of *Phyllanthus amarus* and *Phyllanthus urinaria* and Their Marker Compounds on Phagocytic Activity of Human Neutrophils. *Evid Based Complement Alternat Med*. 2013;2013:603634. doi: 10.1155/2013/603634.
- Yue S, Xue N, Li H, Huang B, Chen Z, Wang X. Hepatoprotective Effect of Apigenin Against Liver Injury via the Non-canonical NF- κ B Pathway In Vivo and In Vitro. *Inflammation*. 2020;43(5):1634-1648. doi: 10.1007/s10753-020-01238-5.
- Zeng L, Zhang G, Lin S, Gong D. Inhibitory Mechanism of Apigenin on α -Glucosidase and Synergy Analysis of Flavonoids. *J Agric Food Chem*. 2016;64(37):6939-49. doi: 10.1021/acs.jafc.6b02314.
- Zhang A, Sun H, Wang X. Recent advances in natural products from plants for treatment of liver diseases. *Eur J Med Chem*. 2013;63:570-577. doi: 10.1016/j.ejmech.2012.12.062.
- Zhang E, Zhang Y, Fan Z, Cheng L, Han S, Che H. Apigenin Inhibits Histamine-Induced Cervical Cancer Tumor Growth by Regulating Estrogen Receptor Expression. *Molecules*. 2020;25(8):1960. doi: 10.3390/molecules25081960.

References

- Zhang J, Hu K, Di L, Wang P, Liu Z, Zhang J, Yue P, Song W, Zhang J, Chen T, Wang Z, Zhang Y, Wang X, Zhan C, Cheng YC, Li X, Li Q, Fan JY, Shen Y, Han JY, Qiao H. Traditional herbal medicine and nanomedicine: Converging disciplines to improve therapeutic efficacy and human health. *Adv Drug Deliv Rev.* 2021;178:113964. doi: 10.1016/j.addr.2021.113964.
- Zhang J, Li H, Wang W, Li H. Assessing the anti-inflammatory effects of quercetin using network pharmacology and in vitro experiments. *Exp Ther Med.* 2022;23(4):301. doi: 10.3892/etm.2022.11230.
- Zhang J, Liu D, Huang Y, Gao Y, Qian S. Biopharmaceutics classification and intestinal absorption study of apigenin. *Int J Pharm.* 2012;436(1-2):311-317. doi: 10.1016/j.ijpharm.2012.07.002.
- Zhang M, Liao Y, Tong X, Yan F. Novel urea derivative-loaded PLGA nanoparticles to inhibit caries-associated *Streptococcus mutans*. *RSC Adv.* 2022;12(7):4072-4080. doi: 10.1039/d1ra09314b.
- Zhang M, Swarts SG, Yin L, Liu C, Tian Y, Cao Y, Swarts M, Yang S, Zhang SB, Zhang K, Ju S, Olek DJ Jr, Schwartz L, Keng PC, Howell R, Zhang L, Okunieff P. Antioxidant properties of quercetin. *Adv Exp Med Biol.* 2011;701:283-289. doi: 10.1007/978-1-4419-7756-4_38.
- Zhang T, Yan T, Du J, Wang S, Yang H. Apigenin attenuates heart injury in lipopolysaccharide-induced endotoxemic model by suppressing sphingosine kinase 1/sphingosine 1-phosphate signaling pathway. *Chem Biol Interact.* 2015;233:46-55. doi: 10.1016/j.cbi.2014.12.021.
- Zhang W, Qiao H, Lv Y, Wang J, Chen X, Hou Y, Tan R, Li E. Apigenin inhibits enterovirus-71 infection by disrupting viral RNA association with trans-acting factors. *PLoS One.* 2014;9(10):e110429. doi: 10.1371/journal.pone.0110429.
- Zhang Y, Huo M, Zhou J, Xie S. PKSolver: An add-in program for pharmacokinetic and pharmacodynamic data analysis in Microsoft Excel. *Comput Methods Programs Biomed.* 2010; 99(3):306-314. doi: 10.1016/j.cmpb.2010.01.007.
- Zhang Y, Yang Y, Tang K, Hu X, Zou G. Physicochemical characterization and antioxidant activity of quercetin- loaded chitosan nanoparticles. *J Appl Polym Sci.* 2008;107(2):891-897. doi: 10.1002/app.26402.

- Zhao J, Yang J, Xie Y. Improvement strategies for the oral bioavailability of poorly water-soluble flavonoids: An overview. *Int J Pharm.* 2019;570:118642. doi: 10.1016/j.ijpharm.2019.118642.
- Zhao L, Zhang J, Hu C, Wang T, Lu J, Wu C, Chen L, Jin M, Ji G, Cao Q, Jiang Y. Apigenin Prevents Acetaminophen-Induced Liver Injury by Activating the SIRT1 Pathway. *Front Pharmacol.* 2020;11:514. doi: 10.3389/fphar.2020.00514.
- Zhao L, Zhang N, Yang D, Yang M, Guo X, He J, Wu W, Ji B, Cheng Q, Zhou F. Protective Effects of Five Structurally Diverse Flavonoid Subgroups against Chronic Alcohol-Induced Hepatic Damage in a Mouse Model. *Nutrients.* 2018;10(11):1754. doi: 10.3390/nu10111754.
- Zhao R, Zhu M, Zhou S, Feng W, Chen H. Rapamycin-Loaded mPEG-PLGA Nanoparticles Ameliorate Hepatic Steatosis and Liver Injury in Non-alcoholic Fatty Liver Disease. *Front Chem.* 2020;8:407. doi: 10.3389/fchem.2020.00407.
- Zhong Y, Jin C, Wang X, Li X, Han J, Xue W, Wu P, Peng X, Xia X. Protective effects of apigenin against 3-MCPD-induced renal injury in rat. *Chem Biol Interact.* 2018;296:9-17. doi: 10.1016/j.cbi.2018.08.005.
- Zhou RJ, Ye H, Wang F, Wang JL, Xie ML. Apigenin inhibits d-galactosamine/LPS-induced liver injury through upregulation of hepatic Nrf-2 and PPAR γ expressions in mice. *Biochem Biophys Res Commun.* 2017;493(1):625-630. doi: 10.1016/j.bbrc.2017.08.141.
- Zhou WC, Zhang QB, Qiao L. Pathogenesis of liver cirrhosis. *World J Gastroenterol.* 2014; 20(23):7312-7324. doi: 10.3748/wjg.v20.i23.7312.
- Zhou Y, Li Y, Zhou T, Zheng J, Li S, Li HB. Dietary Natural Products for Prevention and Treatment of Liver Cancer. *Nutrients.* 2016;8(3):156. doi: 10.3390/nu8030156.
- Zhu X, Zeng X, Zhang X, Cao W, Wang Y, Chen H, Wang T, Tsai HI, Zhang R, Chang D, He S, Mei L, Shi X. The effects of quercetin-loaded PLGA-TPGS nanoparticles on ultraviolet B-induced skin damages in vivo. *Nanomedicine.* 2016;12(3):623-632. doi: 10.1016/j.nano.2015.10.016.
- Zielińska A, Carreiró F, Oliveira AM, Neves A, Pires B, Venkatesh DN, Durazzo A, Lucarini M, Eder P, Silva AM, Santini A, Souto EB. Polymeric Nanoparticles: Production, Characterization, Toxicology and Ecotoxicology. *Molecules.* 2020; 25(16):3731. doi: 10.3390/molecules25163731.

References

Ziessman HA. Hepatobiliary scintigraphy in 2014. J Nucl Med. 2014;55(6):967-75. doi: 10.2967/jnumed.113.131490.

Zubair H, Azim S, Ahmad A, Khan MA, Patel GK, Singh S, Singh AP. Cancer Chemoprevention by Phytochemicals: Nature's Healing Touch. Molecules. 2017;22(3):395. doi: 10.3390/molecules22030395.

Soumya Ganguly
01/06/23

Fabrication of surfactant-free quercetin-loaded PLGA nanoparticles: evaluation of hepatoprotective efficacy by nuclear scintigraphy

Soumya Ganguly · Raghuvir H. Gaonkar · Samarendu Sinha ·
Amit Gupta · Dipankar Chattopadhyay · Sankha Chattopadhyay ·
Satbir S. Sachdeva · Shantanu Ganguly · Mita C. Debnath

Received: 26 May 2016 / Accepted: 6 July 2016
© Springer Science+Business Media Dordrecht 2016

Abstract The purpose of this study was to develop surfactant-free quercetin-loaded PLGA nanoparticles (Qr-NPs) and investigate the hepatoprotective efficacy of the product non-invasively by nuclear scintigraphy. The nanoparticles were prepared using PLGA by dialysis method and ranged in size between 50 and 250 nm with a narrow range of distribution. They were found to arrive at the fenestra of liver sinusoidal epithelium for accumulation. The sizes of nanoparticles (batch S1) were optimal to reach the target and offer enough protection of the hepatocytes degenerated by CCl₄ intoxication as determined by various biochemical and histopathological tests. In vitro studies exhibited the cytotoxic effect of the formulation against HepG2 cell line. The hepatoprotective efficacy of Qr-NPs evaluated non-invasively by nuclear scintigraphic technique using ^{99m}Tc-labelled sulphur

colloid revealed abnormality in liver at the area of decreased uptake in rats of CCl₄-treated group, which disappeared in Qr-NP-treated group. In dynamic studies with ^{99m}Tc-mebrofenin, excretion was severely impaired in CCl₄-treated group but was moderate in drug-treated group, proving the recovery of animals from damage.

Keywords Quercetin-loaded PLGA nanoparticles · Dialysis method · CCl₄ intoxication · Hepatocellular degeneration · Nuclear scintigraphy · Non-intrusive visualization · Biomedicine

Introduction

Various natural products have been used in clinical practice as hepatoprotective agents. These flavonoids

S. Ganguly · R. H. Gaonkar · M. C. Debnath (✉)
Infectious Diseases and Immunology Division, CSIR-
Indian Institute of Chemical Biology, 4 Raja S. C. Mullick
Road, Kolkata 700 032, India
e-mail: mitacd@iicb.res.in;
mita_chdebnath@yahoo.com

S. Sinha · A. Gupta · S. Ganguly
Regional Radiation Medicine Centre, Thakurpukur
Cancer Centre and Welfare Home Campus,
Kolkata 700 063, India

D. Chattopadhyay
Department of Polymer Science & Technology,
University College of Science & Technology, University
of Calcutta, Kolkata 700009, India

S. Chattopadhyay
Radiopharmaceuticals Laboratory, Board of Radiation
and Isotope Technology, Variable Energy Cyclotron
Centre, Kolkata, West Bengal 700 064, India

S. S. Sachdeva
Radiopharmaceuticals Production, BRIT/BARC Vashi
Complex, Sector 20 Vashi, Navi, Mumbai 400 703, India

are considered to be highly efficient against reactive oxygen species by virtue of their antioxidant activities and could be effectively used for the prevention and treatment of liver diseases and damages. Quercetin (Qr), an important dietary flavonoid present ubiquitously in fruits and vegetables, exhibits promising hepatoprotective activity (Casas-Grajales and Muriel 2015). Recently, there has been a growing interest in the therapeutic application of Qr for the treatment and prevention of various diseases. Qr possesses a wide array of pharmacological activities, e.g. antioxidative (Hu et al. 2015; Seufi et al. 2009), hypolipidemic (Bashir 2014), ROS scavenging, anti-inflammatory (Bast et al. 2008), antifibrotic (Chung et al. 2013), anti-cancer (Dajas 2012) and hepatoprotective (Casas-Grajales and Muriel 2015).

The hepatoprotective efficacy of Qr has been investigated against CCl₄-induced hepatocellular injury (Ma et al. 2015), acrylonitrile-induced hepatotoxicity (Abd-Ellah et al. 2011), ethanol-induced liver injury (Kahraman et al. 2012) as well as diethylnitrosamine-induced hepatocarcinoma model in animals (Vikram et al. 2010), wherein it was observed that free radical scavenging as well as modulation of signalling pathways is an important therapeutic strategy of the flavonoids. Liver protects our body by detoxifying poisonous chemicals. Chemical-induced liver impurities are associated with oxidative damages and lipid peroxidation leading to liver dysfunction. Qr combats the damage by stimulating the production of protective antioxidant enzymes and protective proteins in liver cells, blocks the cancer replicative cell cycle and reduces toxin-induced DNA mutations (Granado-Serrano et al. 2012; Aherne and O'Brien 1999).

In spite of the potential therapeutic efficacy of the flavone, its use as a drug in pharmaceutical field is restricted due to its poor aqueous solubility in the gastrointestinal tract. This results in poor bioavailability, poor permeability and extensive first-pass metabolism before reaching the systemic circulation. All these restricted its clinical application. Due to the extremely low hydrophilicity and instability in alkaline medium, the bioavailability of Qr after oral administration is less than 1 % in humans (Dengler et al. 1975). These problems may be circumvented by entrapping/adsorbing the drug molecules either into liposomes (Wang et al. 2013) or into biodegradable polymeric nanoparticles, i.e. NPs (Ghosh et al. 2013). NPs (diameter in the range of 10–1000 nm) have a

great potential as a drug carrier. Due to their small size, they exhibit unique physicochemical and biological properties, as well as high biocompatibility and bioavailability. Nanoencapsulation can protect the drug from rapid degradation and enhance drug concentration in target tissues, thus doses can be lowered and undesirable side effects minimized.

Successful nanoencapsulation of Qr on poly D,L-lactide (PLA) has been achieved by solvent evaporation method to attain sustained delivery of the drug in biological fluids (Pandey et al. 2015). Encapsulation of Qr into liposomes (Gang et al. 2012) and chitosan NPs (Tang et al. 2008) resulted in higher aqueous solubility and constant release of the flavonoids. Qr-loaded lecithin–chitosan NPs were developed for topical application (Tan et al. 2011) to enhance the permeation of the drug in the epidermal layer of the skin. PLGA [Poly D, L-lactide-co-glycolide], a widely used biodegradable and biocompatible polymer approved by USFDA and European Medical Agency (Ansorena et al. 2012), has also been used to encapsulate Qr. There is a rapidly growing interest in this field to use the different molecular weights of PLGA and its copolymers to influence drug release, drug delivery, cellular uptake and biodistribution.

Dispersal of drug in preformed polymers is a very common method used to prepare biodegradable NPs from PLGA and can be accomplished by solvent evaporation, nanoprecipitation, solvent diffusion, salting out, dialysis, etc. (Rao and Geckeler 2011). Although solvent evaporation and nanoprecipitation are the most widely accepted methods, they are associated with several problems related to the removal of non-chlorinated organic solvents and surfactants. Besides, drug inactivation during the preparation procedure and drug loss during the washing step result in low drug-loading efficiency (Cho et al. 2001). To avoid these, the dialysis method has been developed and many workers in this field used this technique for the preparation of liposomes and polymeric micelles. However, the application of this method for the preparation of Qr-NPs has not been reported earlier.

In this study, we report the preparation of Qr-NPs by dialysis method avoiding surfactants. The prepared NPs were characterized by physicochemical characterization technique such as field emission scanning electron microscopy (FE-SEM), FTIR and zeta

potential measurements. Drug-loading and encapsulation efficiency, in vitro drug release studies and particle size measurements by DLS were also performed. In vitro studies were conducted in HepG2 cell line to observe the binding efficiency of Qr-loaded NPs using fluorescence microscopy, while cytotoxicity of the formulation was evaluated using MTT assay to determine optimum dose. Therapeutic efficacy of the Qr-NPs to combat liver dysfunction was also ascertained by monitoring different biochemical parameters. Finally, the hepatoprotective efficacy of Qr-NPs in CCl₄-induced hepatocellular degeneration in rat model was monitored by scintigraphic imaging technique using technetium-99 m-labelled sulphur colloid and mebrotfenin.

Materials and methods

Materials

Qr was purchased from Alfa Aesar. PLGA with an L/G molar ratio of 50:50 (PURASORB PDLG 5002A), 75:25 (PURASORB PDLG 7502A) and 85:15 (PURASORB PLG 8531) was kindly gifted by Purac Biomaterials. Dialysis membranes with a molecular weight cutoff 3.5 or 7.5 kDa were bought from Thermo Fischer, while a membrane of 12–14 kDa was obtained from Hi-Media. Fluorescein isothiocyanate (FITC) and 4',6-diamidino-2-phenylindole (DAPI) were procured from Sigma-Aldrich and Invitrogen, respectively. Dimethylformamide (DMF) was acquired from Spectrochem. All other materials and reagents used were of analytical grade. ^{99m}TcO₄⁻ was obtained by 2-butanone extraction of a 5 N NaOH solution of ⁹⁹MoO₄⁻, procured from Bhabha Atomic Research Centre (Mumbai, India). Tissue and organ radioactivities were measured in an ECIL gamma ray spectrometer (type GRS23C). Scintigraphic imaging of animals was done in GE Infinia Gamma camera equipped with Xeleris workstation.

Preparation of NPs

Qr-NPs were prepared using dialysis method without surfactant. A 5 mg portion of Qr was dissolved in DMF (1 ml) and added to a solution of 50 mg of PLGA in acetone (5 ml). The mixture was stirred for 5 min and dropwise added to 15 ml of distilled water

with continuous stirring. The resulting turbid solution was introduced into the dialysis tube which was placed into an external aqueous phase. The external phase was kept under gentle stirring to aid diffusion and replaced at an interval of 3 to 4 h for a period of 24 h. During the process of dialysis, the organic solvent diffused out of the membrane and water diffused inside, leading to precipitation of polymers which in turn self-assembled to form spherical NPs encapsulating the drug. After 24 h, the content of the dialysis bag was collected and centrifuged at 11,500 rpm for 30 min in high-speed centrifuge (Sorvall RC-5C). The NP pellet thus obtained was freeze dried to obtain a free-flowing powder.

Characterization of NPs

Determination of NP yield, encapsulation efficiency and loading capacity

Qr-NPs were weighed and the percent yield was calculated from the weight of the polymer and the drug taken initially. Encapsulation efficiency was calculated by knowing the amount of Qr added initially and the amount of the flavonoids extracted from the drug-loaded NPs. Briefly, NP pellet (2 mg) was dissolved in acetone (10 ml) and centrifuged, and the amount of Qr was determined by UV absorbance (370 nm) using Shimadzu-1700 spectrophotometer. Encapsulation efficiency and loading efficiency were calculated as per the reported method.

Morphology of NPs

The morphology of the NPs was observed using FE-SEM (Jeol JSM-7600F, Tokyo, Japan). One drop of NP suspension was placed on a glass cover slip and freeze dried. The dried sample was then placed on a copper stud with a double-sided conductive tape followed by ion coating with gold (4–5 nm) by a sputter coater (QUORUM Q150T ES) for 40 s in vacuum at a current intensity of 40 mA. The acceleration voltage was set at 2–5 kV during scanning.

Drug physical state characterization

The physical status of Qr-NPs was ascertained by measuring the differential scanning calorimetric (DSC), X-ray powder diffractometric (XRPD) and

Fourier transform infrared spectroscopic (FTIR) patterns. For DSC analysis, 10 mg of sample was sealed in standard aluminium pans with lids and purged with pure dry nitrogen at a flow rate of 150 ml/min. The temperature ramp speed was set at 12 °C/min and the heat flow was recorded from 0 to 400 °C. Indium powder was used as the standard reference material to calibrate the temperature and energy scales of the DSC instrument (Pyris Diamond TG/DTA, Perkin Elmer, Singapore). The X-ray powder diffraction patterns of pure Qr, polymer and Qr-NPs were measured in X-ray powder diffractometer (XRD-2000, Rigaku, Tokyo, Japan). The measurements were performed in the 2θ range of 2–50° using CuK α radiation (45 kV, 40 mA) as an X-ray source and the rate of scanning was 1° min⁻¹. FTIR (Bruker Tensor-27) analysis was conducted in potassium bromide pellets to verify the possibilities of chemical interaction between the flavonoid and the polymer matrix. Free Qr, PLGA and Qr-NPs were scanned in the range of 400–4000 cm⁻¹.

Particle size and zeta potential analysis

The mean particle size and zeta potential of the Qr-NPs were determined using a Zeta Potential analyser (Zeta Plus, Brookhaven Instruments, Holtsville, NY, USA). To measure the particle size, 10 mg of drug-encapsulated NP sample was suspended in 1 ml deionized water which was further diluted 10 times and subjected to analysis. The zeta potential of the drug-encapsulated NPs was determined by dispersing the sample (1.5 mg) in 1.5 ml KCl (1 mM). The dispersed sample was loaded into disposable optical cuvette to run the measurements. Analysis was carried at least three times for each batch of sample and the mean values were recorded.

In vitro release studies

NPs (20 mg) were dispersed in 4 ml of phosphate-buffered saline (PBS; 0.1 M pH 7.4) and transferred into a dialysis bag (MWCO 12–14 kDa). The bag was placed in a beaker containing 400 ml phosphate-buffered saline (PBS; 0.1 M, pH 7.4) and incubated at 37 °C under horizontal shaking (100 rpm). At fixed time intervals, 4 ml of release medium was withdrawn and replaced with the same volume of fresh PBS. The concentration of the released Qr was determined by UV spectrophotometric analysis at 370 nm. The average

values of these experiments were taken. Cumulative percent of drug release as a function of time was calculated and plotted graphically against time.

In vitro cytotoxicity studies

The effect of free Qr and Qr-NPs on the viability of HepG2 cell line was determined by MTT [3-(4,5-dimethylthiazol-2-yl)-2,5-diphenyltetrazolium bromide] assay using a microplate reader (GENios). HepG2 cells were cultured in DMEM (Dulbecco's Modified Eagle Medium) in 90 % relative humidity and 5 % CO₂ at 37 °C. The cells were harvested using Trypsin–EDTA and the medium was changed every alternate day. The cells were transferred to a 96-well plate to ensure 1 × 10⁴ cells per well. The medium was changed every other day till 80 % confluence was reached. Then 100 μl of freshly prepared solution of free drug (of different concentrations) and drug-encapsulated NPs was added to the growth medium and incubated for 24 h under the same conditions as mentioned above. One row of 96-well plate was used as the control without adding NPs. To evaluate the cell survival after specific time intervals, the medium containing the drug was removed, the wells were washed with PBS three times, and 10 μl of MTT solution (5 mg/ml in PBS) and 90 μl of medium were added to each well and incubated for another 4 h. At the end of the incubation period, medium containing MTT was gently replaced by 100 μl dimethyl sulfoxide (DMSO) to dissolve the formazan crystals and the absorbance was measured by a microplate reader at 550 nm. The absorbance of the test (treated cells) and the control (untreated cells) were used for the determination of the percentage cell viability (Eq. 1). Cell survival in control was assumed to be 100 %.

$$\% \text{ Cell viability} = \frac{\text{Absorbance of test sample}}{\text{Absorbance of control}} \times 100 \quad (1)$$

Confocal laser scanning microscopy

Confocal laser scanning microscopy (Andor spinning disc confocal microscope, UK) was performed to determine cellular uptake. HepG2 cells (1 × 10⁵) were incubated in cover slips placed inside 35-mm cell culture dish. After 80 % confluence was reached in each dish, the medium was replaced with FITC-loaded

PLGA NP suspension (250 µg/ml) and incubated for 2 h. The suspension was removed, and 1 ml of 70 % ethanol was added into each petri dish and kept at -20°C for 15 min to fix the cells. Ethanol solution was removed, each dish was washed three times with PBS, and nuclei were stained with DAPI stain solution for 5 min. Cellular internalization was evaluated using confocal laser scanning microscopy.

Animal experiments

All animal experiment protocols complied with the institutional guidelines and were approved by the committee for the Purpose of Control and Supervision of Experiments on Animals (CPCSEA), Government of India, New Delhi. Adult male Swiss Albino rats (body weight 120–150 g) were kept for 7 days under controlled conditions of $30 \pm 2^{\circ}\text{C}$, 60–80 % relative humidity and 12-h light–dark cycles and allowed free access to food and drinking water. The animals were divided into five groups with six animals in each group. Animals in Group I (normal control) received subcutaneously (S.C.) single dose of olive oil (1 ml/kg body weight). Group II was given CCl_4 (40 % v/v in olive oil, 1 mg/kg body weight) subcutaneously. Animals in groups III, IV and V were treated by oral gavage with free drug (0.5 ml suspension of 0.2 % Tween 80 aqueous solution containing 8.98 µmol/kg b.w. Qr), empty NPs (0.5 ml suspension) and Qr-NPs (0.5 ml suspension containing 8.98 µmol/kg b.w. Qr), respectively. Two hours after oral feeding of drugs, all animals in groups III to V were injected subcutaneously with CCl_4 (40 % v/v, 1 ml/kg b.w.). Twenty-four hours after CCl_4 challenge, the animals were anaesthetized to collect the blood sample from heart and sacrificed to collect the liver. A portion of the liver was fixed in 10 % formalin to prepare paraffin section for histological study and the remaining parts were immediately stored at -80°C for other assays.

Serum biochemistry

The collected blood samples were allowed to stand for 30 min to clot and centrifuged (2000 g) for 10 min at 4°C , and the serum was stored at 4°C for further analysis. Serum marker enzymes, e.g. serum glutamate pyruvate transaminase (SGPT), alkaline phosphatase (AP), and also serum urea and creatinine were determined in accordance with methods provided by the manufacturers of the commercial kits (Span Diagnostics, Surat, India).

Measurement of GSH, catalase, lipid peroxide and SOD in liver homogenate

A portion of liver tissue was homogenized in chilled sodium phosphate buffer (0.1 M, pH 7.4) containing 0.15 M KCl. The homogenate was used for the assessment of levels of oxidative stress markers, e.g. reduced glutathione (GSH) and lipid peroxide, and for the estimation of antioxidant enzyme (catalase) activity.

Estimation of GSH was done as per the reported method (Acosta et al. 1991). Briefly, 2 ml of 10 % liver homogenate was added to a tube containing a mixture of 5 % trichloroacetic acid (TCA) and 1 mM EDTA solution, gently shaken for 5 min and centrifuged at 3000 g for 30 min at 4°C . An aliquot of the resultant supernatant was transferred to a tube containing 5 ml of phosphate buffer (0.1 M, pH 8.0) and 0.4 ml DTNB (0.01 % in 0.1 M phosphate buffer of pH 8.0) and mixed well. The absorbance of the yellow-coloured solution was measured at 412 nm using a UV–Vis spectrophotometer (Shimadzu 1700) and plotted on a standard curve obtained from a known GSH concentration to estimate the GSH content in the homogenate.

Catalase estimation was done as per the protocol reported earlier (Mandal and Das 2005) with modifications. Liver homogenate (5 ml, 10 %) was subject to centrifugation at 300 g for 15 min at 4°C ; the supernatant was collected after separation of small debris and recentrifuged at 105000 g for 60 min at 4°C . To an aliquot of the supernatant containing the cytosolic fraction, ethanol (10 µl) was added and kept in an ice bath for 30 min before the addition of 10 % Triton X-100 (10 µl). H_2O_2 solution (6 mM) was then added to initiate the enzymatic reaction. After 3 min, the reaction was terminated by the addition of H_2SO_4 (6 N). Estimation of the enzyme activity was done by measuring the absorbance at 480 nm after the addition of KMnO_4 solution (0.01 N) to the above mixture. The results were expressed as µM of H_2O_2 decomposed per milligram of protein/min.

The cytosolic fraction of the liver homogenate obtained during catalase estimation was used for measuring superoxide dismutase (SOD) activity. To an aliquot (0.2 ml) of the fraction, 1.5 ml of Tris–cacodylate buffer (pH 8.5, 50 mM), 0.1 ml DTPA (1 mM), 0.1 ml catalase (0.2 µM) and 0.1 ml pyrogallol were added and the mixture was kept at room

temperature for 90 s. Absorbance was measured at 420 nm. Estimation of SOD is based on the ability of the enzyme to inhibit the auto-oxidation of pyrogallol. One unit of enzyme per 2 ml of assay mixture is expressed as the amount of enzyme required to cause 50 % inhibition of pyrogallol auto-oxidation (Marklund and Marklund 1974).

Lipid peroxides were estimated as per the reported method (Mandal and Das 2005). To an aliquot (0.5 ml) of supernatant obtained after centrifugation (2000 g for 15 min at 4 °C) of liver homogenate, methanol (1.75 ml) and chloroform (3.5 ml) were added successively. The mixture was kept at room temperature for 10 min and centrifuged at 260 g for 5 min at 4 °C. The aqueous layer was separated out and the organic layer was evaporated under nitrogen. The residue obtained was dissolved in cyclohexane and the absorbance was measured at 234 nm. Results were expressed as μmole lipohydroperoxide/mg protein.

Histopathological analysis

A part of the liver which was previously fixed in 10 % formalin was used for the histopathological analysis. After fixation for 48 h, the liver portion was embedded in paraffin block and cut into 5- μm -thick sections using a rotary manual microtome. The sections were stained using haematoxylin–eosin dye and visualized under microscope (Leica, Germany) to determine the changes in liver architecture.

Scintigraphic imaging studies

Adult male Swiss Albino rats (b.w. 150–200 g) were divided into three groups (three animals in each group). Each animal of the third group was fed (orally) with Qr-NPs (8.9 μmole Qr/kg body weight), whereas all animals belonging to the first and second groups received 0.5 ml saline orally. Two hours after oral feeding of NPs and saline, all animals in the second and third groups were injected subcutaneously with CCl_4 in olive oil (40 % v/v, 1 ml/kg b.w.), whereas animals of the first group received only olive oil (1 ml/kg b.w.). After 24 h, 30 μl (3.7 MBq) of $^{99\text{m}}\text{Tc}$ -labelled sulphur colloid (prepared as per the reported method) was administered to each anaesthetized animal through precannulated femoral vein. The

animals were placed under gamma camera and whole-body images were acquired at 30 min post injection. The above scintigraphic experiments in different sets of animals were also carried out using $^{99\text{m}}\text{Tc}$ -labelled mebrotfenin kit (procured from BRIT India). Radiolabelling with $^{99\text{m}}\text{TcO}_4^-$ was done according to the instructions provided in the commercial kit. The amount of free pertechnetate in the labelled sulphur colloid and mebrotfenin was checked for each preparation by ascending thin-layer chromatography (silica gel plates, Merck) using saline and acetone, respectively, as the mobile phase. Any preparation showing more than 5 % free pertechnetate was discarded.

Statistical analysis

Statistical analysis was performed with Student's *t* test. The *p* values of the experimental results were calculated and found to be < 0.05 (statistically significant).

Results and discussion

In recent years, the antioxidant properties of Qr, a natural flavonoid, have attracted increasing attention. Hepatoprotective activity of the flavonoids via the oxidative stress pathways has been well studied. Extensive efforts have also been made to develop suitable liposomal and nanoparticulated Qr formulations to render better protection of liver against oxidative attack. In this study, the dialysis method was used for the preparation of Qr-loaded surfactant-free PLGA NPs. During the process of dialysis, water diffused into the organic solvent inside the dialysis tube and the organic solvent in turn diffused into water outside. The displacement of the organic solvent inside the tube resulted in the precipitation of the polymer as micro- and nanoparticles and the drug was encapsulated inside the particles.

Although the technique is simple and effective, so far no report describing the preparation of Qr-NPs by direct dialysis has been available. Different types of dialysis membranes of MWCO 3.5, 7 and 12–14 kDa were used. The process was continued for 24 h to remove the solvent completely and a milky suspension was obtained at the end.

Surface morphology, particle size and zeta potential

FE-SEM was done to ascertain the formation of NPs. The particle size was measured by a zeta potential analyser (Table 1). Different grades of polymer as well as dialysis membrane with different ranges of MWCO were used to fabricate formulations of nanoparticulated drug delivery systems of optimum particle size, drug-loading capacity and encapsulation efficiency. The particle sizes of batches bearing formulation codes S1–S3 and S7–S9 which were fabricated using a dialysis membrane of MWCO 3.5 and 12–14 kDa, respectively, were comparatively less, whereas encapsulation efficiencies were comparatively higher in batches S1 and S2. Encapsulation efficiency of batch S1 fabricated from PLGA grade 50:50 was the highest, while drug-loading capacity and mean particle size were also optimal. The value of polydispersity index exhibited narrow distribution profile of the particles and was used for further studies. FE-SEM image (Fig. 1A, B) showed smooth spherical-shaped particles. Particle size distribution profile analysed by a zeta potential analyser revealed the size distribution (%) by intensity (Fig. 1C). The size distribution pattern determines the route of administration and the drug release behaviour. Small-sized NPs facilitate tissue penetration in vivo by extravasation. The zeta potential values of the NPs were found to be negative in the range of -70 to -12 mV (Fig. 1D). This is due to the carboxylic group

of the polymer on the particle surface. The measurement of zeta potential is important to assess the stability of the colloidal systems and predict the fate of NPs in vivo.

Drug physical status characterization

DSC, XRD and FTIR analyses were performed to understand the physical status of the drug encapsulated in the PLGA NPs. Figure 2A shows the DSC curves of free Qr, PLGA and Qr-NPs.

Free Qr showed two endothermic peaks at 118 and 313 °C, which are in agreement with the previously reported values. These peaks were not visible in Qr-NP formulation possibly because the drug loses its crystallinity due to entrapment into nanoparticles. X-ray powder diffraction data of free Qr, PLGA and Qr-NPs are shown in Fig. 2B. A number of distinct peaks characteristic of the crystalline sample were observed in free drug, whereas no such peaks were observed in Qr-NPs and in PLGA. This indicates that the free drug gets converted from crystalline to amorphous state due to nanoencapsulation. This finding also corroborates the results obtained from DSC analyses.

Infrared absorption peaks of Qr, PLGA and Qr-NPs were determined (Fig. 3) to confirm nanoencapsulation of the drug. The FTIR spectra of free PLGA showed the characteristic peaks between 2996 and 2949 cm^{-1} due to $-\text{CH}$, $-\text{CH}_2$, $-\text{CH}_3$ stretching, at 1754 cm^{-1} due to $-\text{C}=\text{O}$ stretching and at 1271 cm^{-1}

Table 1 Particle characterization

Dialysis membrane (MWCO)	Formulation codes	PLGA grade	Size (nm)	PDI	Drug loading (DL, %)	Encapsulation efficiency (EE, %)
3.5	S1	50:50	97.1 ± 26	0.211	5.1 ± 2.3	75.1 ± 1.6
	S2	75:25	312.1 ± 15	0.118	4.9 ± 2.8	70.5 ± 3.4
	S3	85:15	278.7 ± 21	0.122	4.6 ± 1.8	54.5 ± 5.2
7.0	S4	50:50	429.6 ± 36	0.210	5.2 ± 2.6	50.2 ± 2.9
	S5	75:25	413.5 ± 25	0.197	5.8 ± 3.4	62.1 ± 5.1
	S6	85:15	424.1 ± 11	0.155	4.2 ± 3.2	51.9 ± 4.3
12–14	S7	50:50	258.5 ± 12	0.072	6.2 ± 4.2	48.5 ± 3.9
	S8	75:25	361.2 ± 26	0.206	3.8 ± 2.5	56.2 ± 5.6
	S9	85:15	118.4 ± 32	0.123	2.9 ± 3.1	42.6 ± 3.3

Each value represents the average of three measurements

Fig. 1 FE-SEM images (A, B), particle size distribution profile (C) and zeta potential distribution profile (D) of Qr-NPs (batch S1)

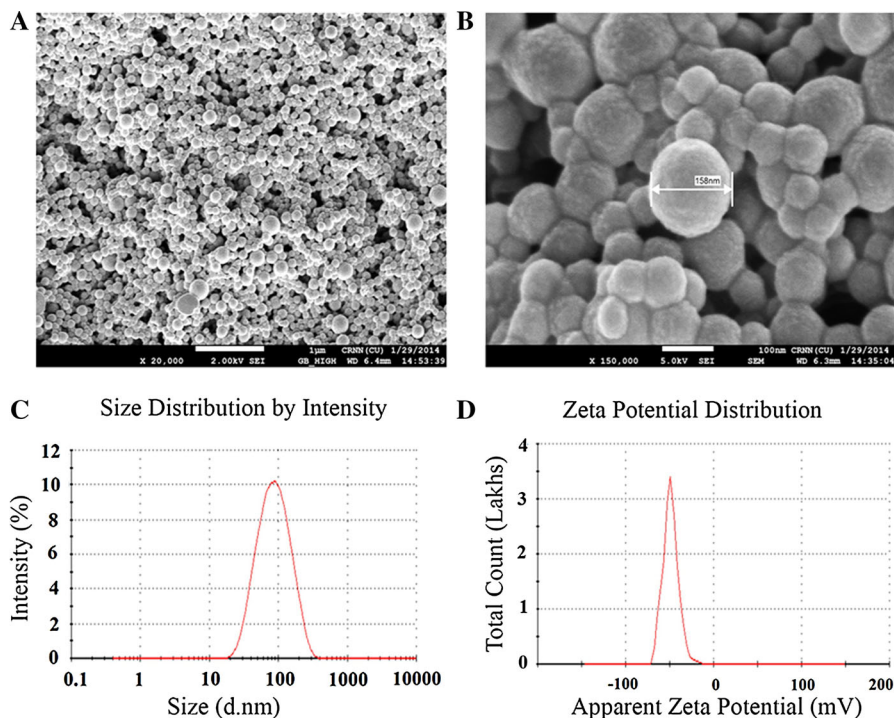
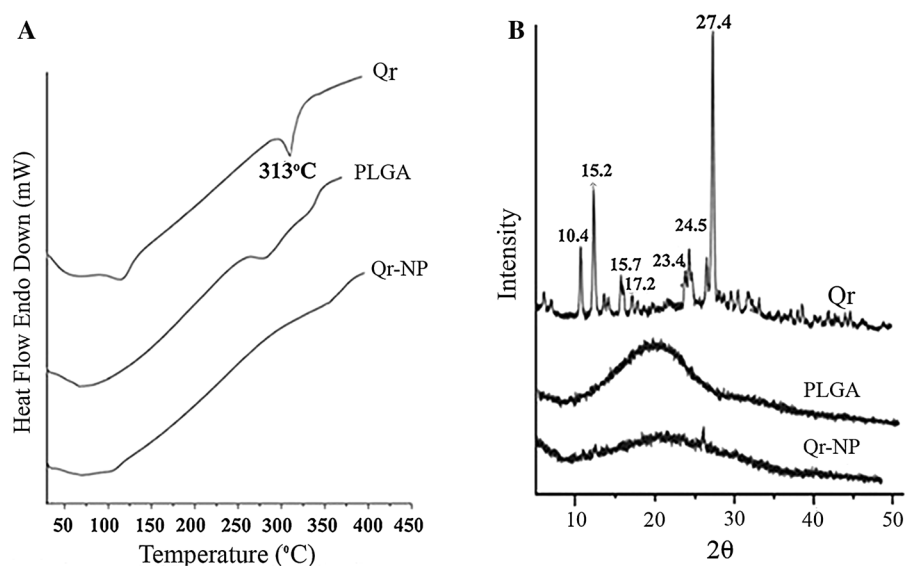


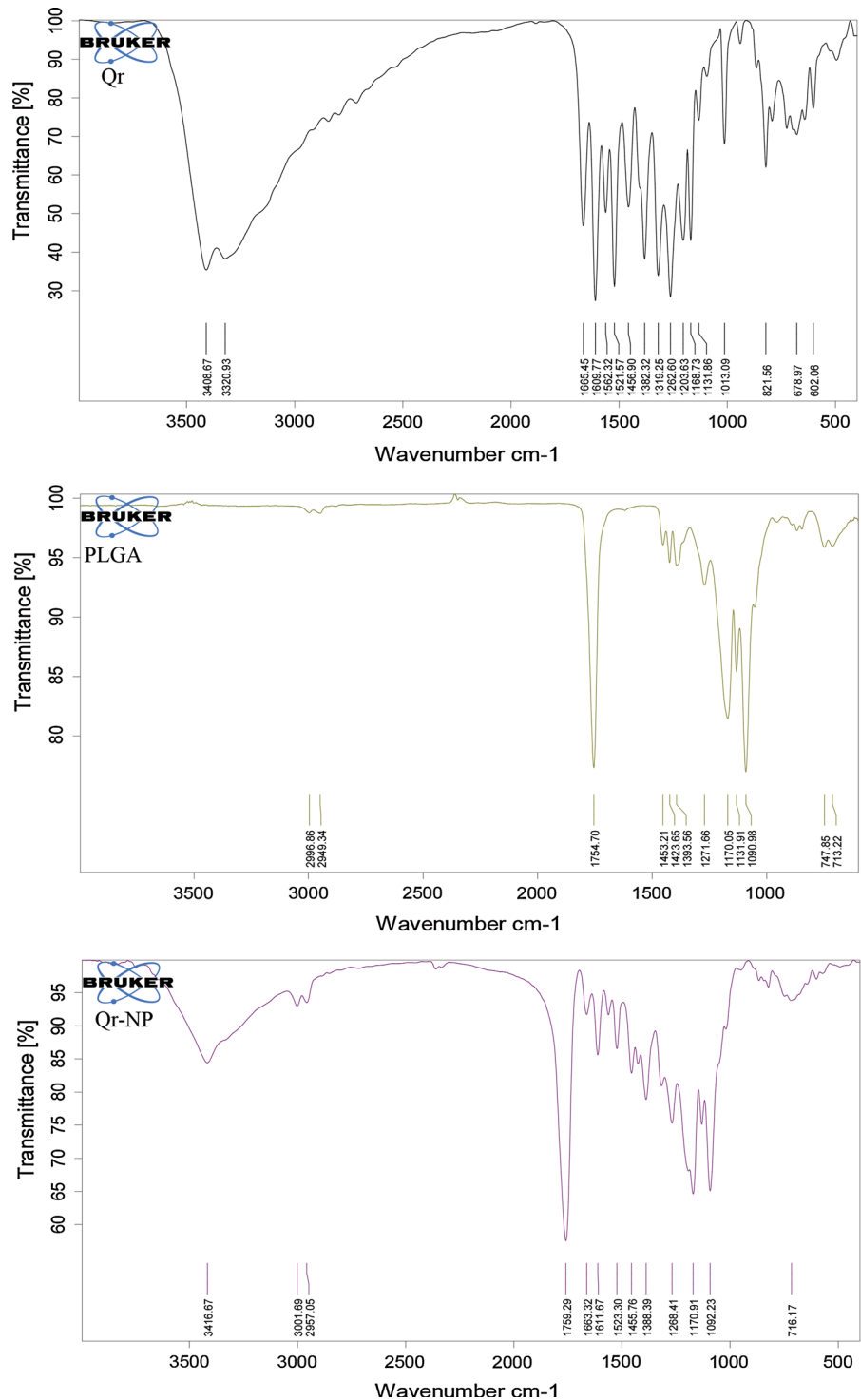
Fig. 2 DSC thermograms (A) and XRD spectra (B) of Qr (free), PLGA and Qr-NPs



for $-C-O$ stretching. For Qr, the spectrum showed characteristic stretching bands due to $-OH$ groups ($3408 - 3320 \text{ cm}^{-1}$), $-C=O$ absorption (1665 cm^{-1}), $-C=C-$ groups (1609 cm^{-1}) and $-C-H$ bending ($1456, 1382 \text{ cm}^{-1}$) besides strong $-C-OH$ and $-C-C$ bending

(aromatic) at 1168 and 1131 cm^{-1} as well as characteristic peaks due to aromatic ring at 1013 and 821 cm^{-1} . All these results are in agreement with the reported values (Yen et al. 2008; Dias et al. 2008). FTIR spectra of Qr-NPs showed slight shifting of $-OH$

Fig. 3 FTIR spectra Qr (free), PLGA and Qr-NPs



stretching band. This could be due to the association of flavonoid with the polymer through hydrogen bonding. In Qr-loaded NPs, the band corresponding to

-C=O stretching (1759 cm⁻¹) was broader which could be due to interactions between the carbonyl and the carboxyl groups of the polymer.

In vitro release profile

The cumulative % drug release curve of Qr-NPs in PBS is shown in Fig. 4A. The curve shows that approximately 69 ± 4.2 % of free quercetin was released over a 6-day period. The high initial burst release (25 ± 2.9 %) during the first 12 h could be attributed to the immediate dissolution of the drug adhered on the surface and located near the surface of the NPs followed by a slower, continuous release at extremely slow rates for a period of almost 6 days. This indicates a slow and sustained release of the drug from the PLGA polymer.

Cytotoxicity test

The cytotoxic activities of free Qr and Qr-NPs on HepG2 cell line were evaluated by assessing the cell viability using the MTT assay (Fig. 4B). The study was continued up to 50 h. The concentration of NPs

was selected so that the amounts of Qr present were in the range corresponding to the plasma levels of the drug achievable in humans. It was observed that the cytotoxicity of drug-loaded NPs was even higher than that of the free drug taken at 10 times higher concentration. Increasing the time of drug exposure resulted in the increase of cytotoxic activity. The higher cytotoxicity of the nanoparticulated formulation may be due to its sustained release properties.

Particle cellular uptake

Confocal laser scanning microscopy was used to evaluate the cellular uptake efficiency of FITC-loaded PLGA NP suspension in HepG2 cell line. Nucleus staining was performed using DAPI. PLGA NP uptake (green colour) is shown in Fig. 4C. The images show the entrapment of the NPs within the intracellular space. Phagocytosis could be the process by which the cell engulfs the NPs.

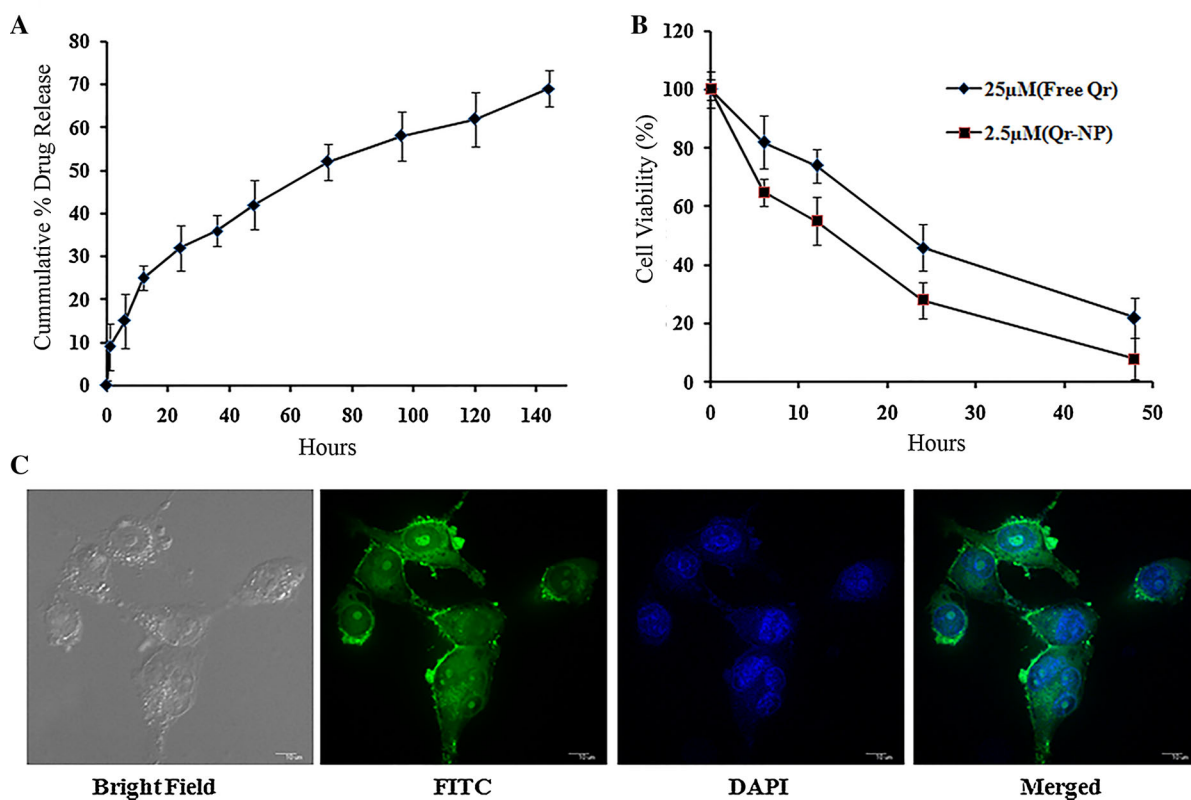


Fig. 4 In vitro drug release profile of Qr-NPs (A), MTT cytotoxicity studies of free Qr and Qr-NPs against HepG2 cells (B) and fluorescent microscopy images of HepG2 cells treated with FITC-loaded PLGA NPs (C)

In vivo study results

Animal experiments were performed to determine the efficacy of the Qr-loaded nanoparticulated formulation. Carbon tetrachloride is one of the most commonly used chemicals in the experimental study of hepatocellular injury. Oxidative stress occurring due to CCl₄ metabolism plays an important role. Liver damage by CCl₄ increases the membrane permeability and releases the enzymes into circulation, which can be measured in the serum. The levels of ALP and SGPT were increased significantly in CCl₄-treated group. Although treatment with free Qr prior to CCl₄ treatment could not significantly reduce elevated enzyme levels, there was a significant restoration of the levels on the administration of Qr-NPs (Table 2) before CCl₄ treatment.

Treatment with Qr-NPs also significantly reduced the elevated levels of serum urea and creatinine in the test group (Table 2). These studies indicate the protection of structural integrity of hepatocyte cell membrane by nanoformulation of Qr. Levels of serum creatinine and urea, significantly elevated in CCl₄-treated rats, were significantly reduced in the test group pretreated with Qr-NPs compared to the free drug-treated groups. However, pre-administration of nanoparticulated Qr caused marked diminutions in the levels of these biomarkers of renal disorder. As kidney is the excretory organ, it might be accumulating some of the bioactive flavonoids offering nephroprotection.

Oxidative stress resulting from the metabolism of CCl₄ in liver plays a crucial role in damaging the liver, promoting hepatic fibrogenesis. CCl₄ intoxication

caused the loss of structure and integrity of the cell membrane. The lipohydroperoxide level was significantly high in liver homogenates of CCl₄-intoxicated rats when compared with the control group. Treatment with Qr-NPs significantly reduced these levels (Table 3).

CCl₄ induces oxidative stress, and cells develop several enzymatic and non-enzymatic defences to combat the stress. Catalase and SOD are antioxidant enzymes, whereas GSH is the endogenous antioxidant that maintains intracellular redox balance and detoxifies reactive oxygen species. CCl₄-induced hepatotoxicity resulted in a significant decrease in SOD, catalase and GSH levels (Table 3). Administration of Qr-NPs provided significant elevation in SOD, catalase and GSH levels. Qr not only scavenges the free radicals formed due to CCl₄ metabolism but also protects the liver by restoring the levels of various antioxidants by modulating the intracellular signalling systems. Histological examinations of liver sample (Fig. 5) also revealed severe liver injury in CCl₄-damaged groups. Liver damage includes gross changes in cellular boundaries, ballooning degeneration and broad infiltration. These changes were markedly reduced by the administration of Qr-NPs before CCl₄ treatment as evidenced by the appearance of normal cellular features with prominent nucleus, absence of ballooning degeneration, minimal cellular infiltration and well brought out central vein as observed in liver section of control groups.

Hepatoprotective activity of nanoparticulated Qr was further studied on CCl₄-induced acute liver damages (in rat model) by radionuclide scintigraphic

Table 2 Effect of oral treatment with Qr-NPs on blood serum biochemical parameters in CCl₄-induced acute hepatocellular injury

Serum enzyme analysis					
Parameters	Normal	CCl ₄ -treated group (A)	(A) + free Qr treated	A + empty NP treated	(A) + Qr-NP treated
Alkaline phosphatase (unit/l)	298 ± 8.2	721 ± 46.7*	651 ± 6.8	765 ± 12.4	353 ± 14.3*
SGPT (IU/l)	81 ± 11.5	193 ± 13.8*	162 ± 21.3	181 ± 8.9	105 ± 6.5*
Urea (g/l)	0.303 ± 0.12	0.551 ± 0.35*	0.495 ± 0.31	0.501 ± 0.22	0.352 ± 0.25*
Creatinine (mg/l)	16.3 ± 1.2	62.1 ± 3.2*	50.0 ± 3.6	59.8 ± 2.1	23.1 ± 4.2*

Results are expressed as mean ± SD of six animals. CCl₄-treated group was compared with the normal group and Qr-NP-treated group was compared with CCl₄-treated group

* $p < 0.001$

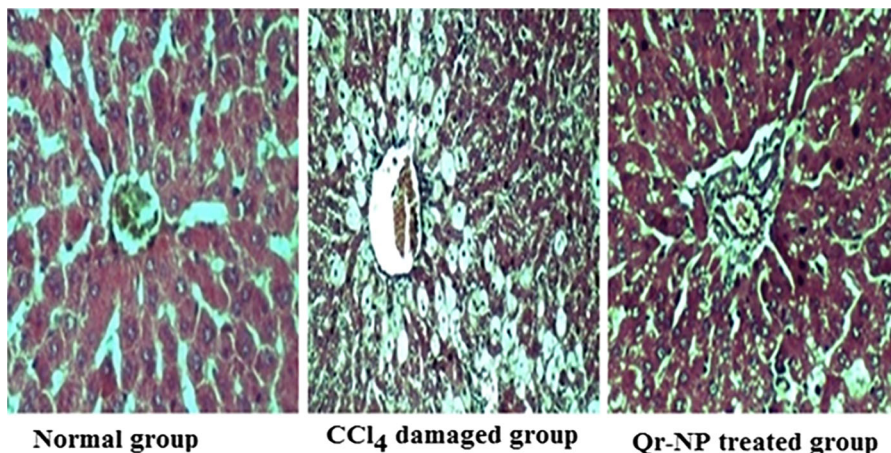
Table 3 Effect of oral treatment with Qr-NPs on GSH, catalase, lipid peroxide and SOD activities of liver in CCl₄-induced acute hepatocellular injury

Liver homogenate analysis					
Parameters	Normal	CCl ₄ -treated group (A)	(A) + free Qr treated	A + empty NP treated	(A) + Qr-NP treated
Lipohydroperoxide (μmole/mg protein)	1.8 ± 0.25	3.9 ± 0.56*	3.6 ± 0.12	3.4 ± 0.52	2.3 ± 0.09*
Catalase (μmole H ₂ O ₂ reduced/min/mg protein)	9.1 ± 1.2	3.6 ± 0.62*	4.1 ± 0.52	3.8 ± 0.22	8.2 ± 0.12*
GSH (μg/g tissue)	11.3 ± 1.3	4.9 ± 0.65*	6.1 ± 0.32	4.5 ± 0.11	10.2 ± 0.12*
SOD (% Inhibition of pyrogallol auto-oxidation)	25.43 ± 1.2	9.61 ± 2.4*	11.92 ± 1.8	11.92 ± 1.8	20.58 ± 2.6*

Results are expressed as mean ± SD of six animals. CCl₄-treated group was compared with the normal group and Qr-NP-treated group was compared with CCl₄-treated group

* $p < 0.001$

Fig. 5 Microscopy images of H & E-stained liver of rats treated with olive oil (normal), CCl₄ (damaged) and CCl₄ + Qr-NPs

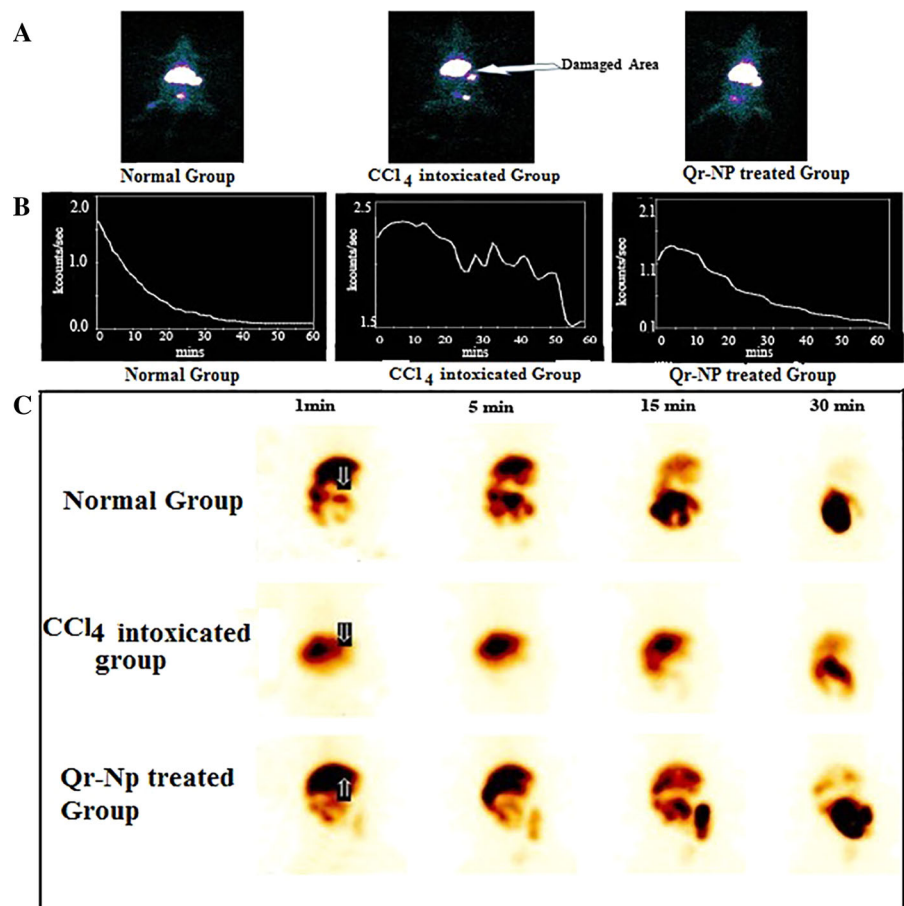


studies using ^{99m}Tc-labelled sulphur colloid and ^{99m}Tc-mebrofenin. We thus developed a new probe for the evaluation of hepatoprotective efficacy of nanoparticulated Qr by non-invasive nuclear scintigraphy. Technetium-99m-labelled sulphur colloid has been well used for years as a liver scintigraphic agent to image the reticuloendothelial system. This is well documented whereas dynamic ^{99m}Tc-mebrofenin SPECT scan has been used to measure total liver function and diagnose parenchymal disorder. Both the radiopharmaceuticals can delineate normal healthy liver tissue from the damaged one. ^{99m}Tc-sulphur colloid imaging studies were performed in rats of normal, acutely damaged and test groups. The anaesthetized animals were placed anteriorly under a gamma camera. Scintigraphic images (Fig. 6A) revealed abnormality (or hole) in liver at the area of

decreased uptake in rats of CCl₄-treated group. This damage disappeared in test group (Qr-NP treated).

In dynamic studies with ^{99m}Tc-mebrofenin, liver was visible very promptly in normal control rats immediately after injection; this was followed by rapid clearance (Fig. 6B). In CCl₄-treated animals, there was not much variation in the overall pattern of ^{99m}Tc-mebrofenin uptake in liver, whereas ^{99m}Tc-mebrofenin excretion was severely impaired in CCl₄-treated group. In Qr-NP-treated group, the excretion pattern of ^{99m}Tc-mebrofenin was moderate, neither very fast nor sluggish, revealing the recovery of animals from damage. Scintigraphic images (Fig. 6C) at different time points (1, 5, 15, 30 min) also exhibit liver uptake and excretion of ^{99m}Tc-mebrofenin. At 1 and 5 min, intense activity in the liver was observed in animals of all the three groups. However, in normal and

Fig. 6 **A** Scintigraphic images of ^{99m}Tc -sulphur colloid acquired at 30 min post injection time period of normal, CCl_4 -intoxicated and Qr-NP-treated rats. **B** Hepatobiliary clearance curve and **C** scintigraphic images at different post injection time periods of ^{99m}Tc -mebrofenin in normal, CCl_4 -intoxicated and Qr-NP-treated rats



nanoparticle-treated animals ^{99m}Tc -mebrofenin began to excrete at 5 min, was substantially cleared out at 15 min and was totally cleared at 30 min leaving a shadow of liver. In contrast, the activity retained in the liver up to 15 min in CCl_4 -treated group and slowly excreted out. These studies have demonstrated the utility of non-invasive scintigraphic methods to evaluate the hepatoprotective efficacy of nanoparticulated Qr.

Conclusion

Various oxidative stresses damage the hepatic cells. Both acute and chronic hepatocellular disorders are very fatal to mankind. During the last two decades, the role of Qr has been widely explored for counteracting chemical-induced hepatotoxicity. Recent research has led to the development of sophisticated nanoparticulate technology to increase the therapeutic efficacy of

bioflavonoids. The present study reports the preparation of Qr-NPs by dialysis method avoiding surfactants and chlorinated solvents. Hepatoprotective efficacy of nanoparticulated Qr has been evaluated non-invasively based on the findings of liver scintigraphy by ^{99m}Tc -sulphur colloid and ^{99m}Tc -mebrofenin. Overall, the studies may be considered as the starting point for the development of a novel method to monitor the hepatoprotective efficacy of nanoparticulated drug delivery system. This approach is being utilized for monitoring the hepatoprotective efficacy of other nanoparticulated bioflavonoids.

Acknowledgments The work has been carried out at CSIR-India Institute of Chemical Biology, funded by BRNS, DAE (Govt. of India) vide Grant No. 2013/35/25/BRNS. The authors gratefully acknowledge Dr. Basudeb Achari, Emeritus Scientist, for his valuable suggestions during the preparation of the manuscript. The authors would also like to acknowledge the Centre for Research in Nanoscience and Nanotechnology (CRNN), University of Calcutta, for allowing to use their FE-SEM facility.

References

- Abd-Allah MF, Ghonaim MM, Abo-Salem OM (2011) Hepatoprotective activity of quercetin against acrylonitrile-induced hepatotoxicity in rats. *J Biochem Mol Toxicol* 25:386–392
- Acosta D, Davila JC, Davis PS (1991) Changes in glutathione and cellular energy as potential mechanisms of papaverine-induced hepatotoxicity in vitro. *Toxicol Appl Pharmacol* 108:28–36
- Aherne SA, O'Brien NM (1999) Protection by the flavonoids myricetin, quercetin, and rutin against hydrogen peroxide-induced DNA damage in Caco-2 and Hep G2 cells. *Nutr Cancer* 34:160–166
- Ansorena E, Danhier F, Silva JM (2012) PLGA-based nanoparticles: an overview of biomedical applications. *J Control Release* 161:505–522
- Bashir SO (2014) Hepatoprotective role for quercetin in diabetic rats: hypolipidemic and antioxidant effects. *Med J Cairo Univ* 82:169–178
- Bast A, Boots AW, Haenen GRMM (2008) Health effects of quercetin: from antioxidant to nutraceutical. *Eur J Pharmacol* 585:325–337
- Casas-Grajales S, Muriel P (2015) Antioxidants in liver health. *World J Gastrointest Pharmacol Ther* 6:59–72
- Cho C, Kim S, Jeong Y et al (2001) Preparation of poly(DL-lactide-co-glycolide) nanoparticles without surfactant. *J Appl Polym Sci* 80:2228–2236
- Chung EJ, Li F, Horton JA et al (2013) Quercetin inhibits radiation-induced skin fibrosis. *Radiat Res* 180:205–215
- Dajas F (2012) Life or death: neuroprotective and anticancer effects of quercetin. *J Ethnopharmacol* 143:383–396
- Dengler HJ, Leschik M, Gugler R (1975) Disposition of quercetin in man after single oral and intravenous doses. *Eur J Clin Pharmacol* 9:229–234
- Dias K, Nikolaou S, De Giovanni WF (2008) Synthesis and spectral investigation of Al(III) catechin/beta-cyclodextrin and Al(III) quercetin/beta-cyclodextrin inclusion compounds. *Spectrochim Acta A* 70:154–161
- Gang W, Jie WJ, Ping ZL et al (2012) Liposomal quercetin: evaluating drug delivery in vitro and biodistribution in vivo. *Expert Opin Drug Deliv* 9:599–613
- Ghosh A, Mandal AK, Sarkar S et al (2013) Neuroprotective role of nanoencapsulated quercetin in combating ischemia-reperfusion induced neuronal damage in young and aged rats. *PLoS One* 8:e57735
- Granado-Serrano AB, Bravo L, Martín MÁ et al (2012) Quercetin attenuates TNF-induced inflammation in hepatic cells by inhibiting the NF- κ B pathway. *Nutr Cancer* 64:588–598
- Hu X, Ding C, Zhou N et al (2015) Quercetin protects gastric epithelial cell from oxidative damage in vitro and in vivo. *Eur J Pharmacol* 754:115–124
- Kahraman A, Çakar H, Köken T (2012) The protective effect of quercetin on long-term alcohol consumption-induced oxidative stress. *Mol Biol Rep* 39:2789–2794
- Ma JQ, Xie WR, Li Z et al (2015) Quercetin protects mouse liver against CCl₄-induced inflammation by the TLR2/4 and MAPK/NF- κ B pathway. *Int Immunopharmacol* 28:531–539
- Mandal AK, Das N (2005) Sugar coated liposomal flavonoid: a unique formulation in combating carbon tetrachloride induced hepatic oxidative damage. *J Drug Targ* 13:305–315
- Marklund S, Marklund G (1974) Involvement of the superoxide anion radical in the autoxidation of pyrogallol and a convenient assay for superoxide dismutase. *Eur J Biochem* 47:469–474
- Pandey SK, Patel DK, Thakur R et al (2015) Anti-cancer evaluation of quercetin embedded PLA nanoparticles synthesized by emulsified nanoprecipitation. *Int J Biol Macromol* 75:521–529
- Rao JP, Geckeler KE (2011) Polymer nanoparticles: preparation techniques and size-control parameters. *Prog Polym Sci* 36:887–913
- Seufi AM, Ibrahim SS, Elmaghraby TK et al (2009) Preventive effect of the flavonoid, quercetin, on hepatic cancer in rats via oxidant/antioxidant activity: molecular and histological evidences. *J Exp Clin Cancer Res* 28:80
- Tan Q, Liu W, Guo C et al (2011) Preparation and evaluation of quercetin-loaded lecithin-chitosan nanoparticles for topical delivery. *Int J Nanomed* 6:1621–1630
- Tang K, Zhang Y, Yang Y et al (2008) Physicochemical characterization and antioxidant activity of quercetin-loaded chitosan nanoparticles. *J Appl Polym Sci* 107:891–897
- Vikram A, Gupta C, Tripathi DN et al (2010) Antioxidant and antimutagenic effect of quercetin against DEN induced hepatotoxicity in rat. *Phytother Res* 24:119–128
- Wang G, Luo J, Wang J et al (2013) PEG2000-DPSE-coated quercetin nanoparticles remarkably enhanced anticancer effects through induced programmed cell death on C6 glioma cells. *J Biomed Mater Res A* 101:3076–3085
- Yen FL, Lin LT, Wu TH et al (2008) Preparation, physicochemical characterization, and antioxidant effects of quercetin nanoparticles. *Int J Pharm* 346:160–168



Apigenin-loaded galactose tailored PLGA nanoparticles: A possible strategy for liver targeting to treat hepatocellular carcinoma

Soumya Ganguly^a, Saikat Dewanjee^b, Ramkrishna Sen^a, Dipankar Chattopadhyay^c, Shantanu Ganguly^d, Raghuvir Gaonkar^a, Mita Chatterjee Debnath^{a,*}

^a Infectious Diseases and Immunology Division, CSIR-Indian Institute of Chemical Biology, Kolkata, India

^b Advanced Pharmacognosy Research Laboratory, Department of Pharmaceutical Technology, Jadavpur University, Kolkata, India

^c Department of Polymer Science & Technology, University College of Science & Technology, University of Calcutta, Kolkata, India

^d Regional Radiation Medicine Centre, Saroj Gupta Cancer Centre and Research Institute, Kolkata, India

ARTICLE INFO

Keywords:

Apigenin
Galactosylated-PLGA
HCC
HepG2 cell
Therapeutic efficacy
Scintigraphic imaging

ABSTRACT

Hepatocellular carcinoma (HCC) is the most common hepatic malignancy worldwide. Recent reports focusing on the efficacy of apigenin-loaded nanoparticles (NPs) in combating the progress of HCC encouraged us to develop galactose-tailored PLGA NPs loaded with apigenin (API-GAL-NPs) for active liver targeting to treat HCC. Two kinds of apigenin NPs, such as apigenin-PLGA NPs (API-NPs) and API-GAL-NPs were fabricated and characterized by size, surface morphology, encapsulation efficacy, and *in vitro* drug release kinetics. *In vitro* assays were performed on HepG2 cells to check the cellular internalization, cytotoxic potential, and apoptotic potential of free apigenin (API), API-NPs, and API-GAL-NPs. In this study, API-GAL-NPs exhibited improved cellular internalization of API resulting in significantly high cytotoxic and apoptotic potentials to HepG2 cells over API and API-NPs. In *in vivo* studies, API-GAL-NPs exhibited a better protective effect against DEN-induced HCC in rats evidenced by the significant reduction of nodule formation, downregulation of matrix metalloproteinases (MMP-2 and MMP-9), and induction of apoptosis in the liver than API and API-NPs. Histopathological studies and scintigraphic imaging also confirmed that API-GAL-NPs treatment achieved better therapeutic efficacy against DEN-induced HCC in rats over API-NPs. In conclusion, API-GAL-NPs may serve as a potential therapeutic agent against HCC in the future by achieving improved liver targeting.

1. Introduction

HCC is one of the leading causes of cancer-associated death around the world [1]. It is the fifth most typical malignancy in men and seventh amongst women [2]. Over a half-million of newly diagnosed cases of HCC appear per year [2]. An extremely poor prognosis worsens the recovery of this disease. Early diagnosis of HCC can have some therapeutic options, such as surgical liver resection, liver transplantation, and chemotherapy [3]. However, HCC is mostly diagnosed at an advanced

stage, where chemotherapy remains the only therapeutic option [1]. Thus, target-specific delivery of chemotherapeutic agents is a primary therapeutic requirement in its therapeutic management. API is an edible naturally occurring flavonoid that exhibited significant anticancer potential in preclinical studies without imparting toxic effects to normal cells [4]. It is an excellent apoptosis inducer to liver cancer cells, and can exhibit significant chemo-preventive and/or tumor-suppressive effects against HCC [4]. API induces apoptosis to liver cancer cells by increasing cellular ROS production mediated through NADPH oxidase activation

Abbreviations: Akt, protein kinase B; ALP, alkaline phosphatase; ALT, alanine transaminase; API, apigenin; API-GAL-NPs, apigenin galactose nanoparticles; API-NPs, Apigenin nanoparticles; ASGP-R, asialoglycoprotein receptors; AST, aspartate transaminase; AUC, area under the curve; b.w., body weight; DAPI, 4',6-diamidino-2-phenylindole; DEN, diethylnitrosamine; FESEM, field emission scanning electron microscope; FITC, fluorescein isothiocyanate; FTIR, Fourier transform infrared spectroscopy; GAL-PLGA, galactosylated PLGA; HCC, hepatocellular carcinoma; HPLC, high pressure liquid chromatography; IL-4R, interleukin 4 receptor; *i.p.*, intraperitoneal; *i.v.*, intravenous; MMP, matrix metalloproteinases; NMR, nuclear magnetic resonance; NPs, nanoparticles; Nrf-2, nuclear factor erythroid 2-related factor 2; PBS, phosphate buffered saline; PDI, polydispersity index; PI3K, phosphoinositide 3-kinase; PLGA, poly (Lactic-co-glycolic acid); TEM, transmission electron microscope; USFDA, United States Food and Drug Administration; USP-18, ubiquitin-specific peptidase 18.

* Corresponding author at: Infectious Diseases and Immunology Division, CSIR-Indian Institute of Chemical Biology, Kolkata, 700032, India.

E-mail address: mitacd2016@gmail.com (M.C. Debnath).

<https://doi.org/10.1016/j.colsurfb.2021.111778>

Received 28 December 2020; Received in revised form 30 March 2021; Accepted 17 April 2021

Available online 20 April 2021

0927-7765/© 2021 Elsevier B.V. All rights reserved.

[4]. In addition, it can inhibit tumor proliferation by arresting the cell cycle at G1 and G2/M phases [4]. cDNA microarray expression analysis revealed that API can regulate 1764 genes in human hepatoma cells [5]. Suppression of USP-18/IL-4R and Nrf-2/PI3K/Akt signaling and activation of P53/P21/Waf-1 and P38/P21/cyclinD1 pathways were found to be accountable for its chemotherapeutic effect against HCC in different preclinical assays [4–6]. However, the chemotherapeutic efficacy of API is largely limited due to its poor pharmacokinetic attributes [7]. A high level of protein binding and its poor release from the protein-bound form also restricts its chemotherapeutic effectiveness following parenteral delivery [8]. In these aspects, nanoencapsulation can serve as efficient drug delivery to overturn the aforementioned limitations of free API. PLGA is a USFDA approved biodegradable and biocompatible polymer. PLGA-based NPs can encapsulate poorly soluble drugs, extravasating through the tumor vasculature by the enhanced permeability and retention effect [9]. Galactosylation of a polymer can improve liver targeting as galactose can recognize asialoglycoprotein receptors which are abundant in liver cells [10]. Galactose-polymer conjugate offers an amphiphilic structure and during NP formulation, the drug gets encapsulated in the inner hydrophobic core and outer hydrophilic shell with galactose moieties is available for asialoglycoprotein receptor recognition [10]. Thus, it has been aimed to develop API-encapsulated in galactosylated-PLGA NPs (API-GAL-NPs) to achieve more effective and target-specific delivery of API to achieve better therapeutic efficacy in the management of HCC. In this study, PLGA was galactosylated by simple esterification reaction and API-GAL-NPs were prepared by nanoprecipitation method using GAL-PLGA as polymer. The developed NPs were characterized and subjected to *in vitro* and *in vivo* assays. The therapeutic efficacy was compared with free API and API-NPs.

2. Materials and methods

2.1. Materials

API was purchased from Otto Chemie Pvt Ltd., Mumbai, India. PLGA with L/G molar ratio of 50:50 (Resomer RG504 H) and Kolliphor P188 (Poloxamer 188) were gifted by Evonik India Pvt. Ltd., Mumbai, India and BASF, Mumbai, India, respectively. FITC, DAPI, and acetone were procured from Sigma Aldrich (St. Louis, MO, USA), Invitrogen (California, USA) and Fischer Scientific (Mumbai, India), respectively. HepG2 cells were procured from NCCS, Pune, India. FITC-Annexin V/propidium iodide (PI) double staining assay kit (Catalog No.: 556547) was purchased from BD Biosciences, USA. Primary antibodies p53 (SC #6243), COX-2 (SC #166475), Bcl-2 (SC #7382), BAX (SC #7480), Bcl-xL (SC #8392) and β -Actin (SC # 47778) were obtained from Santa Cruz Biotechnology. Horseradish peroxidase (HRP) conjugated secondary antibody (A9044) was obtained from Sigma-Aldrich, St. Louis, MO, USA. ^{99}Mo was procured from Bhabha Atomic Research Centre (Mumbai, India) and $^{99\text{m}}\text{TcO}_4^-$ was obtained by 2-butanone extraction of a 5 N NaOH solution of $^{99}\text{MoO}_4^-$. All the remaining chemicals used in the experiments were of analytical grade.

2.2. Synthesis of GAL-PLGA

Synthesis of GAL-PLGA was carried out as reported earlier [10]. Briefly, 4 μL of methane sulfonic acid was added to a solution of galactose (1 $\mu\text{g}/\text{L}$) in dry dimethylformamide with continuous stirring for 5 min, to which 200 mg PLGA was added and stirred for 24 h at 60 $^\circ\text{C}$. Ice-cold distilled water was added to it and the synthesized polymer was separated by centrifugation (10000 rpm). Pellet was washed repeatedly with ultrapure water and lyophilized to yield PLGA-galactose conjugate. Galactosylation of PLGA was confirmed by $^1\text{H-NMR}$ spectroscopy (Bruker, DPX300 MHz NMR Spectrometer, Wissembourg, France) [10].

2.3. Formulation of NPs

API-GAL-NPs and API-NPs were prepared using nanoprecipitation technique as described by Fessi and colleagues [11]. Briefly, 125 mg of the polymer (PLGA or GAL-PLGA) and 12.5 mg of API were dissolved in 25 mL of acetone. The resulting organic solution was poured into 50 mL ultrapure water containing 250 mg of poloxamer 188 under moderate magnetic stirring. The aqueous phase immediately turned milky due to formation of NPs. Stirring was continued overnight to evaporate acetone diffused towards the aqueous phase. NPs were then recovered by ultra-centrifugation at 18,000 rpm for 30 min. The pellet thus obtained was washed (3–4 times) using ultrapure water and finally lyophilized to obtain free flowing powder of NPs. The formulated API-GAL-NPs and API-NPs were stored at 4 $^\circ\text{C}$ for further use. Fluorescent NPs were prepared following the same protocol by replacing API with FITC (12.5 mg).

2.4. Characterization of NPs

2.4.1. Particle size distribution and zeta potential analysis

Size distribution, mean particle size, polydispersity index (PDI) and zeta potential of NPs in the suspension were determined using zeta potential analyzer (Zeta Plus, Brookhaven Instruments, Holtsville, NY, USA) [12].

2.4.2. Surface morphology of NPs

The surface morphology of API-NPs and API-GAL-NPs was observed using FESEM (Jeol JSM-7600 F, Tokyo, Japan) and TEM (FEL, Tecnai G2 SPIRIT Bio Twin, Czech Republic) as per methods reported earlier by this laboratory [12].

2.4.3. Physicochemical characterization of NPs

Drug loading, encapsulation efficiency and percentage (%) yield were calculated using UV–vis spectroscopic technique following established protocol by our group [13]. FTIR, differential scanning calorimetry, and X-ray powder diffraction analyses ascertained the physicochemical compatibility between API, polymer, and the other formulation ingredients [13].

2.4.4. *In vitro* release studies

The release of API from API-NPs and API-GAL-NPs in PBS (0.1 M, pH 7.4) at different time intervals was investigated for 8 days following a cumulative drug release protocol reported elsewhere [14].

2.4.5. Stability study

Lyophilized API-NPs and API-GAL-NPs were stored at 4 ± 1 $^\circ\text{C}$ for 90 days and analyzed for size distribution, zeta potential, PDI, drug loading and encapsulation efficiency as per methods described by Gaonkar and co-workers [13].

2.5. *In vitro* studies

2.5.1. Cell culture

Human liver hepatocellular carcinoma (HepG2) cells were cultured in EMEM (Eagle's minimum essential medium) fortified with 10 % FBS and antibiotics solution (Hi-Media, Mumbai, India) and the culture was maintained at 5 % CO_2 , 90 % humidity, and 37 $^\circ\text{C}$ temperature in an incubator [14].

2.5.2. Cellular uptake studies

In vitro cellular uptake of API-NPs and API-GAL-NPs by HepG2 cells was determined qualitatively and quantitatively by confocal laser scanning microscope (Olympus FluoView FV10i, Olympus, Tokyo, Japan) and flow cytometer (BD LSRFortessa™, BD Biosciences, CA, USA), respectively [13]. The cellular uptake of API-GAL-NPs in presence of galactose was determined by blocking studies [15].

2.5.3. Cytotoxicity studies

The cytotoxic potentials of API, API-NPs and API-GAL-NPs against HepG2 cells (1×10^4 cells/well) were ascertained at two different time intervals (24 and 48 h) by MTT-based colorimetric assay [14].

2.5.4. Apoptosis assay

Apoptotic potentials of API, API-NPs and API-GAL-NPs on HepG2 cells were determined in a flow cytometer (BD LSRFortessa™, BD Biosciences, CA, USA) using FITC-Annexin V/propidium iodide (PI) double staining assay kit (BD Biosciences, NJ, USA) following manufacturer protocol.

2.6. In vivo studies

2.6.1. Pharmacokinetic studies

The pharmacokinetic study of API, API-NPs and API-GAL-NPs were performed in plasma samples collected from Wistar rats following the established protocol by our group [13]. Briefly, the animals were treated with the aforementioned formulations (equivalent dose of 9.2 μ M of API/animal, *i.v.*) and blood samples were collected at predetermined time points (1, 2, 4, 8, 12, 24 and 48 h) post-administration, and plasma was separated. The samples were then analyzed in Dionex UltiMate 3000 HPLC system (Dionex, Idstein, Germany) using a Hypersil GOLD-C18 column (250 \times 4.6 mm and particle size of 5 μ m; Thermo Scientific™ Hypersil GOLDTM, MA, USA) and eluted with water: acetonitrile: methanol (40:35:25 v/v/v) at a flow rate of 1.0 mL/min. API was detected by UV detector at 340 nm [16]. The pharmacokinetic parameters were determined using PKSolver (A freely available add-in program for pharmacokinetic data analysis in Microsoft Excel). Zhang and colleagues [17] validated PKSolver with respect to other professional PK softwares and established the reliability of this software. Different research groups successfully employed PKSolver to determine pharmacokinetic parameters [18,19].

2.6.2. In vivo antitumor efficacy study

Adult male Wistar rats were randomly divided into five groups (N = 7). Animals in Gr-I (normal control) received three doses of olive oil (0.5 mL/animal). All animals in Gr-II, Gr-III, Gr-IV, and Gr-V received DEN (200 mg/kg b.w. in olive oil, *i.p.*) three times at an interval of 15 days. Gr-III, Gr-IV, and Gr-V were treated with API, API-NPs, and API-GAL-NPs (equivalent dose of 9.2 μ M of API/animal, *i.v.*) once in a week for 16 weeks, respectively. Gr-I and Gr-II (DEN-treated control) were treated with normal saline [20]. DEN-treated control served as HCC control group. After 18 weeks, two animals (from each group) from Gr-I, Gr-II, and Gr-V were injected with ^{99m}Tc -labeled sulfur colloid (30 μ L; 3.7 MBq/animal) and ^{99m}Tc -labeled mebrofenin (50 μ L), and viewed under gamma camera [14].

2.6.3. Serum enzyme parameters

Blood samples collected from animals of control and treated groups were processed as per reported method [14] and level of AST, ALT, and ALP were determined using commercially available bioassay kits (Coral Clinical Systems, Goa, India) following manufacturer protocols.

2.6.4. Western blot analysis

Liver tissues collected from different treatment groups and protein samples were separated as per established protocol [21]. Briefly, The sample proteins (10 μ g) were subjected to 10 % SDS-PAGE gel electrophoresis and resolved proteins were transferred into nitrocellulose membrane. Membrane was blocked and then incubated with primary antibody at 4 °C overnight. The membrane was washed and subsequently treated with a suitable HRP-conjugated secondary antibody at room temperature for 1 h. The immunoblot was developed by ECL substrate (Millipore, MA, USA) and detected in a ChemiDoc touch imaging system (Bio-Rad, USA). β -Actin served as a loading control protein. The intensity of normal control band was assigned 1 [22]. The

densitometric analysis was performed using Image Lab software (Bio-Rad, USA). The expressions of P53, Bcl-xL, Bcl-2, and Bax were studied.

2.6.5. Gelatin zymography analysis

MMP-9 and MMP-2 activities were measured using gelatin zymography analysis [23]. Briefly, PBS extracts of liver tissue was resolved in 10 % SDS-PAGE gel containing 1 mg/mL gelatin under non-reducing conditions. The gels were then washed and incubated in a calcium assay buffer for 24 h at 37 °C. Finally, it was stained using 0.5 % (w/v) Coomassie blue followed by destaining with methanol:acetic acid:water (4:1:5 v/v/v) until the bands were clearly visible. The zones of gelatinolytic activity appeared as negative staining.

2.7. Statistical analysis

The data was statistically analyzed using one-way ANOVA followed by post hoc Dunnett and Sidak test using Graph Pad Prism Software 7.0. $p < 0.05$ was considered as a minimum level of significance.

3. Results

3.1. Structural confirmation of galactosylation of PLGA

The anomeric OH— functional group of galactose reacted with the free —COOH group of PLGA in acidic condition catalyzed by methane sulfonic acid. This esterification was conducted in DMF media. The conjugation was confirmed by $^1\text{H-NMR}$ spectroscopy (Figure S1). $^1\text{H-NMR}$ spectra of PLGA depicted various chemical shifts between 1.57 ppm correspond to methyl proton (—CH₃), 4.82 ppm due to methylene proton (—CH₂), and between 5.22 ppm due to methyne proton (—CH). The chemical shifts were observed in the $^1\text{H-NMR}$ spectra of galactosylated-PLGA, wherein an additional peak at 4.32 ppm appeared due to the galactose unit. The extent of galactosylation can be measured by comparing the relative peak areas of the —CH₃ and —CH₂ of PLGA and peaks of galactose.

3.2. Characterization of NPs

The prepared NPs were characterized on the basis of particle size, size distribution, and zeta potential. The mean particle size of API-NPs was 110.0 nm (Fig. 1A) with a PDI of 0.041 ± 0.004 (Table S1); while, API-GAL-NPs exhibited a mean particle size of 129.0 nm (Fig. 1A) and PDI of 0.059 ± 0.007 (Table S1). Low PDI values indicate that the formulations exhibit even-sized particles. The mean zeta potential values of API-NPs and API-GAL-NPs as determined by the DLS technique were found to be -25.0 and -14.0 mV, respectively (Fig. 1B). The decrease of zeta potential value of the NPs prepared from GAL-PLGA may be due to galactosylation of the PLGA. The negative zeta potential also favors reticuloendothelial system (RES) uptake by the liver and spleen. The formulations stored at 4 °C for 90 days did not show any significant change in particle size, PDI, and zeta potential, which confirmed the stability of the NPs (Table S1).

3.2.1. Drug loading and encapsulation efficiency

API-NPs and API-GAL-NPs exhibited ~5.1 and 5.3 % w/w of drug loading and ~70.3 and 75.4 % of encapsulation efficiency, respectively (Table S1). Drug loading in NPs was optimum; whereas, encapsulation efficiencies were sufficiently high. Galactosylation of PLGA does not affect API entrapment in NPs.

3.2.2. Surface characteristics of NPs

FESEM images of API-NPs and API-GAL-NPs showed that the NPs were spherical in shape, homogeneously, and thickly distributed having a smooth outer surface (Fig. 1C). TEM images revealed a smooth surface characteristics and entrapment of drug within the NPs (Fig. 1D). The diameter range of the NPs as obtained from FESEM (60–120 nm) and

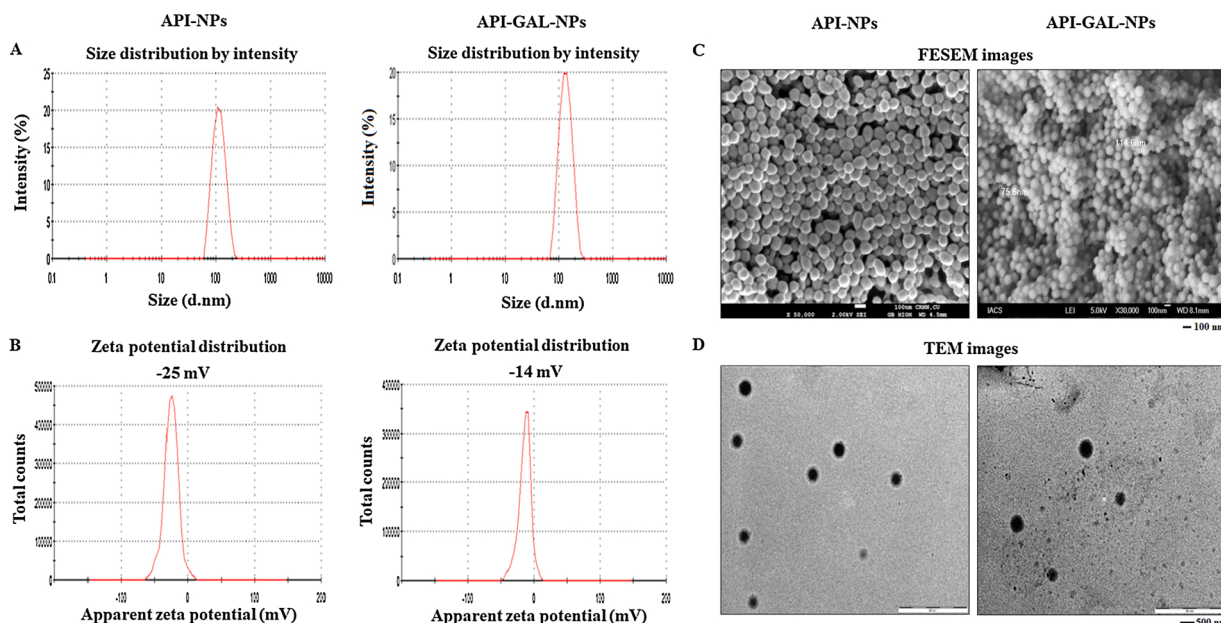


Fig. 1. Size distribution, zeta potential, and morphology of API-NPs and API-GAL-NPs. (A) Particle size distribution profile, (B) zeta potential distribution pattern, (C) FESEM images, and (D) TEM images.

TEM (85–160 nm) analyses were corroborated with the data obtained in DLS.

3.2.3. Physicochemical characteristics of NPs

3.2.3.1. DSC and XRD study. The DSC thermogram of API showed a melting endothermic peak at 359.2°C (Fig. 2A). PLGA and GAL-PLGA being amorphous did not exhibit any sharp endothermic peak in their respective DSC thermograms. The disappearance of the endothermic peak of API in the respective DSC thermogram of API-NPs and API-GAL-NPs may be due to the conversion of API from the crystalline state to the amorphous state during nano-formulation. This loss of crystallinity and amorphization due to nanoencapsulation may increase the stability of the formulation. The above findings from the DSC analyses were well corroborated with the results obtained from the X-RD study. The XRD spectra of API exhibited sharp distinct peaks due to its crystalline nature (Fig. 2B). The absence of any sharp peak in the respective XRD spectra for PLGA and GAL-PLGA confirmed their amorphous nature (Fig. 2B). The disappearance of the distinct peaks of API in API-NPs and API-GAL-NPs suggested the conversion of the crystalline state of API to an amorphous state during nanoencapsulation (Fig. 2B).

3.2.3.2. FTIR spectroscopic analysis. FTIR spectroscopy was done to investigate the interactions between drug and excipients. Fig. 2C depicts FTIR spectra of API, PLGA, GAL-PLGA, poloxamer, physical Mixture, API-NPs, and API-GAL-NPs. Most of the characteristic peaks (discussed in supplementary section) of API, PLGA, GAL-PLGA and poloxamer appeared in the FTIR spectra of the physical mixture with only minor shifts. The minor shifting of peaks occurred due to minor physical interaction, weak hydrogen bond formation, Vander-Waals force of attractions, dipole-dipole interactions, etc. The presence of characteristic peaks of API also suggests that no chemical interactions took place between the drug and the excipients.

3.2.4. In vitro drug release and kinetic study

In vitro drug release profile of nanoformulations revealed a biphasic release profile of the formulations as characterized by initial burst release followed by a slow and sustained drug release for about 8 days as depicted in Fig. 2D. An initial burst release of API (at the end of 8 h) were

~31.5 % from API-NPs and ~21 % from API-GAL-NPs. At the end of 8 days, % cumulative drug releases were ~88 and 86 % from API-NPs and API-GAL-NPs, respectively. The release of API from API-GAL-NPs was slower than from API-NPs. Moreover, the release patterns of API from API-NPs and API-GAL-NPs were almost comparable indicating no effect of galactosylation on the drug release profile. The drug release kinetic pattern was further assessed using zero-order, first-order, Korsmeyer-Peppas and Higuchi kinetic models. Various regression coefficient (R^2) values for the kinetic models are shown in Table S2. The data suggest that Higuchi kinetic model ($R^2 = 0.991$ and 0.994 for API-NPs and API-GAL-NPs, respectively) indicated better linearity for both the formulations over other models. The drug release mechanism is Fickian in nature as indicated by 'n' value from the Korsmeyer-Peppas equation for both the formulations.

3.3. In vitro studies

3.3.1. Cellular uptake and internalization

The quantitative measurement of cellular uptake behaviour of FITC-labelled galactose conjugated (FITC-GAL-NPs) and unconjugated (FITC-NPs) NPs by HepG2 cells were determined at different intervals (15, 30, 60, and 120 min) by flow cytometric analysis (Fig. 3A and B). The internalization of galactosylated-NPs by the cells was significantly decreased in presence of excess galactose (Fig. 3C). FITC-GAL-NPs exhibited favourably high cellular internalization relative to FITC-NPs at all the time points (Fig. 3D). The decrease of internalization of galactosylated-NPs in presence of excess galactose may arise due to competitive inhibition of asialoglycoprotein receptors present on the surface of the HepG2 cells by the excess of galactose. Qualitative analysis by confocal microscopic studies also revealed that the intracellular fluorescence intensity of the cells treated with galactosylated-NPs was stronger than that treated with non-galactosylated one (Fig. 3E). Thus, galactosylation enhances cellular internalization and may strengthen the biological activity of the formulation.

3.3.2. MTT assay

The cytotoxic potentials of free API, API-NPs, and API-GAL-NPs were evaluated at two different time intervals (24 and 48 h) by MTT assay using HepG2-cells (Table S3). The concentrations of NPs were selected on the basis of API available to exert the anti-proliferative effect. In both

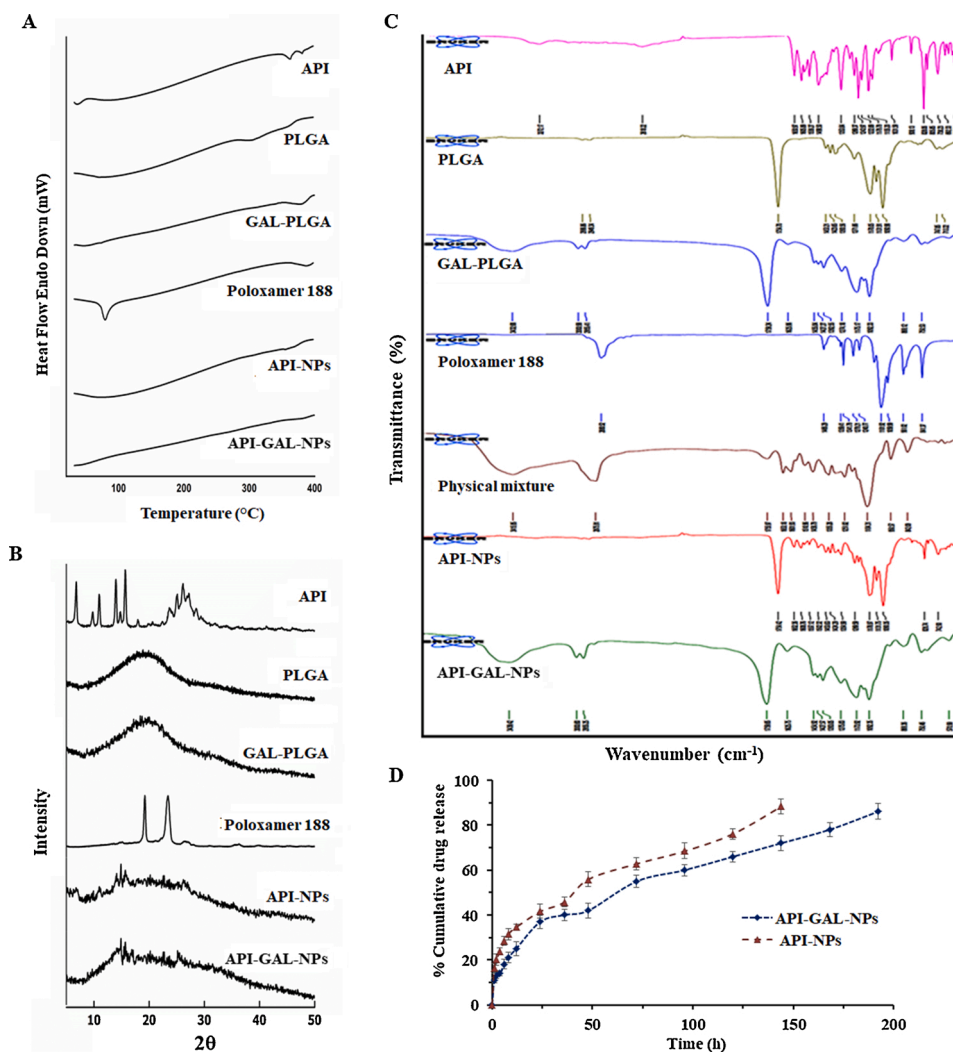


Fig. 2. (A) DSC thermograms, (B) XRD diffractograms, and (C) FTIR spectra of API, PLGA, GAL-PLGA, PELOXAMER, API-NPs, and API-GAL-NPs. (D) *in vitro* drug release showing cumulative % of drug release of API-NPs and API-GAL-NPs.

cases API-GAL-NPs exhibited better cytotoxic potential than API-NPs and API-GAL-NPs. After 24 h of incubation, the IC_{50} value of API-GAL-NPs ($37.1 \pm 3.4 \mu M$) was significantly ($p < 0.01$) lower than the IC_{50} values of API-NPs ($77.2 \pm 6.4 \mu M$) and API ($130.2 \pm 8.9 \mu M$). The anti-proliferative effect was more pronounced after 48 h of incubation and the corresponding IC_{50} values of API-GAL-NPs, API-NPs, and API were found to be 60.1 ± 7.1 , 40.2 ± 5.9 , and $15.9 \pm 4.8 \mu M$, respectively. Better cellular internalization of API-GAL-NPs increased cytotoxic behavior and may attribute better anticancer potential.

3.3.3. Apoptosis study

The induction of apoptosis to HepG2 cells following treatment (IC_{50} dose for 24 h) with API, API-NPs, and API-GAL-NPs were assessed by flow cytometric assay (Fig. 4B). API treatment induced apoptosis to HepG2 cells with 8.8 and 4.1 % of apoptotic cells were seen at early and late phases, respectively. These values were relatively high with API-NPs treatment, which exhibited 22.5 and 10.9 % apoptotic cells at early and late phases, respectively. The apoptotic activity following API-GAL-NPs treatment was highest, which showed 27.9 and 11.3 % of apoptotic cells at early and late phases, respectively. Optimum particle size, sustained release of API from NPs, and promising cytotoxic effect might have resulted in higher apoptotic potentials of API-NPs, which was further intensified in API-GAL-NPs due to improved cellular penetration through asialoglycoprotein receptors.

3.4. Pharmacokinetic analysis

Pharmacokinetic analysis was performed to understand the plasma profile of the drug in experimental rats following treatment with API, API-NPs, and API-GAL-NPs (Table S4). Despite an initial high plasma level of API was seen in the free drug-treated group, it was rapidly eliminated (Fig. 4C). In contrast, both the nanoformulations were capable to restore a steady plasma concentration of API up to 72 h (Fig. 4C). At 48 h, plasma API concentration remained ~ 2.6 and 2.1 -fold ($p < 0.001$) high in API-GAL-NPs and API-NPs-treated animals as compared to free drug-treated group, respectively. Elimination half-life ($t_{1/2}$) and AUC_{0-t} values of API-GAL-NPs were found to be significantly ($p < 0.001$) higher than API-NPs. Similarly, MRT value of API-GAL-NPs increased by ~ 1.27 -fold ($p < 0.001$) than the value for API-NPs. Drug clearance of API-GAL-NPs is decreased by ~ 1.33 -fold ($p < 0.001$) as compared to API-NPs. All these parameters indicate that API-GAL-NPs maintained a steady and significantly high level of API in the blood even up to 72 h and could provide better therapeutic efficacy than API and API-NPs.

3.5. Antitumor efficacy of NPs in vivo

3.5.1. Efficacy of NPs against DEN-induced HCC

Visible nodules were observed on the liver surface of all animals in

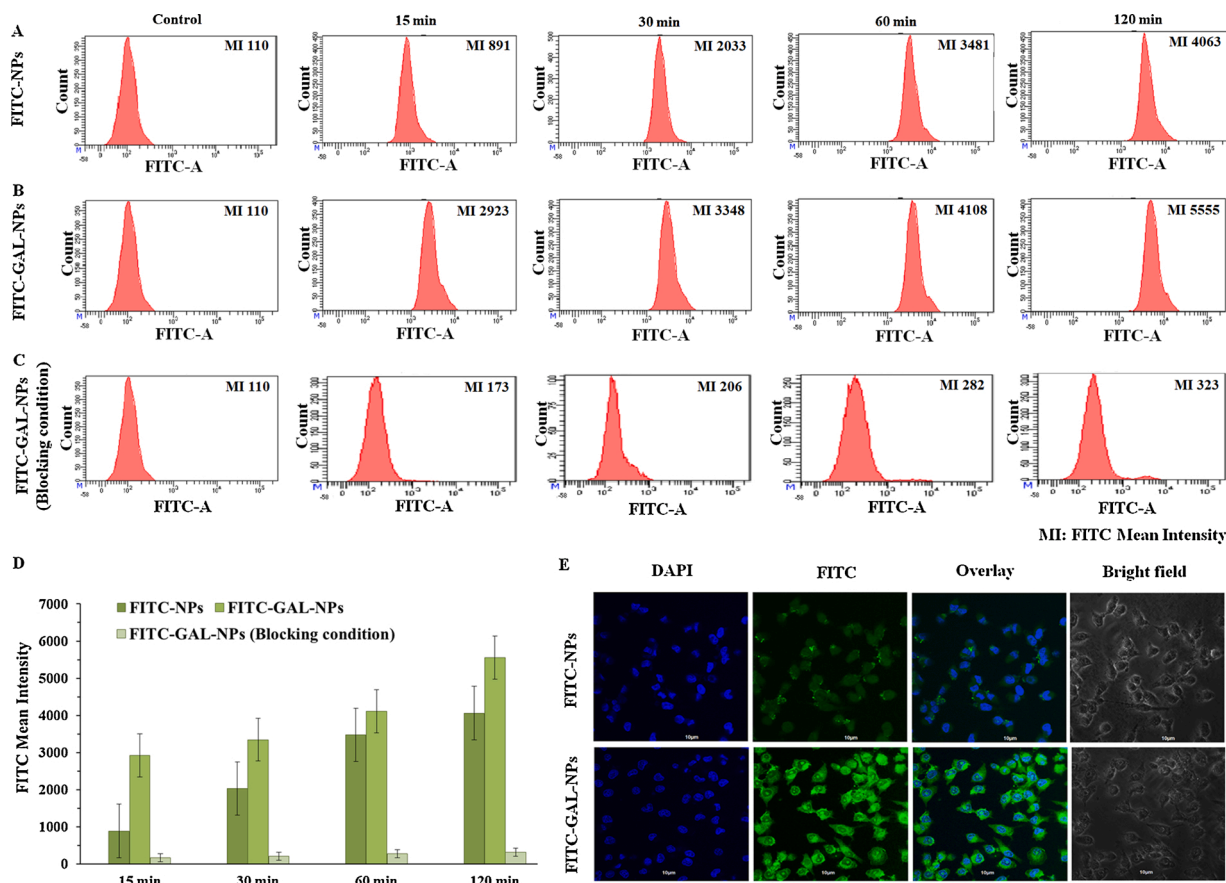


Fig. 3. *In vitro* cellular uptake of galactosylated and non-galactosylated NPs in HePG2 cells at different time points. (A) Cellular uptake of FITC-NPs. (B) Cellular uptake of FITC-GAL-NPs. (C) Cellular uptake of FITC-GAL-NPs in the presence of galactose (blocking condition). (D) Histogram representing the cellular uptake of FITC-NPs, FITC-GAL-NPs, and FITC-GAL-NPs (blocking condition) at different time points. Results are expressed as \pm SD ($n = 3$). (E) Confocal microscopic images representing cellular uptake of FITC-NPs and FITC-GAL-NPs in HePG2 cells at a time interval of 2 h. FITC exhibits green fluorescence and DAPI (nuclear stain) exhibits blue fluorescence.

DEN-treated group (HCC control), which signified the establishment of HCC in rats caused by DEN treatment. A large number of nodules was developed mostly at the edge of liver parenchyma (Figure S2). It was observed that the average number of nodules were significantly reduced in API-NPs (~ 1.43 -fold; $p < 0.01$) and API-GAL-NPs (~ 3.43 -fold; $p < 0.001$) in carcinogenic animals as compared to HCC control group (Table S5). However, no significant change in nodule number was observed in API-treated animals. Relative liver weight (RLW) was increased in DEN-treated animals and it was significantly reduced in carcinogenic animals treated with API-GAL-NPs (~ 1.32 -fold; $p < 0.001$) and API-NPs (~ 1.15 -fold; $p < 0.05$) as compared to HCC control rats (Table S5).

Serum ALP, ALT and AST levels were significantly increased in HCC control animals as compared to normal control group (Table 1). However, treatment with API-NPs ($p < 0.01$) and API-GAL-NPs ($p < 0.001$) to carcinogenic rats significantly reduced and ALP, AST, and ALT levels in sera as compared to HCC control animals (Table 1). API-treatment though reduced serum ALP, AST, and ALT levels; however, changes remained insignificant as compared to DEN-treated animals (Table 1).

3.5.2. Histopathological analysis

The effects of API, API-NPs, and API-GAL-NPs on DEN-induced HCC in rats was examined by the histopathological investigation. Haematoxylin-eosin-stained liver sections collected from the normal control animals (Gr-I) exhibited normal hepatocytes arranged in the cords and the portal tracts also appeared normal. The liver section collected from HCC animals (Gr-II) exhibited scattered lesions with cells of ground-glass opacity, dilated hepatic veins, and loss of normal hepatic

architecture (Fig. 5A). Cells with pyknotic nucleus and multinucleated hepatocytes were observed in the HCC control group (Gr-II) as compared to Gr-I. No distinguishable change was observed in the liver sections of API-treated carcinogenic rats (Fig. 5A). API-NPs treatment to carcinogenic rats demonstrated some improvement in liver architecture and structural integrity; however, dilated hepatic veins and lesions were still evident (Fig. 5A). In contrast, API-GAL-NPs treatment to carcinogenic rats resulted in perceptible recovery in the liver architecture showing increased cell density with increased eosinophilic staining and more distinct cord structure. Significant reduction in hepatic lesions and abnormal cells was observed in API-GAL-NPs-treated group (Fig. 5A). No PAS-positive cells appeared in PAS-stained liver section collected from normal rats (Gr-I) (Fig. 5B). However, the liver sample collected from HCC control rats showed an appreciable extent of PAS-positive reaction; whereas, adjacent pale staining of centrilobular hepatocytes indicated an ischemia/reperfusion injury (Fig. 5B). Free API treatment did not have much effect as the staining intensity was not reduced (Fig. 5B). API-NPs-treated group (IV) exhibited better results than free drug-treated group evidenced by the reduction of PAS-positive cells and nodules (Fig. 5B). API-GAL-NPs treatment to carcinogenic rats caused a significant reduction in the intensity of PAS-positive staining in the cytoplasm with a concomitant reduction in pre-neoplastic nodules, which signified that API-GAL-NPs exhibited better therapeutic efficacy over API-NPs against HCC in rats (Fig. 5B).

3.5.3. Western blot analysis of apoptosis markers

The therapeutic efficacy of API-GAL-NPs against DEN-induced HCC was further estimated by studying the signaling events involved in

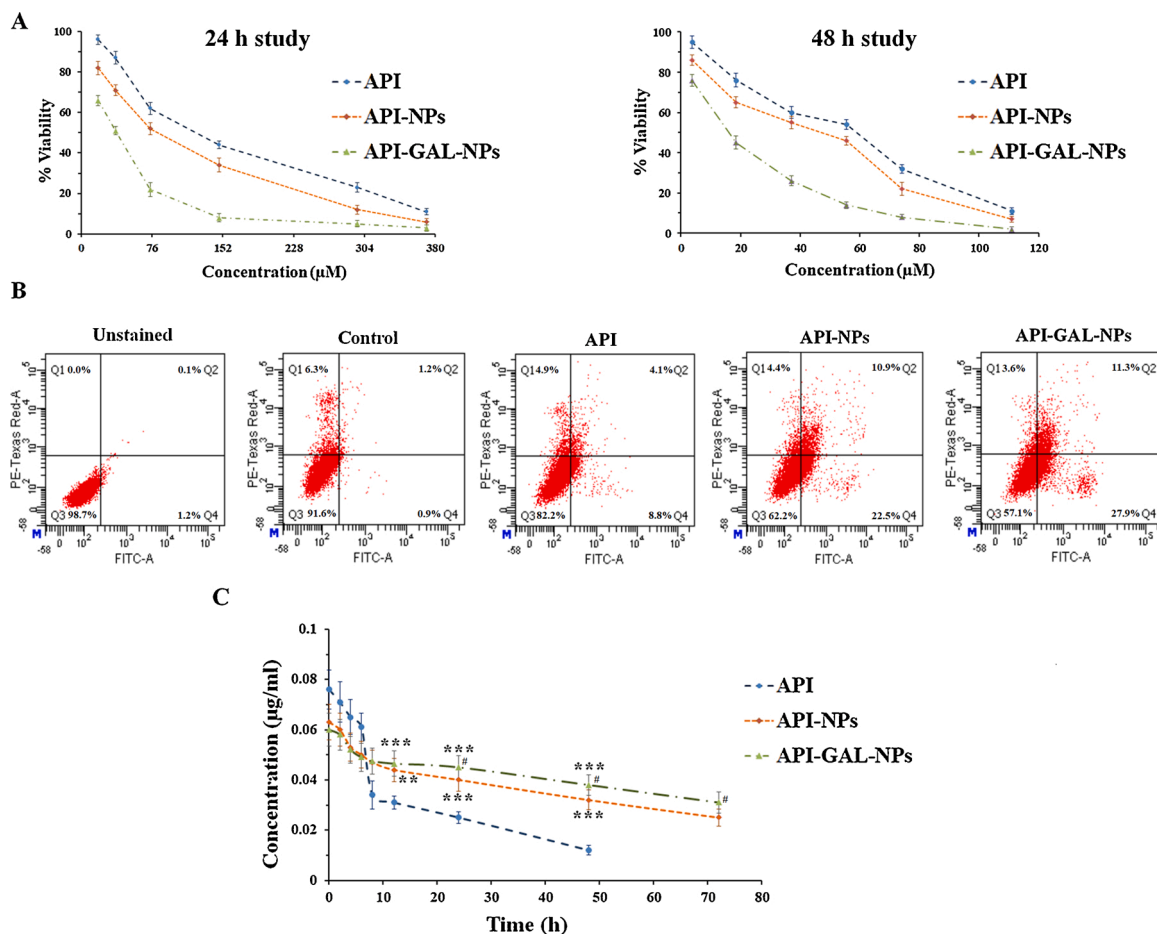


Fig. 4. (A) Cytotoxic effect of API, API-NPs, and API-GAL-NPs on HepG2 cells at 24 and 48 h measured by MTT assay. (B) Apoptosis induction by API, API-NPs, and API-GAL-NPs to HepG2 cells measured by flow cytometry. (C) Plasma concentration-time profile of API at different time points following API, API-NPs, and API-GAL-NPs treatments. Results are expressed as \pm SD ($n = 3$). **Values significantly ($p < 0.01$) differed from API-treated group. ***Values significantly ($p < 0.001$) differed from API-treated group. #Values significantly ($p < 0.05$) differed from API-NPs-treated group.

Table 1

Effect of API and nanoparticulated API on serum enzyme parameters.

Parameters	Gr-I	Gr-II	Gr-III	Gr-IV	Gr-V
ALP (KA units)	20.22 \pm 1.82	112.04 \pm 4.46 [#]	107.09 \pm 6.68 ^{NS}	71.01 \pm 2.12 ^{**}	32.14 \pm 1.14 ^{***}
AST (IU/L)	70.14 \pm 2.11	354.92 \pm 8.86 [#]	346.50 \pm 9.13 ^{NS}	212.33 \pm 4.89 ^{**}	86.54 \pm 0.65 ^{***}
ALT (IU/L)	30.89 \pm 1.65	165.44 \pm 9.55 [#]	156.21 \pm 7.96 ^{NS}	79.67 \pm 2.39 ^{**}	42.37 \pm 2.22 ^{***}

Results are expressed as mean \pm SD ($n = 5$).

[#] Values significantly ($p < 0.001$) differed from Gr-I.

^{**} Values significantly ($p < 0.01$) differed from Gr-II.

^{***} Values significantly ($p < 0.001$) differed from Gr-II. NS: Non-significant.

apoptotic pathways (Fig. 5C). In this study, a significant downregulation ($p < 0.001$) was observed in the expression of P53 and Bax proteins in the livers of HCC control animals. In contrast, API-NPs ($p < 0.01$) and API-GAL-NPs ($p < 0.001$) treatments to carcinogenic rats significantly activated P53 and Bax expression in the liver as compared to HCC control rats. No significant change was seen in the expression of either of the proteins in the liver of API-treated carcinogenic rats. In search of the effects on anti-apoptotic factors, the expressions of Bcl-2 and Bcl-xL were studied in the liver of rats that received different treatments. HCC control animals exhibited significant upregulation ($p < 0.001$) in the expression of Bcl-2 and Bcl-xL in the liver. In contrast, API-NPs ($p < 0.01$ – 0.001) and API-GAL-NPs ($p < 0.001$) treatments significantly reduced Bcl-2 and Bcl-xL expressions in the liver of carcinogenic animals. API treatment could only suppress ($p < 0.05$) Bcl-xL expressions in carcinogenic rats. The expression analyses of the apoptotic factors clearly indicated that

API-GAL-NPs could induce apoptosis more intensively than API-NPs.

3.5.4. Gelatin zymography analysis

Gelatin zymography analysis of liver tissue exhibited significant downregulation of the expression of MMP-2 ($p < 0.01$ – 0.001) and MMP-9 ($p < 0.05$ – 0.001) in API-NPs and API-GAL-NPs treated carcinogenic rats as compared to HCC control animals. However, API-GAL-NPs treatment caused \sim 1.1 and 1.5-fold intense reduction in hepatic MMP-2 and MMP-9 levels as compared to API-NPs treated group (IV).

3.5.5. Evaluation of hepatoprotective efficacy by scintigraphic imaging analysis

The mechanistic evaluations stated above suggested the potential efficacy of API-GAL-NPs to treat DEN-induced HCC in rats, which could be further corroborated with scintigraphic imaging analysis. The

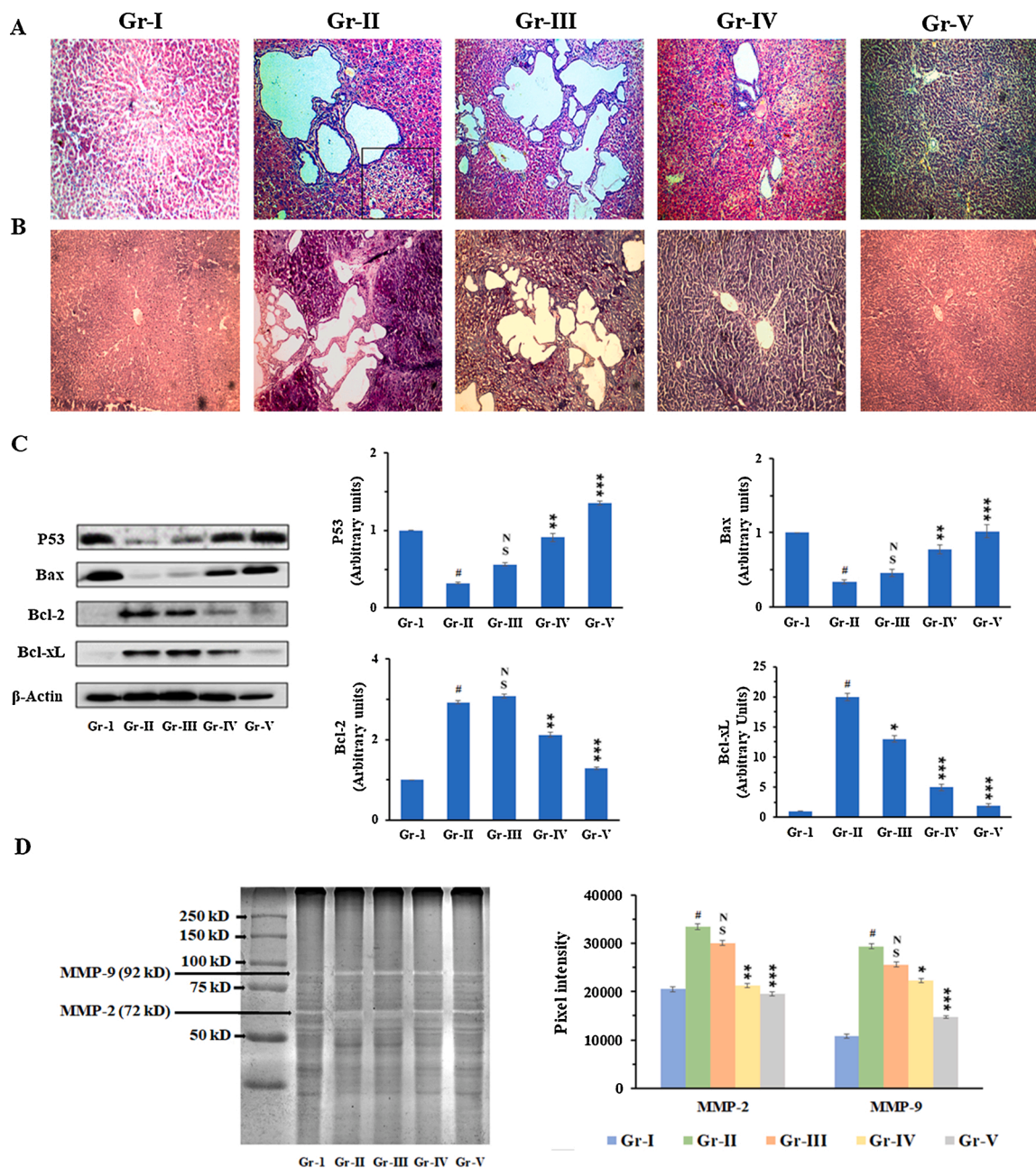


Fig. 5. (A) Representative photomicrographs of haematoxylin-eosin-stained liver section. (B) Representative photomicrographs of PAS-stained liver section. (C) Western blot analysis expression of different apoptotic proteins and histogram showing their relative expressions in liver. β -Actin served as a loading control protein. The intensity of normal control band was assigned 1 (D) Zymogram and histogram showing the effect on MMP-9 and MMP-2 in liver. Results are expressed as \pm SD ($n = 5$). #Values significantly ($p < 0.001$) differed from Gr-I. **Values significantly ($p < 0.01$) differed from Gr-II. ***Values significantly ($p < 0.001$) differed from Gr-II. NS: Non-significant.

function of hepatic RES was qualitatively assessed using ^{99m}Tc -labelled sulphur colloid imaging protocol. The anterior view of the scinti-photos revealed that uniform distribution of ^{99m}Tc -sulphur colloid in the liver of normal control animals (Gr-I) indicating good functioning of RES (Fig. 6A). In contrast, hepatic distribution was discontinuous in HCC control animals (Gr-II) (Fig. 6A). However, API-GAL-NPs treatment significantly reciprocated hepatic distribution in carcinogenic animals (Gr-V), which signified that RES function could have recovered with API-GAL-NPs treatment (Fig. 6A). The liver function of the normal, HCC control, and API-GAL-NPs-treated group were also monitored non-invasively by nuclear scintigraphy approach using ^{99m}Tc -labeled mebrofenin. The normal group exhibited immediate liver accumulation following injection of ^{99m}Tc -labeled mebrofenin and rapid excretion.

The sharp rise and fall were observed in the curve as generated from the instrument (Fig. 6B). The nature of the curve was very irregular in HCC control (Gr-II) group representing slow and erratic uptake with sluggish excretion (Fig. 6B). However, these irregularities in uptake and excretion were relatively reversed following treatment with API-GAL-NPs to carcinogenic animals (Fig. 6B). The serial images of liver uptake and subsequent clearance for a period of 1 h at 3 min interval was also depicted in Fig. 6C.

4. Discussion

Emerging evidence highlighted chemopreventive role of API against various types of cancer including HCC [4,24]. It exerts anticancer effects

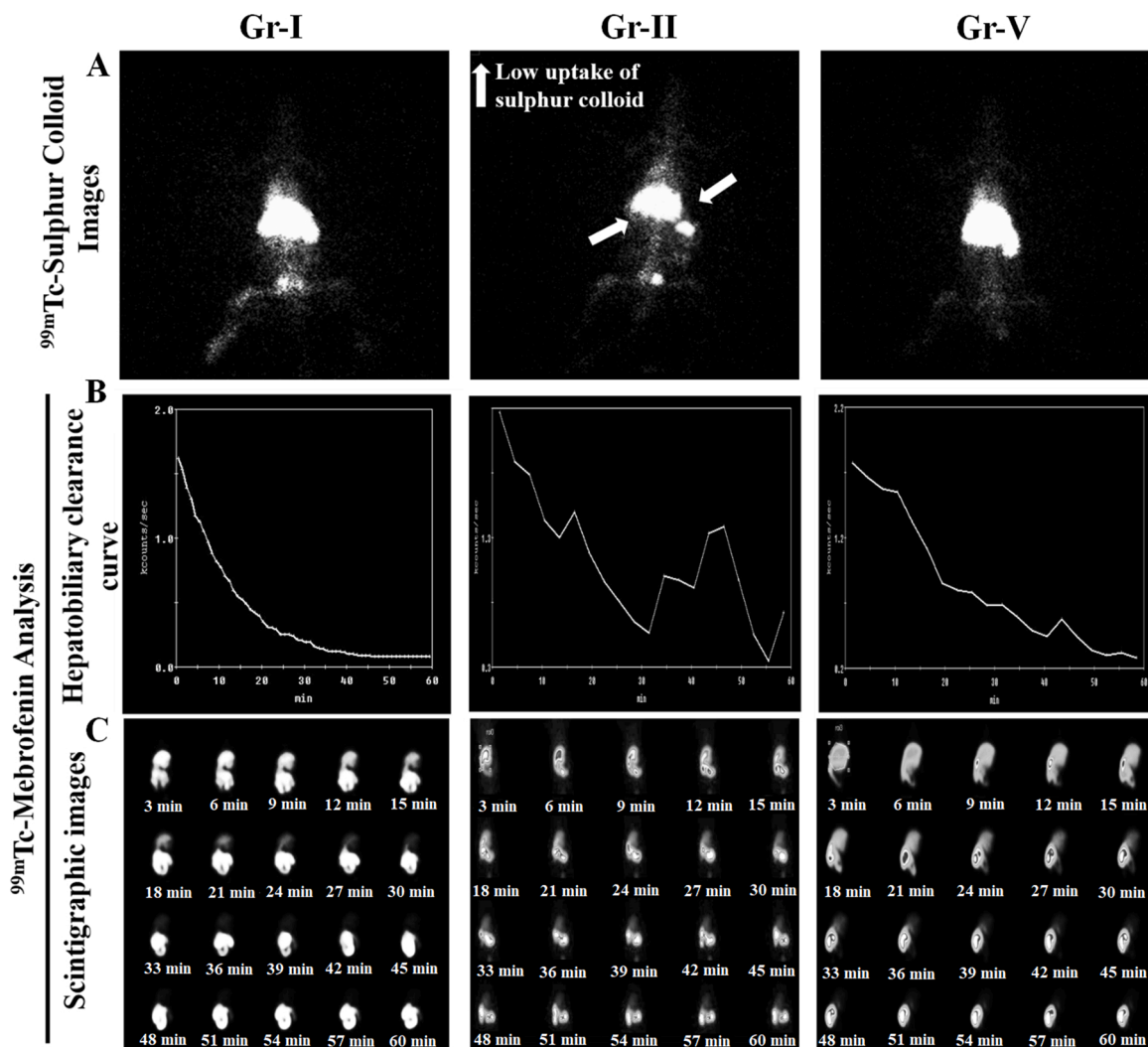


Fig. 6. Nuclear scintigraphic image analyses of normal (Gr-I), HCC control (Gr-II), and API-GAL-NPs-treated rats (Gr-V). (A) Representative scintigraphic images of ^{99m}Tc -sulphur colloid acquired at 1 h post-injection. (B) Representative hepatobiliary clearance curves of ^{99m}Tc -mebrofenin. (C) Representative scintigraphic images at different post-injection time periods of ^{99m}Tc -mebrofenin. White arrows represented area of low uptake of sulphur colloids.

on human liver cancer cells by inhibiting cell growth, arresting cell cycle, and inducing apoptosis without imparting any toxic manifestation to normal liver cells [25]. However, a gap exists between *in vitro* and *in vivo* observations. Poor solubility in both aqueous and non-aqueous solvents, high metabolic transformation, and high inter-individual variability limit its *in vivo* effectiveness [7]. Thus, a much higher *in vivo* dosing of API is required to achieve a therapeutic effect against HCC in preclinical assays [26,27]. In this aspect, nanoformulation of API can stand as a solution to improve its therapeutic efficacy. Our recent observations showed that API-loaded PLGA NPs can improve the chemopreventive efficacy of API in a murine model of HCC [28], which encouraged us to fabricate API-PLGA-NPs to achieve better therapeutic efficacy of API *via* active targeting to the liver tissues. Galactose conjugation to NP surface can improve liver targeting as galactose is actively taken up by asialoglycoprotein receptors which are abundant on the hepatic parenchymal cells [10]. In this study, we aimed to prepare galactose-tailored API-NPs to improve the therapeutic efficacy of API-NPs against HCC by improving site (liver) specificity.

To prepare galactosylated API-loaded polymeric NPs, polymer (PLGA) was galactosylated by simple esterification reaction [10]. Galactose conjugation was confirmed by $^1\text{H-NMR}$ spectroscopy [10]. The galactosylated-PLGA was used to formulate API-loaded galactosylated polymeric NPs by nanoprecipitation technique using poloxamer

188 as a surfactant. In selecting surfactant, poloxamer 188, polyvinyl alcohol, and vitamin E-TPGS were initially tried; however, poloxamer 188 stood optimum and included in this formulation. DSC thermograms, XRD diffractograms, and FTIR spectra indicated that no chemical reaction occurs between API and excipients; however, some physical interactions and changes in physical form (crystalline to amorphous) might be involved in the formation of NPs. Developed API-GAL-NPs were spherical in shape with a smooth surface and mean diameter of 129 nm. A low PDI value indicated that API-GAL-NPs exhibit even-sized particles [28]. An observed zeta potential of -14.0 mV was well within the recommended range (-30 mV to +30 mV), which suggested that API-GAL-NPs would not settle down so quickly and could be delivered intravenously [28]. API-GAL-NPs exhibited $\sim 5.3\%$ w/w of drug loading and can restore stability at least for 90 days at 4 °C. API-GAL-NPs exhibited an initial burst release of API ($\sim 21\%$ within 8 h) in PBS followed by a sustained release up to 8 days (cumulative release $\sim 86\%$ in 8 days). Initial burst release might occur due to the presence of API close to the surface of the NPs; while a sustained-release profile was achieved due to the drug present in the inner core of NPs [29]. Drug diffusion from API-GAL-NPs followed Higuchi kinetics exhibiting good linearity (as assessed by R^2 values) and the release of API was Fickian in nature.

FITC-labeled API-GAL-NPs exhibited better cellular uptake by HepG2 cells compared to API and API-NPs. Galactosylation might

facilitate intracellular uptake through asialoglycoprotein receptors present on the surface of HepG2 cells [10]. This has been verified by blocking studies. Asialoglycoprotein receptor-mediated active targeting improved cytotoxic and apoptotic effects of API-GAL-NPs to HepG2 cells over API-NPs. All these findings suggest that improved internalization of API by HCC cells from API-GAL-NPs would potentiate its chemotherapeutic efficacy to combat HCC *in vivo*. In this study, the *in vivo* anticancer potential of API-GAL-NPs was compared with API and API-NPs in DEN-induced HCC in rats. DEN-induced HCC is a well-established murine model of liver carcinoma [30]. API-GAL-NPs treatment to carcinogenic rats more effectively reduced the number of nodules and RLW than API-NPs. A gross reduction of nodule number and RLW signifies low incidence of HCC development and/or chemotherapeutic potential of API-GAL-NPs against HCC in rats [28]. Emerging evidence revealed that an increased risk of HCC is conferred by the increased levels of AST, ALT, and ALP in sera [31]. In this study, HCC control rats exhibited significant elevation in the levels of AST, ALT, and ALP as compared to normal. In contrast, API-NPs and API-GAL-NPs both could significantly reciprocate AST, ALT, and ALP levels in sera of carcinogenic rats; however, API-GAL-NPs exhibited better therapeutic efficacy. Histological examination revealed that API-GAL-NPs could significantly reduce hepatic lesions, abnormal cells, and glycogen deposition in liver and restore hepatic architecture to near-normal status. API-NPs also improved the tissue structure; however, it was not to the extent of API-GAL-NPs-mediated improvement.

Induction of apoptosis is a primary requirement in chemotherapy [1]. Bcl-2 family proteins regulate apoptosis through a complex interplay between pro-apoptotic and anti-apoptotic proteins. Pro-apoptotic factors, such as Bax protein promotes apoptosis through mitochondrial stress [32]. In contrast anti-apoptotic factors of Bcl-2 family, such as Bcl-2 and Bcl-xL inhibit apoptosis *via* binding to pro-apoptotic proteins [32]. P53, a tumor suppressor protein, can impart pro-apoptotic role and can arrest cell cycle [32–34]. Emerging evidence established the cross-talk between P53 and Bcl-2 family proteins in human HCC [35]. In this study, immunoblotting showed that API-GAL-NPs treatment to carcinogenic animals significantly activated the expression of pro-apoptotic factors (P53 and Bax) and suppressed anti-apoptotic factors (Bcl-2 and Bcl-xL), which signifies induction of apoptosis to the liver in HCC bearing animals. API-NPs also induced apoptosis to the liver of carcinogenic animals, but the extent was much less as compared to API-Gal-NPs. MMP-2 and MMP-9 are involved in epithelial-mesenchymal transition of HCC and play important role in disease progression [36]. Gelatin zymography showed that significant up-regulation of MMP-2 and MMP-9 in the livers of DEN-treated rats, which signifies the progression of HCC in rats. In contrast, API-GAL-NPs treatment to carcinogenic animals prevented HCC progression by reducing the levels of MMP-2 and MMP-9 in the livers. API-NPs also reduced hepatic MMP-2 and MMP-9 in carcinogenic animals; however, the extent was much less as compared to API-Gal-NPs. Hepatoprotective efficacy of the nano-formulations was also evaluated non-invasively by nuclear scintigraphic analyses using ^{99m}Tc -sulphur colloid and ^{99m}Tc -mebrofenin. ^{99m}Tc scintigraphy is a routinely used technique to study hepatobiliary function [37]. In this study, HCC control rats exhibited significant disruption in hepatobiliary function. In contrast, API-GAL-NPs treatment to carcinogenic animals significantly attenuated hepatocellular degeneration and restored hepatobiliary function to near normal status as observed in both qualitative and quantitative scintigraphic analyses.

Apigenin is a naturally occurring molecule with exciting anticancer potential against HCC. However, poor pharmacokinetic and biopharmaceutical features reduce its *in vivo* therapeutic effect. Earlier report revealed that API-NPs exhibited improved chemotherapeutic effect against HCC over free API *via* improving pharmacokinetic and biopharmaceutical attributes. In this study, galactose tailoring to API-NPs caused further improvement in therapeutic efficacy over API-NPs, which has been shown to be mediated through active targeting and

improved internalization of API by HCC cells. In conclusion, API-GAL-NPs may serve as a novel drug delivery with improved therapeutic efficacy achieved by active liver targeting in the management of HCC in the future.

CRediT authorship contribution statement

Soumya Ganguly: Conceptualization, Methodology, Software, Formal analysis, Investigation, Data curation, Writing - original draft. **Saikat Dewanjee:** Resources, Conceptualization, Supervision, Writing - original draft. **Ramkrishna Sen:** Software, Investigation, Visualization. **Dipankar Chattopadhyay:** Resources. **Shantanu Ganguly:** Resources. **Raghuvir Gaonkar:** Investigation, Visualization. **Mita Chatterjee Debnath:** Conceptualization, Validation, Writing - review & editing, Resources, Supervision, Project administration, Funding acquisition.

Declaration of Competing Interest

The authors report no declarations of interest.

Acknowledgements

The authors are indebted to Mr. Satyabrata Samadder for FTIR analysis, Mr. Budhaditya Ghosh for TEM analysis, Mr. Tanmoy Dolui, Mrs. Debalina Chakraborty for flow cytometry analysis, Mr. Binayak Pal for confocal microscopy analysis at CSIR-IICB Kolkata. The authors would also like to acknowledge Mr. Samrat Kundu, Centre for Research in Nanoscience and Nanotechnology (CRNN), University of Calcutta for FE-SEM analysis. BRNS, DAE (Govt. of India) is being acknowledged for awarding research project (Grant No. 2013/35/25/BRNS). Finally, authors are thankful to CSIR-IICB for support in carrying out the research work at the institute.

Appendix A. Supplementary data

Supplementary material related to this article can be found, in the online version, at doi:<https://doi.org/10.1016/j.colsurfb.2021.111778>.

References

- [1] S. Chakraborty, Z.Y. Dlie, S. Chakraborty, S. Roy, B. Mukherjee, S.E. Besra, S. Dewanjee, A. Mukherjee, P.K. Ojha, V. Kumar, R. Sen, Aptamer-functionalized drug nanocarrier improves hepatocellular carcinoma toward normal by targeting neoplastic hepatocytes, *Mol. Ther. Nucleic Acids* 20 (2020) 34–49, <https://doi.org/10.1016/j.omtn.2020.01.034>.
- [2] S. Mittal, H.B. El-Serag, Epidemiology of hepatocellular carcinoma: consider the population, *J. Clin. Gastroenterol.* 47 (2013) S2–6, <https://doi.org/10.1097/MCG.0b013e3182872f29>.
- [3] J.D. Yang, P. Hainaut, G.J. Gores, A. Amadou, A. Plymoth, L.R. Roberts L, A global view of hepatocellular carcinoma: trends, risk, prevention and management, *Nat. Rev. Gastroenterol. Hepatol.* 16 (2019) 589–604, <https://doi.org/10.1038/s41575-019-0186-y>.
- [4] M. Imran, T. Aslam Gondal, M. Atif, M. Shahbaz, T. Batool Qaisarani, M. Hanif Mughal, B. Salehi, M. Martorell, J. Sharifi-Rad, Apigenin as an anticancer agent, *Phyther. Res.* 34 (2020) 1812–1828, <https://doi.org/10.1002/ptr.6647>.
- [5] J. Cai, X.L. Zhao, A.W. Liu, H. Nian, S.H. Zhang, Apigenin inhibits hepatoma cell growth through alteration of gene expression patterns, *Phytomedicine* 18 (2011) 366–373, <https://doi.org/10.1016/j.phymed.2010.08.006>.
- [6] Y. Li, X. Cheng, C. Chen, W. Huijuan, H. Zhao, W. Liu, Z. Xiang, Q. Wang, Apigenin, a flavonoid constituent derived from *P. villosa*, inhibits hepatocellular carcinoma cell growth by CyclinD1/CDK4 regulation via p38 MAPK-p21 signaling, *Pathol. Res. Pract.* 216 (January (1)) (2020) 152701, <https://doi.org/10.1016/j.prp.2019.152701>.
- [7] S. Dewanjee, P. Chakraborty, B. Mukherjee, V. De Feo, Plant-based antidiabetic nanoformulations: the emerging paradigm for effective therapy, *Int. J. Mol. Sci.* 21 (2020) 2217, <https://doi.org/10.3390/ijms21062217>.
- [8] H. Cao, L. Chen, J. Xiao, Binding Citrus flavanones to human serum albumin: effect of structure on affinity, *Mol. Biol. Rep.* 38 (2011) 2257–2262, <https://doi.org/10.1007/s11033-010-0356-z>.
- [9] S. Acharya, S.K. Sahoo, PLGA nanoparticles containing various anticancer agents and tumour delivery by EPR effect, *Adv. Drug Deliv. Rev.* 63 (2011) 170–183, <https://doi.org/10.1016/j.addr.2010.10.008>.
- [10] I.N. Peça, K.T. Petrova, M.M. Cardoso, M.T. Barros, Preparation and characterization of polymeric nanoparticles composed of poly(DL-lactide-co-

- glycolide) and poly(DL-lactide-co-glycolide)-co-poly(ethylene glycol)-10%-Triblock end-capped with a galactose moiety, *React. Funct. Polym.* 72 (2012) 729–735, <https://doi.org/10.1016/j.reactfunctpolym.2012.06.019>.
- [11] H. Fessi, F. Puisieux, J.P. Devissaguet, N. Ammoury, S. Benita, Nanocapsule formation by interfacial polymer deposition following solvent displacement, *Int. J. Pharm.* 55 (1989) 1–4, [https://doi.org/10.1016/0378-5173\(89\)90281-0](https://doi.org/10.1016/0378-5173(89)90281-0).
- [12] R. Baishya, D.K. Nayak, D. Kumar, S. Sinha, A. Gupta, S. Ganguly, M.C. Debnath, Ursolic acid loaded PLGA nanoparticles: in vitro and in vivo evaluation to explore tumor targeting ability on B16F10 melanoma cell lines, *Pharm. Res.* 33 (2016) 2691–2703, <https://doi.org/10.1007/s11095-016-1994-1>.
- [13] R.H. Gaonkar, S. Ganguly, S. Dewanjee, S. Sinha, A. Gupta, S. Ganguly, D. Chattopadhyay, M. Chatterjee Debnath, Garcinol loaded Vitamin E TPGS emulsified PLGA nanoparticles: preparation, physicochemical characterization, in vitro and in vivo studies, *Sci. Rep.* 7 (2017), <https://doi.org/10.1038/s41598-017-00696-6>.
- [14] S. Ganguly, R.H. Gaonkar, S. Sinha, A. Gupta, D. Chattopadhyay, S. Chattopadhyay, S.S. Sachdeva, S. Ganguly, M.C. Debnath, Fabrication of surfactant-free quercetin-loaded PLGA nanoparticles: evaluation of hepatoprotective efficacy by nuclear scintigraphy, *J. Nanopart. Res.* 18 (2016), <https://doi.org/10.1007/s11051-016-3504-0>.
- [15] F.Y.K. Siu, S. Ye, H. Lin, S. Li, Galactosylated PLGA nanoparticles for the oral delivery of resveratrol: enhanced bioavailability and in vitro anti-inflammatory activity, *Int. J. Nanomedicine* 13 (2018) 4133–4144, <https://doi.org/10.2147/IJN.S164235>.
- [16] R. Sahu, T.K. Dua, S. Das, V. De Feo, S. Dewanjee, Wheat phenolics suppress doxorubicin-induced cardiotoxicity via inhibition of oxidative stress, MAP kinase activation, NF- κ B pathway, PI3K/Akt/mTOR impairment, and cardiac apoptosis, *Food Chem. Toxicol.* 125 (2019) 503–519, <https://doi.org/10.1016/j.fct.2019.01.034>.
- [17] Y. Zhang, M. Huo, J. Zhou, S. Xie, PKSolver: An add-in program for pharmacokinetic and pharmacodynamic data analysis in Microsoft Excel, *Comput. Methods Programs Biomed.* 99 (2010) 306–314, <https://doi.org/10.1016/j.cmpb.2010.01.007>.
- [18] K. Balakumar, C.V. Raghavan, N.T. Selvan, R.H. Prasad, S. Abdu, Self-nanoemulsifying drug delivery system (SNEDDS) of rosuvastatin calcium: design, formulation, bioavailability and pharmacokinetic evaluation, *Colloids Surf. B Biointerfaces.* 112 (2013) 337–343, <https://doi.org/10.1016/j.colsurfb.2013.08.025>.
- [19] N.S. Abdelwahab, A. Morsi, Y.M. Ahmed, M.H. Hassan, A.M. AboulMagd, Ecological HPLC method for analyzing an antidiabetic drug in real rat plasma samples and studying the effects of concurrently administered fenugreek extract on its pharmacokinetics, *RSC Adv.* 11 (2021) 4740–4750, <https://doi.org/10.1039/D0RA08836F>.
- [20] A. Ghosh, D. Ghosh, S. Sarkar, A.K. Mandal, S. Thakur Choudhury, N. Das, Anticarcinogenic activity of nanoencapsulated quercetin in combating diethylnitrosamine-induced hepatocarcinoma in rats, *Eur. J. Cancer Prev.* 21 (2012) 32–41, <https://doi.org/10.1097/CEJ.0b013e32834a7e2b>.
- [21] S. Joardar, S. Dewanjee, S. Bhowmick, T.K. Dua, S. Das, A. Saha, V. De Feo, Rosmarinic acid attenuates cadmium-induced nephrotoxicity via inhibition of oxidative stress, apoptosis, inflammation and fibrosis, *Int. J. Mol. Sci.* 20 (2019) 2027, <https://doi.org/10.3390/ijms20082027>.
- [22] T.K. Dua, S. Joardar, P. Chakraborty, S. Bhowmick, A. Saha, V. De Feo, S. Dewanjee, Myricitrin, a glycosyloxyflavone in *Myrica esculenta* Bark ameliorates diabetic nephropathy via improving glycemic status, reducing oxidative stress, and suppressing inflammation, *Molecules* 26 (2021) 258, <https://doi.org/10.3390/molecules26020258>.
- [23] V. Sivaramakrishnan, S. Niranjali Devaraj, Morin regulates the expression of NF- κ B-p65, COX-2 and matrix metalloproteinases in diethylnitrosamine induced rat hepatocellular carcinoma, *Chem. Biol. Interact.* 180 (2009) 353–359, <https://doi.org/10.1016/j.cbi.2009.02.004>.
- [24] C. Rodríguez-García, C. Sánchez-Quesada, J.J. Gaforio, J.J. Gaforio, Dietary flavonoids as cancer chemopreventive agents: an updated review of human studies, *Antioxidants* 8 (2019) 137, <https://doi.org/10.3390/antiox8050137>.
- [25] L.C. Chiang, L.T. Ng, I.C. Lin, P.L. Kuo, C.C. Lin, Anti-proliferative effect of apigenin and its apoptotic induction in human Hep G2 cells, *Cancer Lett.* 237 (2006) 207–214, <https://doi.org/10.1016/j.canlet.2005.06.002>.
- [26] J.P. Singh, K. Selvendiran, S.M. Banu, R. Padmavathi, D. Sakthisekaran, Protective role of apigenin on the status of lipid peroxidation and antioxidant defense against hepatocarcinogenesis in Wistar albino rats, *Phytomedicine.* 11 (2004) 309–314.
- [27] P.V.S. Jeyabal, M.B. Syed, M. Venkataraman, J.K. Sambandham, D. Sakthisekara, Apigenin inhibits oxidative stress-induced macromolecular damage in N-nitrosodiethylamine (NDEA)-induced hepatocellular carcinogenesis in Wistar albino rats, *Mol. Carcinog.* 44 (2005) 11–20.
- [28] S. Bhattacharya, L. Mondal, B. Mukherjee, L. Dutta, I. Ehsan, M.C. Debnath, R. H. Gaonkar, M.M. Pal, S. Majumdar, Apigenin loaded nanoparticle delayed development of hepatocellular carcinoma in rats, *Nanomedicine Nanotechnology, Biol. Med.* 14 (2018) 1905–1917, <https://doi.org/10.1016/j.nano.2018.05.011>.
- [29] P.J. Das, P. Paul, B. Mukherjee, B. Mazumder, L. Mondal, R. Baishya, M. C. Debnath, K.S. Dey, Pulmonary delivery of voriconazole loaded nanoparticles providing a prolonged drug level in lungs: a promise for treating fungal infection, *Mol. Pharm.* 12 (2015) 2651–2664, <https://doi.org/10.1021/acs.molpharmaceut.5b00064>.
- [30] R. Tolba, T. Kraus, C. Liedtke, M. Schwarz, R. Weiskirchen, Diethylnitrosamine (DEN)-induced carcinogenic liver injury in mice, *Lab Anim. (NY)* 49 (2015) 59–69, <https://doi.org/10.1177/0023677215570086>.
- [31] H.W. Hann, S. Wan, R.E. Myers, R.S. Hann, J. Xing, B. Chen, H. Yang, Comprehensive analysis of common serum liver enzymes as prospective predictors of hepatocellular carcinoma in HBV patients, *PLoS One* 7 (2012) e47687, <https://doi.org/10.1371/journal.pone.0047687>.
- [32] S. Das, S. Joardar, P. Manna, T.K. Dua, N. Bhattacharjee, R. Khanra, S. Bhowmick, J. Kalita, A. Saha, S. Ray, V. De Feo, S. Dewanjee, Carnosic acid, a natural diterpene, attenuates arsenic-induced hepatotoxicity via reducing oxidative stress, mapk activation, and apoptotic cell death pathway, *Oxid. Med. Cell. Longev.* 2018 (2018), 1421438, <https://doi.org/10.1155/2018/1421438>.
- [33] B.J. Aubrey, G.L. Kelly, A. Janic, M.J. Herold, A. Strasser, How does p53 induce apoptosis and how does this relate to p53-mediated tumour suppression? *Cell Death Differ.* 25 (2018) 104–113, <https://doi.org/10.1038/cdd.2017.169>.
- [34] N. Takagaki, Y. Sowa, T. Oki, R. Nakanishi, S. Yagosawa, T. Sakai, Apigenin induces cell cycle arrest and p21/WAF1 expression in a p53-independent pathway, *Int. J. Oncol.* 26 (2005) 185–189.
- [35] C.T. Chiu, T.S. Yeh, J.C. Hsu, M.F. Chen, Expression of Bcl-2 family modulated through p53-dependent pathway in human hepatocellular carcinoma, *Dig. Dis. Sci.* 48 (2003) 670–676, <https://doi.org/10.1023/a:1022816204831>.
- [36] C. Scheau, I.A. Badarau, R. Costache, C. Caruntu, G.L. Mihai, A.C. Didilescu, C. Constantin, M. Neagu, The role of matrix metalloproteinases in the epithelial-mesenchymal transition of hepatocellular carcinoma, *Anal. Cell Pathol.* (2019) (2019), 9423907, <https://doi.org/10.1155/2019/9423907>.
- [37] F. Al-Saeedi, I. Loutfi, ^{99m}Tc sulfur colloid and ^{99m}Tc mebrofenin hepatobiliary functional liver imaging in normal and diabetic rats, *Med. Princ. Pract.* 20 (2011) 129–132, <https://doi.org/10.1159/000321216>.

Apigenin-Loaded PLGA-DMSA Nanoparticles: A Novel Strategy to Treat Melanoma Lung Metastasis

Ramkrishna Sen, Soumya Ganguly, Shantanu Ganguly, Mita Chatterjee Debnath,* Subrata Chakraborty, Biswajit Mukherjee, and Dipankar Chattopadhyay



Cite This: *Mol. Pharmaceutics* 2021, 18, 1920–1938



Read Online

ACCESS |

Metrics & More

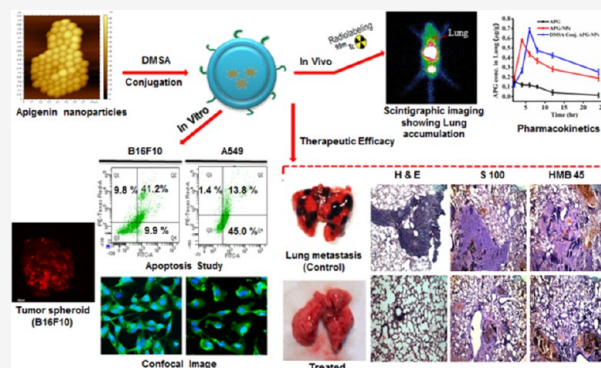
Article Recommendations

Supporting Information

ABSTRACT: The flavone apigenin (APG), alone as well as in combination with other chemotherapeutic agents, is known to exhibit potential anticancer effects in various tumors and inhibit growth and metastasis of melanoma. However, the potential of apigenin nanoparticles (APG-NPs) to prevent lung colonization of malignant melanoma has not been well investigated. APG-loaded PLGA-NPs were surface-functionalized with *meso*-2,3-dimercaptosuccinic acid (DMSA) for the treatment of melanoma lung metastasis. DMSA-conjugated APG-loaded NPs (DMSA-APG-NPs) administered by an oral route exhibited sustained APG release and showed considerable enhancement of plasma half-life, C_{max} value, and bioavailability compared to APG-NPs both in plasma and the lungs. DMSA-conjugated APG-NPs showed comparably higher cellular internalization in B16F10 and A549 cell lines compared to that of plain NPs.

Increased cytotoxicity was observed for DMSA-APG-NPs compared to APG-NPs in A549 cells. This difference between the two formulations was lower in B16F10 cells. Significant depolarization of mitochondrial transmembrane potential and an enhanced level of caspase activity were observed in B16F10 cells treated with DMSA-APG-NPs compared to APG-NPs as well. Western blot analysis of various proteins was performed to understand the mechanism of apoptosis as well as prevention of melanoma cell migration and invasion. DMSA conjugation substantially increased accumulation of DMSA-APG-NPs given by an intravenous route in the lungs compared to APG-NPs at 6 and 8 h. This was also corroborated by scintigraphic imaging studies with radiolabeled formulations administered by an intravenous route. Conjugation also allowed comparatively higher penetration as evident from an *in vitro* three-dimensional tumor spheroid model study. Finally, the potential therapeutic efficacy of the formulation was established in experimental B16F10 lung metastases, which suggested an improved bioavailability with enhanced antitumor and antimetastasis efficacy of DMSA-conjugated APG-NPs following oral administration.

KEYWORDS: apigenin, nanoparticles, DMSA surface conjugation, lung metastasis, gamma scintigraphy



INTRODUCTION

With more than 12 million new cases every year, cancer has become one of the most devastating diseases worldwide. Lung cancer is one of the deadliest cancers with a high mortality rate. According to the GLOBACON report in 2018, lung cancer affected 2.1 million of the population (11.6% of all cancers) worldwide and caused 1.8 million deaths (comprising about 18.4% of all cancer-related deaths).¹ Meanwhile, in India, according to the Indian Council of Medical Research statistics, there were 57,795 new cases of lung cancer estimated to occur in 2012, which is expected to increase by 67,000 (5.9% of all cancers) annually by the year 2020.² Metastatic cancers, especially lung metastasis cases, are almost incurable. Conventional chemotherapy, radiotherapy, and surgery remain the mainstay for treating primary or metastasizing tumor cells. Malignant melanoma causing metastasis still accounts for most of the cancer-related deaths, as multiple metastases cannot be

treated by surgery. Radiotherapy and chemotherapy are the only treatment modalities.

In this context, the ability of natural agents to suppress carcinogenesis has received widespread attention in the research community. Many reports have shown that consumption of phytochemical-rich diets such as fruits and vegetables can decrease the risk of certain types of human cancers.³ Flavonoids comprise a class of low-molecular-weight polyphenolic compounds widely distributed in the plant kingdom, possessing potent antioxidant and anti-inflammatory

Received: September 29, 2020

Revised: March 11, 2021

Accepted: March 12, 2021

Published: March 29, 2021



Journal Pre-proofs

Folate decorated epigallocatechin-3-gallate (EGCG) loaded PLGA nanoparticles; *in-vitro* and *in-vivo* targeting efficacy against MDA-MB-231 tumor xenograft

Julekha Kazi, Ramkrishna Sen, Soumya Ganguly, Tarun Jha, Shantanu Ganguly, Mita Chatterjee Debnath

PII: S0378-5173(20)30433-6
DOI: <https://doi.org/10.1016/j.ijpharm.2020.119449>
Reference: IJP 119449

To appear in: *International Journal of Pharmaceutics*

Received Date: 5 February 2020
Revised Date: 13 May 2020
Accepted Date: 18 May 2020

Please cite this article as: J. Kazi, R. Sen, S. Ganguly, T. Jha, S. Ganguly, M. Chatterjee Debnath, Folate decorated epigallocatechin-3-gallate (EGCG) loaded PLGA nanoparticles; *in-vitro* and *in-vivo* targeting efficacy against MDA-MB-231 tumor xenograft, *International Journal of Pharmaceutics* (2020), doi: <https://doi.org/10.1016/j.ijpharm.2020.119449>

This is a PDF file of an article that has undergone enhancements after acceptance, such as the addition of a cover page and metadata, and formatting for readability, but it is not yet the definitive version of record. This version will undergo additional copyediting, typesetting and review before it is published in its final form, but we are providing this version to give early visibility of the article. Please note that, during the production process, errors may be discovered which could affect the content, and all legal disclaimers that apply to the journal pertain.

© 2020 Published by Elsevier B.V.



RESEARCH ARTICLE



Cite this: *Med. Chem. Commun.*,
2018, 9, 812

Development of a peptide-based bifunctional chelator conjugated to a cytotoxic drug for the treatment of melanotic melanoma†

Raghuvir H. Gaonkar,^{†a} Rinku Baishya,^{†b} Brahamacharry Paul,^{†a}
Saikat Dewanjee,^c Shantanu Ganguly,^d Mita C. Debnath,^{†*a} and Soumya Ganguly^{†a}

The cytotoxic drug gemcitabine (GEM) has been conjugated to receptor-binding peptides to target melanoma tumors. A hexapeptide having a Lys–Gly–His–Lys sequence (pep-1), an octapeptide with an Arg–Gly–Asp–Lys–Gly–His–Lys sequence (pep-2), a GEM-conjugated Lys–Gly–His–Lys peptide (GEM-pep-3) and a GEM-conjugated Asp–Gly–Arg peptide (GEM-pep-4) were synthesized and characterized. *In vitro* uptake of fluorescently labeled GEM-pep-3 and GEM-pep-4 on B16F10 cells was investigated. Fluorescence microscopy studies demonstrated significant uptake of GEM-pep-3 in the B16F10 mouse melanoma cell line. The peptides and GEM-coupled peptides were radiolabeled with [^{99m}Tc(CO)₃(H₂O)₃]⁺ and examined for *in vitro* cell binding in the B16F10 melanoma cell line and *in vivo* biodistribution and scintigraphic studies in a B16F10 melanoma tumor-bearing mice model. *In vitro* cellular uptake studies and biological evaluation confirmed significant deposition of GEM-pep-3 at the melanoma tumor site. The MTT assay depicted higher cytotoxic behaviour of GEM-pep-3 than free GEM. A considerable amount of cell apoptosis was also observed in B16F10 cells. Finally, the *in vivo* therapeutic efficacy study revealed a significant decrease in tumor growth in the GEM-pep-3-treated animal model. These studies reveal enough potentiality of GEM-pep-3 to treat melanoma and underline the need for further evaluation.

Received 18th December 2017,
Accepted 28th February 2018

DOI: 10.1039/c7md00638a

rs.c.li/medchemcomm

Introduction

Recent contribution of research in different areas of modern biology includes finding novel ways to suppress tumor growth using low-toxicity therapies. An effective therapeutic approach is to eliminate cancerous cells while sparing the normal cells. Conventional chemotherapeutics (*i.e.* DNA alkylating agents) target proliferating cancer cells. These may damage healthy growing cells but fail to eliminate quiescent or non-proliferating cancer cells. As many primary and metastatic human tumors are associated with overexpression of different endogenous regulating peptides,^{1–3} conjugation of cytotoxic drugs to receptor-binding peptides is an attractive approach of various cancer research laboratories.^{4,5}

Advancement in the field of peptide synthesis over the last few decades has resulted in the development of new tumor-specific peptides exhibiting high affinity to receptors for research, diagnosis and therapy.^{6–8} Small, synthetic, receptor-binding peptides are preferable over proteins and antibodies for tumor targeting because of their easy chemical modification, favourable pharmacokinetics (high uptake in target tissues, rapid clearance from blood and non-target organs), and broad range of biological activities against many chronic diseases.⁴ In recent years, specifically designed radiolabeled small peptides have been increasingly being used for diagnostic imaging and radionuclide therapy in nuclear oncology.^{6,9} Highly sensitive molecular imaging techniques like single-photon emission computed tomography (SPECT) and positron emission tomography (PET) can be used to monitor tumor localization, progression as well as therapeutic intervention and control.^{10,11} Somatostatin, bombesin, neurotensin, vasoactive intestinal peptide and many others are currently under investigation for possible clinical applications in the diagnosis and treatment of human cancers.^{4,6} The overexpression of somatostatin receptors on various cancers led to the development of US FDA-approved ¹¹¹In-labeled DTPA-octreotide (¹¹¹In-octreoscan) as a diagnostic radiopeptide for scintigraphic imaging of neuroendocrine tumor in patients.¹² A wide variety of chelating agents and

^a Infectious Diseases and Immunology Division, CSIR-Indian Institute of Chemical Biology, Kolkata, India. E-mail: mitacd@iicb.res.in

^b Natural Product Chemistry Group, Chemical Science and Technology Division, North East Institute of Science and Technology, Assam, India

^c Advanced Pharmacognosy Research Laboratory, Department of Pharmaceutical Technology, Jadavpur University, Kolkata, India

^d Regional Radiation Medicine Center, Thakurpukur Cancer Center and Welfare Home Campus, Kolkata, India

† Electronic supplementary information (ESI) available. See DOI: 10.1039/c7md00638a

‡ These authors contributed equally to this work.

SCIENTIFIC REPORTS



OPEN

Garcinol loaded vitamin E TPGS emulsified PLGA nanoparticles: preparation, physicochemical characterization, *in vitro* and *in vivo* studies

Raghuvir H. Gaonkar¹, Soumya Ganguly¹, Saikat Dewanjee², Samarendu Sinha³, Amit Gupta³, Shantanu Ganguly³, Dipankar Chattopadhyay⁴ & Mita Chatterjee Debnath¹

Garcinol (GAR) is a naturally occurring polyisoprenylated phenolic compound. It has been recently investigated for its biological activities such as antioxidant, anti-inflammatory, anti ulcer, and antiproliferative effect on a wide range of human cancer cell lines. Though the outcomes are very promising, its extreme insolubility in water remains the main obstacle for its clinical application. Herein we report the formulation of GAR entrapped PLGA nanoparticles by nanoprecipitation method using vitamin E TPGS as an emulsifier. The nanoparticles were characterized for size, surface morphology, surface charge, encapsulation efficiency and *in vitro* drug release kinetics. The MTT assay depicted a high amount of cytotoxicity of GAR-NPs in B16F10, HepG2 and KB cells. A considerable amount of cell apoptosis was observed in B16F10 and KB cell lines. *In vivo* cellular uptake of fluorescent NPs on B16F10 cells was also investigated. Finally the GAR loaded NPs were radiolabeled with technetium-99m with >95% labeling efficiency and administered to B16F10 melanoma tumor bearing mice to investigate the *in vivo* deposition at the tumor site by biodistribution and scintigraphic imaging study. *In vitro* cellular uptake studies and biological evaluation confirm the efficacy of the formulation for cancer treatment.

In recent years a great deal of attention has been given to identify novel pharmacophores from natural resources that can be used to suppress cancers as well as reduce the risk of cancer development¹. Garcinol (GAR) is a polyisoprenylated benzophenone derivative isolated from the fruit rind of *Garcinia indica* known as Kokum. Like turmeric, this plant is also used as a garnish in cooking and has been extensively used to treat gastric disorders and skin irritation². Studies by different groups have revealed the potential antioxidant, anti-inflammatory and anti-cancer effects of GAR. The anti oxidative property is due to its polyphenolic structure³. *In vivo* studies in animal models have shown its efficacy in suppressing azoxymethane induced colon cancer⁴, 4-nitroquinoline-1-oxide induced tongue cancer⁵, and nicotine-induced human breast cancer⁶. *In vitro* studies in different cancer cell lines reveal the efficacy of the compound in modulating cell signaling pathways involved in apoptosis and cancer development⁷. Though a large number of *in vitro* and *in vivo* studies have been done to establish its wide array of pharmacological effects, little is known about its pharmacokinetic properties and toxicity parameters. A study report claimed that oral administration of 285.71 mg/kg GAR in a mouse model bearing MDA-MB-231 did not result in systemic toxicity and mortality⁷. The compound is a hydrophobic polyphenol exhibiting extremely low aqueous solubility whereas freely soluble in common hydrophilic or organic solvents (0.344–1 g/ml). This necessitates the development of potential delivery systems to enhance its stability and bioavailability.

¹Infectious Diseases and Immunology Division, CSIR-Indian Institute of Chemical Biology, Kolkata, India. ²Advanced Pharmacognosy Research Laboratory, Department of Pharmaceutical Technology, Jadavpur University, Kolkata, India. ³Regional Radiation Medicine Center, Thakurpukur Cancer Center and Welfare Home Campus, Kolkata, India. ⁴Department of Polymer Science & Technology, University College of Science & Technology, University of Calcutta, Kolkata, India. Raghuvir H. Gaonkar and Soumya Ganguly contributed equally to this work. Correspondence and requests for materials should be addressed to M.C. (email: mitacd@iicb.res.in)

Exploring the Potential of $^{99m}\text{Tc}(\text{CO})_3$ -Labeled Triazolyl Peptides for Tumor Diagnosis

Raghuvir H. Gaonkar,¹ Soumya Ganguly,¹ Rinku Baishya,¹ Saikat Dewanjee,² Samarendu Sinha,³ Amit Gupta,³ Shantanu Ganguly,³ and Mita C. Debnath¹

Abstract

In recent years the authors have reported on $^{99m}\text{Tc}(\text{CO})_3$ -labeled peptides that serve as carriers for biomolecules or radiopharmaceuticals to the tumors. In continuation of that work they report the synthesis of a pentapeptide (Met-Phe-Phe-Gly-His; pep-1), a hexapeptide (Met-Phe-Phe-Asp-Gly-His; pep-2), and a tetrapeptide (Asp-Gly-Arg-His; pep-3) and the attachment of 3-amino-1,2,4-triazole to the β carboxylic function of the aspartic acid unit of pep-2 and pep-3. The pharmacophores were radiolabeled in high yields with $[\text{}^{99m}\text{Tc}(\text{CO})_3(\text{H}_2\text{O})_3]^+$ metal aqua ion, characterized for their stability in serum and saline, as well as in His solution, and found to be substantially stable. B16F10 cell line binding studies showed favorable uptake and internalization. *In vivo* behavior of the radiolabeled triazolyl peptides was assessed in mice bearing induced tumor. The $^{99m}\text{Tc}(\text{CO})_3$ -triazolyl pep-3 demonstrated rapid urinary clearance and comparatively better tumor uptake. Imaging studies showed visualization of the tumor using $^{99m}\text{Tc}(\text{CO})_3$ -triazolyl pep-3, but due to high abdominal background, low delineation occurred. Based on the results further experiments will be carried out for targeting tumor with triazolyl peptides.

Key words: *fac*- $[\text{}^{99m}\text{Tc}(\text{CO})_3(\text{H}_2\text{O})_3]^+$ core, internalization, triazolyl peptide synthesis, tumor imaging

Introduction

Technetium-99m (^{99m}Tc) is the most widely used radioisotope in diagnostic nuclear medicine. Significant advancement in technetium radiolabeling is associated with the availability of a wide variety of ligand systems as well as bifunctional chelating agents.¹ Further advances have led to the development of organometallic labeling strategy based on the *fac*- $[\text{}^{99m}\text{Tc}(\text{CO})_3(\text{H}_2\text{O})_3]^+$ core, the synthon developed by Alberto et al., for labeling receptor-specific bioactive molecules.^{2,3} This core due to its low spin, d^6 electronic configuration of Tc(I), exhibits remarkable stability over a wide range of pH values. Excellent labeling efficiencies with a number of donor groups, including amines, thioesters, phosphines, carboxylates, and thiols have been achieved due to the lability of the three water molecules coordinated to the *fac*-M(CO)₃ moiety.⁴

Their laboratory in recent years has made notable attempts toward the development of $^{99m}\text{Tc}(\text{CO})_3$ -labeled peptides coupled to bioactive pharmacophores to be used as diagnostic

radiopharmaceuticals for tumor targeting.^{5,6} During the last 10 years several receptor-specific peptides have been radiolabeled with various radionuclides for scintigraphic applications and therapeutic purposes.⁷ Small peptides are less likely to be immunogenic, possess rapid blood clearance, and are easy to synthesize and modify. Thus, for the development of target-specific radiopharmaceuticals they are considered to be excellent candidates.⁸ L-type amino acid transporter 1 (LAT 1) is responsible for the transport of various natural amino acids, such as methionine, phenylalanine, tyrosine etc. In cancer cells too LAT 1 is found to be highly expressed. Therefore, many natural amino acids and their synthetic analogues are being explored as tumor imaging agents, which have been radiolabeled with different radioactive isotopes.^{9,10}

Recently the pharmacological activities of 1,2,4-triazoles have been extensively explored. In many cases 1,2,4-triazoles have been found to exhibit significant antitumor activity.^{11,12} In an effort to develop radiopharmaceuticals that can localize and image tumors, $^{99m}\text{Tc}(\text{CO})_3$ -labeled triazole-coupled peptides have been synthesized (Fig. 1), characterized, and evaluated for

¹Infectious Diseases and Immunology Division, CSIR-Indian Institute of Chemical Biology, Kolkata, India.

²Department of Pharmaceutical Technology, Jadavpur University, Kolkata, India.

³Regional Radiation Medicine Center, Thakurpukur Cancer Center and Welfare Home Campus, Kolkata, India.

Certificate for Poster Presentation



G-29



Indian Pharmaceutical Congress Association
hereby declares that

Dr / Mr / Ms SOUMYA GANGULY

Theme :
Pharma Vision 2030 :
Indian Pharma Industry-
A Global Leader

has presented a paper entitled

**EVALUATION OF RADIO-PROTECTIVE EFFICACY OF
NANOPARTICULATED MYRICETIN IN COMBATING WHOLE BODY
GAMMA-IRRADIATION INDUCED LIVER TISSUE DAMAGE IN RAT
MODEL.**

in the Scientific Session during 70th IPC 2018

Venue:

Amity University, Noida

Dilip Shanghvi
President - IPCA

B.R. Sikri
Chairman - LOC

Atul Nasa
Organizing Secretary

Dr. A. Ramkishan
Convenor, Scientific Services - IPCA

Dr. Arun Garg
Chairman, Scientific Committee - LOC



Organised by :
Indian Pharmaceutical Congress Association (IPCA)



Hosted by :
Indian Pharmacy Graduates' Association (IPGA)

NATIONAL SEMINAR
on
Pharmacy & Healthcare:
Traditional Knowledge to Modern Techniques

14th September, 2018



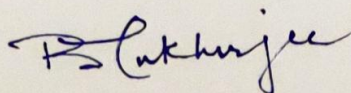
Certificate

This certificate is awarded to Prof. / Dr. / Mr. / Mrs. / Ms.

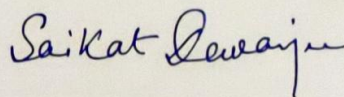
SOUMYA GANGULY

for participation as Delegate/ ~~Resource Person~~/ ~~Chairing a session~~/

Presenting a paper (~~Oral~~/ Poster).



Prof. Biswajit Mukherjee
Co-Chairman



Dr. Saikat Dewanjee
Organizing Secretary



Sponsored by:



Science and Engineering Research Board
Department of Science and Technology
Government of India, New Delhi

Organized by:



Advanced Pharmacognosy Research Laboratory
Department of Pharmaceutical Technology
Jadavpur University, Kolkata 700032



69th IPC 2017

CHANDIGARH
22nd - 24th December, 2017



Certificate

This is to certify that

Prof./Dr./Mr./Ms.

SOUMYA GANGULY

has presented a paper entitled OF THE THERAPEUTIC EFFICACY OF

..NANOPARTICULATED MYRISCTIN..IN..COMBATING..OXIDATIVE..HEPATOCELLULAR...
DEGENERATION BY NON -INVASIVE NUCLEAR IMAGING TECH USING 99mTc Radio Phosphorus
in the Scientific Poster Session of 69th IPC held at Chitkara University, Rajpura

from December 22nd to 24th, 2017.

Signature

Signature

Signature

Signature

Dr. Mahesh Burande
President - IPCA

Dr. Shailendra Saraf
Chairman - LOC

Dr. A. Ramkishan
Convener, Scientific Services - IPCA

Dr. Harish Dureja
Chairman, Scientific Committee - LOC

INTERNATIONAL SYMPOSIUM ON CHEMICAL BIOLOGY AND DRUG DISCOVERY

(ISCBDD-2016)

&

3rd Annual Meeting of Chemical Biology Society (CBS), India

March 1-3, 2016

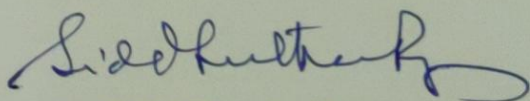
Organized by

National Institute of Pharmaceutical Education and Research-Kolkata,
Bose Institute, Kolkata and Chemical Biology Society, India

Certificate

This is to certify that Prof. /Dr. /[✓]Mr. /Ms. SOUMYA GANGULY

participated / delivered an invited lecture / [✓]presented a paper / chaired scientific session / panel discussant in the International Symposium on Chemical Biology and Drug Discovery organized by National Institute of Pharmaceutical Education and Research, Kolkata, Bose Institute, Kolkata and Chemical Biology Society, India.



Prof. Siddhartha Roy
President, ISCBDD-2016



Prof. P. Jaisankar
Convener, ISCBDD-2016

46th Annual Conference

SOCIETY OF NUCLEAR MEDICINE (INDIA)



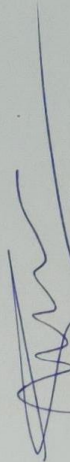
SNMICON2014 (11th - 14th December)

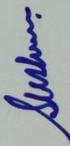
Saha Institute of Nuclear Physics, Kolkata

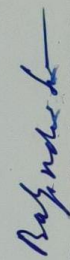
Certificate of Participation

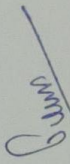
Soumya Ganguly

Certified that **Dr / Mr / Ms**
has Chaired a Scientific Session / presented a paper / participated in Radiation Safety Awareness Walk and Seminar in
the **46th Annual Conference of Society of Nuclear Medicine (INDIA)**.


Dr G P Bandopadhyaya
President, Society
of Nuclear Medicine (India)


Dr SK Sharma
Chairman
Organizing Committee


Dr Baljinder Singh
Dean, ICNM


Col PG Kumar
Organizing Secretary